SPH SIMULATION OF NONLINEAR WATER WAVES

A THESIS

submitted by

SWAPNADIP DE CHOWDHURY

for the award of the degree

of

DOCTOR OF PHILOSOPHY

DEPARTMENT OF OCEAN ENGINEERING

INDIAN INSTITUTE OF TECHNOLOGY MADRAS.

JULY 2014

THESIS CERTIFICATE

This is to certify that the thesis titled **SPH SIMULATION OF NONLINEAR WATER WAVES**, submitted by **Swapnadip De Chowdhury**, to the Indian Institute of Technology Madras, Chennai for the award of the degree of **Doctor of Philosophy**, is a bona fide record of the research work done by him under my supervision. The contents of this thesis, in full or in parts, have not been submitted to any other Institute or University for the award of any degree or diploma.

Professor S. A. Sannasiraj
Research Guide
Professor
Department of Ocean Engineering
IIT-Madras, 600 036

Place: Chennai

Date: 9th July 2014

To my parents and kutty Oishi

ACKNOWLEDGEMENTS

The author is grateful to his research supervisor and soul guru for his guidance, affection and support during his research work. His equal willingness to spend time for discussing results, irrespective of whether it is erroneous or correct is remarkable. In fact, it is quite difficult to frame sincere thanks in words with a scanty vocabulary. Yet, the author feels very proud to be and remain as one of his students.

The author would like to thank all the former Heads of the Department (Prof. S. K. Bhattacharaya and Prof. J. S. Mani) during the tenure of the author and the present Head of the Department Prof. V. Anantha Subramanian, for their effort in maintaining a research friendly environment throughout the department. He is grateful to Prof. S. K. Bhattacharya for approving the upgradation from MS to PhD program. For the same reason, he is grateful to the GTC members: Prof. R. Velmurugan (Department of Aerospace Engineering) and Prof. R. Paneerselvam (Department of Ocean Engineering) for providing their kind support in such program. Among the other Doctoral Committee members, Prof. V. Anantha Subramanian (Department of Ocean Engineering) and Prof. B.S.V. Prasad Patnaik (Department of Applied Mechanics) have provided numerous suggestions and encouragement for work. In particular, the author would like to thank Prof. K. Murali for exploring the world of numerical techniques during one of the courses that he taught in earlier semester. The author has benefited from attending that course which helped him to go for learning SPH from a fast growing literature.

The author is spellbound by the encouragement provided by the Prof. V. Sundar for working on fascinating research problems in coastal hydrodynamics. It was a great learning experience to come in contact with many researchers working in the group headed by him. The author has been fortunate to get senior Research Scholars like, Dr. C. Rajasekharan, Mr. P. Sunny Kumar, Mr. A.C. Mayilvahanan, Mrs. R. Manjula, Mrs. Jeremy Stephen and Mr. K.V. Anand with whom it was a great pleasure to engage in stimulating discussions. The author would like to thank them for providing their kind encouragement for his work.

During these years, the author also has got a number of good friends who made his stay at IIT Madras memorable and enjoyable. For this reasons, he wishes to thank Mr. N.N.V. Rakesh and Mr. Pritam for their kind help in initial days. Among his old friends he wishes to thank Mr. Parsesh Halder for spending his time in hard times. He is grateful to Mr. G. Saravanan, Mrs. N. Sasikala for their helps in numerous occasions. In particular, he needs to recall Mr. E.D.K. Dinesh Kumar for his endless supports, helps and affections.

The author would like to thank the people working in the Department Office and Academic Section for their kind cooperations in administrative procedures. He is grateful to the people in High Performance Computing Facility centre at IIT Madras for their effort in assuring smooth access to the facilities.

The author would like to thank Prof. Alexander Babanin for granting a short term research visit at Swinburn Universuty of Technology, Melbourne, Australia which gave the author the novel opportunity to interact with researchers in his research group and have a glimpse of the work that is going on upper ocean turbulence, among others. This has motivated the author for the future research work.

Lastly, the author would like thank to Prof. V. Sriram who indeed has been an idol during this work. Many suggestions that he used to share on numerical coding from his vast experience were vital. The author is grateful to him for his time and useful comments that the author got during discussions.

'*Man Proposes, God Disposes*'

Hence, let the blessings usher in finding truths in lives of all such people: People who keeps belief, believes in hope and hopes for the best.

Swapnadip De Chwodhury

ABSTRACT

KEYWORDS: Mesh free Particle Methods, Smoothed Particle Hydrodynamics, Incompressible Flow, Navier Stokes Equation, Wave-structure interaction, nonlinear water waves, Numerical simulation.

Free surface waves are one of the numerous magisterial manifestations of nature: be it in the form of oscillating harmonic modes of the free surface of water in a moving pot, interacting ripples in a pond due to rain or the foaming waves lashing over coasts. The evolution of free surface waves closely depends on: i) the initial conditions and ii) the boundary conditions to which it is subjected. It is the latter that often brings complicacies while seeking for exact and closed form solutions for the governing equations (i.e., Navier- Stokes Equations). It requires a numerical tool to solve through computer programs to get approximate solutions. The Smoothed Particle Hydrodynamics (SPH) method is one of many numerical tools which can be adopted for solving Navier-Stokes equations. During seventies and eighties, significant contributions were made in the Finite Element and Boundary Element Method and subsequently, these have been applied to simulate nonlinear water waves with moderate steepness. Similarly, numerous developments have incurred in Smoothed Particle Hydrodynamics methods for free surface flow problems in the last decade. The present study is thus focused on developing a numerical model based on Smoothed Particle Hydrodynamics for simulating nonlinear water waves, including violent cases for which traditional mesh based method like Finite Element or Finite Volume methods are known to have difficulties.

Initial applications of Smoothed Particle Hydrodynamics method to simulate free surface flow problems showed its' capability as a method for dealing with highly nonlinear event like wave breaking. However, from engineering point of view, the real effectiveness of a numerical method remains in the fact whether it can give acceptable solution for a useful flow quantity (say, pressure). The time evolution of pressure was found to be fluctuating unrealistically with the traditional weakly compressible (e.g.,

Weakly Compressible SPH, WCSPH) approach. Therefore, numerous solutions were proposed to rectify and improve the prediction. Present study adopts few notable techniques in order to investigate the performances for a given problem. This includes: a) δ- SPH (Molteni and Colagrossi, 2009) in the framework of weakly compressible SPH; and, b) Incompressible SPH (ISPH) (Cummins and Rudman, 1999; Lo and Shao, 2002). It is explored that the effectiveness of the chosen method is related to the Reynolds number of the flow. Moreover, among the numerous parameters which are required to tune for enhancing the numerical stability, smoothing length (h) and XSPH factor (ε) are identified as the most important parameters. Suitable ranges of these parameters have been proposed based on the requirement of the problem i.e., depending on whether non violent or violent flow. The ISPH model has been improved by i) adopting XSPH smoothing for velocity, ii) Considering higher order source terms in the Pressure Poisson Equation and, iii) Utilizing ISPH_DFDI (Hu and Adams, 2007) algorithm to maintain uniform particle distribution during the course of simulation.

In addition, in contrast to a mesh based method, implementation of boundary conditions poses difficulties in Smoothed Particle Hydrodynamics. Present study employs innovative techniques for the enforcement of boundary conditions. The Ghost particle technique for modelling boundaries satisfies the consistencies of the particle based differential operators. Hence, it has been adopted to perform the convergence studies. But, it has been found to have difficulty in geometric corners. Therefore, Dummy Particles have been adopted with proper formulae to extrapolate flow properties at the solid region. In overall, a robust and reliable numerical model has been developed which can be equally effective in both violent and non-violent flow simulation.

The analysis has been presented in two main parts. For simulation of non violent with low to moderate steepness using the present SPH model prediction has been compared with solutions from potential flow based analytical and/ or a Finite Element Method (FEM) solvers (Sriram, 2008) with nonlinear terms retained in the combined free surface boundary condition. Good performance has been achieved for problems such as i) Propagation of regular monochromatic wave over fixed depth, and, ii) Non violent sloshing in a prismatic tank undergoing external excitation with low amplitude. Whereas,

for violent problems, the pressure time history has been compared with experimental data and the overall flow has been qualitatively compared.

The improved WCSPH and ISPH models developed in this study have been applied to perform inter comparison for problems like- i) Wave impact, ii) sloshing and iii) wave overtopping over coastal structures under given wave conditions. These studies are necessary in order to prescribe a version of SPH model for a general problem where one needs both accuracy and fast computation. A number of findings have been obtained based on these comparative studies.

Finally, the success of the present δ- SPH model has further been highlighted by reproducing the experimental work of Anand (2010) where an in depth investigation has been carried out in understanding suitability of a given sea wall for a given wave climate.

Understanding of violent waves is increasingly becoming vital with respect to the recent marine industry trend for utilizing the offshore wave environment (for example, harnessing the energy of breaking waves). The developed numerical model can thus be employed in order to replicate such extreme wave climate in a computational framework. The salient observations and associated experiences gained by applying the same model to different problems (like sloshing, wave impact due to dam break, wave overtopping over seawalls) showed the efficacy of the numerical method for its generic implementation in many other applications.

CONTENTS

Table of Contents (Contd.) **Page**

Table of Contents (Contd.) **Page**

Table of Contents (Contd.) **Page**

Table of Contents (Contd.) **Page**

LIST OF TABLES

LIST OF FIGURES

List of Figures (Contd.) **Page**

List of Figures (Contd.) **Page**

List of Figures (Contd.) **Page**

List of Figures (Contd.) **Page**

List of Figures (Contd.) **Page**

List of Figures (Contd.) **Page**

ABBREVIATIONS

ALE	Arbitrary Lagrangian Eulerian
BEM	Boundary Element Method
CFL	Courant Friedrichs Levy Criteria
CISPH	Corrected Incompressible Smoothed Particle Hydrodynamics
CPM	Constraint Particle method
CPU	Central Processing Unit
CUDA	Compute Unified Device Architecture
2D	Two Dimensional
3D	Three Dimensional
EFG	Element Free Galerkin
FDM	Finite Difference Method
FEM	Finite Element Method
FNPT	Fully Nonlinear Potential flow Theory
FVM	Finite Volume Method
FVPM	Finite Volume Particle Method
GPU	Graphical Processing Unit
ISPH	Incompressible SPH
ISPH_DFDI	Incompressible Smoothed Particle Hydrodynamics with Density Free and Divergence Invariance
MBT	Multiple Boundary Tangent
MLPG	Meshless Local Petrov Galerkin
MLS	Moving Least Square
MPI	Massage Passing Interface
MPS	Moving Particle Semi implicit
NNPS	Nearest Neighbouring Particle Searching
NS	Navier Stokes Equation
NWF	Numerical Wave Flume
NWT	Numerical Wave Tank

ODE	Ordinary Differential Equation
PC	Personal Computer
PDE	Partial Differential Equation
PFEM	Particle Finite Element
PPE	Pressure Poisson Equation
QALE- FEM	Quasi Arbitrary Lagrangian Eulerian Finite Element Method
RANS	Reynolds Averaged Navier Stokes Equation
RK4	Fourth Order Runge Kutta Method
RKPM	Reproducing Kernel Particle Method
SPH	Smoothed Particle Hydrodynamics
SWL	Still Water Level
TLP	Tension Leg Platform
WCSPH	Weakly Compressible SPH
VOF	Volume of Fluid
VS-1,2,3,4	Violent Sloshing cases 1,2,3,4

NOTATIONS

α	Density relaxation factor for the source term in Pressure Poisson Equation
γ	Adiabatic factor
Γ	Boundary of the Support Domain
δ	Dirac Delta Function
∇	Gradient Operator
∇^2	Laplacian Operator
Δ	Delta denoting a small increment over a variable (e.g., time t)
ε	XSPH velocity correction factor
η	Wave elevation
θ	Random Phase
μ	Dynamic Viscosity
ν	Kinematic Viscosity
ρ	Density
φ	Velocity Potential
ω	Angular frequency of wave
Ω	Support Domain
a	amplitude of the standing wave
a_h	Amplitude of the wavemaker
A	Coefficient matrix for the Pressure Poisson Equation
B	Source term vector for the Pressure Poisson Equation
B_f	Body Force term
c_w	Solitary wave celerity
c_s	Numerical Sound Speed
d	Initial water depth
dt	Time step
dzp	Initial particle spacing along z- coordinate
$f(x)$	Function of variable x

$\boldsymbol{g}$	Acceleration due to gravity
h	Smoothing Length
H_s	Significant Wave Height
H	Wave Height
k	Scale factor for the smoothing length
k_n	Standing wave number
k_p	Wave Number for the progressive wave
L	Wave Length
L_x	Domain length along x- coordinate
L_2	Error norm
m	Mass
m_f	Number of free surface particles
n	Total number of particles of all kind
N	Number of Neighbouring particles
N_p	Number of fluid particles
N_b	Number of boundary particles
p	Pressure
$\boldsymbol{r}$	Position vector of a point in a Cartesian plane ($\mathbb{R}^2$) with components (x,z)
R	Wave runup
S	Stroke of the wavemaker
t	Time
t_s	Physical start time of simulation
t_e	Physical end time of simulation
$\boldsymbol{v}$	Velocity
W	Kernel function
V	Volume
V_s	Specific Volume
X	Solution vector the Pressure Poisson Equation
VW,FSS,CPS,GS	Type of swawalls: Vertical Wall (VW), Flaring Shaped Seawall (FSS), Circular Cum Parabolic Seawall (CPS) and Galvenston

	Seawall (GS)
T	Time period of the wave

Normalized parameters

t_n	Time scale normalized in two ways: 1. $t_n = t\omega$ 2. $t_n = t\sqrt{(\lvert \mathbf{g} \rvert / d)}$

CHAPTER 1

INTRODUCTION

1.1. GENERAL

A bright sunny day in a sandy beach with a blue sky and patches of cirrostratus clouds like casual strokes from a painter's brush on an empty canvas is probably one of the most popular stress busters during a weekend for an urban individual. Many beaches are natural or artefacts of some artificial ports enhancing offshore- onshore interactions. It takes a significant effort to maintain the smooth accessibility of a beach throughout the seasonal changes. Fig. 1.1 presents some snapshots of a beach showing its various morphological and man made aspects. Such environment becomes dangerous during severe weather condition. Fig. 1.2 shows wave overtopping over a coastline during an extreme wave climate.

In deep sea, a cargo vessel (Fig. 1.3) carrying oil container may face severe stability challenges due to the violent sloshing of the liquid inside the containers in a harsh marine environment. For a passenger carrier vessel, the rolling of the ship affects the comfort of on board members. A jacket structure installed in an intermediate water depth for exploring natural resources is also subjected to extreme marine environment (Fig. 1.4). Turbine kept in chambers in order to harness wave energy is supposed to retain stability during adverse wave climate ensuring uninterrupted and efficient operation.

(a) (b) (c)

Fig. 1.1. Different aspects of a beach: (a) a jetty at Car Nicobar, (b) a geometrically shadow zone providing habitats for migrating birds and (c) a recreational place (Location: St. Kilda beach, Melbourne, Australia).

Design and development of such entities (e.g., coastal areas, oil containers, ship etc.) which are vital for human lives, material and financial resources, cover a significant potion of understanding the physics of water waves: their generation, propagation and interaction with different structures.

Fig. 1.2. Wave overtopping over coastline

Fig. 1.3. A liquid cargo vessel carrying oil container
source:
http://seaspout.wordpress.com/2012/07/23/alternatives-to-bunker-fuel-lng/

Fig. 1.4. A jacket structure subjected to an extreme wave climate

The study of wave structure interaction can be performed either in a physical laboratory tank with wave generation facilities or, based on an analytical model seeking for exact solutions, or, in a computer program based on a well established numerical

method for solving a fluid flow problem subjected to proper boundary conditions. All approaches have their own advantages and disadvantages and hence it can be taken as one approach as a supplementary to others. Installation of physical tanks with wave generation facilities is costly and may not easy to avail for a variety of purposes. The prediction from a numerical model can also be used to design complicated experimental activity efficiently. The physical phenomenon in a numerical simulation may in turn motivate an observer to have specific views on some aspects of the experiment. Moreover, the information obtained from the model scale in experiment can be effectively correlated with real scale using numerical simulation. On the other hand, an analytical model (e.g., the airy wave theory) is useful for understanding the basic wave mechanics for small wave steepness (ratio of wave height to wave length). Analytical model capable of dealing with highly steep waves are also available (e.g., Chalikov and Sheinin, 2005). The resulting expression for estimating wave forces on different structures may be complicated while going for a closed from solution. Situation may be further difficult if the structure is considered as floating with its all degrees of freedom including free surface effect. Therefore, approximate solutions are sought for practical purposes. Even though, these solutions are subjected to a number of assumptions which may not remain valid in some cases. So, researchers have put effort in developing numerical models which solves the governing equations of the flow with provision for adopting certain initial or boundary conditions permitted for the governing equations. This makes possible to investigate a test involving wave structure interaction under a number of cases and provides useful information for designing an object which is supposed to face non linear water waves.

The numerical models can be broadly categorized into two divisions:

(a) models based on Fully Nonlinear Potential flow Theory (FNPT): It differs from the Airy wave theory in terms of the higher order terms contained in the combined dynamic and kinematic free surface boundary conditions, which are non linear in nature. In this approach, it is possible to express the flow by the Laplace equation in terms of velocity potential. FNPT model are most suitable while the flow may be safely considered to be irrotational (i.e., non breaking, mildly steep waves).

(b) Full set of Navier- Stokes (NS) equations: It is essential if other details of the flow (like viscosity, turbulence, effect of wind on waves etc.) apart from flow quantities such as velocity and pressure are required. Thus, NS model facilitates detail analysis of the fluid flow.

1.2. NUMERICAL MODELS FOR STEEP NONLINEAR WAVES

With the increase in trend of utilising offshore region for different purposes (like harnessing wave energy), the necessity to understand the flow behaviour of violent waves is becoming important. A number of numerical models dealing with steep nonlinear waves is made available. For any such numerical model, a challenge is to capture the plunging breaking of a wave (Fig. 1.5).

Fig. 1.5. Plunging breaking wave with swirling (Source: http:// www.pdphoto.org).

Physically this phenomenon may be caused by several reasons and is extremely complex involving several flow features like fluid fragmentation, jet evolution, air entrapment, fluid coalescence, turbulence, momentum and energy transfer between air and water through a deformable interface and so on. It is indeed a significant success for a numerical model if it can simulate the onset of such wave breaking due to similar initial and boundary conditions as in a physical case.

Past studies focused on numerical simulation of such steep non linear water waves have adopted numerical methods like Finite Element Method (FEM), Finite Difference method (FDM), Boundary Element Method (BEM) or Finite Volume Method (FVM). Few of these studies have been summarized in Table 1.1. There has been a significant progress achieved in understanding the complex flow behaviour of violent waves.

Table 1.1. Few numerical models used for simulation of steep nonlinear water waves.

Method	**Description**	**Application**
BEM (Grilli and Subramanya, 1996)	solves Laplace equation	Solitary wave shoaling and breaking over gentle slope
FDM (Constraint Interpolation Profile (CIP)) (Kishev et al., 2006)	solves NS with two phases	violent sloshing inside a container
FEM (Yan and Ma, 2010)	solves Laplace equation using FNPT	3D Over turning waves over varying bathymetry
FVM (Xie, 2014)	solves NS with two phases	effect of wind on solitary wave breaking

The presence of time evolving free surface in the computational domain makes the problem as a unique flow problem in the case of nonlinear water wave simulation. In most of the above mentioned studies, major focus has been paid in order to capture this free surface as accurate and efficient as possible. For example, Yan and Ma (2010) used QALE- FEM technique to deal with movements of the nodes at the free surface. Xie (2014) used the Volume of Fluid (VOF) technique to track the dynamic air water interface. One needs to exercise very careful choices while implementing these

techniques by ensuring minimum effect of spurious losses of energy. Remeshing of the domain becomes inevitable to maintain the mesh quality on which the solution of the numerical model depends greatly. Sriram et al. (2006a) investigated a few of these techniques to find which among these yields minimum energy loss for a given mildly steep wave. Also, the influence of those techniques are not significant if it is expected to model waves with low steepness in deep water depths. Thus the model lacks its robustness for general purpose use while one tries to use this model for wave propagation from deep to shallower region. Because, it may be difficult to know a priori when to use special technique to deal with increasing steepness.

A second alternative for the above problems with mesh based numerical methodologies is to adopt meshfree or particle based description of the domain. A particle with associated flow properties like mass, volume, pressure, velocity represents a fluid portion. The kinematic free surface boundary condition is intrinsically satisfied. Due to the absence of mesh connectivity, it easily adopts the flow pattern without having much numerical issues. In this way, it appears to be possible to develop a robust numerical model for simulating nonlinear water waves irrespective of their steepness.

1.3. PARTICLE METHODS FOR NONLINEAR WATER WAVES

Some of the popular particle methods used for simulation of nonlinear water waves are: Smoothed Particle Hydrodynamics (SPH, Dalrymple and Rogers, 2006); Corrected Incompressible Smoothed Particle Hydrodynamics (CISPH, Khayyer et al., 2008); Moving Particle Semi (MPS) implicit method (Koshizuka et al., 1998); Meshless Local Petrov Galerkin (MLPG) method (Ma and Zhou, 2009); Particle Finite Elemet Method (PFEM) (Idelsohn et al., 2004) etc. Generally speaking, in order to achieve qualitatively correct results, one needs to use sufficient number of particles. Also, in contrast to a grid/ mesh based numerical model (like FEM), most of these particle based numerical model do not have the flexibility to use non uniform initial spacing for a given length. But, for most of the problems in nonlinear water waves, the length through which the wave has to propagate to capture a physical process is comparatively higher than the initial water depth. This leads to a quite large number of particles to be used even in the description of wave propagation of waves with small steepness in deep water region (i.e., $d/L > 0.5$, d

and L are water depth and wave length, respectively). Thus it is quite slow in computation compared to a grid based model. But, even with this time consuming tasks, the user does not need to adopt any further action to maintain numerical stability if the steepness of the wave increases during propagation. Therefore, particle based methods have the potential to form a robust numerical model. Regarding the issues with computational times, it should be noted that now a days many computing architectures are being utilized (like GPU computing) for performing faster computation. In fact, efficient and optimal computation of the existing particle based numerical model for large scale problems (flooding of a beach due to a tsunami wave, green water overtopping over a TLP etc.) are a major research topic.

Yet, it is only in recent times, researchers have started exploring the convergence properties of kernel function based differential operators and the effect of choice of input parameters in particle models. Although, the numerical tests used to check the theoretical findings are much simpler (e.g., in many cases restricted to one dimension) than a non linear water wave problem, still the findings from theoretical analysis has brought some facts which inspires further research. Some of these questions have been of particular interest in this present study. It reports the development of an independent particle based numerical model for simulating non linear water waves. Chapter 2 conducts a literature survey to set a definite objective for the study. Chapter 3 discusses the basic principles upon which the developed numerical model is situated and provides validation and quantification of error for the numerical solution of a benchmark case in nonlinear water wave problem. Chapter 4 presents some techniques adopted to enhance the model performance. Then the next two chapters are devoted to application of the developed numerical model to two important problems in non linear water waves: sloshing in a prismatic tank (Chapter 5) and wave overtopping on a seawall (Chapter 6). The length and time scale pertaining to these two problems differ significantly and hence, successful simulation from the same numerical model for both of these problems reflects its robustness. The thesis summarizes with conclusions and future prospective of the present work.

1.4. SUMMARY

In this chapter, the importances of studying non linear water waves have been highlighted. Specific emphasize has been made on highly steep violent water waves. Some of the successful numerical models simulating violent breaking waves have been highlighted. Particle based numerical methods have been selected for simulating non linear water waves. Similar to any numerical method, particle method also contains certain pitfalls which should be addressed for the development of the numerical model.

CHAPTER 2

LITERATURE REVIEW

2.1. GENERAL

On 1977, a numerical technique came into light dealing with evolution of gas clouds in the background of interstellar medium by two independent studies: Lucy (1977) and Gingold and Monaghan (1977). While the work of Lucy (1977) is regarded as revolutionary for the idea of estimating a physical property based on smoothing which has been nurtured using the concept of Monte- Carlo method of Hammersley and Handscomb (1964), the study by Gingold and Monaghan (1977) is undoubtedly ingenious for the original mathematical development of the technique. Lucy (1977) presented the scheme in a contemporary way which might well be appreciated by people working with finite difference codes. Whereas, Gingold and Monaghan (1977) showed the new technique which basically does explicit numerical integration on a system of particles interacting within themselves with respect to Newton's Law of motion, played a potential competitor with finite difference scheme. Later, Monaghan and his co workers (e.g., Durisen et al., 1986) studied the performance of this newborn technique along with finite difference codes on similar problems and noted advantages and disadvantages. Since then, this technique has been maturing into a numerical method, called Smoothed Particle Hydrodynamics (SPH) dealing with complex physical problems found in celestial objects, industry and everyday life. The name SPH was coined by Gingold and Monaghan (1977).

Since then SPH was proposed, it has sailed through a number of stages in terms of method development and diverse applications. So, a survey made on these developments can hardly be claimed as complete. However, hovering over these numerous fields where SPH has been applied, one can get a definite trace of gradual development for an emerging numerical technique. With this aim, the purpose of the present chapter is focused. Although the central theme of the present study is non linear free surface flow, to highlight a coherent outlining of the salient developments of the numerical model, it is

found to be necessary to consider other fields like astrophysics and solid mechanics. Notably, SPH has got its unique numerical form while applying in various problems in astrophysics. As far as a standard systematic stability analysis is considered, SPH has gone through the critical and subtle tests while studying problems in solid mechanics. Most of the techniques to enforce essential boundary conditions in SPH have been proposed while solving fluid flow problems. These show development of SPH including fluid flow with either a free surface or an interface with another media (i.e., a multiphase flow). The latter section discusses more recent applications (e.g., microfluidics, flow of Non Newtonian fluids etc.) of SPH. A brief discussion has been given highlighting the gradual development of numerous particle methods like SPH and their off springs.

2.2. SPH: ASTROPHYSICAL PROBLEM

With the works of Chandrasekhar (part of which was compiled in the books authored by him, such as, on Stellar structures (Chandrasekhar, 1939) and on ellipsoidal figures (Chandrasekhar, 1969)) among others, astrophysicists in 70's were able to discuss on pure theoretical grounds about the physical parameters that have to work on while analysing the stability or a particular shape of a known star. In general, the equations which describe the evolution of stellar structures are integro- differential type combining a range of ideas from a diverse fields of physics (such as, relativity, thermodynamics, electromagnetics and so on) and may be complicated while seeking for an exact solution. Scientists were equally interested to know the key parameters that play a major role in the development of a particular stellar structure from a given state of known mass distribution. The age of computing architecture has also been progressing at a faster rate towards its extreme usage in solving problems in astrophysics. With the advent of SPH, people interested in studying evolution of star and N body problems got a comprehensible and easy to use numerical technique with which they can perform a number of numerical experiments on the possible form of gas clouds. A few of these important works have been summarized by Benz (1988). An overview of salient contributions made towards the development of SPH is given below.

- **Monaghan, Gingold and their co workers (1977 ~ 1990) and Wood (1981, 1982):** During this period, a series of papers emerged from their work for

understanding the behaviour of gas clouds in the formation of stars and other stellar structures in stable and unstable regime. Those problems can be broadly categorized as:

- ***Fission of polytropes:*** The process of fission of a polytrope (i.e., a stellar structure where pressure is related with density through a given polytropic index) rotating with non uniform and angular velocity damped at specified regime was shown to form a system of binary star. While simulating this phenomenon using SPH code (Gingold and Monaghan, 1978), it was able to successfully capture the characteristic bone shape of the so formed binary star system.
- ***Collapse of non axisymmetrically rotating gas cloud:*** A good agreement between finite difference and SPH methods in terms of free fall time has been achieved by Gingold and Monaghan (1981). But in contrast to the former, they obtained merged rod shaped structure in SPH.
- ***Study of fission instabilities:*** An extensive comparison between FDM and SPH by Durisen et al. (1986) provides more information. One important finding from SPH is that it was able to resolve the density at the inner region better than in the outer region with lower resolution. Whereas, in FDM, a uniform performance has been evaluated and therefore, at the inner region, the fluid properties were less resolved compared to SPH.

- **Miyama et al. (1984):** A detailed account was given for the criteria under which an initial gas cloud is likely to take the form of diverse structures. The occurrences of z- bounce and ω- bounce (i.e., a peak in density in rotational plan or in a plane perpendicular to it) along the free fall time scale indicated the possible shape of the object at the end of simulation.
- **Benz (1984):** One of the unique papers, in which the effect of magnetic field was included in the SPH simulation of similar fission processes.

Apart from the above quoted works, there were number of papers appeared in SPH. Analysing these works, the following major contributions in the development of SPH have been explored from the astrophysics problems.

2.2.1. Shock simulation

Physically, when a discontinuity occurs at a given point in a homogenous space (e.g., during an explosion), the energy so released tends to dissipate in the surrounding at a rapid rate in the form of a wave. In one dimensional case, it is interpreted as the propagation of information from a space of higher potential to lower potential due to difference in the given initial condition between these two regions (standard shock tube problem, Sod, 1978). Theoretically such exchange of energy between two given energy states is treated by shock. In standard SPH which was introduced to simulate fission of a rotating gas cloud or collision between two clouds (Lattanzio et al., 1985), it is apparent that two interacting particles may cause a shock along their position vector as they stays at two energy states and pressures at them are calculated by solving an equation of state. This shock so created may lead to artificial oscillation on a calculated numerical value at a particle and thereby cause numerical instability. In order to rectify this, following techniques were proposed in SPH.

- ***Artificial viscosity:*** By showing an analogy with the well known von Neumann and Richtmyer (1950) artificial viscosity, Monaghan and Gingold (1983) proposed a similar form for SPH to smooth the shock front and stabilize the simulation. This form or some of it is later developments (as mentioned in Chapter 3) has been used in most of the SPH models with application in problems in other fields. This artificial viscosity possesses some coefficients which should be tuned properly depending on the problem. Also, the artificial viscosity may bring unwanted numerical diffusion in the solution. However, Balsara (1995) proposed entropy preserving artificial viscosity to retain its major advantages.
- ***Godunov SPH:*** An alternate formulation was proposed by Inutsuka (2002) where the interaction between two interacting particles is resolved by solving a Riemann problem along their position vector. In this approach, there is no need to use artificial viscosity. But it may be computationally more expensive compared to the former, requiring to solve a matrix of size depending on the dimension of the problem, for each interaction in the entire particle system. Also, the basic Godunov scheme was found to suffer from significant numerical dissipation. For this reason latter it was found useful to incorporate HLLC (Harten Lax and van

Leer Contact) and MUSCL (Monotone Upwind Centred Schemes with Conservation Laws) to improve Godunov SPH (see e.g., Rafiee, 2011). Apart from shock tube problem, the Godunov SPH scheme was equally found to yield good results for impact problem in solid mechanics (Parshikov et al., 2000) and sloshing (Rafiee et al., 2012).

In a recent paper by Puri and Ramachandran (2014), a comparative study has been performed between most of proposed techniques dealing with shocks in SPH for a variety of shock tube problems.

2.2.2. Variable smoothing length

While simulating fission of a star, the length scale varies from a few to several higher orders. In order to model, either a huge number of particles have to be employed which might be quite prohibitive in some cases, or, a variable smoothing length can be used through which more number of neighbouring particles are allowed in the interpolation of 'property' in the region of interest. Now, this can be achieved in several ways. In one approach, one can update the smoothing length particle wise, so as to retain a desired range of density (Monaghan, 1992). In another, a separate equation may be solved for the time evolution of particle wise smoothing length by preserving conservation of energy (Hernquist and Katz, 1989; Benz, 1989; Nelson et al., 1994). For slamming problem, Oger et al. (2006) obtained good results using SPH model with variable smoothing length. A more recent implementation of variable smoothing length techniques is available in GRADSPH code (Vanaverbeke et al., 2009) or in NDSPMHD code developed by Price (Price, 2004).

2.2.3. Nearest Neighbouring Particle Searching (NNPS) strategy

One of the computationally expensive parts in any SPH model is the identification and storage of neighbouring particles to calculate a physical property using interpolation at a given particle. The algorithm through which it is done is called Nearest Neighbouring Particle Searching (NNPS). In 3D problems in astrophysics, several NNPS have been proposed. Few details of these algorithms are presented in Chapter 3. In most of the SPH models, the particles are sorted in 'linked- list' based on square cells discretizing the

domain (Monaghan and Gingold, 1983; Hockney and Eastwood, 1988). An effective approach, particularly with variable smoothing length formulation, is to create a hierarchical tree based on successive splitting of the entire domain into octants that contain one particle (Hernquist and Katz, 1989). An implementation of Tree search based NNPS algorithm is available in SPH code GADGET (Springel et al., 2001) which has been used to simulate the formation of giant nebula.

2.3. SPH: SOLID MECHANICS

Since early nineties, SPH has been extensively being applied to solve solid mechanics problems. Authors were mainly interested in studying ballistic impact problems or growth of crack using a Lagrangian method like SPH. In doing so, some of the intrinsic features of SPH which thought to be advantageous in previously attempted problems in astrophysics, now fetched serious doubts on the applicability in solid mechanics problems. While dealing with those issues, researchers made several improvements in SPH.

2.3.1. Tension instability:

In astrophysical problems, where density is varied over large domain, non uniform distribution of particle is apparent due to the relation of pressure with density for a polytrope. When same kind of equation was used to calculate pressure (i.e., stress in solid mechanics), unrealistic accumulation occurred in the presence of tension (a negative stress state). The error due to that was not previously studied in problems in astrophysics but found to bring unacceptable results in basic problem like deflection of a column. In order to rectify that several techniques were proposed. Some of the important corrections in the context of solid mechanics problems are as follows:

- ***Stress points:*** Dyka and Ingel (1995) and Dyka et al. (1997) introduced the concept of stress points. The derivative through which information is obtained for the upgradation of nodes is calculated using these fixed stress points. Using stress points, tension instability was effectively reduced for problems like deflection of a cantilever beam subjected to dynamic load.
- ***Lagrangian kernel:*** Rabczuk et al. (2004) explored that the tension instability can be removed from the solution if one use Lagrangain kernel which is more

consistent for linear transformation than Eulerian kernels. Here, SPH model was used to carry out simulation of a variety of problems like impact of a rod on a beam, defection of a plate, collision between two rubber bands etc.

- ***Total Lagrangian formulation of SPH:*** By investigating the root cause of tension instability in SPH, Bonet and Kulasegaram (2001) found that this happens due to zero eigen modes of the tangent stiffness matrix. It was noted as a characteristic feature of the then used SPH formulation. So, in order to avoid that they proposed a new scheme where the gradient of the kernel function was calculated with respect to a fixed frame of reference. The success of this approach was highlighted by simulating large defection of a column.
- ***Moving Least Square SPH (MLSPH):*** By using a kernel function based on Moving Least Square (MLS) interpolation (Dilts, 1999, 2000) of a given order and dimension, the prediction from the SPH model was shown to improve for similar problems. Moreover, an effective technique was proposed in Dilts (2000) to accurately identify the particles at the deforming boundary.
- ***Addition of repulsion terms with pressure gradient (Monaghan, 2000):*** By this additional term which partly repels two approaching material particles, tension instability was shown to be rectified.

Swegle et al. (1995) found that tension instability is inherent in a kernel based approximation when the second derivative of kernel operates on internal stress and yields a negative value. Physically speaking, under negative change of internal stress state, the kernel based approximation in SPH is unstable. This finding has also been utilized to investigate tension instability in another particle method named Moving Particle Semi implicit (MPS) by Khayyer and Gotoh (2011).

Many more solutions are proposed to remove tension instability. Even in fluid flow problem in fluid flow with moderate Re, tension instability may not be overlooked. So, while SPH was subsequently being applied in fluid flow problems, several other techniques were proposed to avoid tension instability in the context of fluid flow problems. Some of them are mentioned in few sections later.

2.3.2. Other particle methods

One of the major outcomes of the application of SPH on solid mechanics problems is that a number of new particle methods are proposed. For example, Reproducing kernel particle method (RKPM) (Liu et al., 1995). Several Galerkin based particle or meshfree methods were also came into light: Element Free Galerkin (EFG) method (Belytschko et al., 1994); Mehless Local Petrov Galerkin Method (MLPG, Atluri and Zhu, 1998) etc. A detailed account of these developments is available in the book on meshfree method by Liu (2002). Overall contributions are made in the general development of particle based meshfree methods to solve complex problems along with SPH.

2.4. SPH: FLUID FLOW

The earliest successful application of SPH to solve incompressible flow with free surface was by Monaghan (1994). Apart from showing the capability of SPH in simulating violent free surface flow problems, he introduced some useful techniques which are still being used in a number of SPH models. For example,

a) XSPH smoothing of velocity: A technique through which particle positions are updated with a velocity that is not obtained directly from solving the momentum equation, but a smoothed one. It retains uniform particle distribution and may alleviate onset of tension instability;

b) Optimum time step: Since, pressure is solved from an explicit equation of state, the time step is rather small due to sound speed restriction. So, an artificial sound speed is required which is much smaller than the original one to yield a practical time step. A thumb rule that was proposed by him to adopt numerical sound speed as at least one order higher of magnitude (i.e., ten times) of maximum expected flow velocity;

c) Time integration scheme: a predictor corrector time stepping was used as time integrator and,

d) Repelling boundary particle to mimic a solid boundary: Using a Lennard Jones type repulsion force, no slip boundary condition was replicated to give realistic flow evolution, etc.

Qualitatively, description of fluid flow problems would be obtained using the above techniques. Also it appeared to be easy to grasp and implement. However, a qualitative prediction requires much more attention in terms of adopting staratgies in dealing with many issues starting from physical to numerical. These pose a number of important questions that need to be addressed while using the basic SPH technique in fluid flow problems. Most of these contributions emerge towards the development of SPH in the last two decades.

2.4.1. Pressure fluctuation

Since the standard SPH technique tries to solve Euler equation, naturally one is interested in looking at the predicted pressure which is one of the important physical quantities in any engineering problems in fluid flow. But, while investigating for pressure, it is noted that it suffers unrealistic fluctuations and it is difficult to extract useful information. Many authors have been working on reducing the pressure fluctuaions. Some of the salient contributions are discussed here.

- ***Spatial Pressure fluctuation control:*** Colagrossi and Landrini (2003) noted that to control the fluctuation of pressure, one needs to have a smooth density, since in SPH model, pressure is obtained directly from density. Density is calculated from particle positions which are non uniform during the course of the simulation. Naturally, standard kernel which is inconsistent for such distribution of particles brings noise in density field. So, a higher order interpolating kernel (previously used by Dilts as mentioned above) was adopted to have better conservation between mass, density and occupied area for a particle. Moreover, they optimized the correction by periodically applying it throughout the time steps, since calculation of MLS interpolating kernel is computationally expensive. Improvements were shown for pressure calculation in classical 2D dam break flow. They were equally trying to simulate multiphase flow with low density ratio with the SPH model. This approach was found to be useful because near the interface or its vicinity pressure field has to be regular to avoid spurious diffusion.
- ***Calculation of pressure time history:*** The problem of slamming is an important problem in marine engineering and has long been known to be difficult due to a number of issues like involvement of violent free surface fragmentation, acoustic

waves, deformation of structure etc. In this paper, Oger et al. (2006) had moved a step towards answering these questions using SPH. For estimating pressure time history at a given location along the hull, they proposed particle sampling technique.

- ***δ- SPH:*** By adding a higher order source term in the continuity equation (from which density is obtained by time integration) Molteni and Colagrossi (2009) tried to smooth the pressure signal. The proposed diffusive term is proportional to the smoothing length and converges to the continuity equation, when the smoothing length decreases with increase in the number of particles. Through many studies in last decade, they were able to get successful simulation for a variety of fluid flow problems: stable pressure during jet impinging on a flat plate (Antuono et al., 2010); impact of wave on structures due to dam break (Marrone et al., 2011a); accurate propagation of gravity waves in a rectangular basin and wave focusing (Antuono et al., 2011); sloshing (Antuono et al., 2012); and trailing waves due to a propagating ship (Marrone et al., 2012). More recent applications include viscous flow around bluff bodies (Marrone et al., 2013) and non linear responses of floating bodies (Bouscasse et al., 2013a).
- ***K2_SPH:*** By employing a higher order gradient estimation using kernel function, Hu et al. (2011) found improved pressure from SPH. Since, many of the other physical parameters like wave elevation is related with pressure, a noise free and accurate pressure is essential. This would also make it possible to evaluate non violent water waves comparable with analytical solution.
- ***Incompressible SPH (Cummins and Rudman, 1999):*** By treating water as strictly incompressible in contrast to the original weakly compressible approach of Monaghan (1994), and thereby solving pressure from projection based Pressure Poisson Equation (PPE), improvement was obtained over standard SPH for required physical quantities for benchmark problems like 2D lid driven cavity and Rayleigh- Taylor instability. Lo and Shao (2002) applied similar technique to free surface flow problems. Till then, a lot of works has been devoted for understanding the suitability of the models, ISPH and WCSPH for pressure (e.g., Lee et al., 2008; Hughes and Graham, 2010).

- ***ISPH with explicit calculation of pressure from PPE:*** Hosseini et al. (2007) calculated the pressure from PPE explicitly. An important extension of this work was achieved by Rafiee and Thiagarajan (2009) who were successful in simulating Fluid Structure Interaction (FSI) problem involving fluid interaction with an elastic structure using this explicit incompressible SPH. Number of validations of this technique are made by Barcaloro et al. (2012).
- ***Godunov SPH:*** Although this technique was proposed to better deal with shocks, it was apparent that improvement might be possible for pressure in fluid flow problems also. Rogers et al. (2010) found good results for pressures on a caisson breakwater using that technique. Clear evidences of improved prediction of pressure in GSPH compared to both WCSPH and ISPH were provided by Rafiee et al. (2012).
- ***SPH with Arbitrary Lagrangian Eulerian (ALE) scheme:*** Koukouvinis et al. (2013) formulated a novel ALE scheme for SPH and found its improvement for pressure for a variety of fluid flow problems like jet impinging on a flat plate, Taylor Green vortices and slamming of wedge shaped structure during its entry into water etc.

Although most of the above mentioned techniques aimed at improving the prediction of pressure, it has also brought significant improvement for other measurable quantities (like velocity, wave elevation) and facilitated quantifiable validation of the SPH simulation. Thus these have contributed for overall development of the SPH as an effective numerical method.

2.4.2. Treatment of boundary conditions

A number of techniques to implement required boundary conditions in SPH has been proposed by many authors in the past while solving fluid flow problems. The repulsion force based approach in Monaghan (1994) is one of them. Among other techniques, few are given here.

- ***Ghost Particles (Libersky et al., 1993; Colagrossi and Landrini, 2003):*** The required boundary condition (e.g., free slip) is enforced at the solid boundary by providing full compact support near the boundary using ghost particles. This has proven to be a powerful technique for boundary modeling in domain with simple

geometry. But, it has problems with complex geometries. Delorme et al. (2009) obtained good results for sloshing due to roll excitation using this technique.

- ***Dummy particles (Takeda et al., 1994):*** A fixed layer of particles are placed in order to mimic a solid boundary. The problem with ghost particles in case of complex geometrical shapes can be partly solved by using this technique. Yet, one needs to extrapolate the required properties at the dummy particle location carefully to have proper implementation of the boundary conditions. Many studies investigated the effectiveness of this technique. Issa et al. (2010) extended this technique to investigate a proper turbulence model in SPH scheme. On the other hand, Adami et al. (2012) proposed a formula for accurate calculation of pressure at the dummy particles based on local force balance. They also validated the technique for benchmark cases.
- ***Fixed Ghost Particles (Marrone et al., 2011a):*** Another approach is based on fixed layer of ghost particles which are set around the solid boundary and each of them is associated with an interpolation node in the fluid region. Then at each time step, the fluid properties are calculated in these interpolation nodes using higher order kernel function. Using this technique, they were also able to successfully simulate wave pattern generated by a passing ship with a complex hull shape (Marrone et al., 2011b).

A rigorous mathematical analysis of the mostly used dummy particle techniques has been provided by Macia et al. (2011). It was found that most of the techniques are not truly continuous when a systematic convergence test is carried out with respect to the particle based differential operator. Therefore, they proposed consistent formulae for conducting accurate extrapolation in the solid region and later, it has been found to give accurate results for flow over bluff bodies in Marrone et al. (2013).

- ***Multiple Boundary Tangent (MBT) technique:*** Yildiz et al. (2009) and Shadloo et al. (2011) were able to get accurate simulation of flow around bodies using traditional ghost particle approach by proposing effective techniques to position ghost particles and fix their properties based on local normal. Shadloo et al. (2011) have uniquely validated flow past a complex shaped aerofoil using SPH.

- ***Semi analytic Boundary condition:*** After the initial proposal of this technique by Kulasegaram et al. (2004), there has been a long pause for the adoption of this novel technique for more general fluid flow problems. Some preliminary attempts were taken by Di Monaco et al. (2011). Complicacies due to calculation of the normalized integrating factor for a given geometrical shape may be a reason for such a delay. Recently, Ferrand et al. (2013) took an effective initiative towards the development of this technique. Substantial progresses have been achieved to generalize this technique (e.g., 3D problems) as reported in Mayrhofer et al. (2013, 2014).
- Fatehi and Manzari (2012) proposed a novel technique to calculate pressure at the wall particle by considering accurate gradient near the wall. They were able to simulate a deformable boundary using this technique.

2.4.3. Multiphase flow

Monaghan and Kocharyan (1995) provided multiphase simulation of gas and dust using SPH. This may occur during a volcanic eruption. From then onwards, the effectiveness of the SPH methods in simulating multiphase flow has been shown by many authors, in particular, modelling the interface between two media.

- Hu and Adams (2007) provided multiphase simulation using a projection based ISPH method.
- Das and Das (2009) showed the evolution of a bubble originating from a submerged orifice.
- Grenier et al. (2009) proposed an Hamiltonian SPH method to simulate gravity current between two fluids with density ratio up to $O(10)$.
- Repalle et al. (2011) showed comparison between Level- Set and SPH simulations for a bubble evolution problem.
- Monaghan and Rafiee (2013) gave an accurate, easy to use and efficient SPH scheme for simulating multiphase problems.
- Grenier et al. (2013) provided simulation of bubbly flows with multiple bubbles. The evolution and interaction were discussed.
- Zainali et al. (2013) conducted numerous multiphase simulations with ISPH method.

2.4.4. Viscous term

Both artificial viscosity and physical viscosity in Navier Stokes equation cause dissipation of energy. Now, how far the dissipation caused by the artificial viscosity is close to the physical is a matter of research. Yet, while solving fluid flow problems where the viscosity plays a significant role, a number of approximate forms were proposed for the viscous part.

- Cummins and Rudman (1999) used a form in which Laplacian of the velocity was approximated retaining first order derivative of kernel. Similar form was adopted in Lo and Shao (2002) for ISPH model.
- Morris et al. (1997) employed a new viscous form for studying flow around cylinder in 2D for low Re.
- Cleary (1998) proposed another form for heat conduction problem in which an empirical coefficient is required for calibration. Delorme et al. (2009) adopted this form simulating sloshing problem.
- Takeda et al. (1994) used a different form for the viscous part.
- Macia et al. (2012) compared the effectiveness of different viscous forms.

Detail theoretical aspects and the discussions of energy dissipation associated with viscous terms used in SPH or in general in the Lagrangian models and Navier- Stokes equation can be found in Violeau (2009). Here it was found that in order to develop a proper viscous term, the chosen kernel function shall follow some conditions. Using viscous from of Monaghan and Gingold (1983), Colagrossi et al. (2013) found that, by prescribing proper number of neighbouring particles, it is possible to describe energy dissipation with sufficient accuracy comparable to an analytical decay for gravity waves.

2.5. OTHER PARTICLE BASED METHODS

Similar to the case in solid mechanics, few new methods or methods that are proposed in solid mechanics, have been finding their places along with SPH in solving fluid flow problems. Some of the most important techniques are:

- **Moving Particle Semi Implicit (MPS) method**: Originally proposed by Koshizuka and Oka (1996), this technique has been proven to be a robust numerical method for free surface flow related problems, similar to SPH. The

development of this method has been achieved through the series of work by Khayyer and Gotoh (Khayyer and Gotoh, 2009a, 2011, 2013). Other salient study include Shakibaeinia and Zin (2010), Lee et al. (2010, 2011), Kim et al. (2011) and Zhang and Wan (2012). A systematic convergence analysis of the MPS method has recently been carried out by Souto Iglesias et al. (2013).

- **Meshless Local Petrov Galerkin (MLPG) method**: Ma (2005a) extended this technique for non linear water wave problems. Further improvements have been achieved by fast gradient estimation in MLPG_R (Ma, 2005b), accurate detection of free surface particles (Ma and Zhou, 2009), wave breaking in 3D problems (Zhou and Ma, 2010), Improved MLPG_R to deal with wave interaction with a flexible elastic stricture (Sriram and Ma, 2012) and Hybrid coupling with FNPT based FEM solver (Sriram et al., 2012).
- **Particle Finite Element Method (PFEM) (Onate et al., 1996):** This method has proven to be effective in Hydroelastic problem (Idelsohn et al., 2008), wave interactions with submerged movable bodies (Onate et al., 2006), breaking waves (Idelsohn et al., 2004) and landing of capsule in water (Ryzhakov et al., 2013).
- **Finite Volume Particle Method (FVPM):** Hietel et al. (2000) and Nestor et al. (2009) have succeeded the application of FVPM for benchmark problems. This method has recently been applied for free surface flow problem by Guo et al. (2012).
- **Constraint Particle Method (CPM):** Koh et al. (2012) proposed this technique for solving free surface flow problems. Later, Koh et al. (2013) used this technique to study the effect of floating baffle on sloshing.

Other important applications of SPH in various fields of science and engineering include Geophysics (Tartakovsky et al., 2007; Vacondio et al., 2013), flow of Non Newtonian fluids (Ellero and Tanner, 2005), microfluidics (Weib et al., 2013) and so on.

2.6. MOTIVATION

Based on the survey as discussed above, it is apparent that with the works on SPH in recent years, there is a great potential to develop an accurate, robust and multipurpose

numerical model based on SPH for simulating a variety of problems in non linear water waves. With the availability of proper boundary modeling techniques, it is plausible that qualitatively correct results would be obtained for violent wave structure interaction problems. Sophisticated techniques for controlling pressure fluctuation would ensure reliable solution for pressure from simulation for violent cases which might be difficult to achieve through a grid based solver. But the applications of SPH models for non violent water waves are rather scanty where traditional grid based methods (like FDM and FEM) have been proven to be highly accurate and efficient. On the other hand, grid based solvers are known to posses difficulties in simulating violent breaking waves. This has motivated the initiation of the study which aims at filling this long lasting void by considering the following two aspects: a) Perform simulation of non violent water waves to validate and quantify the error with respect to a reference solution obtained from an analytical model or grid based solver and, b) Follow the exercises on violent waves with the same model to test how far qualitatively accurate solutions can be obtained.

In order to achieve that goal, one has to face a number of questions as follows:

- What formulation has to be adopted for the pressure gradient? Whether it is ISPH, or WCSPH or their improved versions.
- What technique should be implemented for modeling boundary? Can it be achieved by combing several approaches? What is the technique through which the model would be able to cope up with any kind of boundary shape prescribed by the user like in commercial CFD software?
- Whether SPH is intrinsically inapplicable for studying non violent cases where one can go for exact quantification of errors by validation, or is it possible to do that? If so, how far the model differs from the basic techniques and what aspects?
- What are the parameters that need calibration for achieving an acceptable solution? How to make an optimum choice of these values?
- Whether a version of the developed model can be equally applicable for both violent and non violent cases or not? Or, it can be done by some change in some input parameters in the same model assuring easy adoption for general purpose use?

2.7. OBJECTIVE AND SCOPE

The salient objective of the present study is thus development of a robust SPH based numerical solver for non linear water waves.

The scope of the study is framed to address the challenges in the model development.

- To tune parameters that control the numerical stability of SPH.
- To implement proper boundary conditions for both fixed and moving surfaces.
- To explore techniques to enhance the computational efficiency of the model.
- To develop improved versions of SPH for specific problems depending on the flow conditions.
- Testing wide range of applications such as sloshing, wave impact and wave overtopping.

Naturally, the research leading to answering those questions may possibly lead to the following contributions: a) For SPH, a number of improvements may be obtained in terms of numerical stability, boundary conditions and time integrators, and, b) A unique numerical model can be casted which will be able to simulate both violent and non violent water waves literally without any constraints. It is the subject matter of the following subsequent chapters which attempt to serve the above research scopes.

CHAPTER 3

THE NUMERICAL MODEL

3.1. GENERAL

This chapter presents the governing equations and the numerical tools required to transform the Partial Differential Equation (PDE) form to Ordinary Differential Equation (ODE) form. This facilitates to design a suitable scheme which can be marched in time domain with an aim to reproduce a dynamical system. The mass and momentum conservation (i.e. continuity and Navier- Stokes equations) equations are described. It is followed by the approximation of these equations in SPH based on the theory of integral interpolations. The success of such an interpolation depends on the chosen kernel or weighting function and its' properties. Therefore, few popular kernel functions are briefly highlighted. Three major differential operators namely: gradient, divergence and Laplacian of a given function are derived using the kernel function. It leads to the formation of the ODEs to be solved in SPH. Finally, an attempt is made to discuss issues related with errors brought into the system due to such a transformation.

3.2. MATHEMATICAL FORMULATION

Fig. 3.1 depicts adopted governing equations and the associated boundary conditions for the unknown variables (namely, pressure p and velocity $\boldsymbol{v}$) to be solved in the domain (D_m) with the boundary Γ ($\Gamma = \Gamma_s \cup \Gamma_f$). Here A_d and Q are appropriate differential operators and a_s and q are the external forces or sources acting over the domain (D_m) and along the boundary Γ respectively. U_{ext} and p_e are the prescribed value of velocity and pressure respectively along Γ. In the present study only one phase (i.e., water) is considered. Hence, p_e is set as 0. The entire domain (D_m) along boundary (Γ) is discretized with particles with known initial quantities including that of unknowns that are to be solved in time. Assuming a strong form formulation, the unknown variables are represented in terms of the variables calculated through a kernel function from a finite

domain for a particle *i*. Then these smoothed variables are substituted in the actual governing equations. The detail procedure of these methodologies is provided in the following sections.

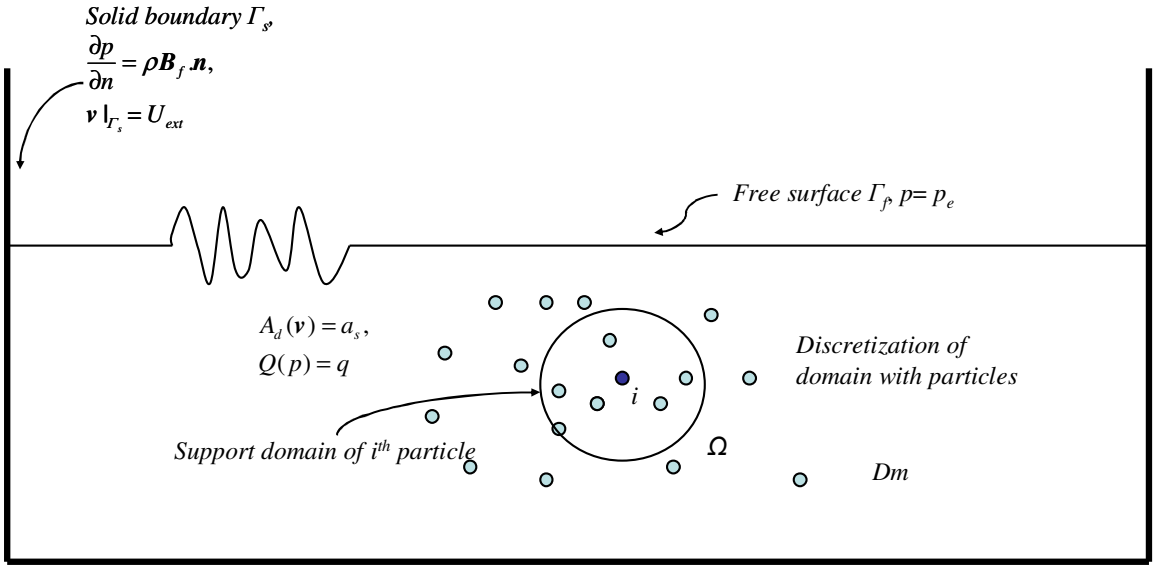

Fig. 3.1. Mathematical formulation of the problem in the given domain.

3.3. GOVERNING EQUATIONS

At macroscopic level, the flow of a Newtonian fluid can be described with sufficient accuracy by considering the following well known continuity and Navier- Stokes equations.

$$\frac{D\rho}{Dt} + \rho\left(\nabla . \boldsymbol{v}\right) = 0 \tag{3.1}$$

$$\frac{D\boldsymbol{v}}{Dt} = -\frac{1}{\rho}\nabla p + \nu\nabla^2\boldsymbol{v} + B_f \tag{3.2}$$

Here, ρ, ν ($=\mu/\rho$), p and $\boldsymbol{v}$ represent fluid density, kinematic viscosity, pressure and velocity respectively. B_f is a body force term. For the fluid flow problems considered in the present study B_f is $\boldsymbol{g}$ (0, -9.8), the acceleration due to gravity. In SPH, a point or a fluid portion is followed in time. Therefore the governing equations are expressed in a Lagrangian frame. Hence, these equations are in non conservative form (Anderson,

1995). If the assumption of incompressible fluid is made, Eqn. (3.1) gives divergence free velocity field. Depending on the Reynolds number (Re) of the flow, there is a mode of dominance in between pressure gradient (∇p) and viscous nature ($\nu\nabla^2\boldsymbol{v}$) in Eqn. (3.2). SPH transforms these equations into an equivalent strong form formulation, where the approximation for a primitive field variable (like ρ) is directly substituted into the governing equation, instead of invoking the minimization of the difference between a predicted variable and its exact value, as generally done in Finite Element Method (FEM) with weak or Galerkin based formulation. The details of the SPH approximation of a field variable and its subsequent higher order derivatives (say, Laplacian) based on the theory of integral interpolation are provided in the next section.

3.4. APPROXIMATION OF A FIELD FUNCTION

While dealing with observables, physicist Paul Adrien Maurice Dirac anticipated the necessity to use a weighting function which would help to yield a better behaviour in the vicinity of an improper function (Dirac, 1930). With this purpose, he wrote:

> "*..the process of multiplying a function of x with δ(x-a) and integrating over all x is equivalent to the process of substituting a for x.*"

$$\int_{-\infty}^{\infty} f(x)\,\delta(x-a)\,dx = f(a) \tag{3.3}$$

This weighting function $\delta(x\text{-}a)$ is named as 'delta (δ)- function'. Latter, it became known as Dirac- delta function. It holds the following two properties:

$$\delta(x-a) = \begin{cases} 1 & x = a \\ 0 & x \neq a \end{cases} \tag{3.4}$$

The Dirac- delta function has been extensively used in various fields (e.g., signal processing). In a particle based numerical method like SPH, it gives a way to construct a field variable and its derivatives at a given point from the knowledge of its surrounding neighbours. Those neighbours which take part in interpolating a property at this given point and their discrete contribution in this process are controlled by the Dirac delta

function. While working with interpolating points movable in space, it is necessary to construct a function which shall approximate a Dirac delta function. Such a function in SPH is interpreted as kernel function, $W(x)$. Theoretically, the neighbours should be selected from an infinite domain. However, it is possible to design the kernel function in such a way that, it tends to zero as the distance increases in between the point and its neighbour. Therefore, in SPH, a function at a point 'a' is approximated as:

$$\left\langle f(a)\right\rangle = \int_{\Omega} f(x) W(x-a)\, dx \tag{3.5}$$

where, the summation is taken over a number of neighbouring points selected from the sub- domain, Ω (area in two- dimension (2D); volume in three- dimension (3D)) which is called a support domain. Now let us assume that the entire domain is represented by particles with known coordinates and masses. Then the integral in Eqn. (3.5) can be substituted by a summation taken over Ω:

$$f(x_i) = \sum_{j=1}^{N} f(x_j) W(x_j - x_i)\, dV_j = \sum_{j=1}^{N} f(x_j) W(x_j - x_i) \frac{m_j}{\rho_j} \tag{3.6}$$

where, dV_j, m_j and ρ_j are the volume, mass and density of the j^{th} particle respectively. There are N number of neighbours in Ω for i^{th} particle. The use of kernel function in SPH makes possible to express a field variable and its derivatives without a grid or mesh. The idea of this integral interpolation is depicted in Fig. 3.2. Generally, the support domain (Ω) is defined by a circle (in 2D) with a radius kh. k is a scale factor and h is called smoothing length.

3.4.1. Approximation of Gradient

In SPH, the gradient of a function using kernel function is given by:

$$\nabla f(x_i) \approx \int_{\Omega} \left[\nabla f(x_j)\right] W(x_j - x_i)\, dx_j \tag{3.7}$$

which is obtained by simply substituting $f(x)$ in Eqn. (3.5) by $\nabla f(x_j)$. We have,

$$\left[\nabla f(x_j)\right] W(x_j - x_i) = \nabla\left[f(x_j) W(x_j - x_i)\right] - f(x_j)\left[\nabla W(x_j - x_i)\right] \tag{3.8}$$

substituting Eqn. (1.8) into Eqn. (1.7), we get,

$$\nabla f(x_i) = \int_{\Omega} \nabla\left[f(x_j) W(x_j - x_i)\right] dx_j - \int_{\Omega} f(x_j)\left[\nabla W(x_j - x_i)\right] dx_j \tag{3.9}$$

The first term in Eqn. (3.9) can be converted into an integral over the boundary of Ω (i.e., Γ) by using Gauss divergence theorem. Hence,

$$\nabla f\left(x_i\right)=\int_{\Gamma}\left[f\left(x_j\right)W\left(x_j-x_i\right)\right].\boldsymbol{n}ds_j-\int_{\Omega}f\left(x_j\right)\left[\nabla W\left(x_j-x_i\right)\right]dx_j \tag{3.10}$$

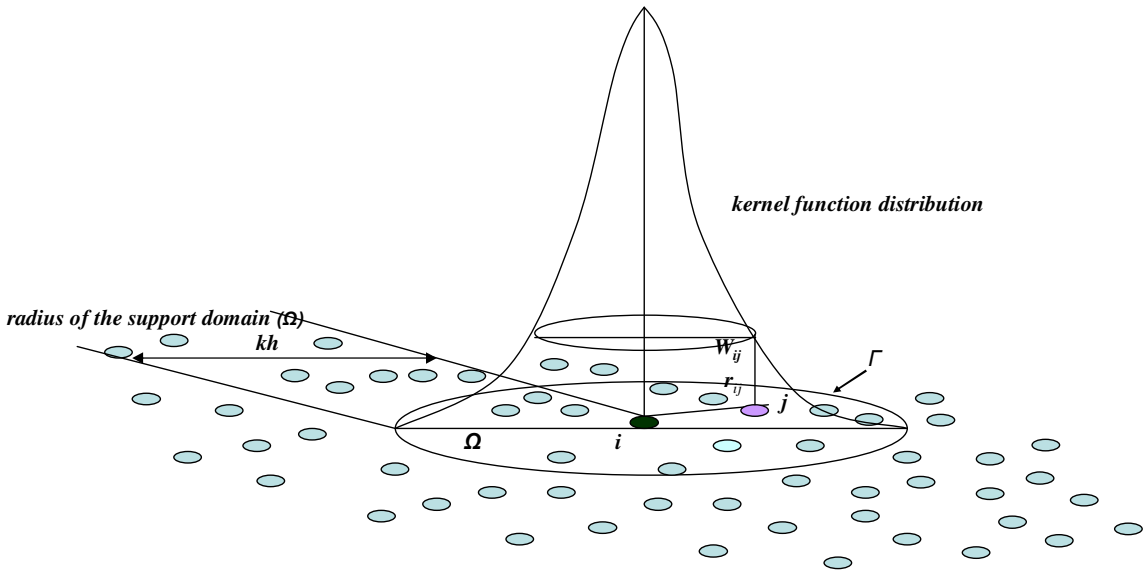

Fig. 3.2. Idea of integral interpolation for representing a function in SPH using kernel function.

For a particle inside the domain with full compact support, the first term in Eqn. (3.10) can be neglected. But, near the edge of the domain (like free surface) it has sufficient contribution. Calculating boundary surface integral in SPH requires identification of particles along the edge and then calculation of associated normals. This makes the computation more complex (Colagrossi et al., 2009). Therefore, most of the SPH models avoid this task. However, recently, some researchers have made significant progress in enforcing necessary boundary conditions through a semi analytic approach (Mayrhofer et al., 2013). In their model, the calculation of surface integral is included. There are other ways through which it can be satisfied in a less rigorous way (Details in Chapter 4). This chapter adopts the standard form for gradient of a function. Following Eqn. (3.10),

$$\nabla f\left(x_i\right)=\int_{\Omega}f\left(x_j\right)\left[\nabla W\left(x_j-x_i\right)\right]dx_j \tag{3.11}$$

Here, the gradient of the kernel is calculated at i^{th} particle with respect to the position of the j^{th} particle. Details of the approximation of a field variable and its subsequent higher order derivatives in SPH can be found in the book by Liu and Liu (2003).

3.5. TRANSFORMATION OF THE GOVERNING EQUATIONS

This section presents the derivation of the ODEs from the governing equations using the principles of SPH approximations as discussed above. Initially, the momentum equation (Eqn. 3.2) is considered. It consists of several differential operators. The techniques used to model those operators is then utilized to deal with the continuity equation (Eqn. (3.1)). Now, the momentum equation is described term by term.

3.5.1. Pressure gradient

Using the expression of representing the gradient of a function using kernel function (Eqn. 3.11), the pressure gradient in SPH may be written as:

$$\nabla p_i = \sum_{j=1}^{N} p_j \nabla W_{ij} dV_j = \sum_{j=1}^{N} p_j \nabla W_{ij} \frac{m_j}{\rho_j} = \sum_{j=1}^{N} \frac{p_j m_j}{\rho_j} \nabla W_{ij} \tag{3.12}$$

where, ∇W_{ij} is the gradient of kernel calculated at i^{th} particle with respect to the position of the j^{th} particle. Therefore, the rate of change of velocity of i^{th} particle due to pressure gradient with respect to the j^{th} particle is $\frac{p_j m_j}{\rho_i \rho_j} \nabla W_{ij}$ which is not necessarily equal to $\frac{p_i m_i}{\rho_j \rho_i} \nabla W_{ji}$, the rate of change of velocity of j^{th} particle due to i^{th} particle, because, $\nabla W_{ji} = -\nabla W_{ij}$ and $p_i \neq p_j$. Hence, the direct approximation of pressure gradient using SPH kernel function does not conserve linear momentum. Non conservation of momentum may have serious stability issues for the numerical model and may yield unphysical pressure distribution. For this reason, Monaghan (1992) adopted a technique that includes density within the pressure gradient. Hence,

$$\begin{aligned} &\nabla\left(\frac{p}{\rho}\right) = \frac{1}{\rho}\nabla p + p\nabla\left(\frac{1}{\rho}\right) = \frac{1}{\rho}\nabla p + p\frac{\partial}{\partial\rho}\left(\frac{1}{\rho}\right)\nabla\rho = \frac{1}{\rho}\nabla p - \frac{p}{\rho^2}\nabla\rho \\ &or,\ \frac{1}{\rho}\nabla p = \nabla\left(\frac{p}{\rho}\right) + \frac{p}{\rho^2}\nabla\rho \end{aligned} \tag{3.13}$$

Now, the rate of change of velocity at i^{th} particle due to j^{th} particle considering pressure gradient alone is: $\frac{p_j}{\rho_j}\nabla W_{ij}\frac{m_j}{\rho_j}+\frac{p_i}{\rho_i^2}\rho_j\nabla W_{ij}\frac{m_j}{\rho_j}=m_j\left(\frac{p_i}{\rho_i^2}+\frac{p_j}{\rho_j^2}\right)\nabla W_{ij}$, which is purely symmetric in form. Therefore considering all the neighbours:

$$\left(\frac{\nabla p}{\rho}\right)_i=\sum_{j=1}^{N}m_j\left(\frac{p_i}{\rho_i^2}+\frac{p_j}{\rho_j^2}\right)\nabla W_{ij} \tag{3.14}$$

This form conserves linear momentum. Apart from the gradient of the kernel, all the other variables are scalar in above equation. Hence, the direction of pressure gradient is same as that of kernel gradient. The resulting force due to pressure gradient is collinear with that of position vector of i^{th} particle with respect to the j^{th}. Therefore, Eqn. (3.14) also conserves angular momentum (see e.g., Khayyer, 2008). Most of the SPH models use this form.

It is equally important to note that there are numerous ways available to derive an approximate SPH form for pressure gradient conserving linear and angular momentum. For example, Eqn. (3.14) can also be derived by writing a Lagrangian for a particle and then following the steps to get the equation of motions (see e.g., Rafiee, 2011). First law of Thermodynamics has to be considered in that case (mathematically, which has same effect as considering the density inside the gradient operator). Although Eqn. (3.14) is symmetric, most of the used standard kernel functions are not even first order consistent (i.e., they may not always able to give zero while taking gradient of a constant). That can be corrected by employing a Moving Least Square (MLS) kernel function. In such case, direct form of pressure gradient (i.e., Eqn. (3.12)) has to be considered. A Hamiltonian form may be preferred if the SPH model is expected to simulate a multiphase flow (see e.g., Grenier et al., 2009).

3.5.2. Viscous stress

Calculation of viscous term in Navier- Stokes equation (Eqn. 3.2) requires estimation of the Laplacian of velocity. Applying the SPH rule similar to pressure gradient to express velocity gradient would lead to a form involving second order derivatives on kernel function. Higher order derivatives of kernel are more susceptible to error due to particle distribution than lower order derivatives. For this reason, it is customary to use a hybrid with an equivalent Finite Difference form where first derivative of kernel function can be

retained to represent the Laplacian operator (Brookshaw, 1985; Morris et al., 1997; Cummins and Rudman, 1999). Let the gradient of $\frac{\nabla \boldsymbol{v}}{\rho}$ be expressed as:

$$\nabla\left(\frac{\nabla \boldsymbol{v}}{\rho}\right)=\frac{d}{dx}\left(\frac{1}{\rho}\right)\frac{d\boldsymbol{v}}{dx}+\frac{1}{\rho}\frac{d^2\boldsymbol{v}}{dx^2}=\frac{dV_s}{dx}\frac{d\boldsymbol{v}}{dx}+V_s\frac{d^2\boldsymbol{v}}{dx^2} \tag{3.15}$$

where, $V_s = 1/\rho$, specific volume. Eqn. (3.15) has been abbreviated in one dimension for the sake of simplicity in derivation. Taking a Taylor series expansion around particle i towards j^{th} particle to express V_s and $\boldsymbol{v}$ yields:

$$V_{sj}=V_{si}+\left(x_j-x_i\right)\frac{dV_s}{dx}+\frac{\left(x_j-x_i\right)^2}{2}\frac{d^2V_s}{dx^2}+\ldots \tag{3.16}$$

$$\boldsymbol{v}_j=\boldsymbol{v}_i+\left(x_j-x_i\right)\frac{d\boldsymbol{v}}{dx}+\frac{\left(x_j-x_i\right)^2}{2}\frac{d^2\boldsymbol{v}}{dx^2}+\ldots \tag{3.17}$$

Ignoring higher order derivatives and combining Eqns. (3.16) and (3.17),

$$\frac{dV_s}{dx}\frac{d\boldsymbol{v}}{dx}=\frac{\left(V_{sj}-V_{si}\right)\left(\boldsymbol{v}_j-\boldsymbol{v}_i\right)}{\left(x_j-x_i\right)^2} \tag{3.18}$$

Now, using Eqn. (3.16) and Eqn. (3.18), the first term in the right hand side of Eqn. (3.15) is expressed as:

$$\frac{dV_s}{dx}\frac{d\boldsymbol{v}}{dx}=\int\frac{V_{sj}-V_{si}}{x_j-x_i}\left(\boldsymbol{v}_j-\boldsymbol{v}_i\right)\frac{\partial W}{\partial x_j}dx_j \tag{3.19}$$

From Eqn. (3.17),

$$\frac{\boldsymbol{v}_j-\boldsymbol{v}_i}{x_j-x_i}=\frac{d\boldsymbol{v}_j}{dx_j}+\frac{x_j-x_i}{2}\frac{d^2\boldsymbol{v}_j}{dx_j^2} \tag{3.20}$$

Multiplying both sides with kernel gradient and integrating over the support domain:

$$\int\frac{\boldsymbol{v}_j-\boldsymbol{v}_i}{x_j-x_i}\frac{\partial W}{\partial x_j}dx_j=\int\frac{d\boldsymbol{v}_j}{dx_j}\frac{\partial W}{\partial x_j}dx_j+\int\frac{x_j-x_i}{2}\frac{d^2\boldsymbol{v}_j}{dx_j^2}\frac{\partial W}{\partial x_j}dx_j \tag{3.21}$$

Due to the property of the chosen kernel function,

$$\int\frac{d\boldsymbol{v}_j}{dx_j}\frac{\partial W}{\partial x_j}dx_j=\frac{d^2\boldsymbol{v}_j}{dx_j^2} \tag{3.22}$$

$$\int W\frac{\partial}{\partial x_j}\left(x_j-x_i\right)dx_j = W\int\frac{\partial}{\partial x_j}\left(x_j-x_i\right)dx_j-\int\frac{\partial W}{\partial x_j}\left(x_j-x_i\right)dx_j$$
$$or,\ W\int\frac{\partial}{\partial x_j}\left(x_j-x_i\right)dx_j = W\left(x_j-x_i\right)=\int W\frac{\partial}{\partial x_j}\left(x_j-x_i\right)dx_j+\int\frac{\partial W}{\partial x_j}\left(x_j-x_i\right)dx_j \tag{3.23}$$

The first line in Eqn (3.23) is obtained by integrating by parts. Since, $\int\left(x_j-x_i\right)Wdx_j=0$,

$$\int W\frac{\partial}{\partial x_j}\left(x_j-x_i\right)dx_j=-\int\frac{\partial W}{\partial x_j}\left(x_j-x_i\right)dx_j \tag{3.24}$$

Hence,

$$\int\frac{x_j-x_i}{2}\frac{d^2\boldsymbol{v}_j}{dx_j^2}\frac{\partial W}{\partial x_j}dx_j=-\frac{1}{2}\int\frac{d^2\boldsymbol{v}_j}{dx_j^2}W\left(x_j-x_i\right)dx_j=-\frac{1}{2}\frac{d^2\boldsymbol{v}_j}{dx_j^2} \tag{3.25}$$

Substituting, Eqn. (3.25) and Eqn. (3.22) into Eqn. (3.21),

$$\frac{d^2\boldsymbol{v}_j}{dx_j^2}=2\int\frac{\boldsymbol{v}_j-\boldsymbol{v}_i}{x_j-x_i}\frac{\partial W}{\partial x_j}dx_j \tag{3.26}$$

Substituting Eqn. (3.26) and Eqn. (3.19) into Eqn. (3.15), the representation of Laplacian operator working on velocity in one dimension is given as:

$$\nabla\left(\frac{\nabla\boldsymbol{v}}{\rho}\right)=\frac{dV_s}{dx}\frac{d\boldsymbol{v}}{dx}+V_s\frac{d^2\boldsymbol{v}}{dx^2}=\int\frac{V_{sj}-V_{si}}{x_j-x_i}\left(\boldsymbol{v}_j-\boldsymbol{v}_i\right)\frac{\partial W}{\partial x_j}dx_j+2V_{si}\int\frac{\boldsymbol{v}_j-\boldsymbol{v}_i}{x_j-x_i}\frac{\partial W}{\partial x_j}dx_j$$
$$=\int\frac{V_{sj}+V_{si}}{x_j-x_i}\left(\boldsymbol{v}_j-\boldsymbol{v}_i\right)\frac{\partial W}{\partial x_j}dx_j \tag{3.27}$$

Generalizing for 2D and representing the above integral as summation over neighbouring particles, the viscous part of Eqn. (3.2) can be represented as:

$$\mu\nabla\left(\frac{\nabla\boldsymbol{v}}{\rho}\right)_i=\sum_{j=1}^{N}\frac{4m_j\left(\mu_i+\mu_j\right)}{\left(\rho_i+\rho_j\right)^2}\frac{\boldsymbol{r}_{ij}.\nabla W_{ij}}{\left(\left|\boldsymbol{r}_{ij}\right|^2+\zeta^2\right)}\left(\boldsymbol{v}_i-\boldsymbol{v}_j\right) \tag{3.28}$$

where, $\boldsymbol{r}_{ij}=\boldsymbol{r}_i-\boldsymbol{r}_j$, ζ is a small number $O(0.1h^2)$ to maintain stability when $\boldsymbol{r}_{ij}\rightarrow 0$ while two particles come too close. This particular form conserves linear momentum, yet conservation of angular momentum is not guarantied (see e.g., Khayyer, 2008). Originally developed in Morris et al. (1997), in this formula, significance of such errors can be problem dependent for low or moderate Reynolds numbers (as observed in Colagrossi et al., 2009). To ensure conservation of angular momentum, one needs to employ a further correction on kernel gradient (Bonet and Lok, 1999). However, for

the fluid media considered (i.e., water), coefficient of kinematic viscosity is noticeably low ($O(10^{-6})$). So, non conservation of angular momentum due to viscous stress part with standard kernel gradient may not have significant influence in numerical simulation, unless one artificially increases the viscosity coefficient. In this case, there is a risk of varying the Re of flow with different flow physics.

Hence, considering the pressure gradient and viscous stress parts approximations in SPH using Eqn. (3.14) and Eqn. (3.28), respectively, Eqn. (3.2) can be written as:

$$\left(\frac{d\boldsymbol{v}}{dt}\right)_i = -\sum_{j=1}^{N} m_j \left(\frac{p_i}{\rho_i^{\,2}} + \frac{p_j}{\rho_j^{\,2}}\right) \nabla_i W_{ij} + \sum_{j=1}^{N} \frac{4m_j\left(\mu_i + \mu_j\right)}{\left(\rho_i + \rho_j\right)^2} \frac{\boldsymbol{r}_{ij}.\nabla W_{ij}}{\left(\left|\boldsymbol{r}_{ij}\right|^2 + \zeta^2\right)} \left(\boldsymbol{v}_i - \boldsymbol{v}_j\right) + \boldsymbol{g} \tag{3.29}$$

This is an ODE. It can solved in time based on an appropriate time integrator (like, fourth order Runge- Kutta Method (RK4)). The key task is to calculate pressure discretely at individual particles (p_i). In the SPH context, there are two distinct approaches to carry out this, viz. weakly compressible and incompressible. The choice of a particular approach controls the selection of a time integrator. Both approaches have been considered in the present study. The details of these two approaches are given in the following sections.

3.6. WEAKLY COMPRESSIBLE SPH (WCSPH)

SPH was formulated to simulate gas dynamics problems in Astrophysics. It was found to be convenient to calculate pressure through an equation of state for a compressible fluid. While it was applied to simulate wave motion, Monaghan (1994) considered the same approach for calculating pressure and proposed to treat water as slightly compressible. The resulting scheme was fully explicit and this idea brought remarkable ease for modelling free surface flow problems. The following equation of state (Batchelor, 1974) was adopted.

$$p_i = \frac{\rho_o c_s^2}{\gamma}\left[\left(\frac{\rho_i}{\rho_o}\right)^{\gamma} - 1\right] \tag{3.30}$$

Here, γ is an adiabatic factor and taken as 7 for water. ρ_0 is the reference density for water (1000kg/m^3). ρ_i is the density of the i^{th} particle. The primary purpose of this equation was to describe propagation of sound waves in water. To adopt a practical time

step during simulation, it is necessary to impose a restriction on sound speed, c_s (Monaghan, 1994).

$$\delta\rho = \frac{|\rho - \rho_0|}{\rho_0} = \frac{{v_b}^2}{{c_s}^2} = M^2 \tag{3.31}$$

i.e., change in variation of density is proportional to square of Mach (M) number. By choosing c_s as ten times of fluid bulk velocity (v_b), it is postulated that the density variation due to compressibility assumption for water is O(0.01% to 0.1%). So, the sound speed (c_s) in water is no longer representing an actual sound wave; but, it is acting like a sort of 'numerical sound speed' and contributes in the overall stability (i.e., time step) of the numerical model.

However, to maintain numerical stability further, several other additional tools are required to be employed in the context of WCSPH. The details are further discussed below.

3.6.1. Artificial viscosity

WCSPH has problems with shocks. Generally, it takes place when two particles with two different energy states (defined by their densities) interact with each other. It was specified by Monaghan and Gingold (1983) to simulate shocks in Astrophysics problems. A separate term (Π) is added with the pressure gradient part in Eqn. (3.29).

$$\begin{cases} \Pi_{ij} = \begin{cases} \dfrac{-\alpha' \overline{c}_{ij} \xi_{ij} + \beta {\xi_{ij}}^2}{\overline{\rho}_{ij}}, & \boldsymbol{v}_{ij}.\boldsymbol{r}_{ij} \le 0 \\ 0, & \boldsymbol{v}_{ij}.\boldsymbol{r}_{ij} > 0 \end{cases} \\ \xi_{ij} = \dfrac{h \boldsymbol{v}_{ij}.\boldsymbol{r}_{ij}}{|\boldsymbol{r}_{ij}|^2 + \kappa^2}, \overline{c}_{ij} = (c_i + c_j)/2, \overline{\rho}_{ij} = (\rho_i + \rho_j)/2 \end{cases} \tag{3.32}$$

where α' and β are empirical coefficients chosen in the range from 0.0 to 0.1. c_i and c_j are the numerical sound speed associated with i^{th} and j^{th} particles. κ= 0.01h. Although it brings some improvements, it is known to cause spurious dissipation. This dissipation can be controlled in water wave simulation by choosing a sufficient number of particles or resolution (Antuono et al., 2011). A better approach may be Godunov scheme adopting Riemann solver (Inutsuka, 2002; Parshikov et al., 2000; Rafiee et al., 2012) or SPH- ALE formulation (Koukouvinis et al., 2013). However, the above schemes are computationally expensive.

3.6.2. Tension instability

Tension instability is a general problem in particle methods where the behaviour of particles becomes unrealistic with the change of internal stress states. The direct consequence of tension instability is particle clustering and breakdown of simulation. Many researchers (Swegle et al., 1995; Monaghan, 2000; Bonet and Kulasegaram, 2001; Khayyer and Gotoh, 2011) have extensively studied tension instability in SPH/MPS and proposed different measures. In the present study, XSPH technique (Monaghan, 1989) is adopted. Here, the particles are moved with a corrected velocity $(\boldsymbol{v}_i)_c$ which is obtained by averaging over its neighbourhood.

$$\left(\boldsymbol{v}_i\right)_c = \boldsymbol{v}_i + \varepsilon \sum_{j=1}^{N} \frac{m_j}{\overline{\rho}_{ij}} \boldsymbol{v}_{ji} W_{ij} \tag{3.33}$$

ε, known as XSPH factor, is a parameter in the range of 0- 0.5. However, for simulating blast waves, higher values may be used (Liu and Liu, 2003). The XSPH technique may not avoid tension instability fully, yet, it gives scope to maintain stability during simulation in an easy manner.

3.6.3. Pressure calculations

To calculate pressure from Eqn. (3.30), one needs density before hand. In WCSPH, density at a particle can be calculated in two different ways, i.e., either by taking a direct summation over the neighbouring particles,

$$\rho_i = \sum_{j=1}^{N} \rho_j W_{ij} dV_j = \sum_{j=1}^{N} \rho_j W_{ij} \frac{m_j}{\rho_j} = \sum_{j=1}^{N} m_j W_{ij} \tag{3.34}$$

or, from the continuity Eqn. (3.1),

$$\left(\frac{d\rho}{dt}\right)_i = \sum_{j=1}^{N} m_j \boldsymbol{v}_{ij} . \boldsymbol{\nabla}_i W_{ij} \tag{3.35}$$

Both of the above techniques have advantages and disadvantages. The summation density approach (Eqn. 3.34) is more susceptible to error compared to continuity density approach (Eqn. 3.35) near the boundary of the domain. That can be corrected by applying a Shepard or MLS (Moving Least Square) correction in Eqn. (3.34). For the free surface flow problems, Eqn. (3.35) is generally preferred.

Looking closely on Eqn. (3.30), it can be understood that it is very stiff in nature. That is, a slight change in density (0.01%- 0.1%) from its desired value may have large

variation in pressure. So, predicted pressure may be fluctuating unrealistically. This is a more serious drawback, if one needs to simulate problems requiring to run for long physical time, i.e., *O*(20- 50s). In this case, instability in pressure may affect the simulation. For this reason, Colagrossi and Landrini (2003) proposed to periodically filter the density at certain time steps by applying a MLS kernel function.

$$\left(\rho_i\right)^{new} = \sum_{j=1}^{N} m_j W_{ij}^{MLS} \tag{3.36}$$

where,

$$\left.\begin{aligned} W_{ij}^{MLS} &= \left[\beta_0\left(\boldsymbol{r}_{ij}\right) + \beta_{1x}\left(\boldsymbol{r}_j\right)\left(x_i - x_j\right) + \beta_{1z}\left(\boldsymbol{r}_j\right)\left(z_i - z_j\right)\right] W_{ij} \\ \beta\left(\boldsymbol{r}_j\right) &= \begin{bmatrix} \beta_0 \\ \beta_{1x} \\ \beta_{1z} \end{bmatrix} = A^{-1} \begin{bmatrix} 1 \\ 0 \\ 0 \end{bmatrix} \\ A &= \sum_{j=1}^{N} W_{ij} A^{*} \frac{m_j}{\rho_j} \\ A^{*} &= \begin{bmatrix} 1 & \left(x_i - x_j\right) & \left(z_i - z_j\right) \\ \left(x_i - x_j\right) & \left(x_i - x_j\right)^2 & \left(x_i - x_j\right)\left(z_i - z_j\right) \\ \left(z_i - z_j\right) & \left(x_i - x_j\right)\left(z_i - z_j\right) & \left(z_i - z_j\right)^2 \end{bmatrix} \end{aligned}\right\} \tag{3.37}$$

Due to inversion of matrix *A* for each particle, the computational cost marginally increases. But it was found to bring significant improvement in pressure distribution. Still, for longer time simulation, it was not that much effective. To enhance the stability for pressure, Molteni and Colagrossi (2009) proposed to add an additional diffusive term in the continuity Eqn. (3.35). This technique was further improved in Antuono et al. (2010) with a conservative and consistent diffusive term for the free surface flow problems.

$$\left(\frac{d\rho}{dt}\right)_i = \sum_{j=1}^{N} m_j \boldsymbol{v}_{ij} . \nabla_i W_{ij} + \underbrace{\delta h C_S \sum_{j=1}^{N} \boldsymbol{\psi}_{ij} . \nabla_i W_{ij} dV_j}_{Diffusive} \tag{3.38}$$

where, the diffusive term in the above equation is given by:

$$\left.\begin{aligned}
\boldsymbol{\psi}_{ij} &= 2(\rho_j - \rho_i)\frac{\boldsymbol{r}_{ij}}{\left|\boldsymbol{r}_{ij}\right|^2} - [\langle\nabla\rho\rangle_i^L + \langle\nabla\rho\rangle_j^L] \\
\langle\nabla\rho\rangle_i^L &= \sum_{j=1}^{N}\left(\rho_j - \rho_i\right)\boldsymbol{L}_i\nabla_i W_{ij}dV_j \\
\boldsymbol{L}_i &= \left[\sum_{j=1}^{N}\left(\boldsymbol{r}_j - \boldsymbol{r}_i\right)\otimes\nabla_i W_{ij}dV_j\right]^{-1}
\end{aligned}\right\} \tag{3.39}$$

With the addition of the diffusive term in the continuity equation approximation (Eqn. 3.38), the above mentioned scheme is referred as δ- SPH. δ is a dimensionless coefficient and takes a value in the range of 0- 0.2. In the present study, δ is taken as 0.1.

3.7. INCOMPRESSIBLE SPH (ISPH)

Another alternative for solving pressure in SPH is by adopting classical time marching procedure for numerically solving Navier- Stokes equation (Chorin, 1968). The required differential operator to solve Pressure- Poisson Equation (PPE) has been proposed by Cummins and Rudman (1999). The first application of this scheme for free surface flow was shown by Lo and Shao (2002). Various other techniques have been proposed to enforce incompressibility in SPH by many researchers (e.g., Hu and Adams, 2007; Lastiwaka et al., 2005; Ellero et al., 2007). The detailed procedure for solving pressure with an incompressible assumption and with a two step projection correction approach is as follows.

Step I. *Update particle positions without considering the pressure gradient terms.*

$$\begin{cases}
\Delta\boldsymbol{v}_* = \upsilon\nabla^2\boldsymbol{v}\Delta t + \boldsymbol{g}\Delta t \\
\boldsymbol{v}_* = \boldsymbol{v}_t + \Delta\boldsymbol{v}_* \\
\boldsymbol{r}_* = \boldsymbol{r}_t + \boldsymbol{v}_*\Delta t
\end{cases} \tag{3.40}$$

where '* ' represents an intermediate step between time step t and $t+\Delta t$. The velocity with which the particle positions need to be updated from time step t to $t+\Delta t$ is calculated as,

$$\begin{aligned}
&\boldsymbol{v}_{t+\Delta t} = \boldsymbol{v}_* + \Delta\boldsymbol{v}_{**} \\
&or,\ v_* = v_{t+\Delta t} - \Delta\boldsymbol{v}_{**}
\end{aligned} \tag{3.41}$$

where, $\boldsymbol{v}_*$ is calculated as shown in Eqn. (3.40). $\Delta\boldsymbol{v}_{**}$ is to be calculated based on pressure gradient part. That is,

$$\Delta \boldsymbol{v}_{**} = -\frac{1}{\rho_*}\nabla p_{t+\Delta t}\Delta t \tag{3.42}$$

Substituting $\Delta \boldsymbol{v}_{**}$ from Eqn. (3.42) to Eqn. (3.41) results in a Helmoltz- Hodge decomposition, where a vector is split up into a divergence free ($\boldsymbol{v}_{t+\Delta t}$) and gradient of a scalar ($\frac{1}{\rho_*}\nabla p_{t+\Delta t}\Delta t$) components. From the requirement of continuity Eqn. (3.1), one can write,

$$\frac{1}{\rho_0}\frac{\rho_0 - \rho_*}{\rho_0} + \nabla.(\Delta \boldsymbol{v}_{**}) = 0 \tag{3.43}$$

Substituting $\Delta \boldsymbol{v}_{**}$ from Eqn. (3.42) into Eqn. (3.43),

$$\nabla.\left(\frac{1}{\rho_*}\nabla p_{t+\Delta t}\right) = \frac{\rho_0 - \rho_*}{\rho_0 \Delta t^2} \tag{3.44}$$

Step II. *Solve PPE to obtain velocity correction based on pressure gradient*

By applying SPH approximation for a Laplacian operator as discussed in section 3.4.2.for viscous part and substituting the average density, $(\rho_i + \rho_j)/2$, the left hand side of Eqn. (3.44) is discretized as,

$$\nabla.\left(\frac{1}{\rho}\nabla p\right)_i = \sum_j m_j \frac{8}{\left(\rho_i + \rho_j\right)^2}\frac{p_{ij}\boldsymbol{r}_{ij}.\nabla \boldsymbol{W}_{ij}}{\left|\boldsymbol{r}_{ij}\right|^2 + \zeta^2} \tag{3.45}$$

where, $p_{ij} = p_i - p_j$. Applying Eqn. (3.45) into Eqn. (3.44), a simultaneous linear algebraic system of the equations of the form $\boldsymbol{AX}=\boldsymbol{B}$ of size $n \times n$, n being the total number of particles, can be obtained. The above PPE in the matrix form can be efficiently solved by using iterative based solver like Conjugate- Gradient (CG) method. Details of the solution of large matrices based on iteration based method like CG are provided in Appendix A. Once pressure is calculated from Eqn. (3.45), velocity correction is obtained from Eqn. (3.42). The final velocity for time step $t+\Delta t$ is obtained from Eqn. (3.41). Then, the particle coordinates are updated from time step t to $t+\Delta t$.

$$\boldsymbol{r}_{t+\Delta t} = \boldsymbol{r}_t + \frac{\boldsymbol{v}_t + \boldsymbol{v}_{t+\Delta t}}{2}\Delta t \tag{3.46}$$

Due to the absence of sound speed restriction in ISPH, a larger time step can be adopted compared to WCSPH. Although, solving PPE consumes additional CPU time, if higher order time integrators (like RK4) is adopted for WCSPH (as followed in the present study), the computational expenses of WCSPH and ISPH can be made to be almost similar order. This gives a chance to make the comparison between WCSPH and ISPH to be more direct compared to using same time integrator (like predictor corrector) in both WCSPH and ISPH.

3.8. BOUNDARY CONDITIONS

In order to have a unique solution for the governing equations, the numerical model shall contain some properly defined and adopted boundary conditions for the field variables (i.e., p and $\boldsymbol{v}$). For the problems pertaining to non linear wave structure interaction as considered in the present study, one might have: a) **Solid boundary**: free slip or no slip for velocity and Neumann boundary condition for pressure; b) **Free surface**: Drichilet boundary condition for pressure (It needs pressure is equal to atmospheric pressure or zero for a single phase model, as considered in the present study). Since, Re number is moderately high for the problems considered, the physical effects (like formation of boundary layer and associated energy dissipation near the solid boundary) due to the viscous part in momentum Eqn. (3.29) are less significant than pressure gradient part. The choice of free slip or no slip condition for velocity adjacent to the solid boundary is controlled by specific interest. In SPH method, reliable solution has been achieved by enforcing no slip while modelling Laplacian operator (i.e., the viscous part) and free slip for the divergence operator (for solving density in Eqn. 3.35 or Eqn. 3.38 and to solve pressure from Eqn. 3.30) while modelling solid boundary. This pressure is used for calculating pressure gradient (Marrone et al., 2013). Since, the current interest is focused on the pressure gradient, free slip boundary condition for velocity at the solid boundary has been used. It is given by,

$$\left.\begin{aligned} (\boldsymbol{v}_p)_t &= (\boldsymbol{v}_b)_t \\ \frac{\partial \boldsymbol{v}_p}{\partial n} &= 0 \end{aligned}\right\} \tag{3.47}$$

where, $\boldsymbol{v}_b$ and $\boldsymbol{v}_p$ are particle velocities at the boundary and at the neighbourhood of the boundary, respectively. Suffix 't' denotes velocity component along the tangent at the particle on the boundary. 'n' is the unit normal pointing outwards from the origin of $\boldsymbol{v}_b$. Following condition is imposed to satisfy Neumann boundary condition for pressure at the solid boundary.

$$\frac{\partial p}{\partial n} = 0 \tag{3.48}$$

This is a general condition when there are no body force components. Whereas, for surface gravity wave problems, the above condition is modified as $\frac{1}{\rho}\frac{\partial p}{\partial n} + \boldsymbol{g}\frac{\partial d}{\partial n} = 0$. This can be obtained from Bernouli's equation imposing free slip condition for the dynamic part. For solving PPE using ISPH, a Drichilet boundary condition, p=0 is applied on the particles located at the free surface. For doing this, particles at the free surface have to be captured. Enforcement of this condition in WCSPH is not straightforward due to its own explicit nature of decoupling between velocity and pressure.

Difficulty arises in enforcing these essential boundary conditions in SPH due to truncation of support domain of the kernel function near the solid boundary. In such cases, one can provide the full support domain by mirroring the fluid properties near the boundary on other side of the boundary. The resulting particles so created are known as 'Ghost particles' (Colagrossi and Landrini, 2003). With Ghost particles, it is possible to satisfy free slip and Neumann conditions properly. But if there is sharp change in the geometry of the boundary, complicacy arises. That can be overcome by using a fixed layer of particles called 'Dummy particles' (Koshizuka et al., 1998) around the solid boundary. However, in that case utmost care has to be undertaken to extrapolate fluid field properties (i.e., $\boldsymbol{v}$ and p) at Dummy particle location, for the proper enforcement of the essential boundary conditions (Eqns. 3.47 and 3.48). Details of these implementations have been provided in Chapter 4 which enhances the present model development.

3.9. KERNEL FUNCTION

The accuracy of SPH simulation depends on the choice of the kernel function, $W(x)$. There are a large number of kernel functions available in SPH literature suitable for

specific applications. For any adopted kernel function with a finite support domain *kh* (i.e., beyond which it has zero value), it shall satisfy the following three important properties:

$$\int_{\Omega} W(x-x',h)dx' = 1 \tag{3.49}$$

$$W(x-x',h)\big|_{x=x} = W(x-x',h)\big|_{x=x'} \tag{3.50}$$

$$W'(x-x',h)\big|_{x=x} = -W'(x-x',h)\big|_{x=x'} \tag{3.51}$$

The first property denotes that when all the weighting contributions for interpolations of a field variable in the neighbourhood of a particular particle is summed up, it shall give unity. For the second property, the kernel function should be symmetric in form when centred at the particle where properties have to be calculated by taking interpolation in its neighbourhood. Since, in SPH the particles move in time, satisfaction of second property (Eqn. (3.50)) is more difficult than the first one (Eqn. (3.49)). These conditions are also got affected due to the presence of a boundary. Using the MLS kernel function or Shepard correction, Eqn. (3.49) can be better satisfied. For example, in Shepard correction, the density in summation density approach can be corrected as,

$$\rho_i = \frac{\sum_{j=1}^{N} m_j W_{ij}}{\sum_{j=1}^{N} \frac{m_j}{\rho_j} W_{ij}} \tag{3.52}$$

This works equally good for both interior and near the boundary.

Fig. 3.3 shows three popular kernel functions with their higher order derivatives for B-Spline (Monaghan and Lattanzio, 1985), Renormalized Gaussian (Colagrossi and Landrini, 2003) and Wedland kernel (Wedland, 1995). Here, α_d denotes a normalizing factor which can be calculated by taking an integration over the support domain for the given dimension of the problem and setting it equal to 1 (i.e., by enforcing first kernel property, Eqn. 3.49). The value of α_d in 2D for B- Spline, Renormalized Gaussian and Wedland kernel are $15/7\pi h^2$, $\{\pi h^2(1-C_1)\}^{-1}$ where, $C_1=C_0(1+k^2)$; $C_0=e^{-k2}$; $k2=k^2$ and $7/64\pi h^2$, respectively. All the kernel functions have the characteristic Dirac δ form, They have a maximum at the centre and symmetric with respect to the centre line. Expressing the gradient of a function through kernel gradient unavoidably contain errors. These

errors get modified further when the laplacian of the same function is expressed by taking higher order derivatives of the kernel. For this reason, for calculating Laplacian, a hybrid form with finite difference has been used keeping the first derivative of kernel function and avoiding the second derivative (as discussed in section 3.4.2). This helps to maintain accumulation of errors within limit while substituting exact derivatives with kernel based differential operators. Compared to B- Spline, Renormalized Gaussian and Wedland have smoother second derivatives. For the present all SPH models, the maximum order of kernel function is up to first order.

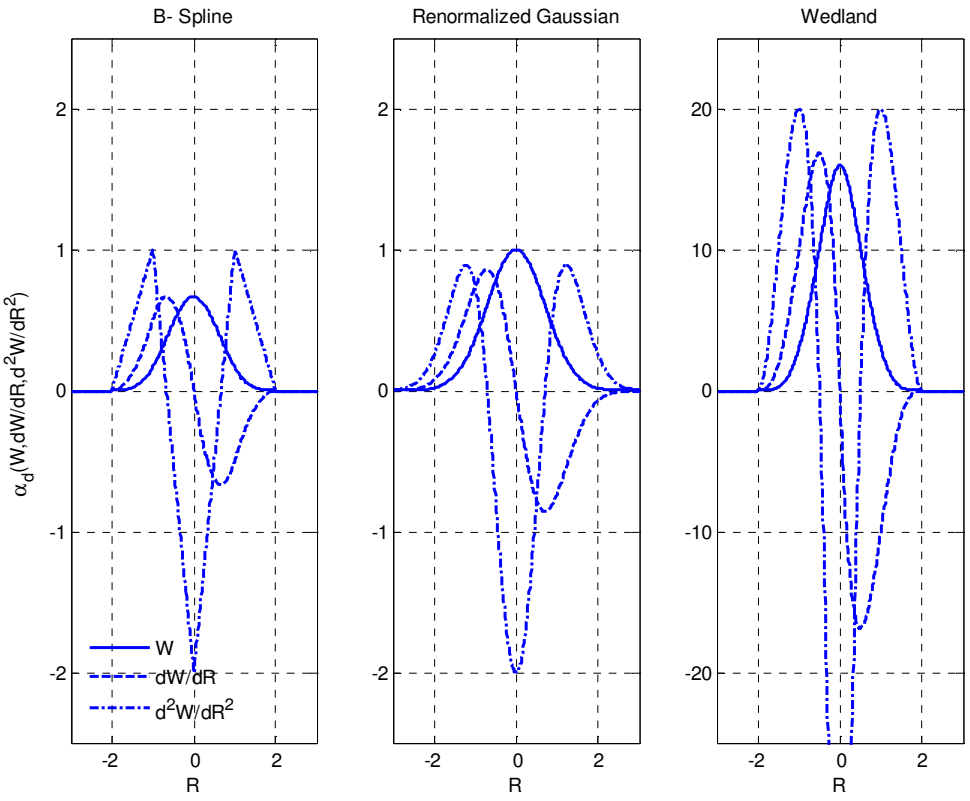

Fig. 3.3. Different kernel functions and their higher order derivatives. R= |$\boldsymbol{x}$-$\boldsymbol{x}$'|/h.

It should be noted that the symmetric form for kernel and anti- symmetric form for its' first derivative (Fig. 3.3) are true only for uniform particle spacing. The necessary conditions (Eqn. 3.50 and Eqn. 3.51) that the kernel function must obey are not valid either when particles start moving during simulation or, near the boundary. This

particular feature of SPH makes a systematic error analysis rather difficult than a grid based numerical method.

3.10. ERROR ESTIMATION

A comprehensive error analysis has been made by Quinlan et al. (2006) for estimating the gradient of a function in SPH. It is learnt that the truncation error in SPH estimation for a gradient is composed of two parts: error due to smoothing (i.e., expressing the exact derivative by taking integral interpolation for kernel gradient over the support domain, Eqn. 3.7) (TE_1) and error due to discretizing (substituting the integral of summation over neighbours (TE_2)). TE_1 is $O(h^2)$. But, TE_2 can vary depending on whether particles are uniformly distributed (during a fluid flow problem with slow dynamics and with sufficient number of particles) or non uniformly distributed (e.g., violent waves). For this reason, in order to develop a robust SPH model dealing with both non violent and violent cases, it is required to conduct separate convergence studies. The rule proposed by Quinlan et al. (2006) for the convergence study in SPH is by varying both initial particle spacing and smoothing length. This has been adopted in the present study.

However, in the context of ISPH or MPS, there is another aspect in this regard, which should also be investigated; yet has been less reported in literature. Due to the presence of Δt^2 in source term of PPE (right hand side of Eqn. 3.44), the time step decreases due to CFL criterion, as one increase resolution or number of particles in the domain. Hence, the convergence is expected for an optimum $\Delta x/\Delta t$ (Δx is the initial uniform particle spacing). This has been performed by Ma and Zhou (2009) with Meshless Local Petrov Galerkin (MPLG) method.

Hence, the convergence study has to be done by varying Δx, h (for WCSPH based schemes) and $\Delta x/\Delta t$ (for ISPH).

3.11. NEAREST NEIGHBOUR PARTICLE SEARCHING (NNPS)

One of the major computationally expensive modules in a SPH based model is to find and store neighbouring particles for all the particles. Allocating a fixed number of neighbours and then finding and storing neighbours individually for all the particles may become impractical for large number of particles. For this reason, the properties of the kernel function as given in Eqn. (3.50) and Eqn. (3.51) are utilized. Using these, an

interaction in between a target particle and its neighbour is counted only once. The required output of the Nearest Neighbour Particle Searching (NNPS) algorithm is basically five arrays. The maximum size of these arrays is a combination on how two particles can form a group of pairs (i.e., nC_2). The first array stores the first member in an interacting pair, second array stores the second member (similar to a typical argument of kernel function $W(x\text{-}x')$, x corresponds to the first and x' the second), third array with the kernel function for this interaction (i.e., $W(x\text{-}x')$) fourth and fifth with the first derivative with respect to the x and z. While all these members are inserted in their arrays, a counter (NIAC) keeps on counting how many times kernel and its derivative are calculated. The output of NNPS also contains this counter. Now, whenever a SPH summation is required, simply a loop is applied over NIAC instead of nC_2 operations for these five arrays as shown in the following pseudo code.

```
DO IK=1, NIAC    ! loop over all the pairs
!collect members in the current pair
I=PAIR_I(IK)
J=PAIR_J(IK)
! calculate volume of the members
VOL(I)=MASS(I)/RHO(I)
VOL(J)=MASS(J)/RHO(J)
! field function and its x and z derivatives
!for member i
f(I) = f(I) + W(IK)*VOL(J)
fx(I) = fx(I) + Wx(IK)*VOL(J)
fz(I) = fz(I) + Wz(IK)*VOL(J)
!for member j
f(J) = f(J) + W(IK)*VOL(I)
fx(J) = fx(J) - Wx(IK)*VOL(I)
fz(J) = fz(J) - Wz(IK)*VOL(I)

END DO
```

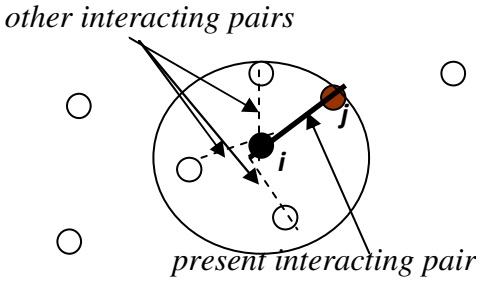

Once these four arrays are formed, SPH summation can be performed in very efficient way using this above technique. Therefore, the program (i.e., NNPS) which gives output for NIAC and these four arrays should be made as computationally cheap as possible so as to have an overall efficient model. In SPH, there are various ways to perform this task. The two techniques that are used in the present study are detailed below.

3.11.1. Directly evaluating the pairs

In this technique, for all i={1,2,3….,n}, j is checked for j={1,2,3,….n}, j≠i, to find neighbouring particles for all the particles. This operation is of $O(n^2)$. Therefore, it is not computationally efficient. For higher number of particles, this approach is impractical.

3.11.2. Linked List Particle searching method

In this technique (Monaghan and Gingold, 1983; Hockney and Eastwood, 1988), initially a grid with squares of $kh \times kh$ is laid in the domain. Then all the particles are sorted inside those squares. In other words, an array of the same size N is formed which stores the particle indices based on their locations in these squares. This array is called a Linked-List, where particles are linked with respect to either inside a particular square or its adjacent squares. For a given particle, in order to identify the neighbouring particles, search is made only inside the square where the particle lies and in its surrounding eight cells. This is done by using the linked list. The grid has to be recreated in each time step based on the maximum reach of the free surface. This technique has the number of operations, roughly $O(n)$. This technique is adopted for most of the SPH runs performed in the present study.

Apart from linked- list, there is another efficient algorithm available for NNPS named tree search. This is more efficient in 3D calculations with the number of operations $O(n\log n)$. This has been adopted in many SPH codes (like GADGET, Springel et al., 2001).

3.12. ALGORITHM OF THE NUMERICAL MODELS

In summary, the flow charts of the basic SPH models (WCSPH and ISPH) as described in previous sections are provided in Fig. 3.4. Many of the steps are similar. However, the

approach adopted for solving pressure make the choice of the time integrator different. Therefore, these two algorithms have to be developed through separate models.

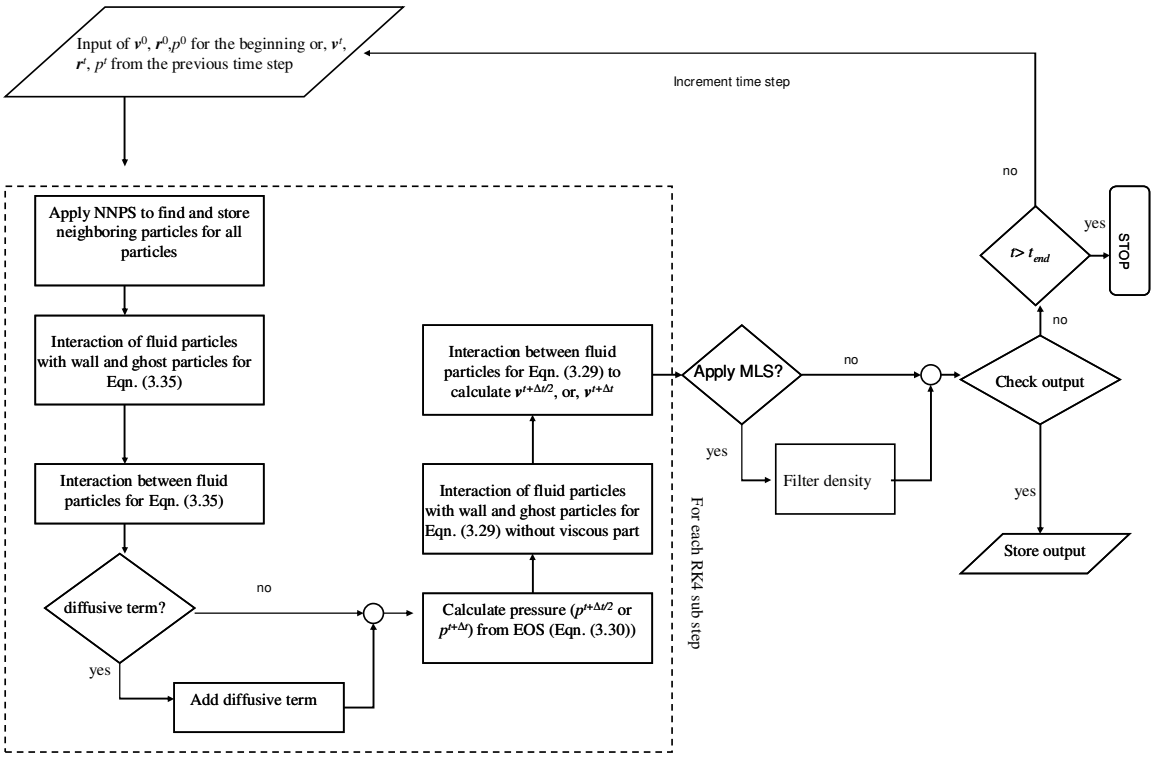

(a)

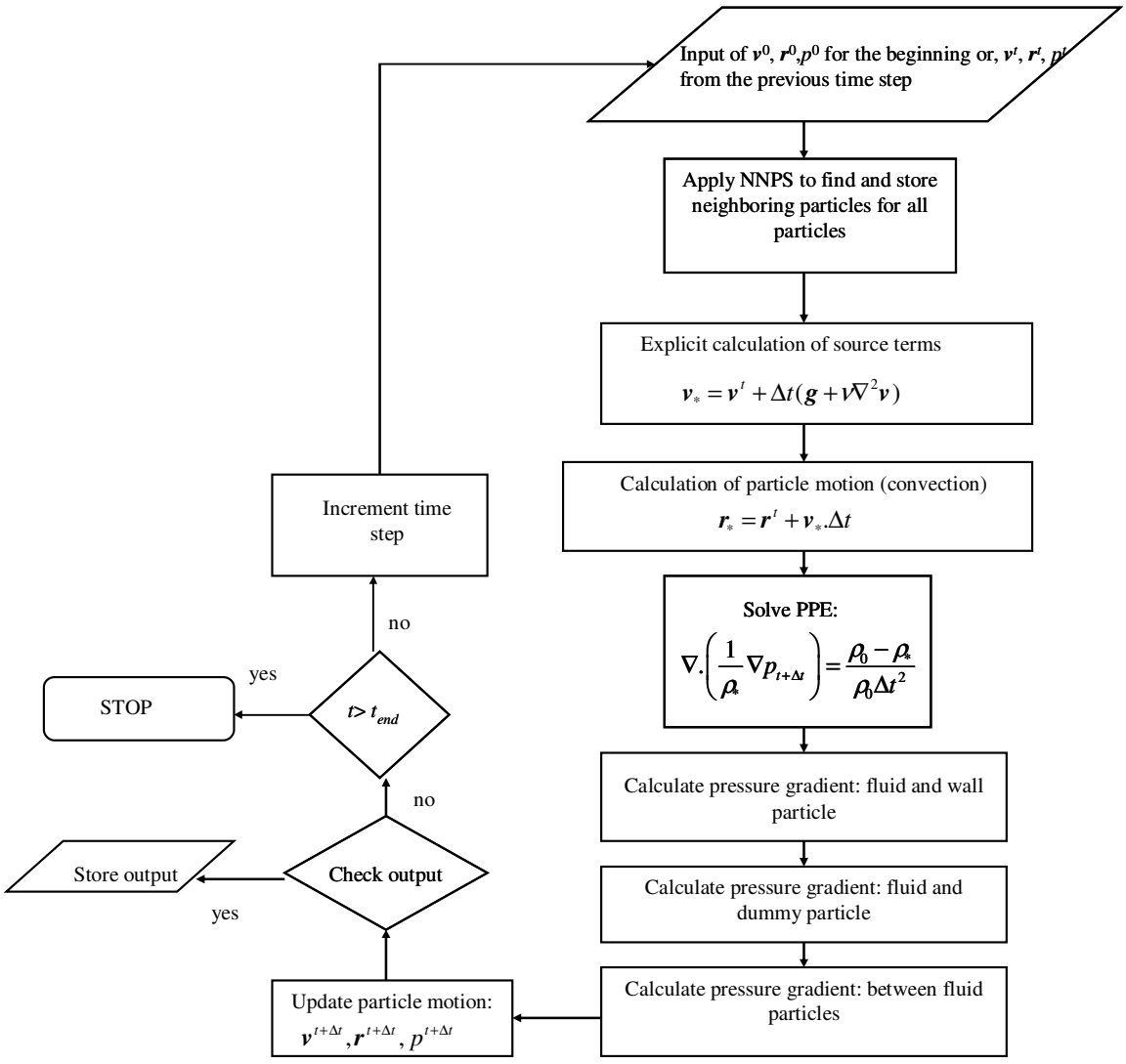

(b)

Fig. 3.4. Flow charts of (a) WCSPH and (b) ISPH algorithms.

3.13. VALIDATION

An independent numerical model whether it has been developed based on well established numerical method or a new novel formulation, has to be validated using various problems with known exact solutions. These kinds of reference problems are called benchmark problems. Even if the model is based on established methods, still it is required to perform this test in order to prove that the algorithm has been implemented properly. This requirement is more prolonged for the SPH models because a number of different numerical techniques have been adopted in order to develop a robust model. The

subsequent sections discuss performances of the SPH models developed in the present study for the non linear wave propagation problem, i.e., the wave generation and propagation in a Numerical Wave Tank (NWT). It is also equally important to systematically quantify the error yielded by the numerical model while predicting against an exact solution for a given benchmark problem. This facilitates for the numerical model to be acceptable as a deterministic model.

The next section begins with describing the NWT problem and the exact analytical solution for this problem adopted from Eatock Taylor et al. (1994). This analytical model along with the numerical model based on Fully Nonlinear Potential Theory using Finite Element Method (FEM) (Sriram, 2008) has been used to validate the present SPH model. Inter comparison has also been performed in between Weakly Compressible SPH (WCSPH) and Incompressible SPH (ISPH) with the reference solutions. Lastly, a detailed convergence study has been performed for the present SPH schemes.

3.14. NUMERICAL WAVE TANK (NWT)

In order to understand the dynamical behaviour of an object either floating (like ship, semi- submersibles, floating platforms for extracting oil and natural resources etc.) or fixed (like breakwater, coastal defence structures), it is required to investigate its response in a marine environment subjected to different wave conditions. Findings from such studies form a major part in designing coastal or marine structures. In a physical model test, this is achieved by conducting experiment in a large tank partially filled with water where nonlinear water waves can be artificially generated by moving a paddle periodically at one end of the tank. In the simplest case, the wave maker or paddle undergoes a sinusoidal motion with a given frequency and amplitude so as to generate a regular monochromatic wave (i.e., a wave that can be described by a single frequency-amplitude pair) in the tank. Following linear wave theory, it is possible to have relationship between stroke (S) of the oscillating piston type wavemaker and the desired wave height (H) for a given wave period (T) (Dean and Dalrymple, 1984).

$$\frac{H}{S} = \frac{2\left(\cosh 2k_p d - 1\right)}{\sinh 2k_p d + 2k_p d} \tag{3.53}$$

where, k_p is the wave number of the required progressive wave.

Installation of a tank with such wave generation system requires substantial technical expertise with financial support. Moreover, placement of the object that is to be studied along with necessary instruments in wave tank is a critical task. Since eighties, hydrodynamists have been spending lot of effort in developing programs through which such tests can be reproduced in computers. These programs are developed based on well established numerical methods for solving partial differential equations with given boundary conditions. This kind of a program or numerical model is called a Numerical Wave Tank (NWT).

The domain that is adopted for solving the NWT problem in 2D is shown in Fig. 3.5. It consists of a tank of length L_x with constant water depth d. The bottom and the right wall are fixed.

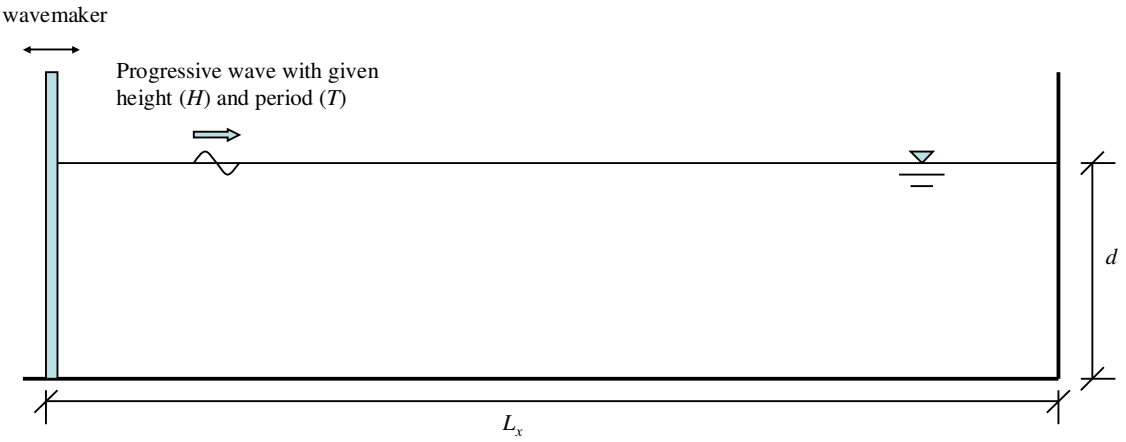

Fig.3.5. Schematic diagram of a 2D NWT problem.

The left wall simulates a moving paddle or the wavemaker. Depending on the choice of the input to the wavemaker, a number of different waves (e.g., regular wave, random wave, solitary wave etc.) can be generated in a NWT. Hence, the wave generation and its evolution along tank length without the presence of any object have been considered. If the model is capable of describing the wave generation and propagation properly, then it is understood that it has the potential to study with more complex physics (i.e, inclusion of floating object, breakwater, beach, sea wall etc.). Thus, an attempt to solve this

problem is a first step towards the development of robust numerical model for solving problems in nonlinear water waves.

3.14.1. Analytical model for predicting wave elevation in NWT

The solution from the analytical model which is taken as reference for the numerical model, is adopted from Eatock Taylor et al. (1994).

$$\eta(x,t) = \frac{2k_0 A_0}{\pi} \int_0^\infty \frac{\cos kx \cos \beta t - \sin k_0 x \cos \omega t}{k^2 - k_0^2} dk + A_0 \sin k_p x \cos \omega t \tag{3.54}$$

where, $\beta^2 = |\boldsymbol{g}|k_p \tanh(k_p d)$ and $\omega = 2\pi/T$. This solution is composed of two parts: the first part represents the transient part where any point on the initial calm free surface takes some finite time to adopt characteristic nonlinear wave form. Whereas, the second part describes a steady state situation. In the limit, when $t \rightarrow \infty$ (i.e., physically, after a long time interval), the above solution asymptotes towards a steady state solution of the form $A_0 \cos(k_p x - \omega t)$ with amplitude $A_0 = \omega/(|\boldsymbol{g}|k_0)$.

As a Navier- Stokes solver, capturing of the steady state part of the above solution is rather demanding for the present numerical model. However, this can be achieved either by incorporating a damping zone adjacent to the right wall restricting wave reflection from there, or, by using sufficiently long tank length (L_x) depending on location of the probe where one wants to measure wave elevation (η) avoiding any possible effect of wave reflection from right wall. Although few SPH/ Particle based Lagrangian models have incorporated damping zones (Lastiwka et al., 2009; Lind et al., 2012; Li et al, 2012; Molteni et al., 2013), its' effectiveness in long time simulation is still a research topic. On the other hand, the elapsed CPU time increases rapidly with increase in number of particles (due to increase in L_x). For most of the problems discussed in the present convergence study, the time series in the transient part alone has been considered. Good convergence for this part also denotes effectiveness of the adopted boundary modelling technique and overall stability of the model. Hence, for the NWT problem, the solution of the present numerical model has been reported within the limit of the transient part only.

3.14.2. The FEM model

Apart from the above analytical model (Eqn. 3.54), a different numerical model has also been used for the purpose of validation. In contrast to the present numerical model solving Navier- Stokes equation using SPH, this numerical model solves Laplace equation assuming irrotational, inviscid flow using FEM. This model is highly accurate when compared to analytical model (Eqn. 3.54) or experiment (specifically, in deep or intermediate water depth regions). It is also computationally cheap and most of the 2D cases, jobs can be performed in desktop PCs with normal ratings. Details of this numerical model can be found in Sriram (2008).

3.15. INTERCOMPARISON BETWEEN WCSPH AND ISPH

The regular wave propagation in a NWT is considered. Initial water depth (d) is 1m. The amplitude (a_h=S/2) and angular frequency (ω) of the motion of the wavemaker is 0.1m and 3.13 rad/s respectively.

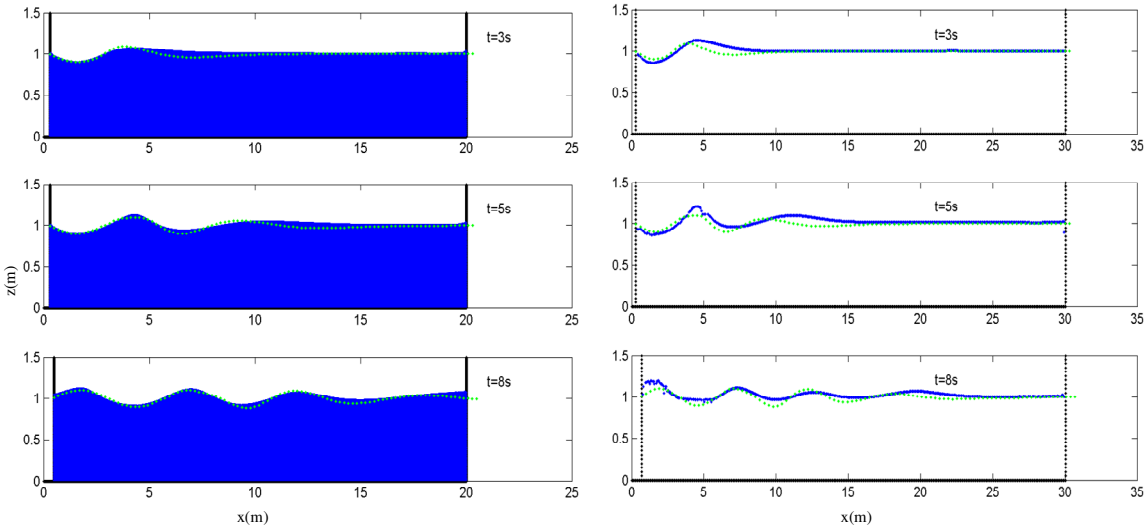

(a) WCSPH (b) ISPH

Note: Green dot represents the analytical solution.

Fig. 3.6. Comparison of the predicted free surface at different time instants between SPH and analytical model (a) WCSPH; (b) ISPH.

Both WCSPH and ISPH models have been extended. Fig. 3.6 shows the model prediction at different time instant. The prediction has been compared with the analytical model (Eqn. 3.54). Both SPH models use same initial particle spacing (around 0.01m). The SPH

models correctly describe the regular wave propagation. However, there are noticeable differences between WCSPH and ISPH prediction. These issues have to be resolved by investigating the effect of resolution depending on the schemes. This is described in a latter section. Due to employment of a higher order time integration scheme (RK4) in WCSPH, the time step size has been found to be higher than that of ISPH, according to CFL criterion. For the same reason, although a single ISPH step is known to be computationally expensive, requiring solving PPE; this cost have been found to be nearly same as that of WCSPH where within each time step, the calculations need to be reported for three times for RK4.

Figs. 3.7 (a) and (b) show spatial distribution of normalized total pressure with respect to the maximum pressure at different time instants for a resolution of about 20. It is found that even at a coarser resolution, the pressure from ISPH is better than WCSPH in terms of the spatial distribution or total pressure along the depth.

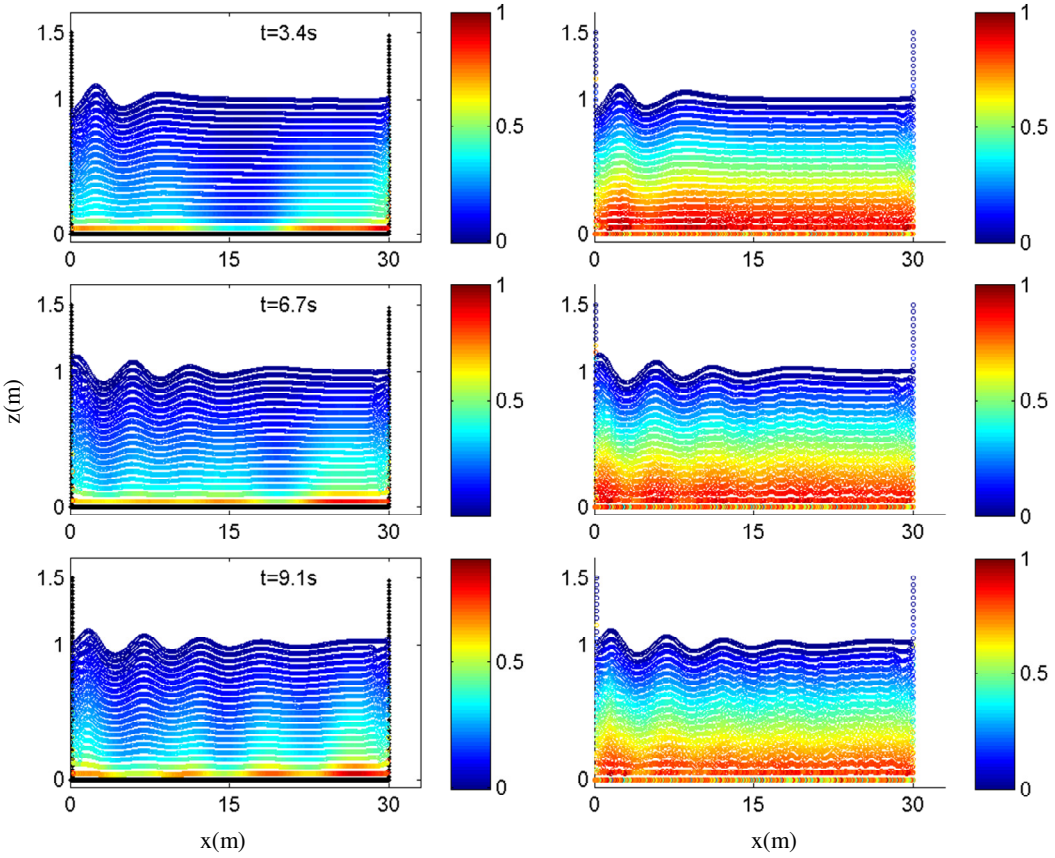

Fig. 3.7. Spatial distribution pressure predicted by (a) WCSPH and (b) ISPH at different time instants. The colour bar is of total pressure normalized with respect to the maximum pressure in the domain.

The improvement in the prediction by WCSPH and ISPH with respect to change in resolution is presented in Fig. 3.8. Mathematically, the resolution property has been defined as the ratio of a characteristic length (e.g., initial water depth, d) to the initial particle spacing (dzp). Comparison of present WCSPH and ISPH models with FEM has been shown for wave elevation (η) measured at 12 m from the mean position of the wavemaker. The number of nodes used in FEM model in x and z coordinates are 400 and 16, respectively. The motion of the wavemaker is prescribed as, $X(t)= a_h \sin(\omega t)$ with a_h=0.1 m and ω=3.13 rad/s. Very fine resolution is required for both WCSPH and ISPH models to obtain better agreement with FEM. Although a perfect match has yet not been

obtained with finest resolution used (e.g., 80 in both WCSPH and ISPH), the transient part of the solution has been recovered well. But the computational expenses are large due to the employment of more number of particles. So, the number of particles have to be optimized based on the required property under investigation (like wave elevation, pressure etc.).

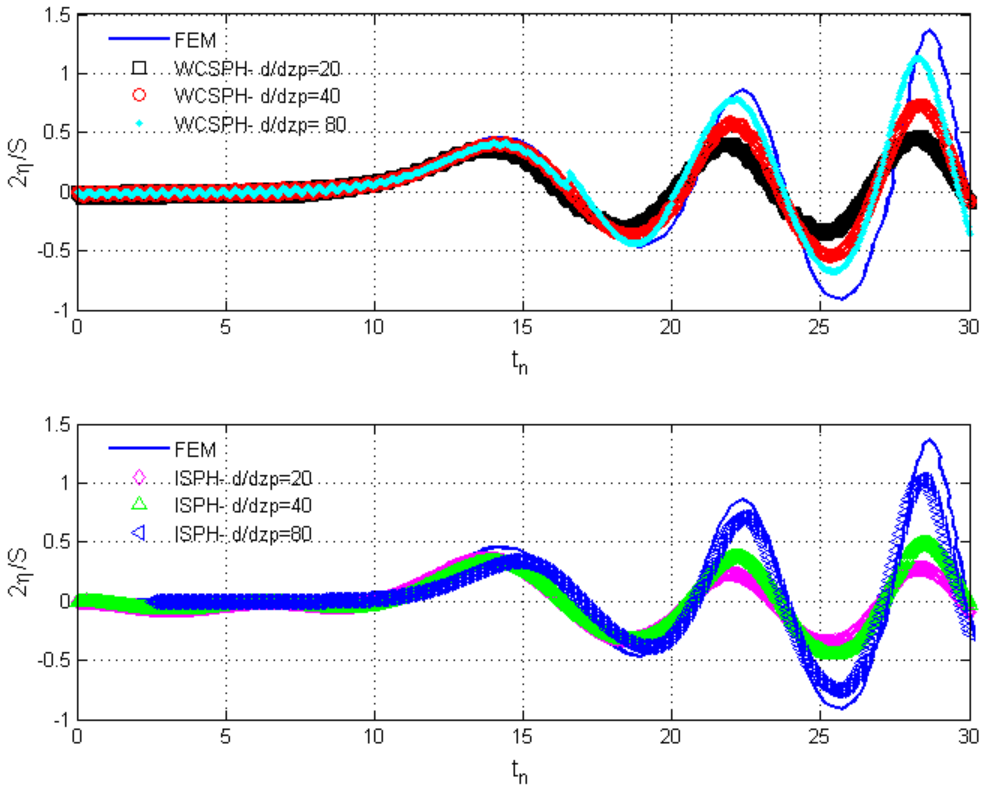

Fig. 3.8. Comparison of the time history of the free surface elevation between FEM and SPH models with different resolution. Time scale is normalized as $t_n = t\omega$. S ($=2a_h$) is the stroke of the wave maker.

Given the fact that none of the SPH schemes has been able to give converged solution for this NWT problem, the convergence study then further been extended by varying h/dzp ratio in addition to the simultaneous variation in d/h. Theoretically, for the chosen particle based representation of differential operators (e.g., gradient) using kernel function, it is required to do the convergence study in SPH by varying both h/dzp and d/h simultaneously, as proposed by Quinlan et al. (2006). While performing such investigations, it has been found that it is possible to get almost a perfect match between

WCSPH and FEM prediction for the NWT problem studied above. Fig. 3.9 shows such a comparison with h/dzp=2 and d/h=50. It should be noted that for all of the above cases (e.g., in Fig. 3.6), h/dzp= 1.33 has been chosen. For the chosen renormalized Gaussian function as kernel function, this has been a standard choice. Yet, for these combinations of h/dzp and d/h, much favourable solution has been obtained in WCSPH. Although, for solving non violent cases like propagation of moderately steep non linear water waves, SPH is relatively less popular compared to that of violent wave structure interactions, it is made clear that with proper selection of smoothing length (h) and resolution, it is possible to get good prediction from SPH.

3.16. CONVERGENCE STUDY FOR WCSPH SCHEME

This section provides detailed convergence study by varying both h/dzp and d/h for the above NWT problem using WCSPH scheme. Although attempt has been adopted to do the same for ISPH, it could not be completed for the constraint of the serial code. With the increase of h, the size of the coefficient matrix in PPE also increases (while using ISPH). Thus, the elapsed CPU time becomes prohibitive with the simultaneous increase in resolution. This restricts relatively lower range of h/dzp and d/h to cover for convergence study.

The test cases selected for three h/dzp ratios (1.0, 1.33, 2.0) with d/h varying from 10 to 60 are summarized in Table 3.1. It should be noted that these test cases have been selected given with the restriction of the present serial code in terms of total number of particles used for simulation. The serial code can be executed with upto 10^5 number of particles.

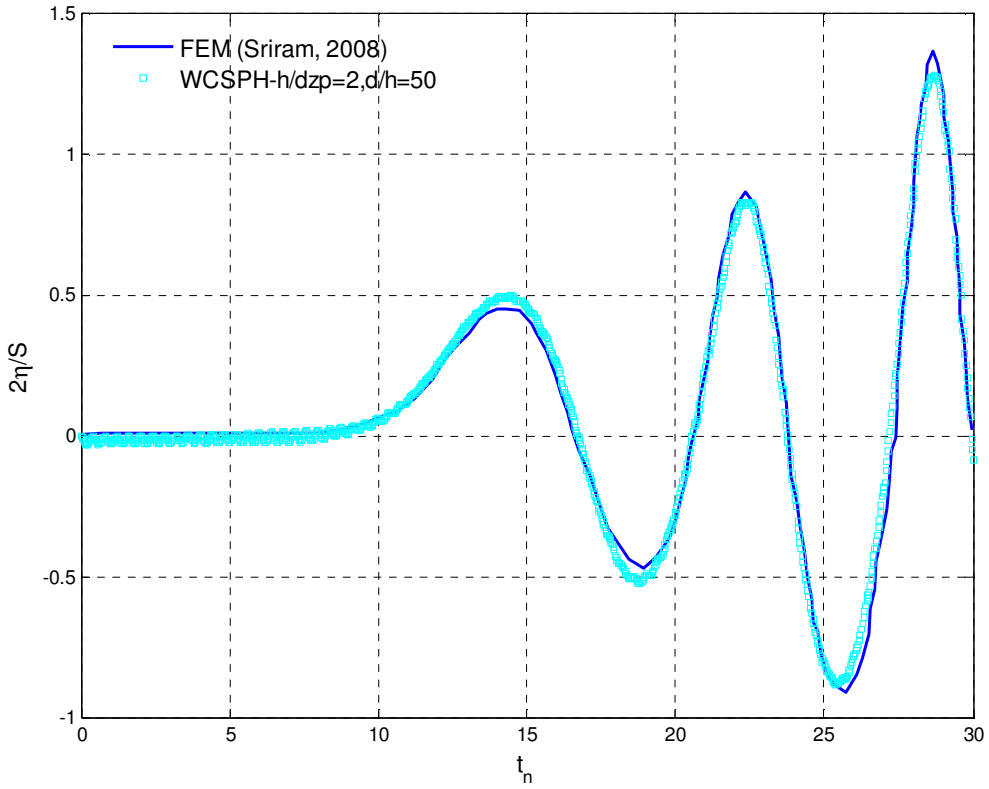

Fig. 3.9. Comparison between WCSPH and FEM for the free surface elevation measured at a given location.

The details of the utilized computational resources based on the number of particles are provided in Table 3.2.

Fig. 3.10 shows the convergence results for the present WCSPH scheme. For all these simulation, ghost particles have been used to model the boundaries. In this way, apart from free surface, the problem associated with truncation of support domain of the kernel function near the boundary has been avoided. In general this gives scope to obtain consistent findings for the present convergence test with that of Quinlan et al. (2006).

In these cases, the error has been quantified based on L_2 error. The adopted procedure for calculating L_2 error is as follows. For each case, at each time step, L_2 error is calculated based on the differences between the predicted free surface profile (η) from Eqn. (3.54) and that from SPH.

$$L_2(t) = \frac{1}{m_f}\sqrt{\sum_{i=1}^{m_f}\left[\eta(x_i,t)\big|_{analytical} - \eta(x_i,t)\big|_{SPH}\right]^2} \tag{3.55}$$

where, m_f is the number of free surface particles at a given time step in SPH. Then the L_2 error has been calculated by taking a time average of these discrete L_2 errors with respect to time.

$$L_2 \ error \ norm = \frac{1}{t_e - t_s}\int_{t_s}^{t_e} L_2(t)dt \tag{3.56}$$

where, t_s and t_e denote start and end time of the simulation respectively. Fig. 3.8 presents the convergence of SPH scheme. The convergence is considered to be achieved when the difference between the L_2 errors from two successive test run is approximately near 10^{-05}. The rate of convergence is faster with increase of *h*/*dzp*. It is of similar nature on the findings of Colagrossi et al. (2013) who studied the standing wave problem with periodic boundary conditions on two sides and ghost particles at the bottom of the domain.

Although higher *h*/*dzp* values have favourable convergence properties, its practical value may be optimized based on the other requirements of the problem.

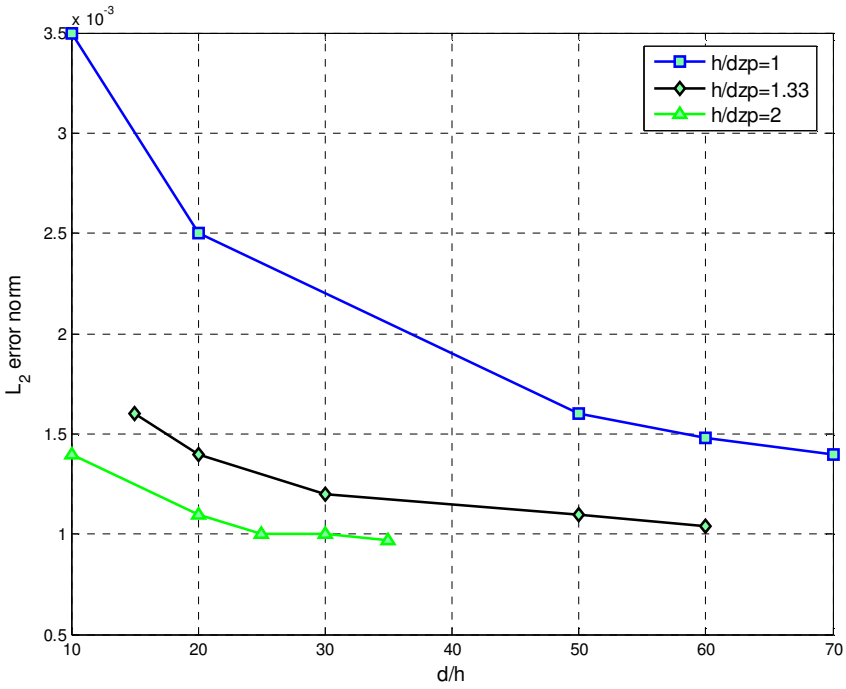

Fig. 3.10. Convergence of the present WCSPH scheme in terms of L_2 error.

3.17. SUMMARY

In this chapter, the fundamental principles of SPH approximation have been explained. The differential operators that are used in the governing equations have been derived using kernel functions. The choice of the boundary conditions for the present problems has been highlighted. Few kernel functions and their properties have been reported. It is found that special techniques are required to restore the consistency of the kernel functions. The detailed strategy for solving pressure gradient in momentum equation has been provided for WCSPH, where flow is assumed as weakly compressible to simplify pressure calculations and for ISPH by retaining true incompressibility for water. A discussion has been provided for the error estimation of both WCSPH and ISPH. The numerical strategy required to develop an efficient SPH model in terms of neighbouring particle searching has also been discussed. These lay the foundation for developing a SPH model for solving particular problems in nonlinear water waves.

The propagation of moderately steep (H/L= 0.044) nonlinear water waves have been simulated with WCSPH and ISPH schemes. Even though the prediction is limited within

the transient part of the solution, very fine resolution is required in both the schemes in order to get converged solution. For the selected (d/L) and wave steepness, the dissipation due to wave propagation has not been considered. But given with proper scale consideration, evidences are available in literature (Babanin and Chalikov, 2012) that non breaking steep waves can trigger turbulence with considerable dissipation. Since, the present SPH models are formulated from Navier- Stokes equation, it has the potential to study such phenomenon with viscous dissipation. A work in this direction has already been indicated by Colagrossi et al. (2013) where WCSPH has been found to correctly predict viscous dissipation when compared to the analytical solution of a Linearized Navier- Stokes equation for the standing wave evolution in a rectangular domain.

Table 3.1. Details of the test cases adopted for the convergence study.

h/dzp=1.0					
d/h	10	20	50	60	70
Nz	5	10	25	30	35
N_p	1495	5990	37, 475	53,970	73,465
h/dzp=1.33					
d/h	15	20	30	50	60
Nz	10	13	20	33	40
N_p	1495	10,127	23,980	65,802	95, 960
h/dzp=2.0					
d/h	10	20	25	30	50
Nz	10	20	25	30	50
N_p	5990	23,980	37,475	53,970	1,49,950

Note: Nz is the number of particles set along water depth (d) and N_p is the total number of fluid particles.

Table 3.2. Computational resources used for NWT problems depending on total number of particles (n).

n<20,000	20,000<n<50,000	50,000<n<100,000
Desktop PC 2.6 GHz Pentium® Dual-Core CPU	HP Z600 workstation (intel® xenon® multi processor (Nos.11))	VIRGO super cluster in High Performance Computing facility at IIT Madras
elapsed CPU time for running 10s of physical time		
4 to 6 hrs. (Aprrox.)	10 to 12 hrs. (Aprrox.)	60 to 72 hrs. (Aprrox.)

CHAPTER 4

DEVELOPMENT OF THE NUMERICAL MODEL

4.1. GENERAL

SPH, an emerging numerical tool, has been undergoing a vast development with its wider application in numerous fields, apart from free surface flow problems. The main purpose of the present study is the development of robust SPH algorithms, applicable for free surface flow problems including interaction with fixed ocean structures. This has been proven by applying SPH methods for different problems and then investigating the ways through which prediction can be enhanced. This chapter presents the salient developments in terms of applications in a number of free surface flow problems. For most of these cases, the benchmark problem of 2D dam break flow has been revisited to show the various stages of improvements brought into different versions of WCSPH and ISPH as part of the model development. Other test cases involve solitary wave evolution as it propagates over constant and varying depths and wave impact over a fixed seahead. The numerical prediction is then compared with experimental measurements and/or analytical/ other numerical prediction as available in the literatures.

4.2. IMPROVED WCSPH MODEL

The improved version of the WCSPH model consists of higher order source terms in continuity equation (δ- SPH, as mentioned in Chapter 3 in Eqn. 3.38). In the initial versions of the WCSPH models, free slip boundary condition for velocity has been implemented using ghost particles. The term 'ghost' denotes repeated appearances and disappearances in the stages of calculation at a given time step based on the requirement of satisfaction of boundary conditions in the numerical model. The details of the ghost particle implementation in case of solid edge boundary are shown in Fig. 4.1. The adopted ghost particle technique is applied in accordance with the free slip boundary

conditions which are explained in section 3.6. At each and every time step (or, in individual RK4 sub time steps), all the fluid particles which are within the range of the

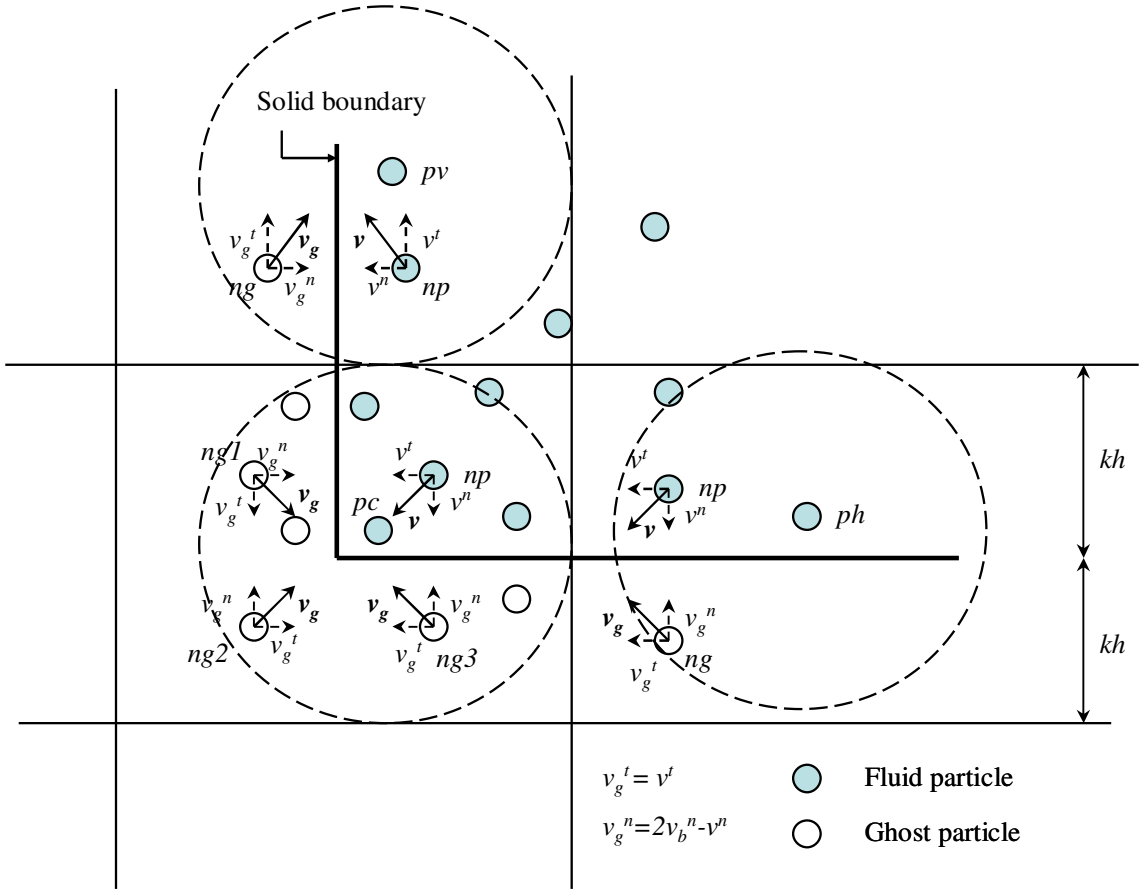

Fig. 4.1. Details of boundary conditions near the solid edge representing a concave angle using ghost particles.

support domain (i.e., *kh*) from the boundary, are reflected on the other side with respect to the boundary. In order to satisfy free slip boundary condition for velocity at the boundary, following velocity field is prescribed at the ghost particles to approximate Eqn. (3.47).

$$\begin{aligned} v_g^t &= v^t \\ v_g^n &= 2v_b^n - v^n \end{aligned} \tag{4.1}$$

where, superscripts *t* and *n* represent tangential and normal components of measured velocity with respect to the plane of reflection at the boundary. $\boldsymbol{v_g}$, $\boldsymbol{v}$ and $\boldsymbol{v_b}$ are the

velocity of the ghost particle, fluid particle and boundary respectively. For example, while solving continuity equation (Eqn. 3.35) for a fluid particle '*pv*' near the vertical edge or fluid particle '*ph*' near the horizontal edge with a ghost particle '*ng*' with its prescribed velocity in accordance with the neighbouring fluid particle '*np*' is considered. Whereas, for a fluid particle '*pc*' near the corner, an additional ghost particle '*ng2*' is accounted in addition to *ng1* and *ng3* corresponding to vertical and horizontal edges, respectively. Velocity at *ng2* is prescribed so as to have a continuous transition in the velocity field while summation is taken over neighbours for *pc* both in interior fluid and corner ghost regions. Apart from velocity, other hydrodynamic variables (such as p, ρ) are prescribed at the ghost particles.

$$\left.\begin{aligned} m_g &= m \\ p_g &= p + \rho_0 \boldsymbol{r}_{fg} . \boldsymbol{g} \\ \rho_g &= \left(\frac{\gamma p}{\rho_0 c_s^2} + 1 \right)^{\frac{1}{\gamma}} \rho_0 \end{aligned}\right\} \tag{4.2}$$

where, $\boldsymbol{r}_{fg}$ is the position vector of the fluid particle relative to the ghost particle. The density (ρ_g) of the ghost particle is calculated from Eqn. (3.30) with known pressure. The pressure (p_g) at ghost particle is defined so as to satisfy Neumann boundary condition (Eqn. 3.48) for pressure at the solid boundary. In overall, this ghost particle technique provides full support domain for the fluid particles near the solid boundary and maintains the consistency of the scheme. It also helps to satisfy the above essential boundary conditions at the discrete level. Ghost particle technique is preferred if the boundary of the domain is relatively simpler (like a rectangle).

Two test cases are considered to study the performance of the above mentioned WCSPH scheme while the boundary is modelled with ghost particles. The first test case is the benchmark problem of 2D dam break flow and the second test case is the evolution of a solitary wave over constant depth.

4.2.1. 2D Dam Break flow

The successive evolution of a large water column due to sudden release of the reservoir gate is the matter of study in the context of dam break flow. The large water column initially retained behind the gate rapidly takes the form of bore upon release and makes impact over the structures situated around the reservoir. Although this happens within a

very short span of time, it gives a fair scope for detailed study of several important hydrodynamic aspects of a free surface flow problem with fluid structure interaction. The schematic of the 2D dam break flow is shown in Fig. 4.2. *H* and *B* are the height and breadth of the water column, respectively.

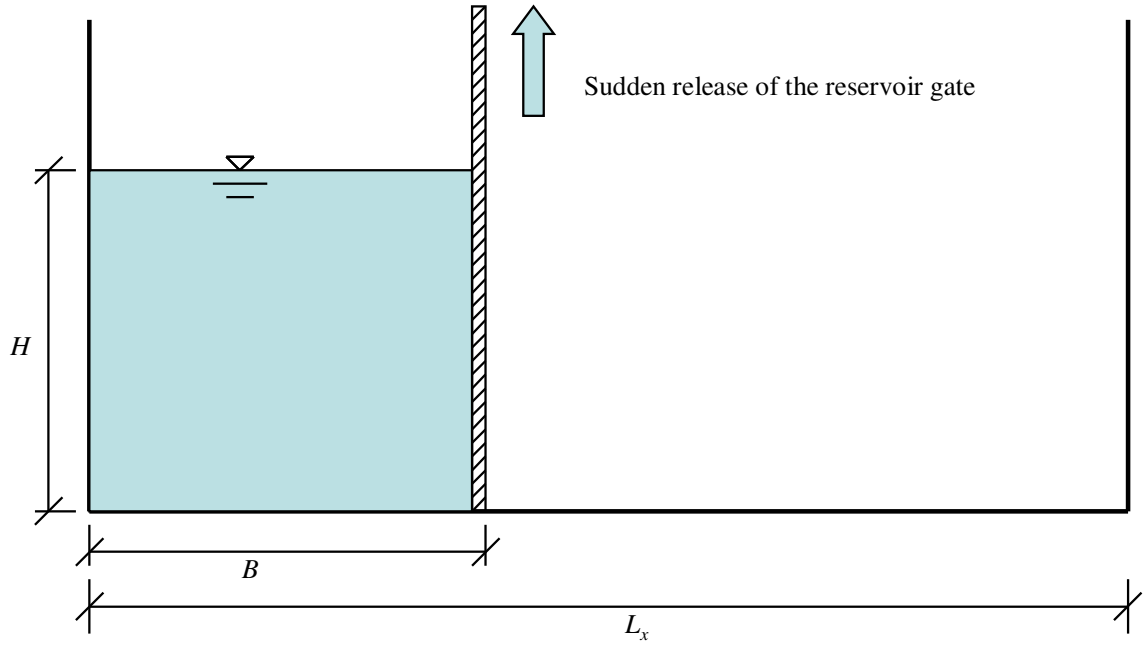

Fig. 4.2. Schematic diagram of the 2D Dam Break problem.

In reality, the gate is released within a finite span of time. But in the numerical model, it is assumed that the gate is released instantaneously, i.e., the problem is simplified by restricting the study of the flow only after the release of the gate without considering the speed at which the gate is withdrawn. This speed is known to have significant effect on the resulting flow evolution. In any case, consideration of sudden release causes maximum impact on the front structure and hence, for practical design purpose, this assumption is appropriate.

Fig. 4.3 shows an inter comparison of numerical simulation from the basic ISPH, WCSPH and δ- SPH at different instants of time for the dam break problem. Here, the length of the domain (L_x), height (H) and breadth (B) of the water column are 0.4m, 0.2m and 0.1m, respectively. The initial particle spacing is kept same (around 0.0025m) in all the SPH models. α' and β have been kept as zero while representing artificial viscosity

(Eqn. 3.32) in order to maintain Re same in all SPH models. The colour bar represents the total pressure. The predicted pressure distribution in standard ISPH and WCSPH has been found to contain noise. All the models capture the point of impact at the toe of right fixed wall around t= 0.3s. There is noticeable improvement in pressure distribution predicted by δ- SPH compared to standard WCSPH and ISPH.

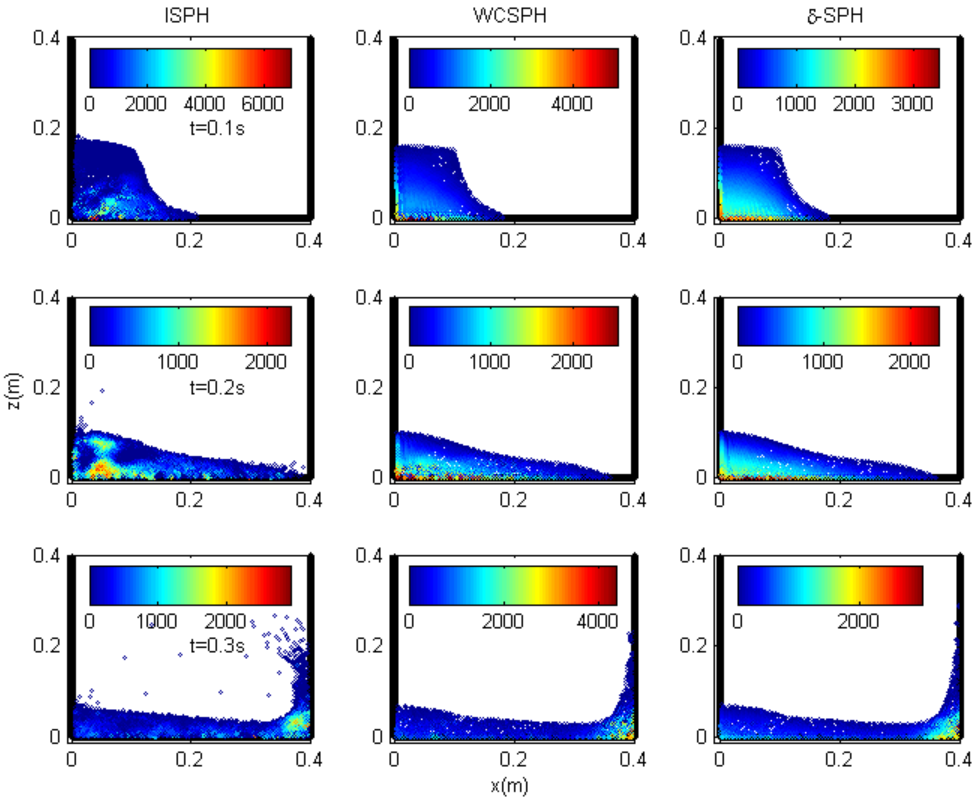

Fig. 4.3. Inter comparison of the flow evolution for the 2D Dam Break problem in between ISPH, WCSPH and δ- SPH models. The colour bar is total pressure (Pa).

The time history of the bore front evolution is compared in Fig. 4.4 with Moving Particle Semi- implicit method (MPS) (Lee et al., 2010) and Volume of Fluid (VOF) method (Hirt and Nichols, 1981). It is also compared with experimental measurements of Martin and Mouce (1952). The WCSPH prediction is found to be closer to experiment compared to ISPH and δ- SPH. Whereas, the simulation from ISPH is in close agreement with MPS and VOF compared to WCSPH and δ- SPH. This may be due to similarity in treating the fluid as truly incompressible as in both MPS and VOF in contrast to WCSPH.

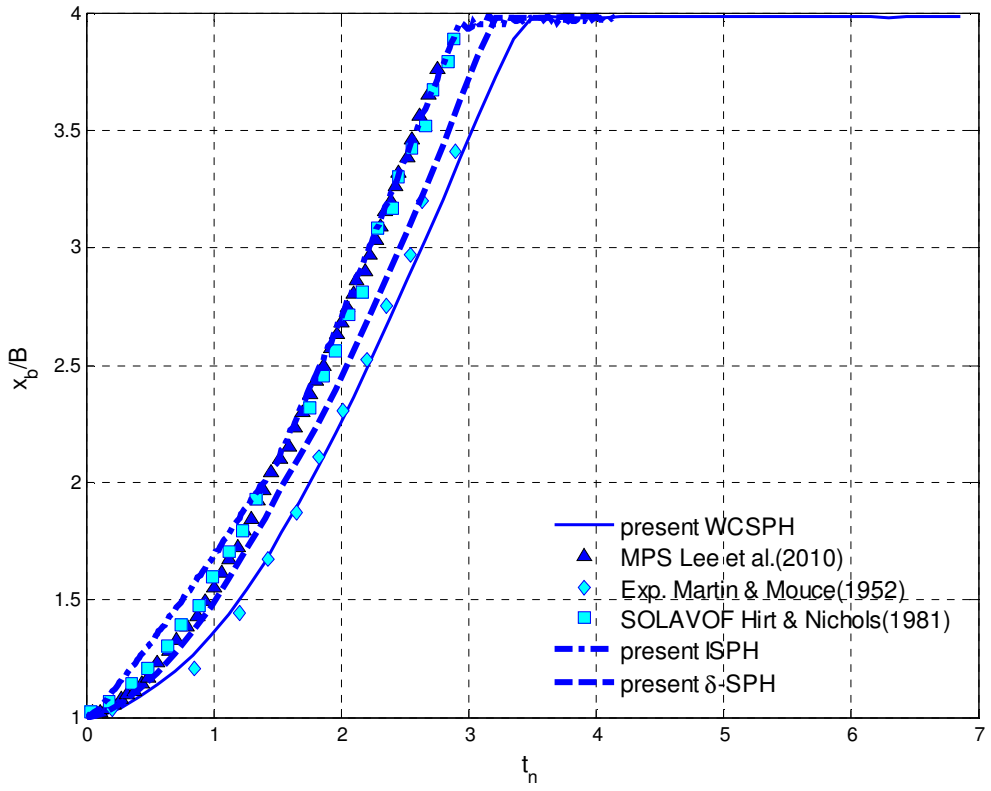

Fig. 4.4. Comparison of the time history of the bore front evolution (x_b) predicted from SPH models with past studies. $t_n = t\sqrt{(2|\boldsymbol{g}|/B)}$.

Another case study on Dam Break problem has been considered where the time history of pressure measured at a given location on the right wall is available from experiment (Zhou et al., 1999). In this case, H= 0.6m, B=1.2m and L_x=3.22m. For this given dimension, the bore undergoes a high swell up on the right wall at 1.2s, as shown in Fig. 4.5. Subsequently, due to the effect of gravity, the swelling bore starts to recess and form a plunging bore (Fig. 4.5, at 1.4s). While this plunging bore touches the upcoming free surface of the fluid towards the right wall, a strong secondary impact occurs and consequently, a strong jet is formed (Fig. 4.5, at 1.9s). Physically, the secondary impact is also enhanced by the burst of the air tube entrapped beneath the plunging bore. Fig. 4.6 gives closer view on the spatial distribution of total pressure (in kPa) around primary (at 1.2s) and secondary impact events (at 1.65s). Due to the presence of the diffusive terms, realistic spatial distribution of pressure has been obtained with δ- SPH. Moreover, it successfully captures physical processes featuring wave breaking, flow separation and

cavity formation which might be more difficult to capture through a grid based numerical model.

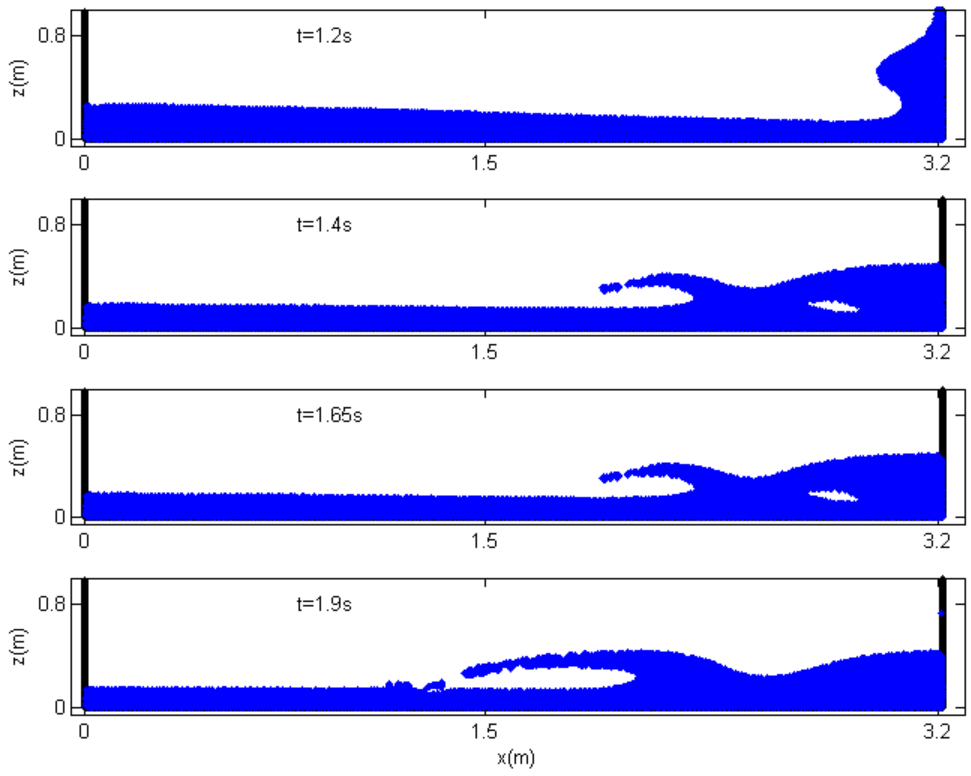

Fig. 4.5. Particle snapshots at different time instants for the dam break flow.

The inter comparison of the pressure time history at 0.16m above the base on the right wall is provided in Fig. 4.7. Compared to standard WCSPH and ISPH, δ- SPH gives least fluctuating pressure time history. In experiment the size of the pressure probe used was 0.09m (see e.g., Marrone et al., 2011a). Whereas, in simulation the pressure is recorded precisely at the location where the probe is located. This may be the reason behind the noticeable global mismatch of the SPH models with experiment. But, the first pressure peak observed in experiment around $t_n = 2.5$ is not properly captured through the present δ- SPH. The time of first pressure peak is well captured in standard WCSPH and ISPH. The prediction from WCSPH is closer to experimental measurement than ISPH. Whereas, for the secondary pressure peak around $t_n = 6$ in the experiment, there is no evidence from the WCSPH prediction. ISPH model shows a peak around $t_n = 7$ which

might be in accordance with the experiment. The pressure rise time and duration of the secondary impact has been relatively best captured in δ- SPH, but with noticeable phase shift.

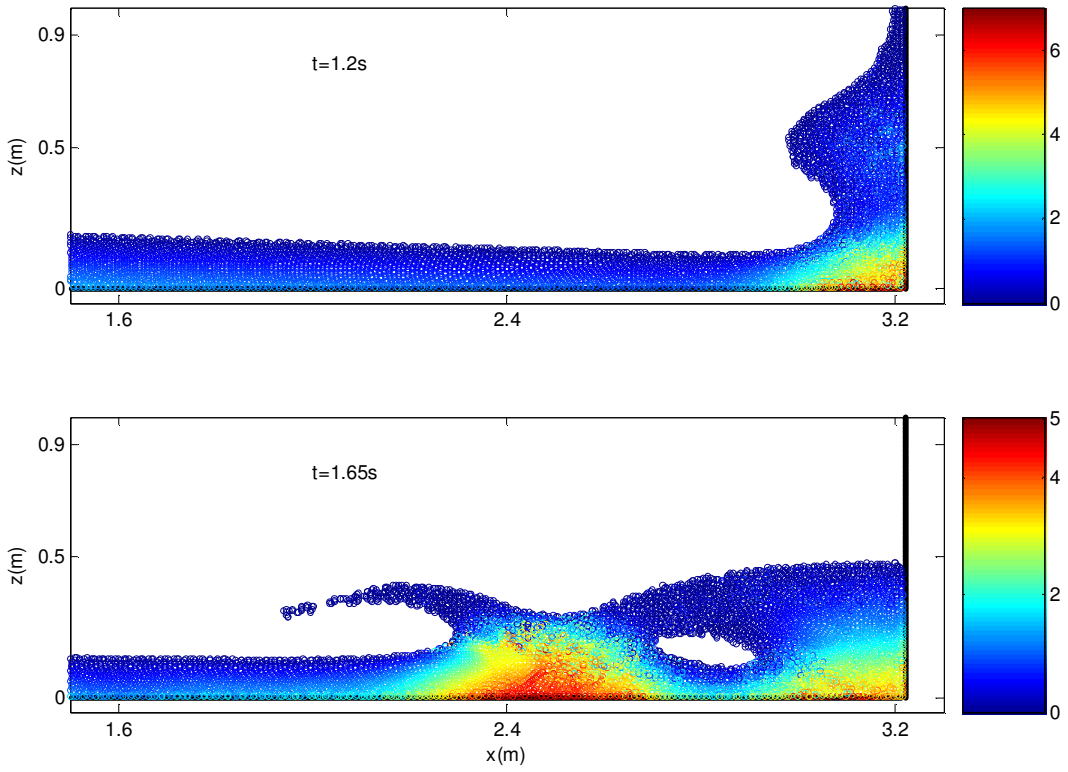

Fig. 4.6. Zoomed view of Spatial distribution of total pressure field at t = 1.2s and t =1.65s. The colour bar is pressure in kPa.

It should be noted that the pressure peak around t_n =7 in experiment starts developing in the process of cavity formation before the closing of the cavity. Whereas, in simulation this peak occurs after the cavity closes. This may be the reason for the slight phase shift. The trend in the pressure time history by δ- SPH near the secondary impact is close to that of experiment. The overshoot near t_n = 7 by δ- SPH is caused due to the sudden collapse of the plunging bore. This kind of overshoot has also been reported by the single phase WCSPH model in Colagrossi and Landrini (2003).

After the first impact with the front vertical wall, the particle distribution becomes scattered specifically in WCSPH and ISPH. Then, at these instances, the interpolated

values for field variable (like density, pressure) and their gradients using kernel function contain error. The accuracy in estimating kernel gradient depends on particle distribution. Thereore, the predicted pressure at the given location suffers from spurious oscillation in WCSPH and ISPH. Whereas, in δ- SPH, these oscillations are damped by using diffusive terms in Eqn. (3.38). This is achieved by applying the gradient correction while calculating density gradients (Eqn. (3.39)). This gradient correction assures conservation of angular momentum (Bonet and Lok, 1999). Hence, the prediction from δ- SPH contains less fluctuation compared to WCSPH and ISPH.

4.2.2. Solitary wave propagation over a constant depth

Having shown the capability of the improved WCSPH (i.e., δ- SPH) in simulating violent wave structure interaction due to dam break flow, its robustness is further highlighted by studying the solitary wave propagation over a constant water depth. The complete understanding of tsunami waves, its generation and propagation are still yet to be revealed. However, there exists some common features between a tsunami and a solitary wave. Therefore, some times, in numerical modelling, a tsunami wave is represented by a solitary wave due to its known physical characteristics.

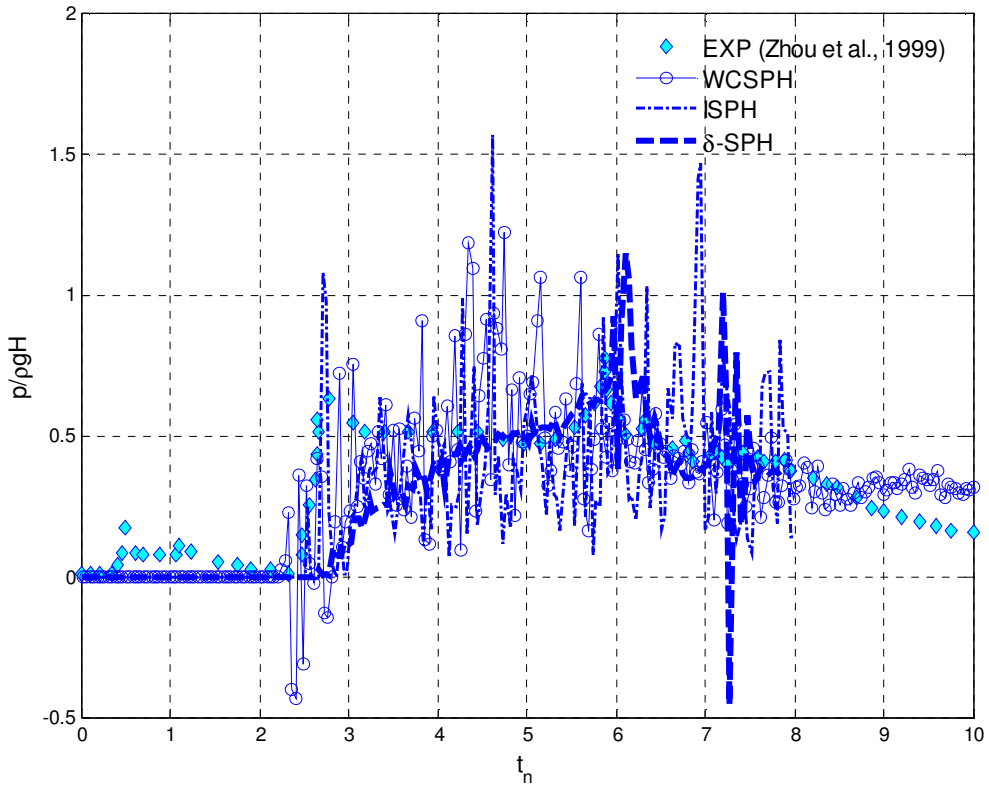

Fig. 4.7. Inter comparison of the pressure time history at 0.16m above the base of the right wall due to dam break flow. $t_n = t\sqrt{(|\boldsymbol{g}|/H)}$.

It is well known that in a numerical flume, a solitary wave can well be generated either by specifying the initial conditions (free surface, η and horizontal component of the water particle velocity, u) or by paddle movement prescribed by the first order wave theory (Goring, 1979). The wave generation schemes of prescribing either as free surface initial condition or left wall boundary condition have been considered in the SPH formulation. In the case of solitary wave propagation over the constant depth, its interaction with a front vertical wall has been investigated in terms of run-up and run-down.

Following Monaghan and Kos (1999) and Lo and Shao (2002), a solitary wave generated by prescribing the initial conditions has been studied by the present SPH model. The solitary wave profile, η at any time t can be described by:

$$\eta(x,t) = a\sec h^2\left[\sqrt{\frac{3a}{4d^3}}\left(x - c_w t\right)\right] \tag{4.3}$$

and the horizontal component of water particle velocity as

$$u = \eta\sqrt{\frac{|g|}{d}} \tag{4.4}$$

where, d is the initial water depth, a is the incident wave amplitude, and, c_w is the wave celerity. Initially, the particles are placed in a tank by removing the particles above the given profile of solitary wave crest on the left wall at $t = 0$ (Eqn. 4.3). Below the solitary wave crest, the velocities of the particles are prescribed by setting the vertical component as zero and the horizontal component (u) following Eqn. (4.4). The domain used for the SPH model is shown in Fig. 4.8. The length of the domain (L_x) is 40m and the initial water depth (d) is 1m. The amplitude of the solitary wave (a) is 0.2m, which leads to a steepness (a/d) of 0.2. The solitary wave profiles at the time instants, 2.34s, 3.26s and 5s have been compared with the Boussinesq model (Eqn. 4.3) as shown in Fig. 4.9. The present SPH model predicts the solitary wave profile well with the Boussinesq model simulation.

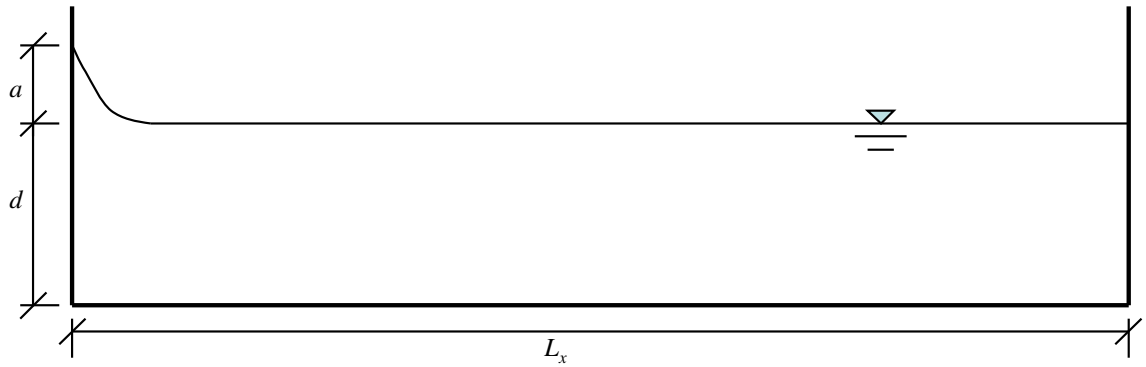

Fig. 4.8. Schematic diagram of the computational domain used for the simulation of a solitary wave by SPH model.

Further, SPH model has been applied to investigate the solitary wave run-up and run-down as it interacts with the front vertical wall. Fig. 4.10 shows the comparison between the prediction made from SPH model and from the ISPH model (Lo and Shao, 2002) as well as experiment (Camfield and Street, 1968). The present SPH model predicts the maximum run- up fairly well similar to the ISPH model. Here, the tank length (L_x) is 2m and the water depth (d) is 0.2m.

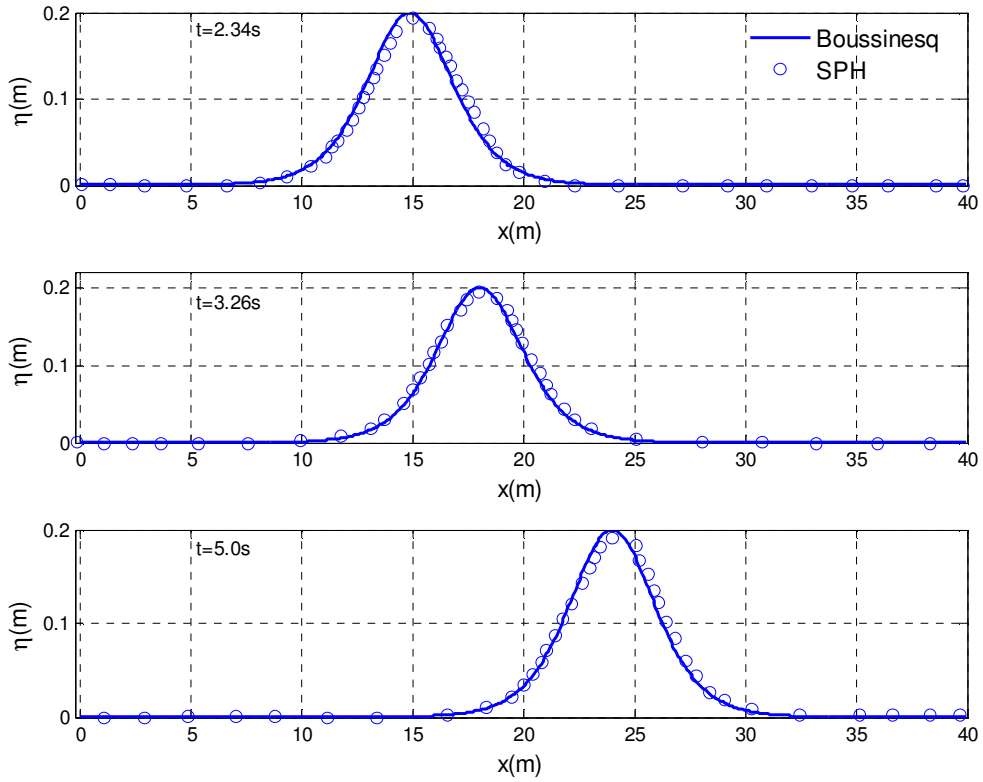

Fig. 4.9. Comparison for the solitary wave profile at t = 2.34s, t= 3.26s and t= 5s between Boussinesq model and the present SPH.

About 6,000 particles were employed in the computation. While interacting with the front vertical wall, the amplitude of the solitary wave increases and induces maximum run- up. The entire process has been simulated well by the present SPH model. Here, the computed wave celerity is found to be 1.778 m/s and the theoretical wave celerity is 1.771 m/s.

The two-dimensional solitary wave has also been simulated by the prescribed paddle movement at one end of the domain. length of the flume (L_x) is 40m. The initial water depth (d) is 1m. In this case, the left boundary of the domain is used as a wave maker with an initial still water condition. The required motion of the wave maker has been given by Goring (1979).

$$x_p(t) = \frac{a}{k_p}\left[\tanh\{\chi(t)\} + \tanh\left\{\frac{k_p}{d}Lx\right\}\right] \tag{4.5}$$

$$\chi(t) = \frac{k_p}{d}\left[c_w t - x_p(t) - Lx\right] \tag{4.6}$$

Here, $k_p = \sqrt{(3a/4d)}$ and $c_w = \sqrt{\{(d+a)|\boldsymbol{g}|\}}$. The above set of equation is implicit in nature for the time series of piston displacement $x_p(t)$. Hence, an iterative technique (like Newton Raphson method) is required to solve for $x_p(t)$. In the present study, a basic iteration technique is applied to solve Eqn (4.5). The MATLAB code is provided in Appendix B. Once $x_p(t)$ is obtained, it can be used as an input to the paddle so as to generate a solitary wave from the still water condition.

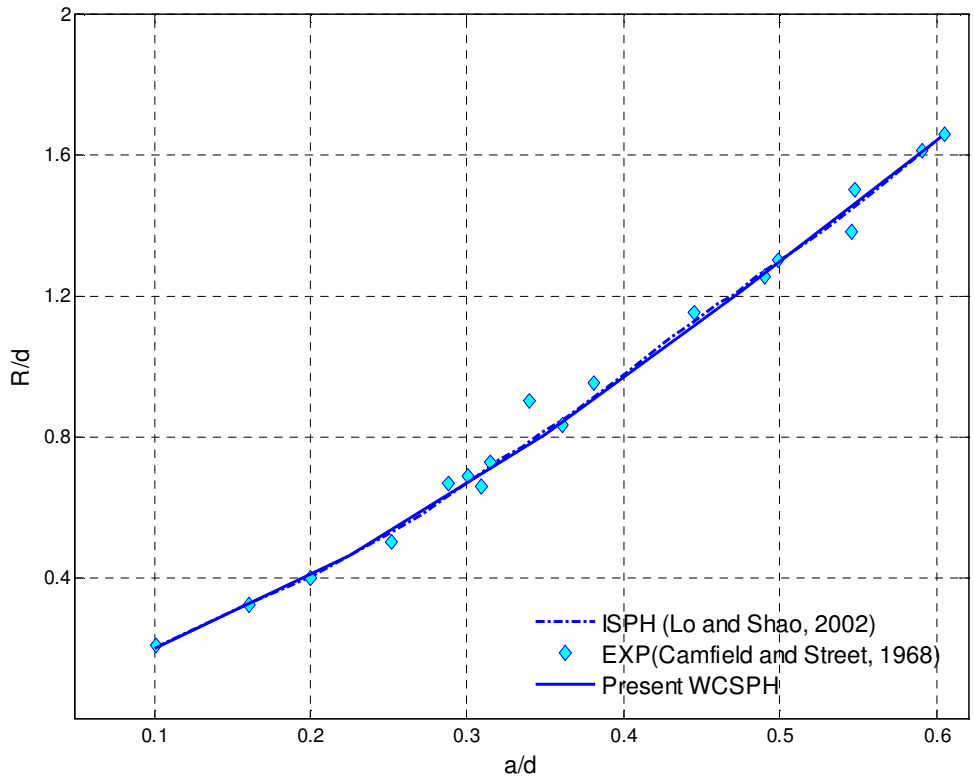

Fig. 4.10. Comparison of maximum run-up (*R/d*) due to solitary wave under different incident wave amplitudes (*a/d*).

The comparison of the solitary wave profile generated by the moving paddle following Eqn. (4.5) with Boussinesq theory (Eqn. 4.3) at two different time instants (t= 5s and t= 7s has been provided in Fig. 4.11. The accurate enforcement of boundary conditions (Eqn. 4.1 and Eqn. 4.2) using ghost particles has resulted in close agreement between the

present SPH and Boussineq model. Hence, the present SPH model has the potential to use as a general purpose Numerical Wave Flume (NWF) code.

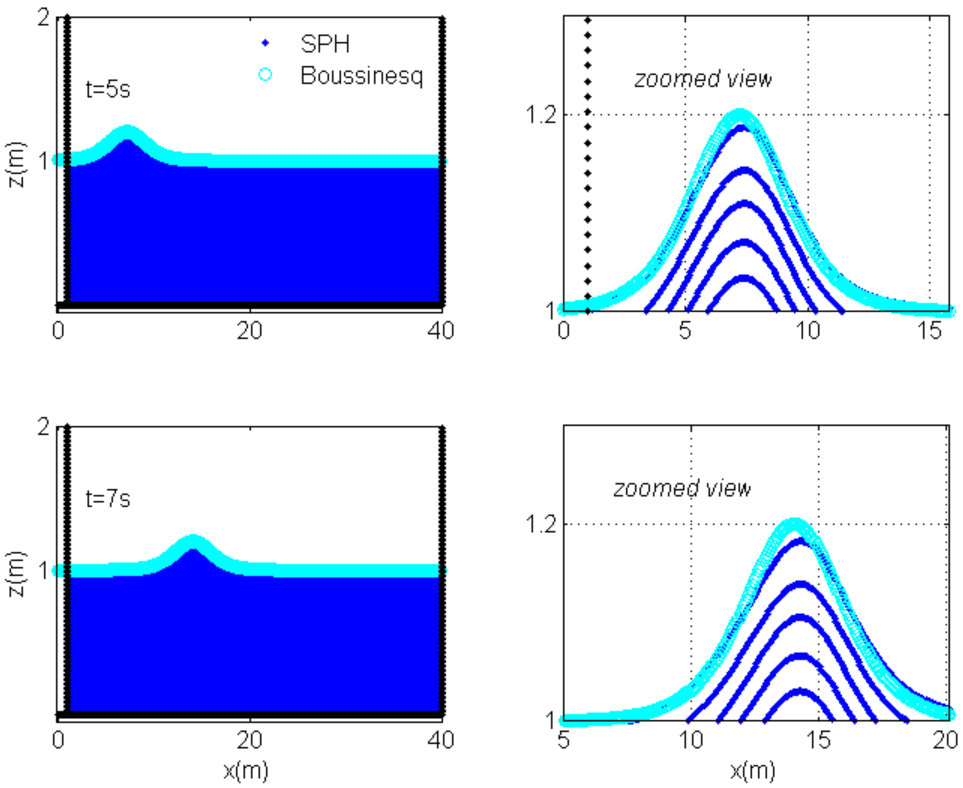

Fig. 4.11. Comparison between the present SPH and Boussinesq theory for the solitary wave generated by paddle movement.

When a solitary wave propagates over a step, indicating a sudden change in the water depth, the crest gradually deforms into second, third and other component of waves due to wave transmission in the presence of the uneven bottom topography. The number of components thus generated may result into several waves as the principal solitary wave travels long distances without dissipation. This physical phenomenon has shown an importance in understanding the propagation of a tsunami wave over a continental shelf. During this process, it splits into few more component waves and consequently, few waves lashes over nearby ports/ coastal structures. Hence the study of solitary wave split up over uneven water depths is equally important as that of constant depths. The domain required to perform such kind of simulation consists of a step staring at a certain distance

from the origin. Standard ghost particle technique poses difficulties in modelling the corner of the step. This is explained in the following.

Let us consider the fluid region near the solid corner in terms of particles as shown in Fig. 4.12. As per the rule of mirroring described earlier, three specific zones namely, zone A, zone B and zone C have to be reflected behind the solid corner. For a particle '*Bp*' in zone B, a particle '*Cp*' from zone C and particle '*Ap*' from zone A are considered as they appear in the range of the support domain (as shown in dotted circle) of '*Bp*'.

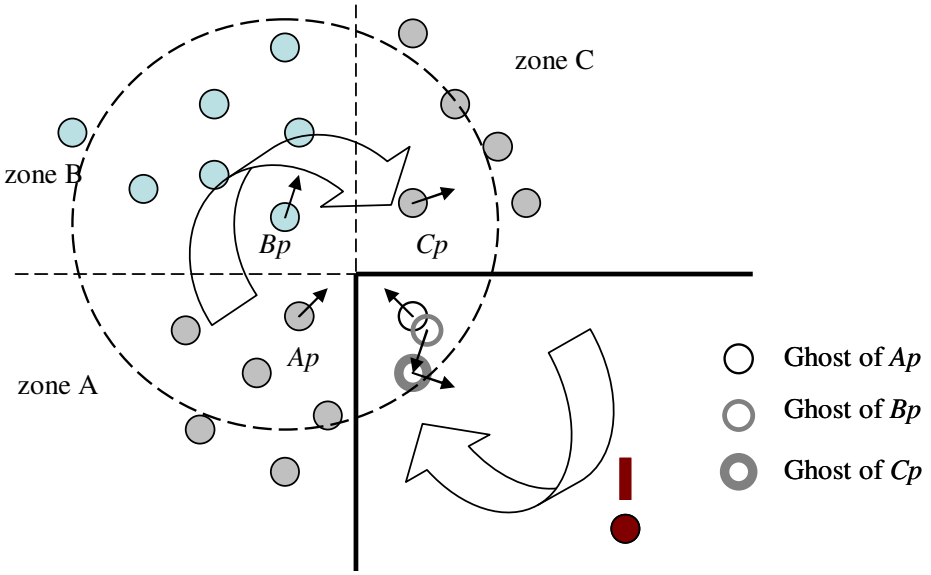

Fig. 4.12. Problem associated with reflecting fluid properties in the solid corner using ghost particle technique.

If the previous rule is applied to prescribe velocity for the ghost particles of '*Ap*', '*Bp*' and '*Cp*', a discontinuous velocity field in the ghost region would occur in the support domain of '*Bp*'. This is seen in Fig. 5.12 as one traverse from zone A to zone C or vice versa. Moreover, there is a possible chance of overlap in ghost particle locations (as happened in the present case for ghost particles of '*Ap*' and '*Bp*'). Hence, the challenge in implementing traditional ghost particle technique to model such corner is two fold: retaining a smooth velocity field in the ghost region near the corner considering reflection of fluid properties from zone B and avoiding overlap in ghost mass. In the present improved WCSPH model, this is achieved in the following ways described in the next section.

4.2.3. An efficient ghost particle technique for solid corners

Solution for velocity

The solution for the problem of discontinuous velocity field is adopted from Le Touze et al. (2006), where velocity for the ghost particle reflected from zone B is prescribed based on the following two cases:

Case A: The particle is supposed to hit inside the sub domain kh × kh (Fig. 4.13a)

In this case, the fluid particle '*Bp*' and its ghost particle share the same impact point. In other words, they shall hit the shared point at the same time. This common impact point can be found using the coordinate and velocity of '*Bp*'. Once this impact point is known, the magnitude of velocity of the ghost particle can be calculated based on condition A (i.e., the fluid and its ghost particle hit the same point within distance *kh* from the corner point). Next, the direction of the velocity can be found from the triangle as shown in the Fig. 4.13a.

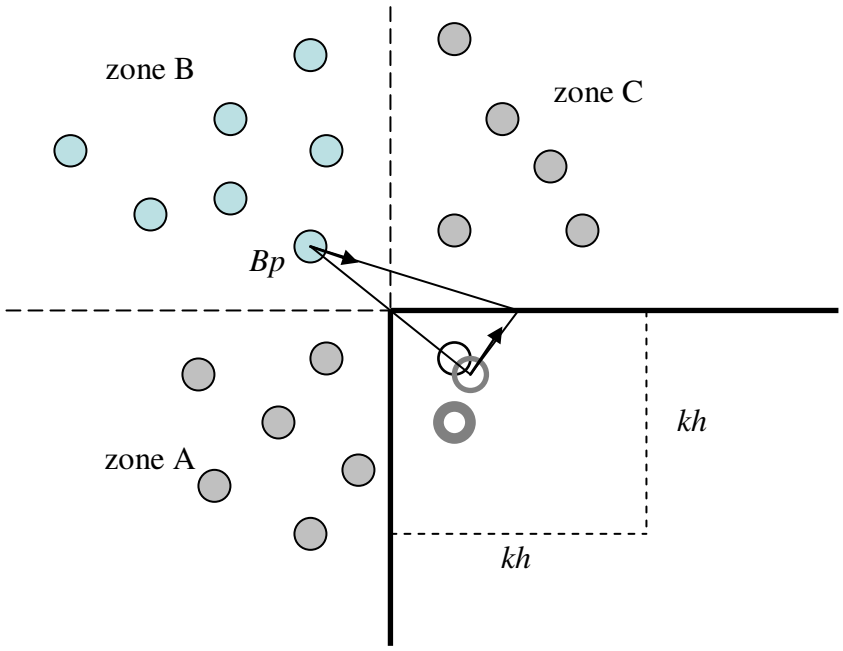

Fig. 4.13a. Condition for obtaining the velocity of the ghost particle for fluid particle *Bp* for case A.

Case B: The particle is supposed to hit outside the sub domain kh × kh (Fig. 4.13 b)

In this case, the ghost particle of *Bp* poses the same velocity as that of *Bp*. Here, the reflected velocity from zone B maintains a continuous velocity field at the ghost region in the corner after the velocity of the ghost particles from zone A and zone C are prescribed as in usual way. However, another correction is required to avoid excessive ghost mass. If two ghost particles are overlapped, error accumulates while taking interpolation for any fluid particles with part of its support domain in ghost region.

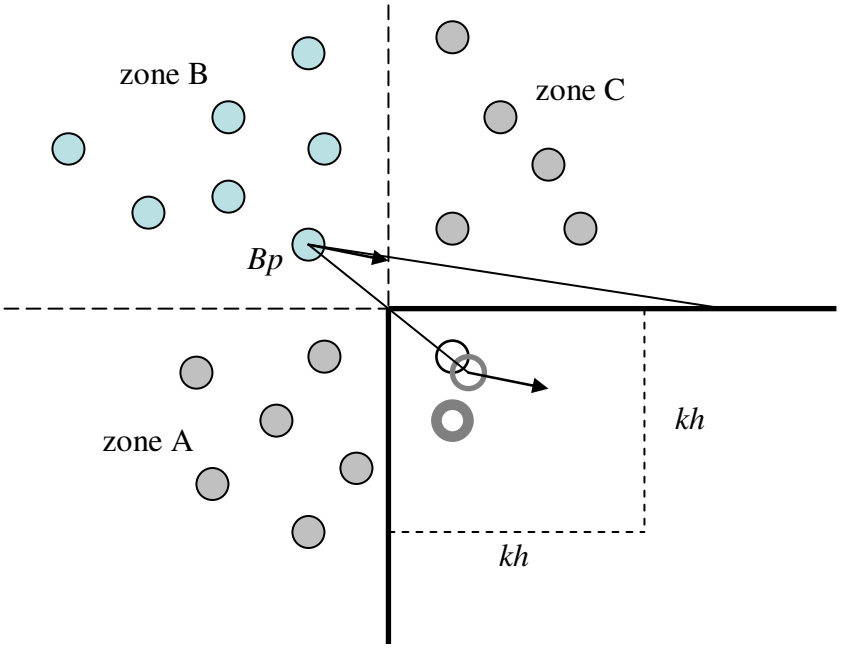

Fig. 4.13b. Condition for obtaining the velocity of the ghost particle for fluid particle *Bp* for case B.

Solution for Mass

From the past works on SPH, primarily there exists few approaches through which this problem of excess ghost mass can be dealt with. One is the Multiple Boundary Tangent (MBT) technique proposed by Yildiz et al. (2009); using fixed ghost particles proposed by Marrone et al. (2011a); using generalized wall boundary conditions of Adami et al. (2012); restricting the interactions between fluid particle and ghost particles at the corner zone by using a local plane of symmetry at the corner zone (Liu et al., 2013) etc. In the present study, a simple and computationally efficient correction is adopted.

In 2D SPH, the mass of a particle represents the area that it occupies. Therefore, when the mass of ghost particle (m_g) is calculated from Eqn. (4.2), the area associated with the fluid particle gets projected on the prescribed position of the ghost particle. In the case of fluid corner (Fig. 4.1), *ng2* is considered in addition so as to have a filled up support domain for the kernel function for all the fluid particles (like *pc*) near the corner. Now, if the masses of the ghost particles are calculated by the same approach for the case of solid corners (Fig. 4.12), a singularity arises in terms of area. For fluid corners, while following the rule of mirroring, the area of the fluid particles near the corner gets projected into three separate and distinct zones whereas, for the case of solid corners, the area associated with the fluid particles from zones A, B and C is projected and then overlapped into a single zone, i.e., the corner area. Naturally, an accumulation of masses occurs in a single zone.

Therefore, the solution of the problem of excess ghost mass lies in an accurate estimation of the masses of the ghost particles staying in the corner zone for the case of solid corners. Once, the positions of the ghost particles in that zone are fixed, the mass of each of these ghost particles should be calculated from the actual area that each of them represents. This can be done by calculating the particle number density ($n_i=\Sigma W_{ij}$) after centering the kernel function at the position of the ghost particle for which mass is to be calculated. The accuracy of that approximation largely suffers when there is lack of neighbours/ improper particle distribution, because then it has to be carried out in the ongoing simulation process. Alternately, the average area (a_{avg}) that a ghost particle posses in that corner can be calculated by $(kh)^2 / N_{gc}$,where, $(kh)^2$ is the area of the corner zone and N_{gc} is the number of ghost particles appearing in the corner zone. Then, the mass of each of the ghost particles is calculated by $\alpha_m \rho g a_{avg}$ where, ρg is the pre-computed density of the ghost particle and α_m is a tuning factor. The proper value of α_m is to be set by numerical trials. Fig. 4.14 reports the performance of the model for two α_m parameters. The optimum performance is achieved for α_m = 0.4. This value has been adopted for all the cases where solitary wave propagation over a step is simulated.

The effectiveness of the adopted correction on modelling solid corner zones using ghost particles is provided in Fig. 4.15, where the vortex created due to the propagation of solitary wave crest over a step is highlighted.

With these improvements, the WCSPH model is now be applied to study evolution of solitary waves as it crosses over a step, replicating a continental self.

4.2.4. Solitary wave split up

Fig. 4.16 presents the schematic diagram of the domain following the similar case study by Seabra-Santos et al. (1987). The location of the probes (3m, 6m, 9m and 12m from the left wall boundary) to measure the free surface elevation with time is also shown in the same figure.

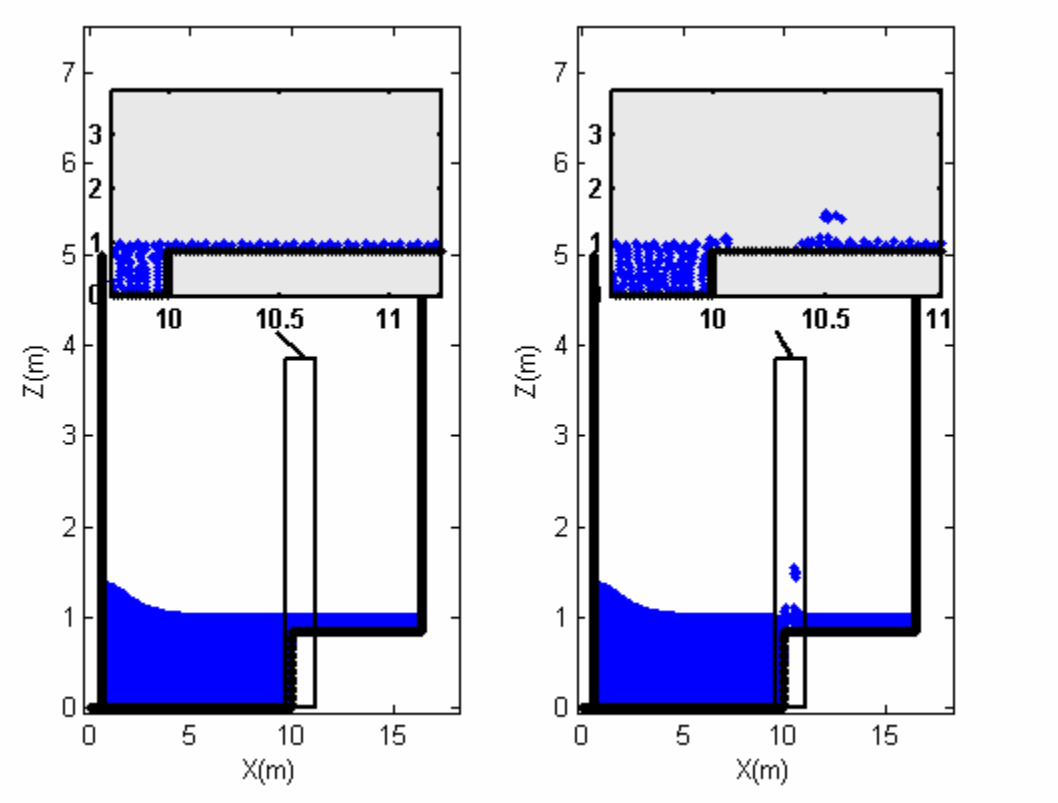

(a) $\alpha_m = 0.4$ (b) $\alpha_m = 0.7$

Fig. 4.14. Effect of the choice of the α_m parameter for avoiding flow separation due to excess ghost mass.

Figs. 4.17 a-f presents the particle configuration at different instant of time while the solitary wave propagates over the vertical step. The initial single soliton disintegrates into few more solitons after passing over the step to propagate over a lesser water depth. The enlarged view of the particle configuration under the wave crests is also shown. The enlarged view of the particle snap shots depicts the process of the splitting up of a solitary

wave during the wave transmission. Nearly 63,000 particles were used in the simulation (excluding boundary particles). It took about 20 days to run for 15s simulation in VEGA super cluster with RK4 time integrator (i.e., four times evaluation of the same SPH procedure per time step).

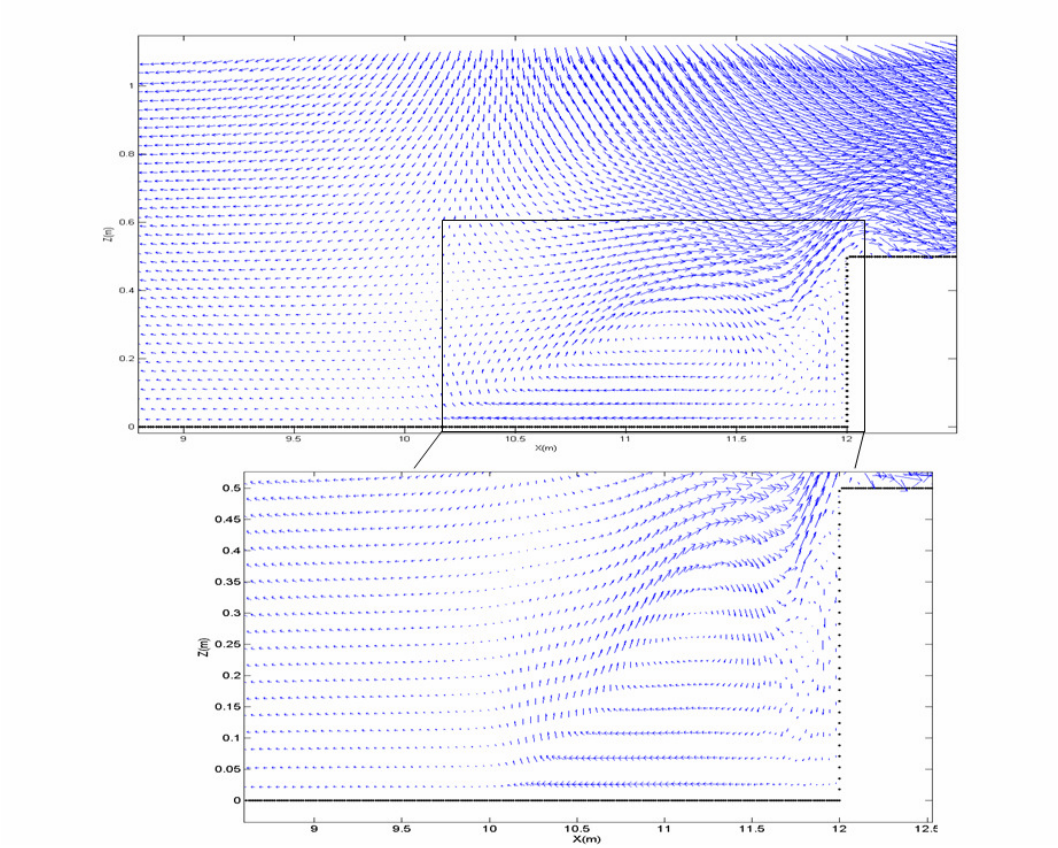

Fig. 4.15. The vortex field created during the crossing of the solitary wave crest above the step.

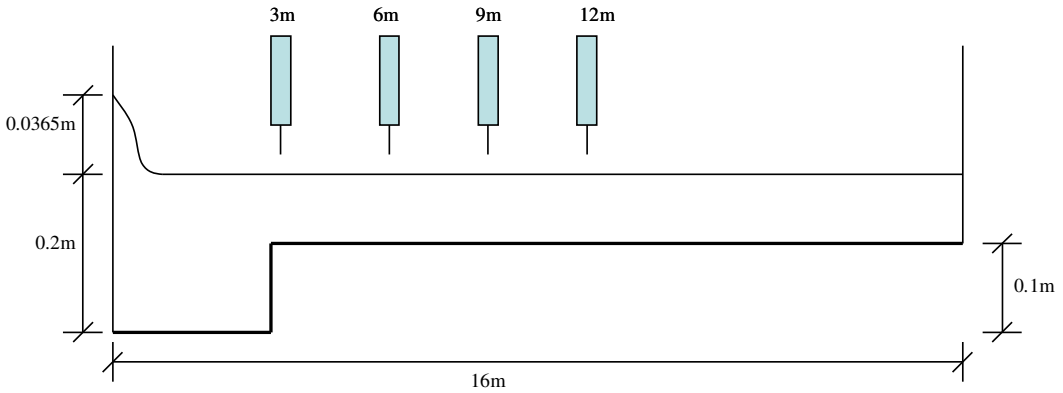

Fig. 4.16. Schematic diagram of the problem domain used for the analysis of the solitary wave split-up problem.

Figs. 4.18 a-d show the time histories of the water surface elevation recorded at four probe locations from the SPH model and compared with the experimental measurements and finite-difference method prediction by Seabra- Santos et al. (1987). The SPH model successfully captures the increase in solitary wave amplitude before splitting- up into multiple solitons. However, the differences both in terms of wave amplitude and phase have been found to be significant at 9m and 12m (probes 3 and 4) from the initial soliton origin when compared to the numerical prediction by Seabra- Santos et al. (1987). Similar observation was noted by Li et al. (2012) while adopting SPH model. However, the comparison between the experimental measurements is found to be good. Since the step was modelled by a half sinusoidal wave in order to avoid numerical instabilities in the finite difference method, the finite difference simulation deviates significantly from the experiment. In SPH, the vertical step can be modelled without any approximation. On comparison with Li et al. (2012), the amplitude of the split-up second soliton is found to be less. It has to be noted that the locations of the probes 3 and 4 are relatively closer to the opposite wall of the numerical wave flume and hence, the wave reflection from the wall might have influenced the prediction. Li et al. (2012) incorporated wave absorbing schemes in order to minimize reflection. However, the present model predicts smoother free surface profile than the SPH prediction by Li et al. (2012).

Although the above proposed technique to resolve the problem of excess ghost mass was quite successful while modelling solid corners, it was found to be not much effective for solid corners apart from right angles. The major problem was to tune the α_m parameter for each problem depending on the geometry of the given domain. For the development of a robust SPH model, a more general approach is required. That has been possible by combining two well established techniques for modelling boundaries with complex geometrical shapes in SPH: the first one is the calculation of pressure at the ghost region by employing a local force balance (Adami et al., 2012) and, the second one is the accurate extrapolation of velocity at the ghost region in order to enforce free slip (Macia et al., 2011; Marrone et al., 2013). In both of these techniques, a fixed layer of ghost particles are set uniformly around the periphery of the given boundary at the beginning of the simulation and their relative position remains fixed. These fixed ghost particles are

also referred as dummy particles. Naturally, this technique does not have problem of excess ghost mass.

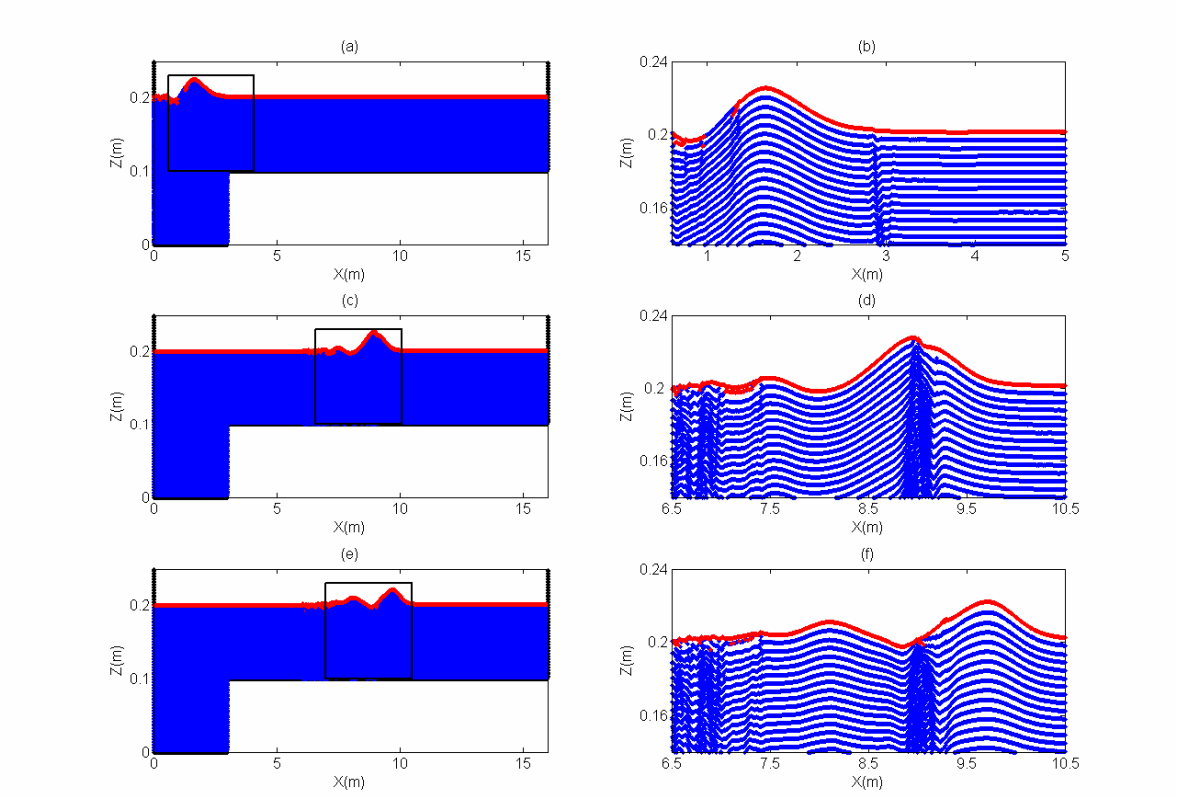

Fig. 4.17. Particle configurations at different instant of time while the solitary wave passes over the step: (a) t=1s, (b) enlarged view of the zone inside the rectangle as shown in (a), (c) t=6.97s, (d) enlarged view of the zone inside the rectangle as shown in (c), (e) t=9.15s, (f) enlarged view of the zone inside the rectangle as shown in (e).

Fig. 4.19 shows a general boundary and dummy particle set up. In order to avoid spurious penetration of fluid particles inside the solid boundary, the pressures on the dummy particles are calculated by the following formula proposed by Adami et al. (2012).

$$p_g = \frac{\sum_f p_f W_{gf} + (\boldsymbol{g} - \boldsymbol{a}_w).\sum_f \rho_f \boldsymbol{r}_{gf} W_{gf}}{\sum_f W_{gf}} \tag{4.7}$$

where, $\boldsymbol{a}_w$ is the acceleration of the moving boundary. The summation is taken over the fluid particles (symbol '*f*'). This formula can be derived by considering the momentum conservation equation in between a fluid and dummy particle. In this technique, it is not required to calculate the normal at the local boundary plane (as required in repulsion force based techniques). Application of first order Shepard correction on kernel gives accurate interpolation. Higher order MLS kernel function can also be used (Marrone et al., 2011a). However, the case studies (discussed in few sections latter) that was conducted using Eqn. (4.7), were found to give equally acceptable results.

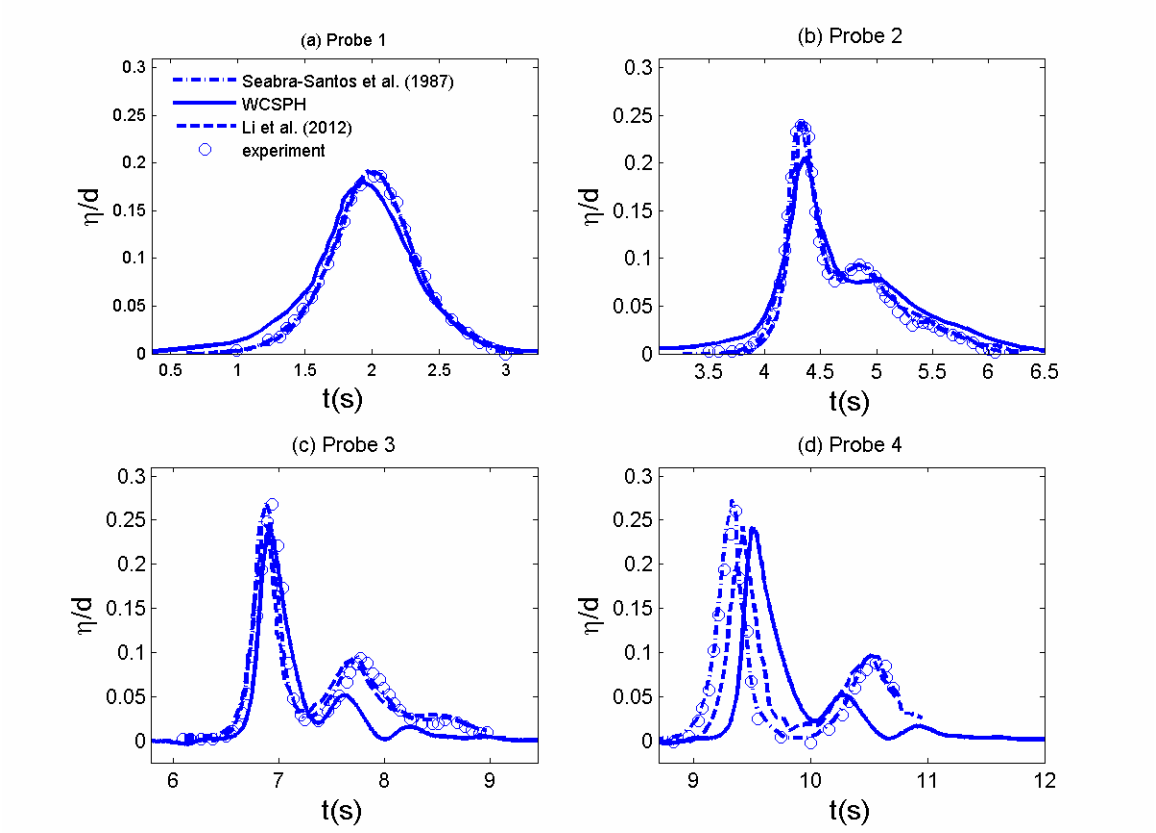

Fig. 4.18. Comparison of the time histories of the free surface elevation at various probe locations: (a) Probe 1 @ 3m, (b) Probe 2 @ 6m, (c) Probe 3 @ 9m, (d) Probe 4 @ 12m.

The velocity at the dummy particles is calculated using the following formula adopted from Marrone et al. (2013)

$$v_g^t = v^t$$
$$v_g^n = v_b^n + (v_b^n - v_n)\frac{dg}{dp + \zeta \Delta p} \tag{4.8}$$

where, the velocity components, distances *dg* and *dp* as shown in Fig. 4.19. ζ is a small parameter which is kept to avoid penetration if a fluid particle comes very close to the boundary. The prescribed value of ζ is 0.25. Δ*p* is the initial particle distance. Eqn. (4.8) is an enhanced version of formula proposed by Takeda et al. (1994), who performed the simulation of flow past a cylinder in 2D using dummy particles to model the boundary of the cylinder.

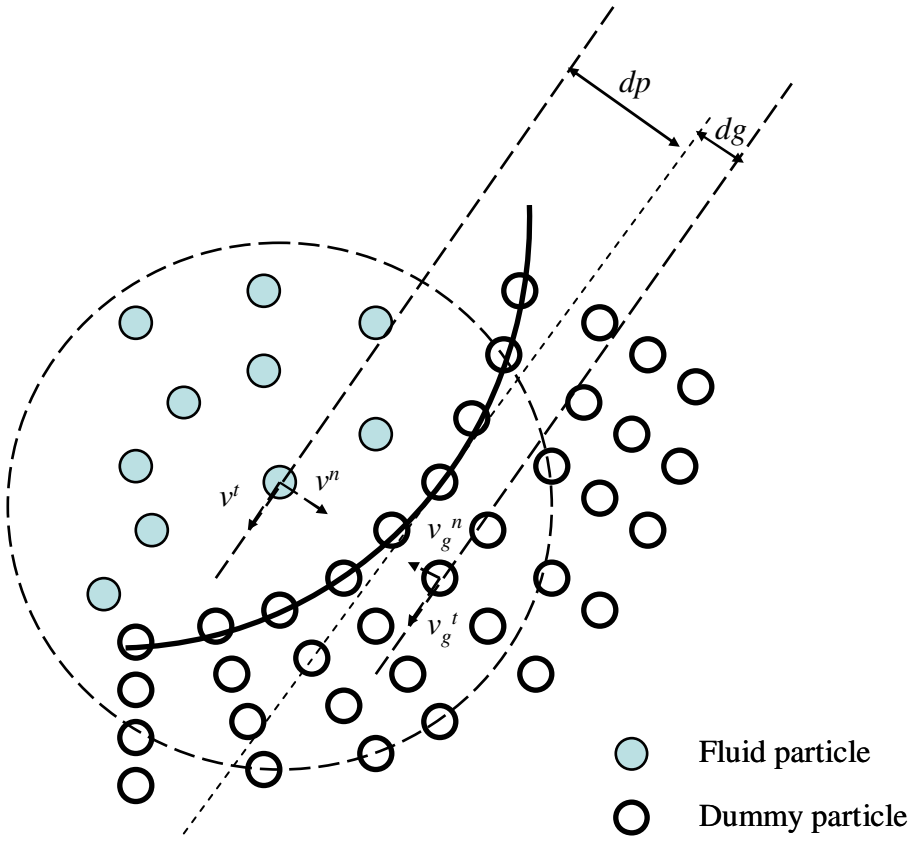

Fig. 4.19. Dummy particle set up near the boundary.

4.2.5. Performance of the improved WCSPH model with generalized boundary modelling technique

4.2.5.1. Simulation of dam break flow

The performance of the WCSPH model including boundary effect is tested with the benchmark dam break problem. The domain is same as discussed in the first dam break problem in subsection 4.2.1. This problem has been addressed using the present SPH model with both Ghost Particle (δ- SPH- GP) and Dummy Particle (δ- SPH-DP) approaches. A comparison of the position of the bore front traced with respect to time is shown in Fig. 4.20. The solution has been found to be recovered with the boundary modelling technique described in Eqn. (4.7) and Eqn. (4.8) using dummy particles. The difference between the experiment and numerical prediction may be due to the bottom wall stress which has not been intentionally incorporated into the SPH models.

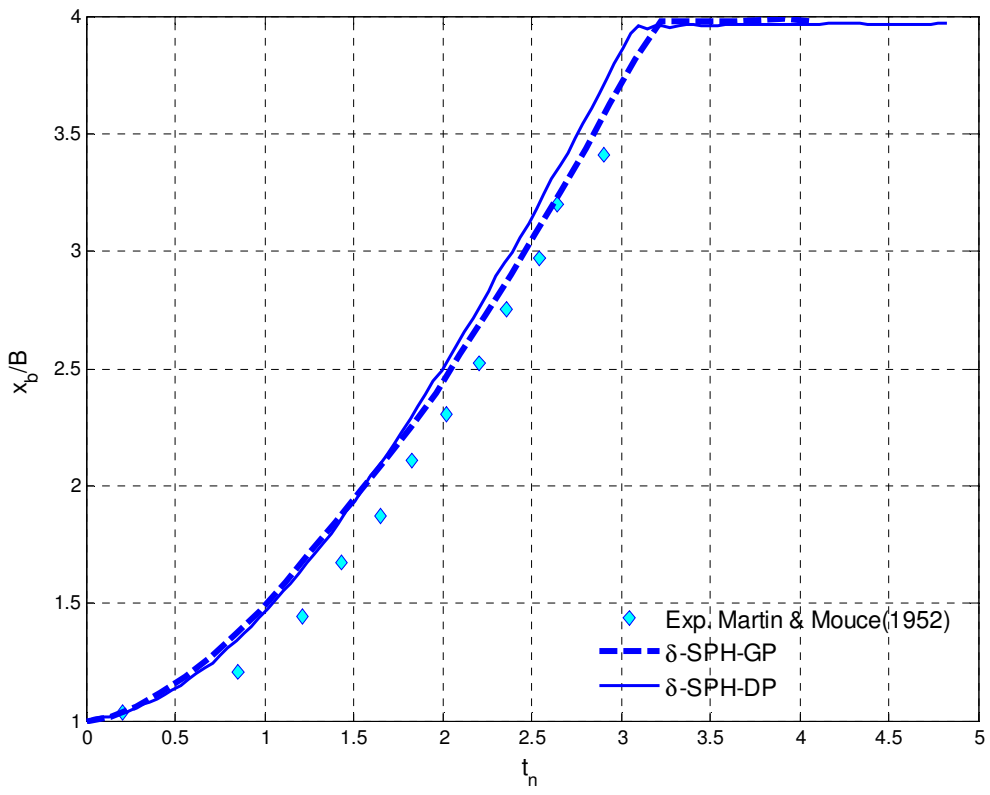

Fig. 4.20. Comparison of the instantaneous bore front position between the present SPH models with two different boundary modelling techniques.

While analysing the elapsed CPU time for running 1.5s of physical time for this case, both SPH models have been run in coarse ($npx \times npz = 25 \times 50$, npx, npz being number of particles along X and Z coordinates respectively) and finer (50×100) resolution. The average time step has been 8.0×10^{-4} s. The computations were performed in a 2.6GHz intel® Dual- Core, 2GB Ram Desktop PC.

Table 4.1: Details of the elapsed CPU time for running dam break case by the present SPH models

SPH model	resolution	elapsed CPU time (s)	resolution	elapsed CPU time (s)
δ- SPH- GP	25×50	331.2500	50×100	5514.594
δ- SPH-DP	25×50	227.9219	50×100	3782.125

The elapsed CPU time for these two SPH models is presented in Table 4.1. It has been found that irrespective of the increase in resolution, the computation cost reduced by 30 % in δ- SPH-DP compared to δ- SPH- GP.

4.2.5.2. Simulation of dam break with an obstacle

The performance of the improved WCSPH model with the boundaries modelled using dummy particles, has further been investigated by introducing a complicated geometrical shape into the domain of the dam break problem. The resulting domain is shown in Fig. 4.21 and has been adopted from Marrone et al. (2011a). Fig. 4.22 shows the comparison of the predicted free surface profile from the present WCSPH model with that of Marrone et al. (2011a). The present WCSPH model provides free surface profile which is very close to that of Marrone et al. (2011a) at different time instants. The evolution of resulting strong jet due to impact of the incoming bore (t_n= 3.53) with the obstacle is also predicted satisfactorily.

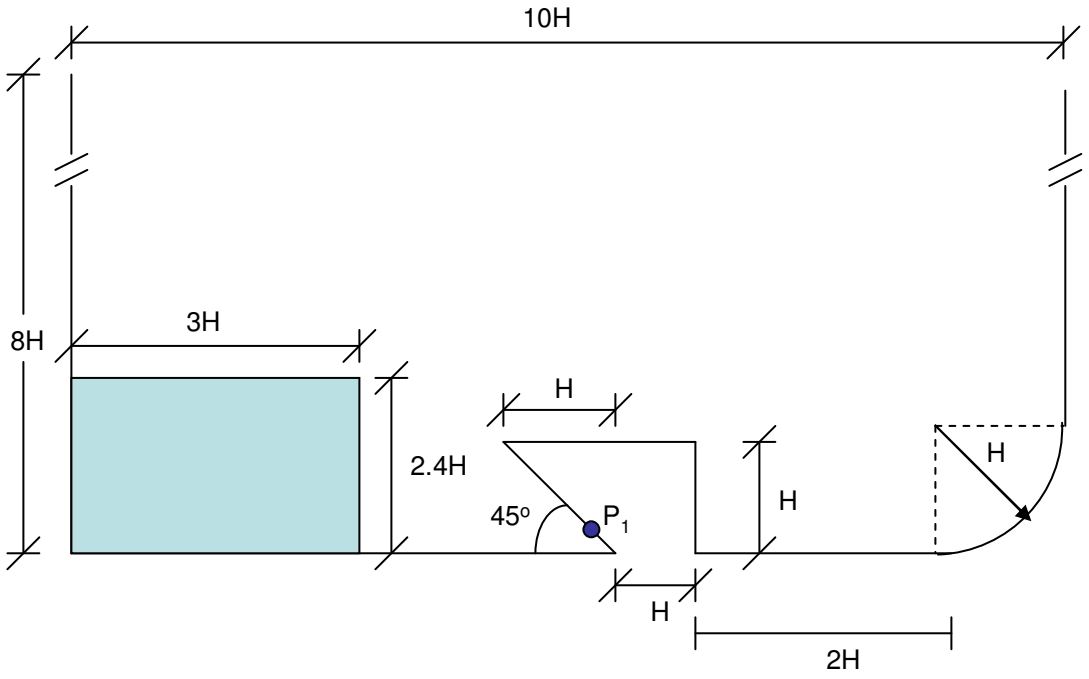

Fig. 4.21. Schematic of the domain used for simulating the case of Dam Break with obstacle.

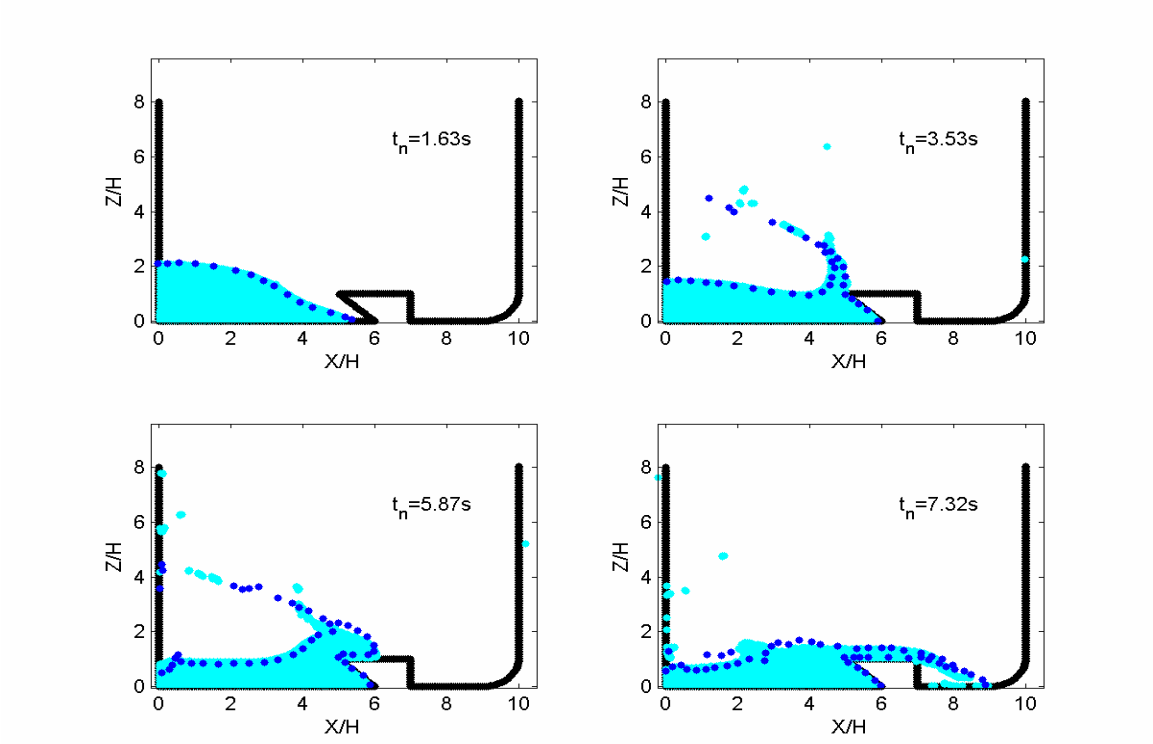

Fig. 4.22. Comparison of the free surface profile for the Dam Break with obstacle case as predicted by the present SPH model with that of Marrone et al. (2011a) (blue dots). $t_n = \sqrt{(t|\boldsymbol{g}|/H)}$.

4.2.5.3. Simulation of solitary wave breaking over a mildly sloping beach

The next test case to highlight the robustness of the present improved WCSPH model is the gradual breaking of solitary wave crest as it propagates over a mildly sloping beach. The domain used is shown in Fig. 4.23. The left boundary of the domain is moved to generate solitary wave of desired height. This problem has been investigated by Li and Raichlen (2003) through laboratory experiments. They provided photographs with close shots near the solitary wave as it breaks over the slope. The height of the solitary wave at offshore region is 0.057m. For the given slope (1:15) and wave height, as the solitary wave gradually propagates over the slope, its' steepness increases due to the effect of shoaling. At the last stage, a bore is formed which breaks as a plunging breaking wave.

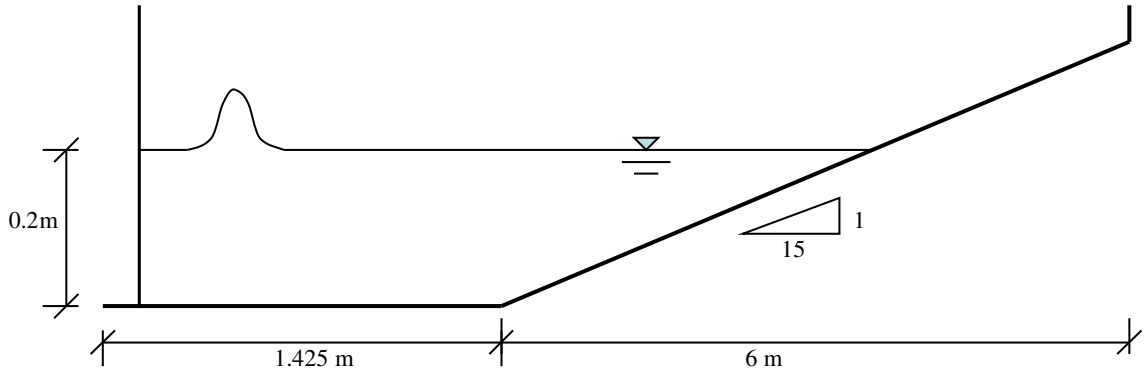

Fig. 4.23. Schematic of the domain used for simulating solitary wave breaking over slope.

Similar problem has been simulated by a number of researchers using different numerical methods: Boundary Element Method (BEM) (Grilli et al., 1997; Fochesato and Dias, 2006), Finite Element Method (FEM) (Yan and Ma, 2010), Meshless Local Petrov Galerkin Method (MLPG) (Ma and Zhou, 2009), Finite Volume Method (FVM) (Xie ,2012), Corrected ISPH (Khayyer et al., 2008) and WCSPH with turbulence model (Issa et al., 2010). Experience from the present study has shown that the correct reproduction of the plunging breaking may not be obtained with the SPH model if the boundary is modelled using standard ghost particle technique. Small errors due to rounding off exact value of sine or cosine functions while positioning the ghost particles at every time step to model the slope, have resulted in overall different flow physics (like a spilling

breaking instead of a plunging breaking), even after using very fine resolutions (high number of fluid particles). The required performance from the WCSPH model has been obtained by using dummy particles to model boundaries and accurate interpolation of the flow properties by using Eqns. (4.7- 4.8).

A qualitative comparison of the present SPH model prediction with that of experimental snapshots (Li and Raichlen, 2003) is shown in Fig. 4.24. Although the present WCSPH model reproduces the formation of plunging jet prior to breaking, formation of cavity (i.e., a void for the present single phase model) and post breaking jet, the overall shape of the breaking wave could not be captured well. However, the evolution of the wave after the first breaking depends on turbulence effect (as can be seen in the experimental photographs). The effect of choosing a particular turbulence scheme in reproducing the jet at the post breaking stages using SPH has been reported by Issa et al. (2010).

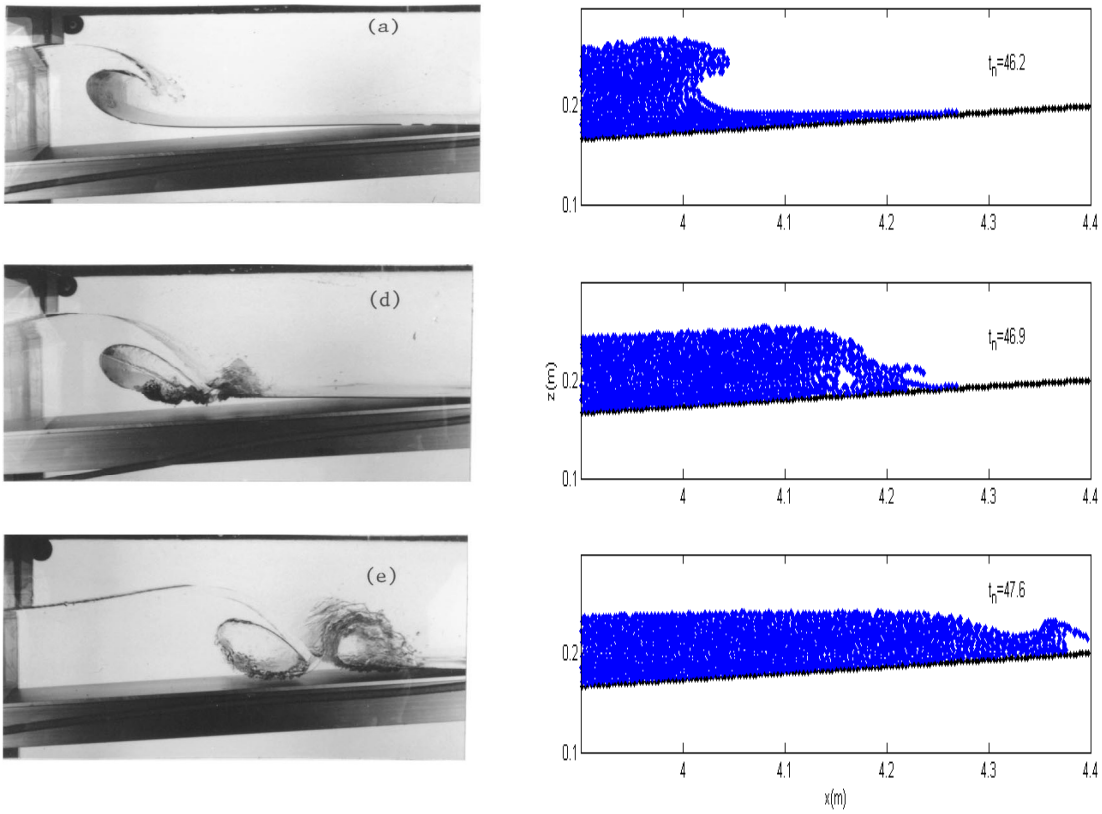

Fig. 4.24. Experimental photographs and snapshots at different time instants from SPH simulation of solitary wave breaking.

4.3. IMPROVED ISPH MODEL

The major improvement in the present ISPH model has been achieved by enhancing its stability through different ways. The boundary is modelled by using wall particle and a fixed layer (depending on the radius of the support domain) of particles called dummy particles. The Pressure Poisson Equation (PPE) is solved on the wall particles. The pressure of the wall particle is transferred to the dummy particle which is next to the wall particle in the normal direction. In this way, Neumann boundary condition for pressure (Eqn. 3.48) is enforced. Moreover, the dummy particles are involved in calculating density of the wall particle in order to keep the density consistent with the nearby fluid particle. For most of the cases ghost particles are not used in ISPH model. However, Liu et al. (2013) has shown improvement in the performance of the ISPH model using Ghost Particles instead of using Dummy particles. In the present ISPH model, Dummy Particles are used with the enforced velocity by Eqn. (4.8).

The corrections adopted in the present ISPH model to enhance the stability are described now.

4.3.1. XSPH smoothing of the velocity field

The pressure is calculated by solving PPE based on a pressure- velocity coupling procedure. So, maintaining an overall smooth velocity ensures a smooth pressure field and vice versa. The easiest way of achieving this is by applying XSPH technique (Eqn. 3.33) which is quite common in WCSPH modeling. The same procedure has been adopted in ISPH following Barcaloro et al. (2012). The XSPH technique also helps to maintain uniform particle distribution to some extent. There are many other approaches available in literature to prevent unrealistic accumulation of particles during simulation: Lennard- Jones repulsive force based correction (Shadloo et al., 2011), particle shifting methodology based on first order Taylor series expansion for the hydrodynamic variables (Xu et al., 2009) etc. The XSPH technique has been used solely in the present study due to its conceptual simplicity and ease in implementation.

4.3.2. Multi- Source term for the PPE

Khayyer et al. (2009) has shown that using a higher order source term for PPE, the ISPH prediction can be improved during impact. However, in this study, a mixture of the two

mostly adopted formulation for source term, that is based on velocity divergence and the time derivative of particle density are used. The combined source term is rewritten as:

$$\nabla.\left(\frac{1}{\rho_*}\nabla p_{t+\Delta t}\right)=\alpha\frac{\rho_0-\rho_*}{\rho_0\Delta t^2}+(1-\alpha)\nabla.\boldsymbol{v}_* \tag{4.9}$$

Similar approach has been adopted by Ma and Zhou (2009) and Asai et al. (2012). The source term in Eqn. (3.44) is obtained by simply setting relaxation factor α as 0.0. The value of α is chosen in the range of [0.0- 0.1]. The dam break problem has been considered to investigate the effect of α. Fig. 4.25 shows a snapshot of a dam break simulation using two values of α. At the time instant when the bore makes impact on the structure, the fluid particles are scattered unrealistically when only the single term (Eqn. 3.44) is used. Whereas, the prediction is improved by using Eqn. (4.9) with α = 0.1. So, for studying wave impact problems due to violent wave structure interaction, this correction is preferred.

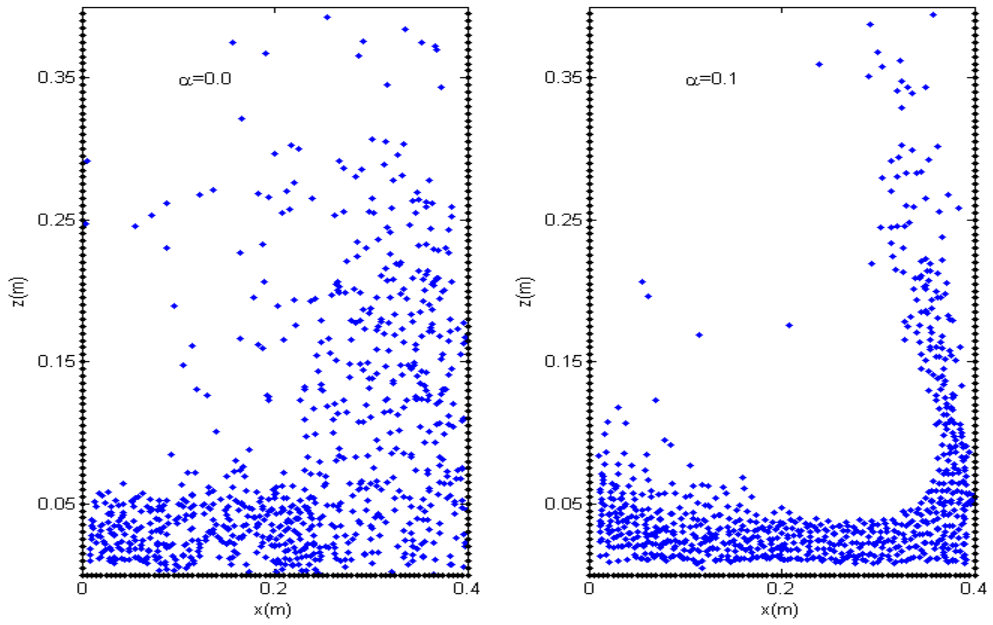

Fig. 4.25. Performance of the ISPH model for two different values of density relaxation factor α.

4.3.3. Enforcement of ISPH with Divergence Free and Density Invariant (ISPH_DFDI, Xu et al., 2009; Hu and Adams, 2007)

Although the adoption of multi source term in the PPE as discussed above, is an attempt to satisfy both divergence free velocity and density invariance, it is to be noted that the numerical technique applied to solve the resulting matrix is not a direct one. So, there occurs several time steps where these conditions are not satisfied and error is accumulated in the density field. As a second step to rectify this issue, the ISPH_DFDI approach is applied. It consists of an iterative scheme where at the end of a single ISPH step, the particle density is recalculated at the modified particle coordinates and the maximum density change is monitored.

$$\left.\begin{aligned} \frac{\Delta t^2}{2}\nabla\cdot\left(\frac{\nabla p}{\rho}\right)_i^{n,m-1} &\leftarrow \frac{\sigma_i^0-\sigma_i^{*,n+1,m-1}}{\sigma_i^0} \\ r^{n+1,m} &\leftarrow r^{n+1,m-1}-\left(\frac{\nabla p}{\rho}\right)^{n,m-1}\frac{\Delta t^2}{2} \\ \sigma_i^{*,n+1,m} &\leftarrow r^{n+1,m} \end{aligned}\right\} \qquad (4.10)$$

Here, $\sigma_i = \Sigma W_{ij}$. n represents a given time step and m represents the iteration step within the specified time step (n). The iterations continue until the maximum density change comes below a certain threshold. Although this requires to solve PPE multiple times in a single ISPH time step, it significantly improves the stability of the model. In most of the cases, the convergence in terms of variation in the maximum density is achieved in iteration steps of 3 to 5. Also, the number of times the Eqn. (4.10) is employed is not frequent. So, in overall the computational overhead is insignificant. Although the present ISPH model uses multi source terms, when ISPH_DFDI is used, only the first part is considered.

The effectiveness of the ISPH_DFDI scheme is investigated by studying the problem of regular wave propagation in a constant depth Numerical Wave Flume (NWF). The left boundary of the domain is moved sinusoidally to generate a regular wave in the domain. For this problem, around t = 3.25s, unrealistic particle accumulation occurs near the bottom boundary at a distance of 16m from the origin (Fig. 4.26). Due to this the spatial distribution of total pressure in the domain becomes spurious (as indicated by the colour

bar at t = 3.25s). At this moment, maximum permitted change in density is violated. Therefore, ISPH_DFDI algorithm becomes activated. Within a very short time, it stabilizes the pressure field by properly shifting the particles from the hot spot and brings the pressure within the desired limit. This is reflected in the subsequent time steps (e.g., t = 3.5s, 3.6s, 3.8s). Therefore, ISPH_DFDI may be useful to perform long time simulation using the ISPH model.

The improved WCSPH and ISPH models so described are then applied to make an inter comparison between them for two wave impact problems: dam break with an obstacle and breaking wave impact on a vertical wall.

4.4. INTER COMPARISON BETWEEN IMPROVED WCSPH AND ISPH

4.4.1. Dam break with an obstacle

The chosen problem domain is same as that adopted in section 4.2.5.2 (Fig. 4.21). The pressure time history at the probe location P_1 is obtained from WCSPH and ISPH models. These pressure time histories have been compared to that of Marrone et al. (2011a) in Fig 4.27. The δ- SPH prediction from Marrone et al. (2011a) was found to be in close agreement with that of a level- set simulation. Taking that as reference, it can be said that for this problem, WCSPH performs better than ISPH. The prediction for the primary peak is underestimated by almost 40 % in ISPH and 10 % in WCSPH. The pressure time history from WCSPH is found to contain less fluctuation than ISPH.

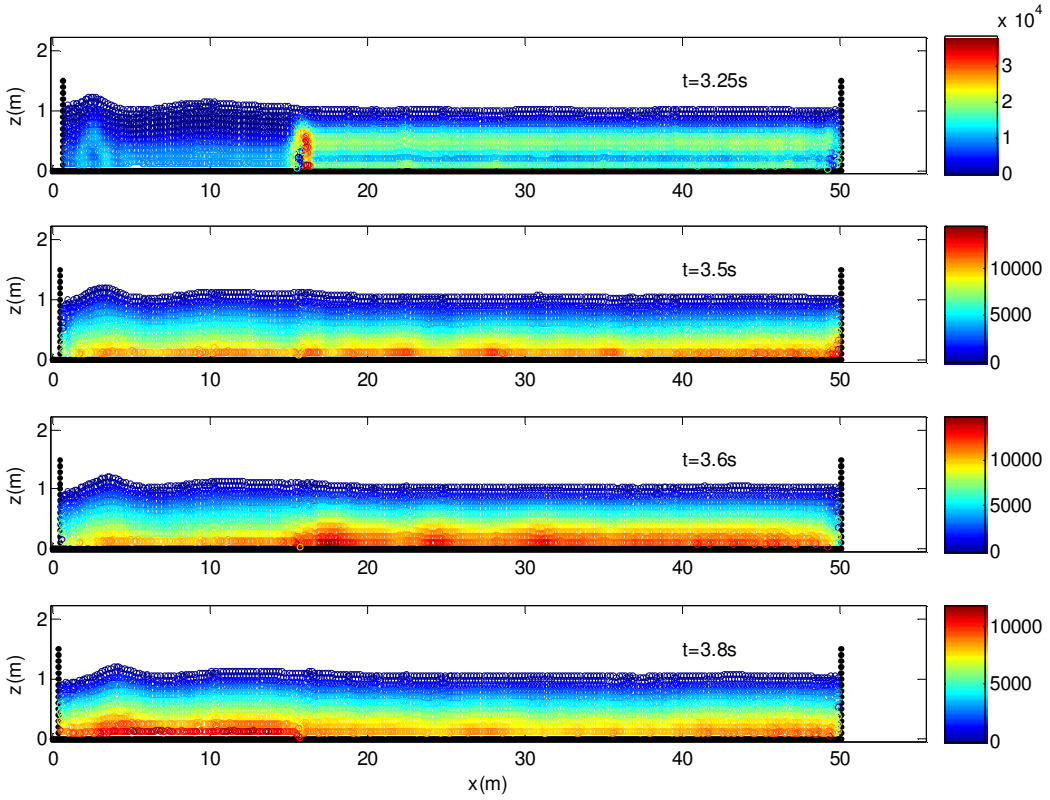

Fig. 4.26. Effect of ISPH_DFDI in maintaining stability in the pressure field for the problem of regular wave propagation in a NWF. The colourbar is of pressure (in Pa).

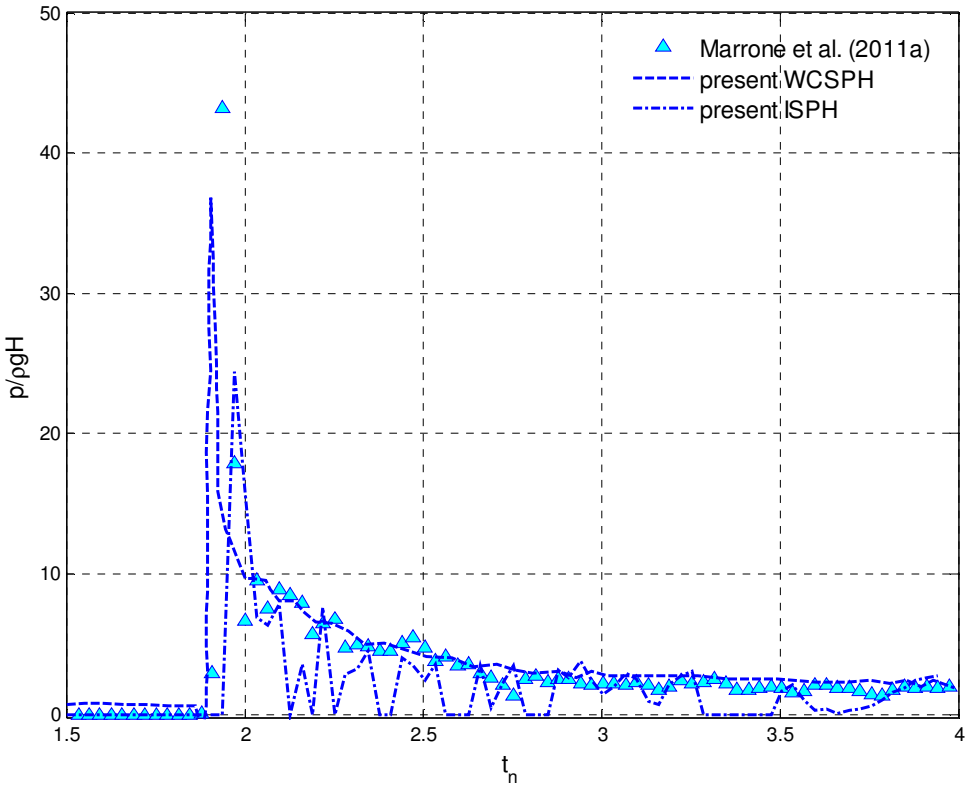

Fig. 4.27. Inter comparison between present WCSPH and ISPH for the pressure time history measured at a location on the obstacle facing a breaking dam.

4.4.2. Breaking wave impact

This test case has been taken from Khayyer and Gotoh (2009a) and the adopted domain is shown in Figure 4.28. For the given wave characteristics (wave height and period) and seabed conditions, a breaking wave impact has occurred during the first cycle of the wave impact. During the simulation, WCSPH and ISPH models record total pressure at the specified location. Figure 4.29 shows comparison for the pressure time history at the given probe location between WCSPH, ISPH and experimental measurements (Goda and Fukumori, 1972). t_s=0 denotes the time instant of maximum run up. The total duration of impact has been found to be better captured through ISPH. The peak pressure is underestimated by 30% in ISPH, whereas, it is overestimated by the same amount in WCSPH. However, as far as the ratio of the magnitude of the first peak to the second peak is concerned, this has been found to be closer to experiment in WCSPH compared to ISPH. Moreover, the amplitude of the pressure fluctuation in the improved ISPH model

as used in this study, is significantly less than reported for few versions of the MPS model of Khayyer and Gotoh (2009a). But, an overshoot near the second pressure peak is observed.

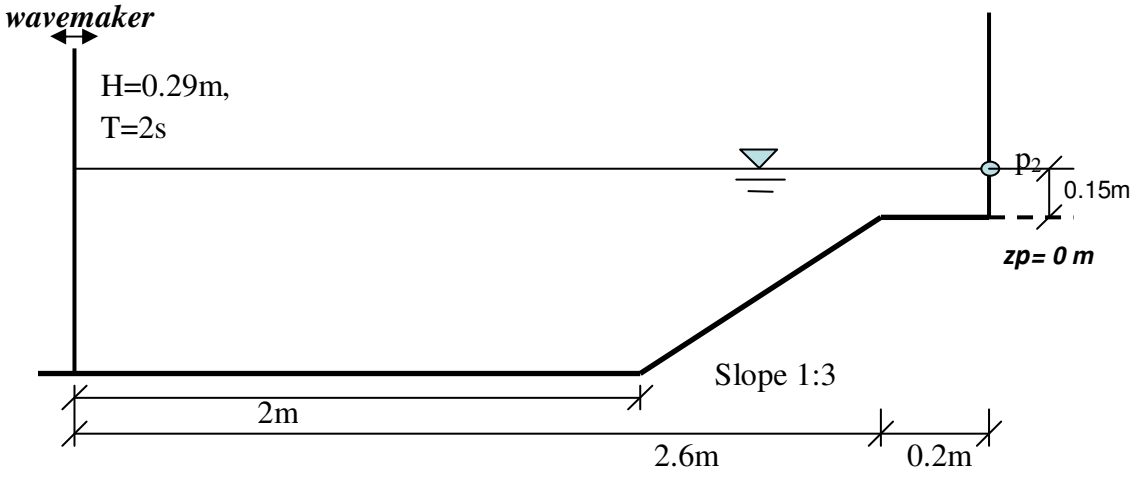

Fig. 4.28. Domain used for the simulation of slightly breaking wave impact over a fixed structure. p_2 is the pressure probe.

4.5. SUMMARY

The accuracy of a numerical model prediction depends on the way the boundary is modelled. Although different problems may be governed by the same governing equation (e.g., the Navier- Stokes equation), the boundary constraints are the key factors which make the dynamics different. In this chapter, the improvement to the WCSPH model has been successively developed mostly in terms of the boundary modeling techniques. This has been achieved by investigating the current version for different problems and then attempting a solution by combining few established techniques. Numerical tests with these improved versions have been found to work equally well when compared to the existing techniques (like standard ghost particle technique) for simple benchmark problem, apart from more complex problems. In this way, a robust and accurate WCSPH model has been obtained.

When comparing improved WCSPH and ISPH models for the same problem with defined input parameters, it has been found that difficulties arise to form a general

conclusion about the suitability of a particular scheme for a problem. Both schemes have been found to poses similar features; yet their relative outcome changes depending on the problem. Therefore the performance of these schemes may be related with the Re of the flow. In general, all SPH schemes employed in this study have been able to describe the free surface profile, in particular when the motion is violent.

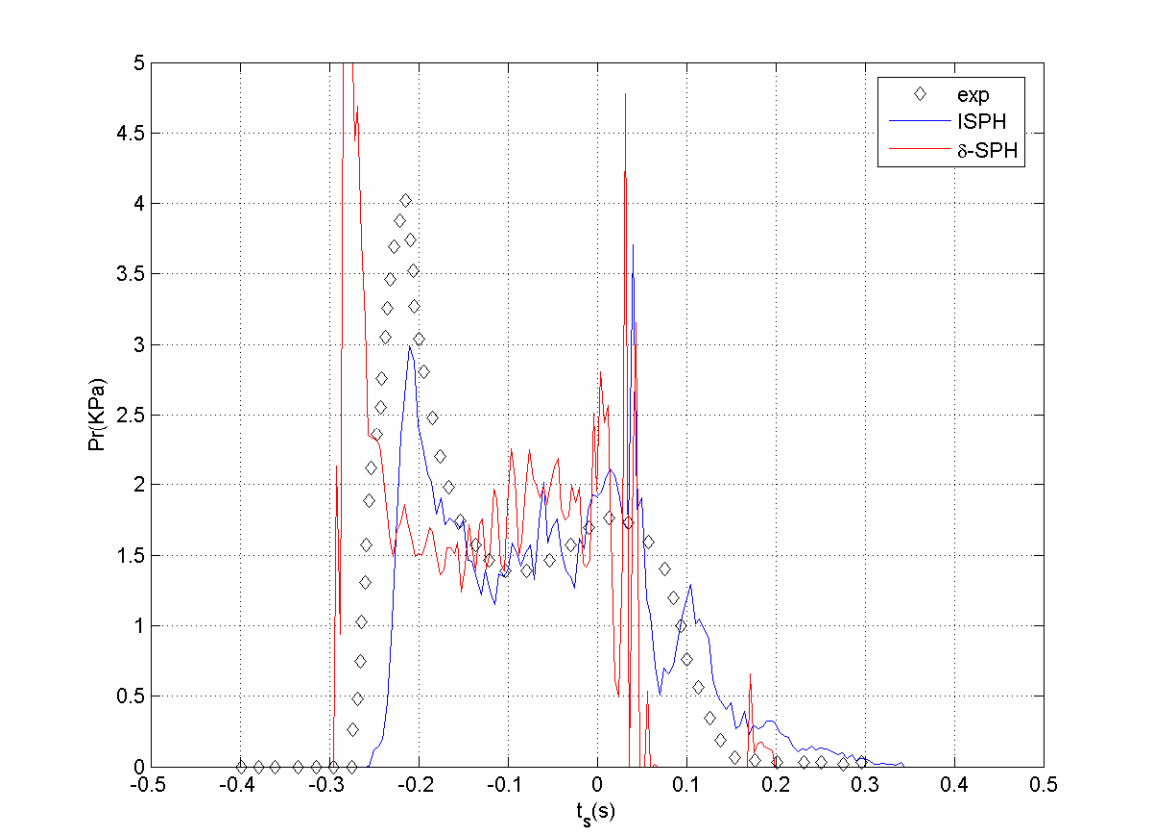

Fig. 4.29. Comparison for the pressure time history at pressure probe p_2.

CHAPTER 5
SLOSHING

5.1. GENERAL

Sloshing is a phenomenon of dynamic evolution of the free surface of the fluid in a partially filled container undergoing external excitation. The study of highly nonlinear water waves due to sloshing has gained significant attention for its relevance in different sectors of industrial application and therefore is regarded as one of the important problems in the broad category of fluid- structure interaction. Closed form analytical solution for different physical parameters (like wave elevation, pressure etc.) involved in sloshing can be found in the works by Ibrahim (2005) and Faltinsen and Timokha (2002). Numerous works based on different methods like finite element method (Wu et al., 1998; Sriram et al., 2006b), finite difference method (Frandsen, 2004; Kim, 2001; Kishev et al., 2006) and finite volume method (Löhner et al., 2006) have also been conducted to simulate sloshing waves. Efficient and accurate capturing of the free surface in sloshing flows have always been a challenging task in both analytical and grid based numerical models, irrespective of the fact that whether it solves a potential flow based formulation or full set of Navier-Stokes equations. Consequently, mesh-free or particle based methods have been preferred to study violent sloshing flows.

Smoothed Particle Hydrodynamics (SPH) has been regarded as the most successful method in simulating sloshing (Bouscasse et al., 2013b; Colagrossi, 2005; Colagrossi et al., 2006; Chen et al., 2013; Delorme et al., 2009; Hu et al., 2011; Rafiee et al., 2011; Shao et al., 2012; etc.) along with Incompressible SPH (ISPH) (Bockmann et al., 2012; Khayyer and Gotoh, 2009b) and other mesh-free or particle based methods like Moving Particle Semi Implicit (MPS) (Khayyer and Gotoh, 2013; Kim et al., 2011); Constraint Particle Method (CPM) (Koh et al., 2013) and so on. Stability issues for the violent sloshing flows in higher Re numbers have extensively been studied by Rafiee et al. (2012) with three versions of SPH, namely, Godunov SPH (GSPH), WCSPH and ISPH. But, apart from the work of Hu et al. (2011), the applicability of SPH in simulating non violent sloshing waves has rarely been reported. In non violent sloshing flows, the free

surface oscillates from lower to higher order harmonics. This particular nonlinearity of the problem is more challenging in a particle based model whose consistency properties have not been fully revealed yet. However, the applicability of SPH method in capturing subtle free surface nonlinearity was probably first demonstrated by Antuono et al. (2011) where wave focusing was simulated by δ- SPH. On the other hand, the quantification on physical and numerical dissipation associated with SPH simulation of standing wave was shown by Colagrossi et al. (2013). Convergence studies were performed there based on error analysis in SPH approximation by Quinlan et al. (2006). With these works, δ- SPH seems to be a promising technique to study sloshing waves for both non violent and violent cases. Present work investigates the performance of δ- SPH for such cases with focus on selection of proper range of values for smoothing length and XSPH factor. Selection of proper value of smoothing length has been found to be of fundamental importance in order to capture the nonlinearity of the free surface correctly. Inter-comparison has been performed with few other versions (namely, fully incompressible SPH (ISPH) and the standard weakly compressible SPH (WCSPH)) for selected cases, showing capability of the present δ- SPH in predicting a smoother pressure field similar to ISPH than WCSPH. The present model prediction has been validated by making comparison with analytical and FEM model for non violent cases and with experiments for violent cases.

5.2. MATHEMATICAL FORMULATION

The sloshing waves are generated in a 2D rectangular tank (Fig. 5.1) through different modes of excitation. The origin of the global coordinate (x, z) system lies at the bottom left corner of the tank when it is at rest (i.e., at time t= 0). The tank is moved with respect to time and the governing equations (Eqn. 3.1 and Eqn. 3.2) are represented with respect to the Cartesian coordinate frame of reference.

5.2.1. Modes of excitation

The purpose is to understand the formation of the nonlinear water waves due to the horizontal movement of the sloshing tank which undergoes either regular or random excitation. These two modes of excitation are prescribed as follows.

The regular harmonic tank excitation is represented either by cosine or sine variation.

$$\boldsymbol{X}(t)=\begin{cases} a_h \cos\left(\omega_h t\right), \ or, \\ a_h \sin\left(\omega_h t\right) \end{cases} \tag{5.1}$$

where, a_h is the amplitude and ω_h is the angular frequency of the oscillation. Due to sloshing, the oscillating free surface can attain different mode shapes. The frequency of these individual modes can be obtained from dispersion relationship from the first order linear wave theory.

$$\omega_n^2 = |\boldsymbol{g}| k_n \tanh(k_n d) \text{ with n=1,2,3..} \tag{5.2}$$

where, k_n is the wave number ($k_n=n\pi/L$, L being the tank length) and d is the initial water depth inside the container. n denotes the corresponding free surface mode.

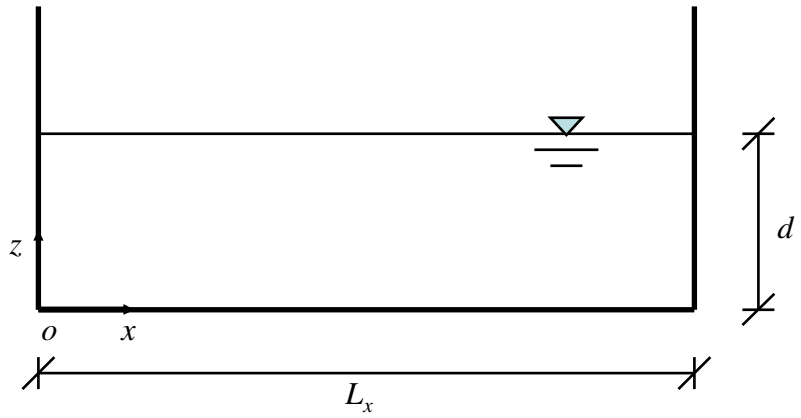

Fig. 5.1. Sloshing tank with its coordinate frame of reference.

The Bretschneider spectrum is used to obtain a random tank excitation time series. The spectrum distribution is given as,

$$S(\omega)=\frac{5H_s^2}{16\omega_p}\left(\frac{\omega_p}{\omega}\right)^5 \exp\left[-\frac{5}{4}\left(\frac{\omega_p}{\omega}\right)^4\right] \tag{5.3}$$

Here, ω_p and H_s are the peak excitation frequency and significant wave height, respectively. Depending on the knowledge of spectrum, the random time series is obtained as,

$$\boldsymbol{X}(t)=\sum_{i=1}^{N_\omega} A_i \sin\left(\omega_i t+\theta_i\right) \tag{5.4}$$

with $A_i=\sqrt{\{2S(\omega_i)d\omega\}}$, N_ω is the number of frequency components and θ_i is a random phase in the range (0, 2π). The spectrum distributes over a small non- zero frequency component to a cut- of frequency ω_c (ω_c= $5\omega_1$, ω_1 being the first mode of tank natural frequency). Moreover, as per the requirement from the numerical model, the following ramp function ($R(t)$) is multiplied with the input random time series to avoid high transitory motion.

$$R(t)=\begin{cases}\dfrac{1}{2}\left[1-\cos\left(\dfrac{\pi t}{t_r}\right)\right], & 0\le t\le t_r\\ 1 & , t>t_r\end{cases} \tag{5.5}$$

where, t_r is taken as some fraction of the peak excitation period.

5.2.2. Analytical Solution

Assuming the inviscid fluid, irrotational flow and the small amplitude of excitation for the sloshing, the following basic sloshing flow quantities (i.e., first order velocity potential φ, velocity $\boldsymbol{v}(u,w)$ and pressure, p) are obtained from the analytical model of Wu (2007) under regular harmonic tank excitation.

$$\varphi=\sum_{n=1}^{\infty}B_n(t)\frac{\cosh\left[k_n(z+d)\right]}{\cosh(k_nd)}\cos\left[k_n(x+0.5L)\right] \tag{5.6}$$

$$p=-\rho(\varphi+\boldsymbol{g}.\boldsymbol{z}) \tag{5.7}$$

$$\left.\begin{aligned}\boldsymbol{u}&=\frac{\partial\varphi}{\partial x}\\ \boldsymbol{w}&=\frac{\partial\varphi}{\partial z}\end{aligned}\right\} \tag{5.8}$$

where,

$$B_n(t)=-\frac{(-1)^n-1}{k_n^2 0.5L}\omega_n\int_0^t\dot{\boldsymbol{X}}(\tau)\sin\omega_n(t-\tau)\,d\tau \tag{5.9}$$

$\dot{X}(\tau)$ contains the instantaneous tank excitation velocity which can be obtained from Eqn. (5.1) by taking derivative with respect to time. The origin of the coordinate system in the analytical model is at the middle of the initial free surface when the tank is at rest. The above analytical solution is used to validate SPH model prediction for non violent sloshing cases.

5.3. SPH MODEL SET-UP

Before discussing the performance of the SPH model for various sloshing test cases, it is required to analyze the dependence of the performance of the model on different input parameters and the choice of the particular scheme.

5.3.1. Resolution

As mentioned in the earlier cahpters, nodes/ particles serve both the purpose of interpolation and advection of required properties in SPH and an improper resolution leads to poor overall approximation. Therefore, the performance of a SPH solver is much more sensitive on selection of proper resolution, compared to that of a grid based solver like FEM/FDM. The resolution has been selected depending on the following two tests as described below. Mathematically, the resolution property has been represented as the ratio of the tank length to the adopted initial particle spacing.

5.3.2. Standing wave problem

While investigating the applicability of SPH method for long time simulation of non-violent gravity waves, the choice of resolution was done by observing the decaying of the total kinetic energy of the system by Antuono et al. (2011). In this problem, the initial conditions are set to obtain a wave whose evolution can be described from first order linear wave theory, without any external forcing as follows.

$$\varphi(x,z,t) = -\left(\frac{a|\boldsymbol{g}|}{\omega}\right)\frac{\cosh\left[k_n(z+d)\right]}{\cosh(k_n d)}\cos(k_n x)\cos(\omega t) \tag{5.10}$$

The initial condition for the velocity ($\boldsymbol{v}$) and pressure (p) field is shown in Fig. 5.2. The initial velocity is obtained from Eq. (5.8) at t= 0. The initial free surface is assumed to be horizontal, so pressure is purely hydrostatic. Theoretically, the standing wave remains

infinitely over time, whereas, due to the presence of artificial viscous terms in momentum equation, the waveform decays gradually and completely damps out after certain number of wave cycles. Defining, $\nu = \alpha C_0 h/8$ as numerical kinematic viscosity, the rate of decaying of the kinetic energy (E_{kt}) in the SPH model was measured as (Lighthill, 2001),

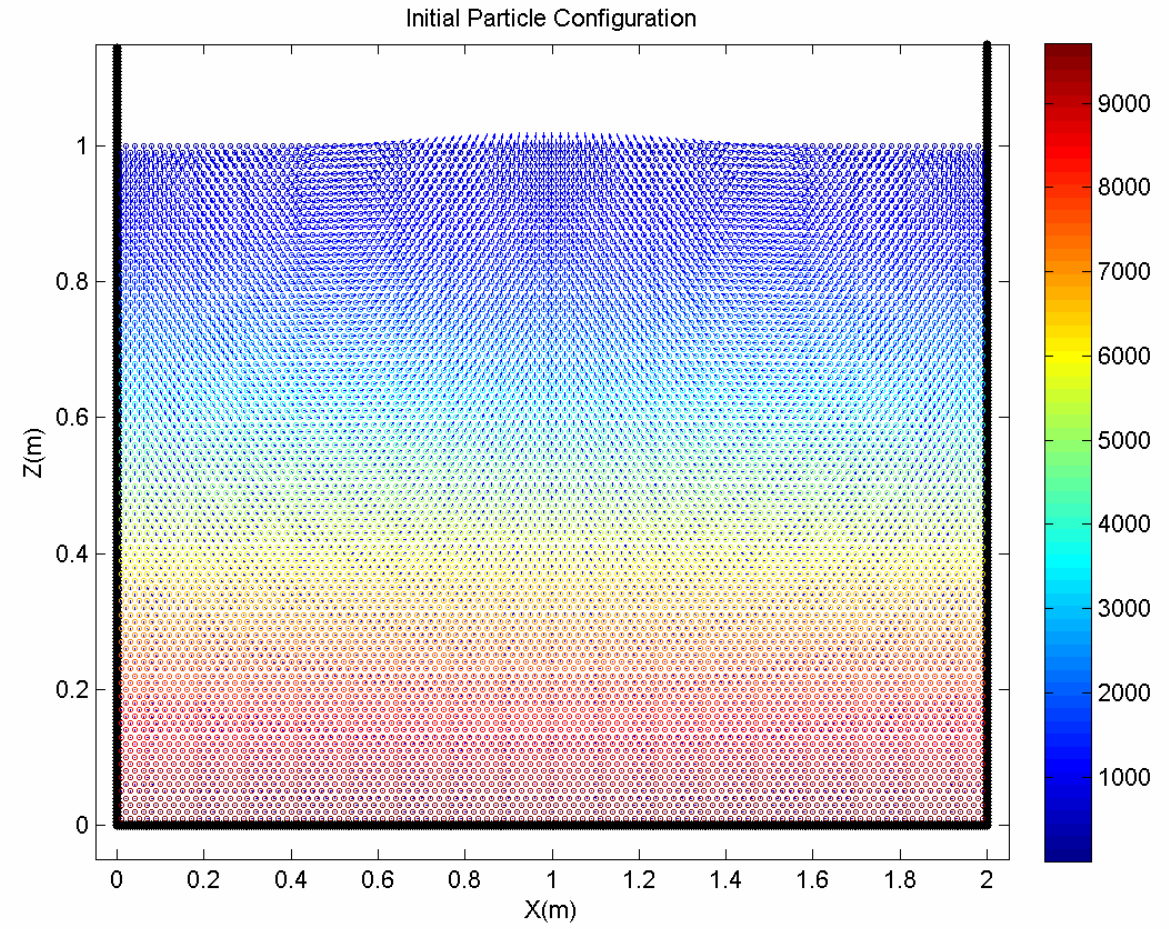

Fig. 5.2. Initial condition set up for the standing wave problem. L_x= 2m, d= 1m. The colour bar is of pressure (p) in Pa.

$$E_{kt}(t) = \left(\frac{2a}{d}\right)^2 |\boldsymbol{g}| \frac{Ld^2}{32} [\exp(-4\nu k_n^2 t)][1+\cos(2\omega t)] \tag{5.11}$$

where, L is the standing wave length and k_n is the corresponding wave number. Eqn. (5.11) gives approximate estimation for the decay of the initial standing wave amplitude.

It was concluded in particular that when the initial particle spacing is chosen close to the amplitude of the wave (a), the kinetic energy decays at a faster rate. Similarly, for non-violent sloshing wave that is desired to be simulated within the range of linear waves, the amplitude of the wave can be thought of to be linearly proportional to the amplitude of the external excitation. Therefore, the same study may reveal the interrelation between the amplitude of the sloshing wave which is proportional to the external excitation with the resolution needed.

For the non- violent sloshing cases, the adopted maximum amplitude of the external excitation was 0.1. So, keeping this as fixed and representative through the standing wave amplitude, the SPH model has run with different resolution. The comparative study has been depicted in Fig. 5.3. It shows that similar to the findings of Antuono et al. (2011), in the presence of the viscous terms in SPH scheme, the kinetic energy decays faster with lower resolution. For the resolution of 100, this decay has been found to be optimum with respect to the analytical solution (Eqn. 5.11).

5.3.3. Forced excitation

The resolution can further be decided from the convergence of the sloshing wave amplitude for a particular input excitation frequency and amplitude and then investigating the convergence with respect to another mesh based FEM solution of a fully non- linear potential theory (Sriram, 2008). For this case, following system characteristics has been considered: L_x= 1m, d=0.163m, $\boldsymbol{X}_t$=$a_h$cos($\omega_h t$). The excitation amplitude (a_h) and frequency (ω_h) have been taken as 0.03d and ω_1 , the first mode frequency, respectively. Since this is a resonance case (ω_h= ω_1), the δ- SPH model is required to predict the gradual increase in sloshing amplitude as time progresses when the damping effect is minimal. The comparison of the water surface elevation measured at the top left corner of the tank is reported for different particle resolutions in Fig. 5.4. Similar to the findings of the standing wave tests, increasing the resolution has been found to improve the SPH model prediction. Further with an increased resolution, a less noisy time history is recovered particularly at the initial stages. The duration of such noisy behaviour depends on the duration taken by the interior particles to get settled in a least fluctuating pressure field in contrast to a pressure field that is obtained through the δ- SPH scheme immediately after the hydrostatic pressure field prescribed at the beginning of the

simulation. So, a better resolution yields a saving in physical solution time that is needed for the particles to get settled in order to provide smoother prediction. From this test, the resolution of almost about 100 has been found to give better prediction. This confirms the findings from the standing wave tests.

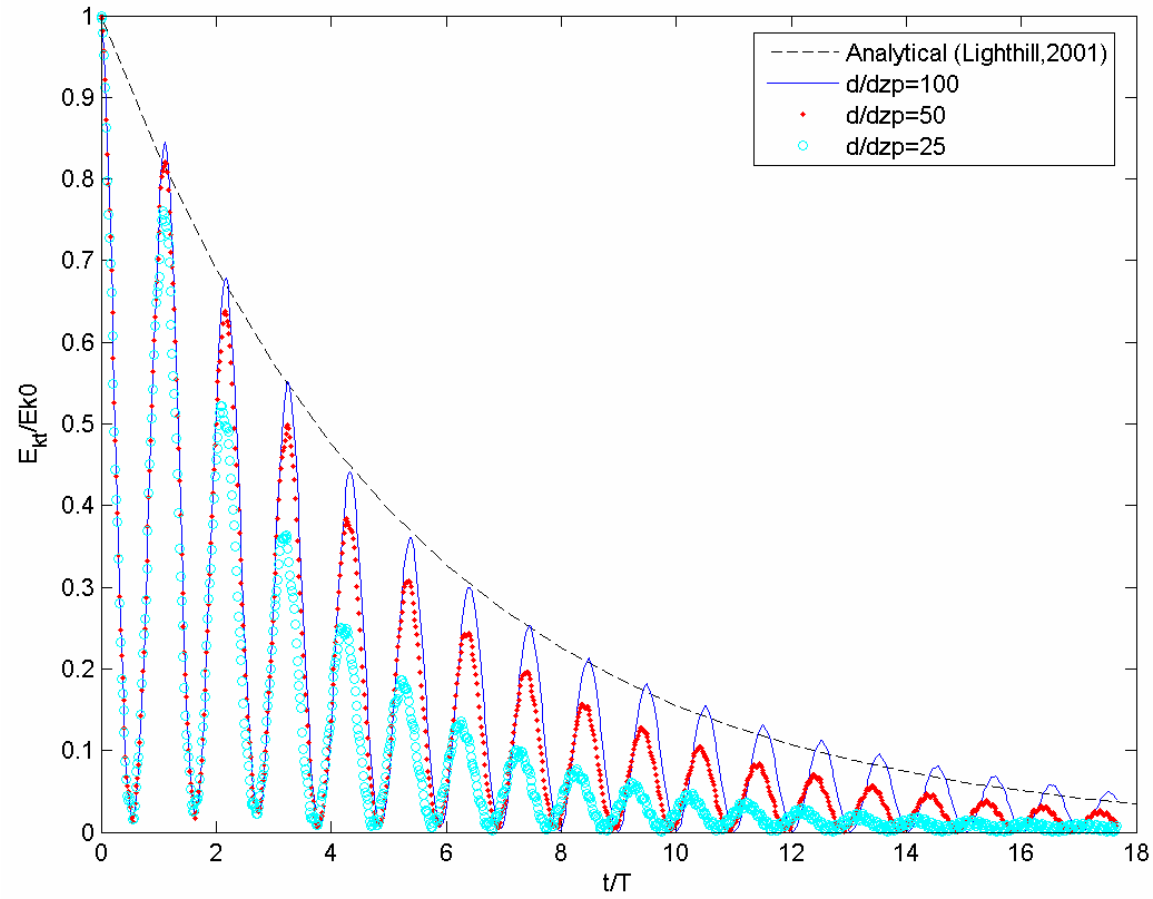

Fig. 5.3. Evolution of the kinetic energy in standing wave problem for different resolution of the SPH model. *T* is the standing wave period. *dzp* is the number of particles set along *z*- coordinate. Standing wave amplitude (*a*)= 0.1, α= 0.01, smoothing length(*h*)= 1.33*dzp*, *dzp*= initial particle spacing along z- coordinate.

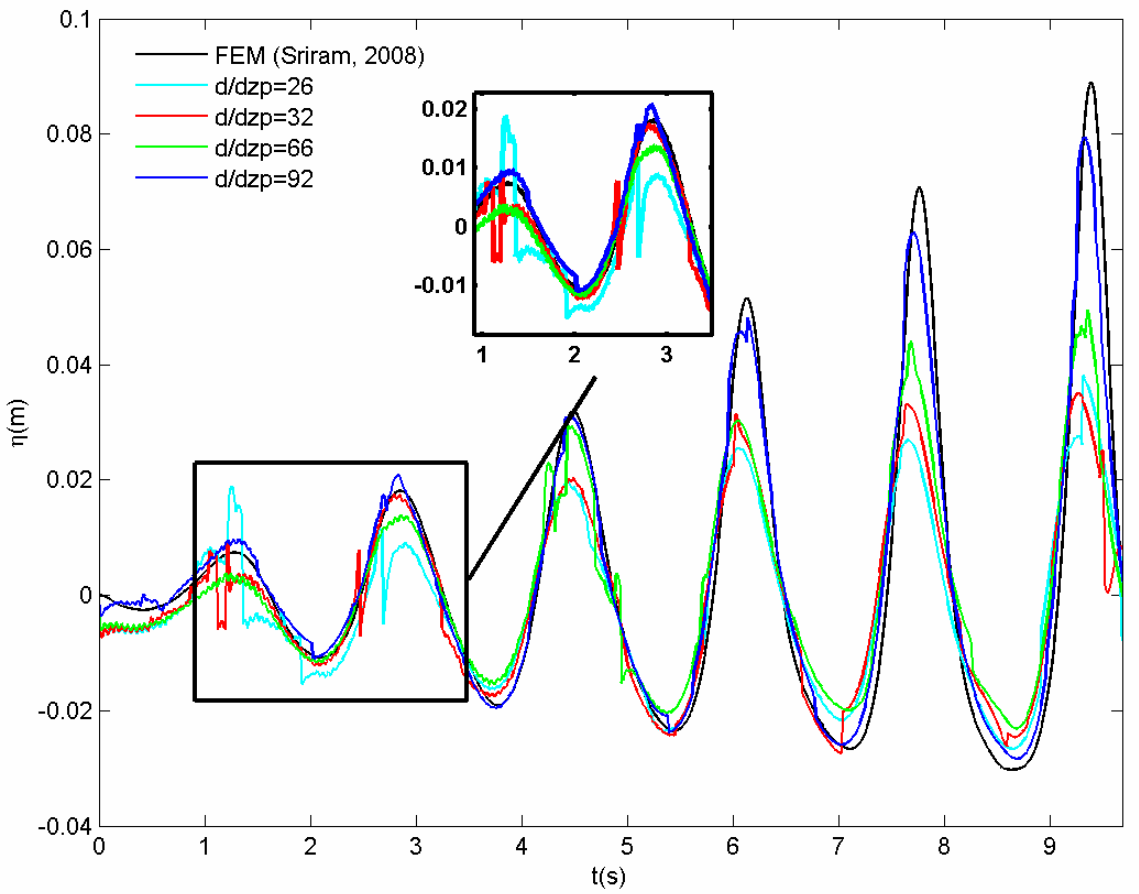

Fig. 5.4. Comparison of time history of the free surface elevation at the top left corner of the tank for various resolutions of the SPH model with FEM (Sriram, 2008).

The convergence study is performed by considering the variation of both smoothing length (h) and initial particle spacing (dzp). The convergence of the present δ- SPH model for the same sloshing test case with respect to the variation of h is considered. The reference solution for non violent sloshing has been adopted from FEM. Fig. 5.5 shows the variation of the L_2 error with respect to the variation of both d/h and h/dzp. For each case, discrete L_2 errors have been calculated based on the differences in the free surface profile predicted by present δ- SPH with FEM solution. The L_2 error has been calculated by taking time average of those discrete L_2 errors over the entire simulation time. It is found that the solution converges at a faster rate with an increase in the particle density. Moreover, while higher h/dzp is used, convergence has been achieved with relatively lower resolution compared to lower h/dzp. Similar findings were also reported by

Colagrossi et al. (2013), while studying evolution of standing waves. The computational efficiency is closely related with *h*/*dzp*. Therefore, the optimum choice of *h*/*dzp* is required to be found out. Further details are provided in the next section.

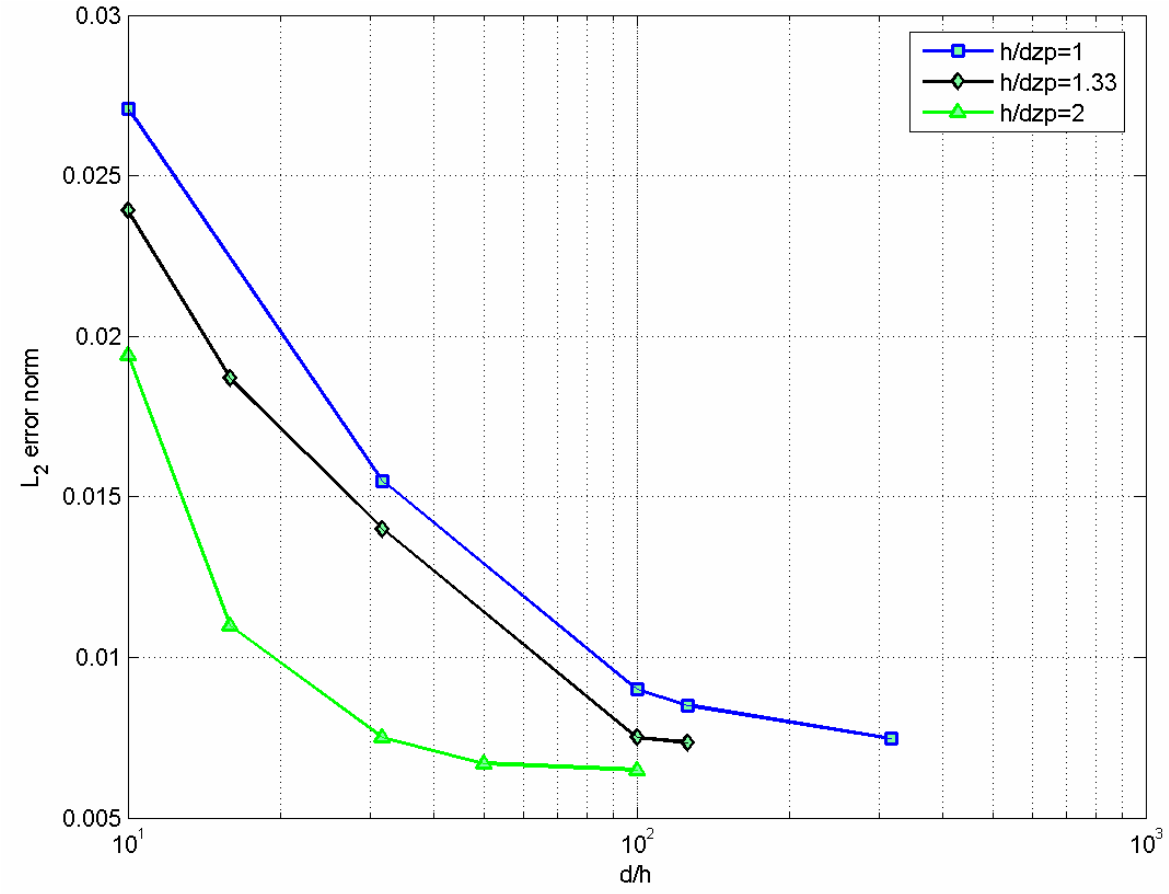

Fig. 5.5. Variation of the L_2 error norm with respect to initial particle spacing (d/h) and smoothing length (h/dzp).

5.4. SIMULATION OF NON VIOLENT SLOSHING

5.4.1. Regular excitation

The sloshing tank with L_x=2m, d=1m, ω_h=0.7ω_1 and a_h=0.05d is considered to analyse δ-SPH model prediction with analytical solution of Eqns. (5.6) to (5.8). The comparison for the overall velocity field between the analytical and SPH model is shown in Fig. 5.6 at t= 2s. The time instant is characterized by the onset of run up along the side wall. The prediction of the velocity field by δ- SPH model is found to be fairly accurate on

comparison with the analytical model. Note, the analytical model solves the no- slip boundary conditions for velocity exactly at the two side wall locations (i.e., at $x = \pm L/2$), whereas in the δ- SPH model, the velocity at the wall particles is prescribed according to the external excitation. Thus, the velocity field at the tank wall locations is not available from the δ- SPH model. The dynamic pressure time history measured at the top left corner of the tank in the SPH model is compared with that of analytical model as shown in Fig. 5.7. The pressure at the wall location is calculated using particle sampling method of Oger et al. (2006). The overall pressure field at different time instants for WCSPH, δ- SPH along with ISPH is shown in Fig. 5.8. δ- SPH predicts improved and smooth total pressure field similar ISPH compared to WCSPH. With the diffusive terms in the continuity equations in δ- SPH, unrealistic fluctuations in pressure time history have been substantially reduced compared to standard WCSPH.

Next, δ- SPH model prediction is compared with FEM (Sriram et al., 2006b) for the same sloshing test case. The comparison for the water surface elevation at the top left corner of the tank is shown in Fig. 5.9. δ- SPH model successfully captures the higher harmonics.

The effect of h/dzp is further investigated by checking its effect on the overall velocity field and associated smooth harmonic free surface. The sloshing flow velocity field along with the predicted free surface has been reported at three different time instants (t= 4s, 4.5s, 6s) and for three different h/dzp ratios (h/dzp = 1.0, 1.33, 2) in Fig. 5.10. Different harmonic waves induce their own velocity fields. In order to capture higher order harmonics in the free surface profile, the smoothness of the velocity field has been monitored. For h/dzp=1.0, the overall velocity field is noisy and the free surface profile does not show any higher order harmonics. Whereas, for relatively higher h/dzp value (i.e., 2), the velocity field is substantially improved to obtain a smooth field and predicts the higher order harmonics which is comparable with FEM simulation as discussed above. The intermediate h/dzp of 1.33, even though contains modest noise in the overall velocity field, has been found to be capable of predicting the higher order harmonics. Since the computational cost increases with h/dzp, the optimum choice of h/dzp is set by testing the velocity field.

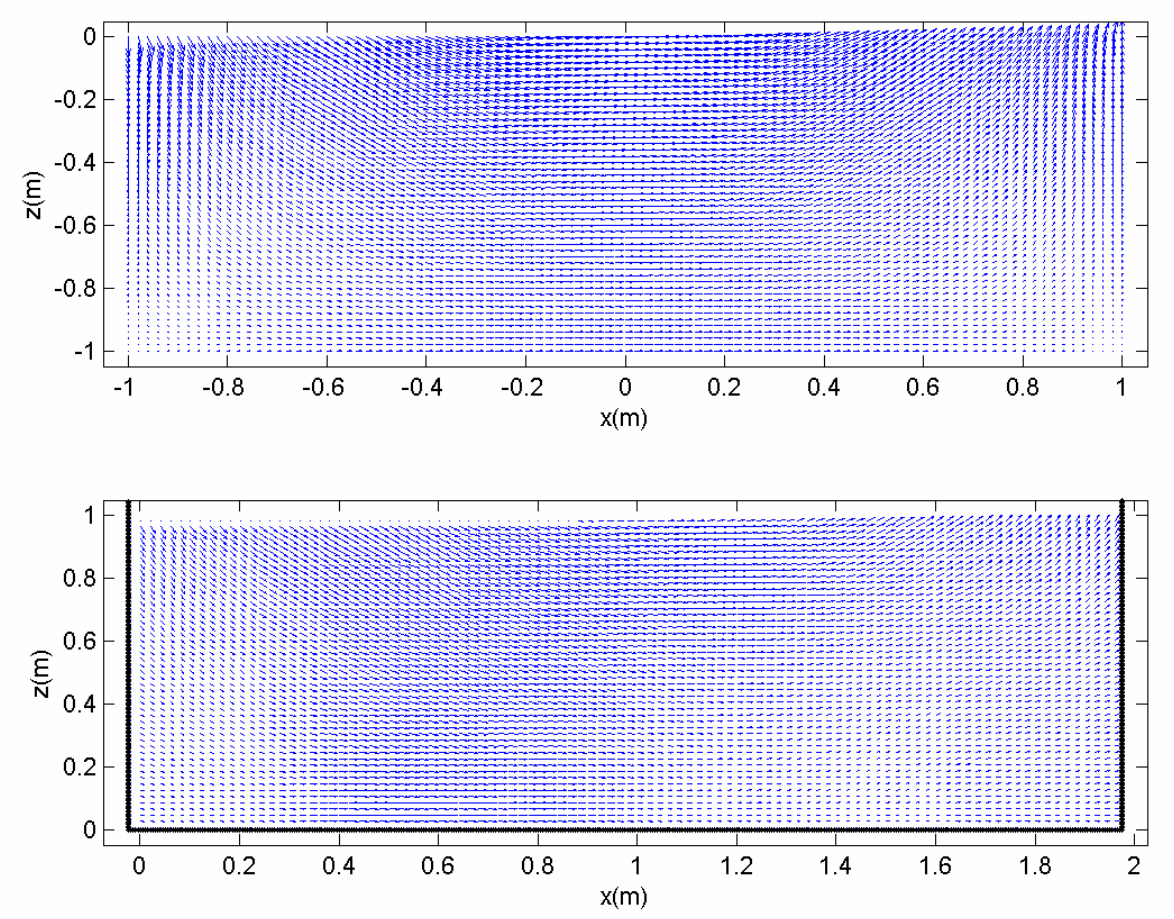

Fig. 5.6. Overall velocity field predicted at t= 2s using analytical (above) and SPH model (below).

The power spectra of sloshing oscillation for different tank excitation frequencies are shown in Fig. 5.11. At least twenty wave cycles are used to generate the spectrum. When the excitation frequency (ω_h) is less than the first mode natural frequency, the maximum spectral peak occurs at the excitation frequency. For excitation frequency equal to the first mode natural frequency, the significant peak is observed at the natural frequency due to the well known resonance condition. For excitation frequencies greater than the first mode natural frequency and less than second modal frequency, primary peak occurs at the second mode followed by a secondary peak at the first mode. When the excitation frequency is equal to or greater than third mode frequency, ω_3 (=1.8 ω_1), the third mode dominates the sloshing motion. Similar findings were obtained from the study based on the FEM model by Sriram et al. (2006b).

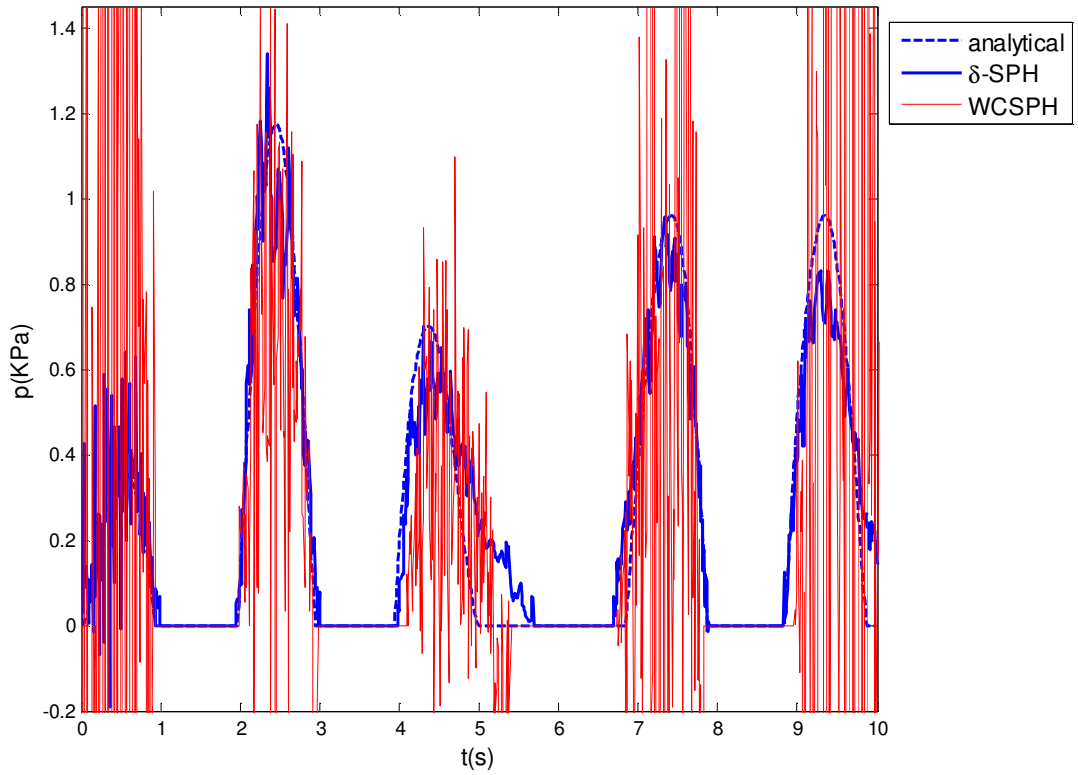

Fig. 5.7. Comparison for the pressure time history at the top left corner of the sloshing tank.

5.4.2. Random excitation

The present δ- SPH model has further been applied to simulate the sloshing waves under the condition of random horizontal excitation of the tank. The random excitation has been generated following Eqn. 5.4. The sloshing tank geometry is similar to the earlier test case. For $\omega_p=\omega_1$ and $H_s= 0.1d$, the time series of tank excitation, simulated free surface elevation and dynamic pressure at top left corner of the tank are presented in Fig. 5.12. The spectra of the measured water surface elevation at top left corner of the tank for various peak excitation frequencies are shown in Fig. 5.13. When the peak excitation frequency is less than or equal to the first mode natural frequency, the dominant frequency of the sloshing oscillation lies only at the natural frequency of the tank. This observation is in contrast with the case of regular tank excitation and in which case, a primary peak at the excitation frequency has been observed followed by a

secondary peak at the first mode of natural frequency. Whereas, when the peak excitation frequency is greater than first mode natural frequency, high frequency waves have been found to coexist which make the spectrum wider compared to the case when $\omega_p < \omega_1$. The maximum energy concentration occurred only at certain frequencies corresponding to higher modes of oscillation when $\omega_p > \omega_1$. This characteristic feature of sloshing oscillation can be positively utilized for an efficient operation of the sea going vessels.

5.5. SIMULATION OF VIOLENT SLOSHING

Meshless method like SPH has been successful in the field of nonlinear water waves, particularly when flow separation/ wave breaking takes place. Thus, for the present SPH model, it is important to investigate its capability to reproduce violent sloshing. The sloshing laboratory experiments conducted at Det Norske Veritas (DNV) (Rognebakke, 2002) have been considered in the first case. The tank length (L) and initial water depth (d) are 1.73m and 0.2m, respectively. The tank height (H) is 1.03m. This is a case defined by shallow water effects which is relatively difficult to simulate by analytical/ grid based model due to the formation of wave bores/ swelling up along the side walls. For an excitation period of 2.6s and amplitude of a_h/d= 0.025, δ- SPH simulation of free surface elevation at 0.05m from the left wall is compared with experimental measurements (Fig. 5.14). The capability of the δ- SPH model for long time simulation is achieved. The differences between the δ- SPH model prediction and the experimental measurements might be due to the difference in the tank excitation time series employed in numerical simulation and experiment. The measured tank excitation time history was not available. Though the input amplitude and excitation frequency are same for both experiment and δ- SPH, no ramp function has been used in δ- SPH model since it is a regular excitation case. But, ramp function is required in experiment to establish flow stabilities.

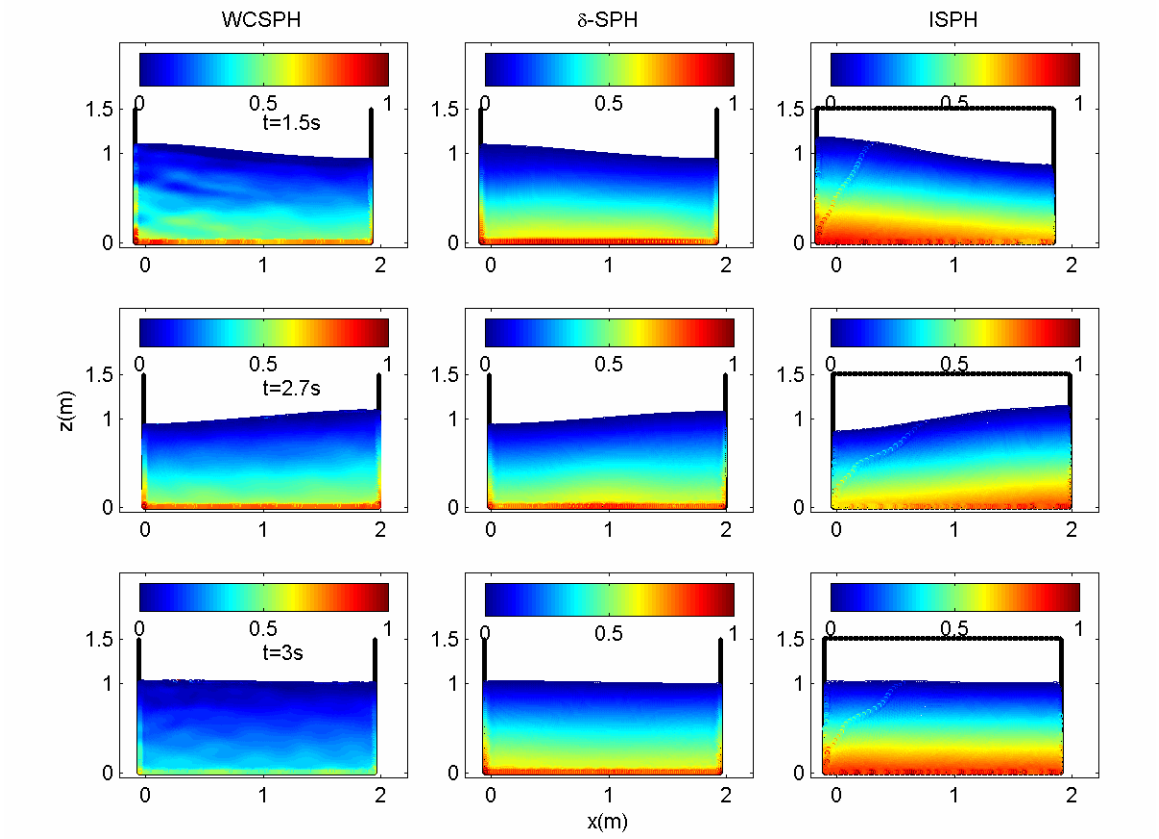

Fig. 5.8. Inter comparison for pressure field at different time instants between WCSPH, δ- SPH and ISPH. The colour bar is the pressure normalized with respect to the maximum pressure.

A number of unique features as encountered in violent sloshing waves has been reported from the experimental findings of Colagrossi (2005) and Colagrossi et al. (2006). From the same experimental set- up (tank length (L_x): 1m, tank height (H): 1m, width (b): 0.1m, initial water depth (d): 0.35m), different sloshing characteristics can be obtained depending on the choice of input excitation frequency and amplitude. From these, four frequency- amplitude pairs have been selected for the violent sloshing test for the δ- SPH model. The details of these cases are shown in Table 5.1. For the case of Violent Sloshing (VS- 3), the free surface state as predicted by the δ- SPH model is compared with the experimental photographs (Colagrossi, 2005) in Fig. 5.15. On a side wall, a smooth plunging bore was obtained, but prior to the formation of another plunging bore at the opposite wall, the nonlinear free surface harmonics interacts in between them strongly. It results in the formation of a hydraulic jump at the middle of the tank and

thereby leading to complete unstable flow conditions. These further cause complete flow separation when the incoming fluid rushes towards the opposite side wall and, while swelling up against it resulted in complete flow fragmentation. Since the δ- SPH model has been set up in a single phase, it has not been able to capture the highly turbulent flow characteristics with bubble formation (specially, left- bottom). However, it captures the complete fragmentation and ruptured water column (right- bottom) during run- up. Fig. 5.16 shows the various sloshing oscillation under different test cases. From the time history of the wave elevation at 0.01m from the left wall (Fig. 5.16d) for the case VS- 1, the steady-state free surface elevation shows oscillation with three- times excitation period, i.e., the sub-harmonics could be identified. This sub-harmonic frequency occurs with the wave breaking frequency at the wall on its subsequent oscillation. Once the wave breaks, it loses its energy and subsequently, builds up energy on its oscillation inside the tank. Every third-wave could build sufficient energy to make the wave breaks. Similar observations were made from the experimental study of Colagrossi et al. (2006).

Another violent sloshing case has been considered from the experimental study of Kashiwagi et al. (2010). In this case, tank length (L_x) is 0.6m; height (H) is 0.3m and, the initial water depth (d) is 0.06m. For an excitation period of 1.3s and amplitude of 0.06m, a violent sloshing case has occurred. A travelling plunging bore traverses back and forth along the tank length and it is followed by run- up along the side walls and associated roof impacts. Fig. 5.17 shows inter comparison of the total pressure field between WCSPH, δ- SPH and ISPH. The event at t=1.15s is representative of the well known flip-through impact. WCSPH has not been able to reproduce the area of impact around the breaking point properly, whereas, both δ- SPH and ISPH predict the impact region satisfactorily (prediction from ISPH being slightly better). The relative performances are found to be similar at t= 1.9s, i.e., characterized by roof impact. Indeed that was a critical task for the numerical model to avoid dispersive pressure distribution in such wave impact cases as occurred in violent sloshing flows (Macia et al., 2013). The comparison of the pressure measured at 0.05m above tank bottom on the right wall is shown in Fig. 5.18a. The dependence of the predicted pressure with resolution has been shown in Fig. 5.18b. In contrast to the non violent case where a higher resolution has always yielded a better prediction, here more noisy pressure time history has been obtained while adopting

d/dzp= 30 compared to d/dzp=24. This might be attributed by the fact that there is a possibility of divergence at higher Re due to the inherent particle based representation of differential operators in SPH (Colagrossi et al., 2013). Another evidence of this same phenomenon was also reported by Zhou (2010), where for studying violent sloshing waves, pressure time history could not always be improved in terms of increasing resolution. Hence the adopted resolution is assumed to be optimized. The occurrences of the maximum impact, the secondary impact and the duration of impact over the cycles have been captured well by the SPH model. However, the energy dissipated through the wave breaking in the experiment has not been exactly reproduced in SPH model. The laboratory measured pressure time history shows an alternate variation in the maximum peak over the subsequent cycles. Probably, this happened due to the reduction in maximum run up on the side wall immediately after the wave breaking. As energy is dissipated due to turbulence in wave breaking, less momentum is available for the resulting bore for swelling up along the side wall on the subsequent instant. Whereas, the numerical time history shows almost a steady state (i.e., energy is preserved) in terms of the maximum wave impact. Incorporation of a turbulence model in this case might improve the SPH model performance.

A parametric study has been performed to monitor the change in maximum wave elevation and maximum impact force (along x- direction) with respect to the wave excitation frequencies in the sloshing tank. The tank dimensions are similar to the last case study. The tank displacement is given by $\boldsymbol{X}_t=a_h\sin(\omega_h t)$. For T_h/T_1=1.02 and a_h/L=0.05, the force time history along x- direction (F_x) is shown in Fig. 5.19. The force has been calculated by integrating the pressure along the tank wall. About twenty steady cycles have been considered. The variation in maximum wave elevation (η_{max}) recorded at a probe located at 0.05m from the right wall and maximum impact force (F_{xmax}) with respect to the input excitation frequencies have been reported in Fig. 5.20. The prediction from the δ- SPH model is found to be fairly good compared to that of experiments.

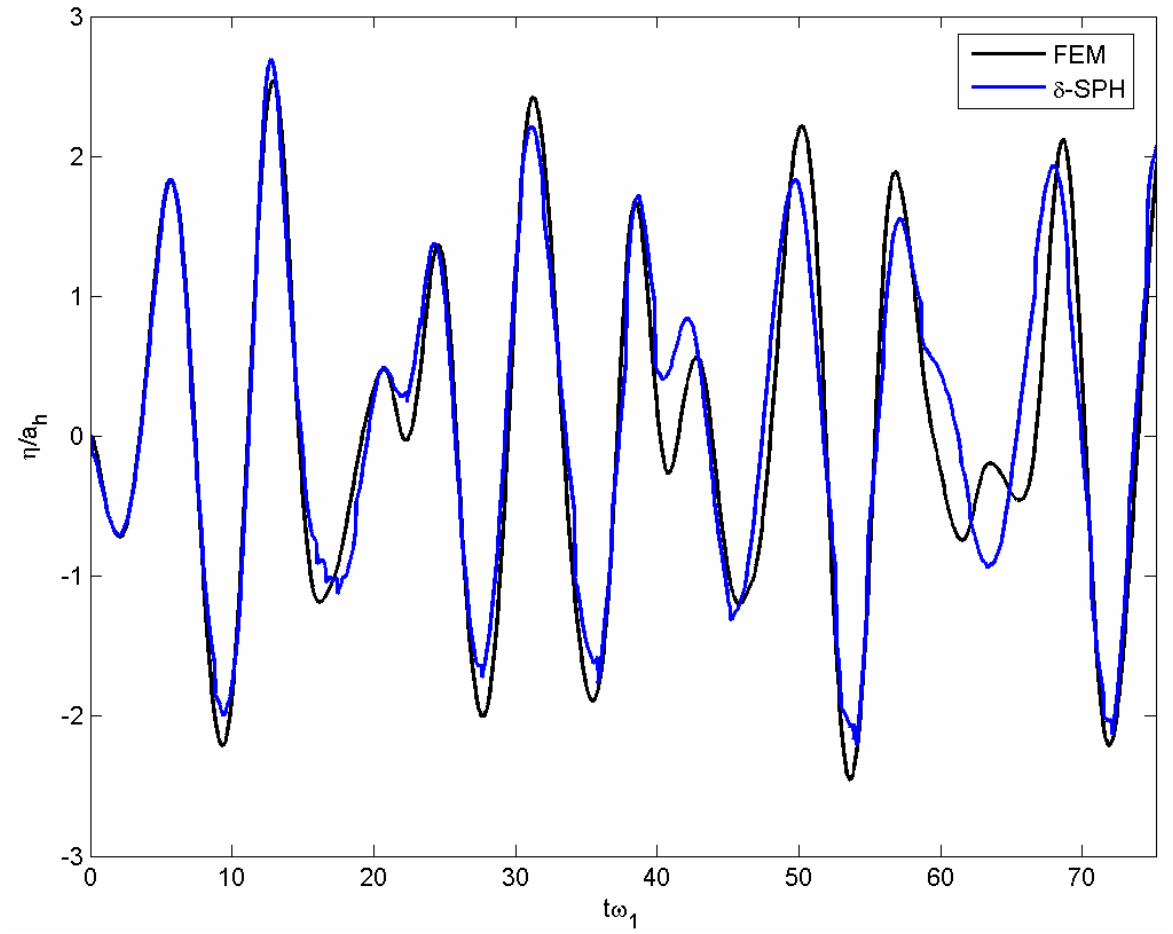

Fig. 5.9. Comparison between FEM and δ- SPH for the measured water surface elevation at the top left corner of the sloshing tank.

From the numerical experiments on non- violent as well as violent sloshing cases, it has been found that the smoothing length (h) and XSPH correction factor (ε) are the two major parameters that need careful calibration in order to maintain the true robust nature of SPH model. For non violent cases, the proper choice of h is based on optimization for the convergence of the scheme in predicting higher order harmonics. Apart from effecting the overall particle approximation by specifying the average number of neighbours available for interpolation, the choice of the smoothing length (h) is found to posses the main control over the adaptive time step size (dt). For a non- violent case, a larger time step size is preferable for the better stability of the RK4 time integrator, whereas, for a violent case, a high resolution in time scale (i.e., a smaller dt) is needed to follow the dynamics of wave breaking. Hence, the smoothing length has to be reduced

intentionally despite of the risk of losing RK4 stability. This compromise has to be managed by a proper choice of XSPH velocity correction factor (ε) which ensures that at the end of each time step, particle coordinates are updated properly. Fig. 5.21 shows the variation of the pressure distribution with respect to the variation in the XSPH factor (ε). The adopted range of smoothing length (h) and XSPH correction factor (ε) have been reported in Fig. 5.22.

There are some overlap zones in between non- violent, moderately to highly violent cases in these scales. The proposed range thus can be taken as an average general prescription while developing an existing weakly compressible SPH based solvers to a robust numerical scheme.

5.6. SUMMARY

This chapter has made an attempt to investigate the potential of SPH to emerge as a unique numerical tool to study sloshing for a variety of d/L and a_h/L ratios covering non violent and violent phenomenon. Addition of diffusive forcing terms in the continuity equation brings the two major improvements in weakly compressible SPH (WCSPH) scheme: less fluctuating and more regular pressure field; and, numerical solution for the time series of the required quantity with less dominating effect of numerical damping (loss in amplitude), recovering the required convergence with respect to the standard solution. Yet, it comes with a higher computational cost. For a single time step, the CPU cost in δ- SPH model has been found to be four times than standard WCSPH with estimation of diffusive terms taking 75% of total cost. OpenMP implementation may improve the computational efficiency of the model. The dissipation of energy as encountered in violent cases has not been predicted well when compared to experiments. Implementation of a particle based turbulence model (for example, the Sub- Particle-Scale (SPS) model within MPS framework, Gotoh et al., 2001) may be considered to improve the model performance for this case.

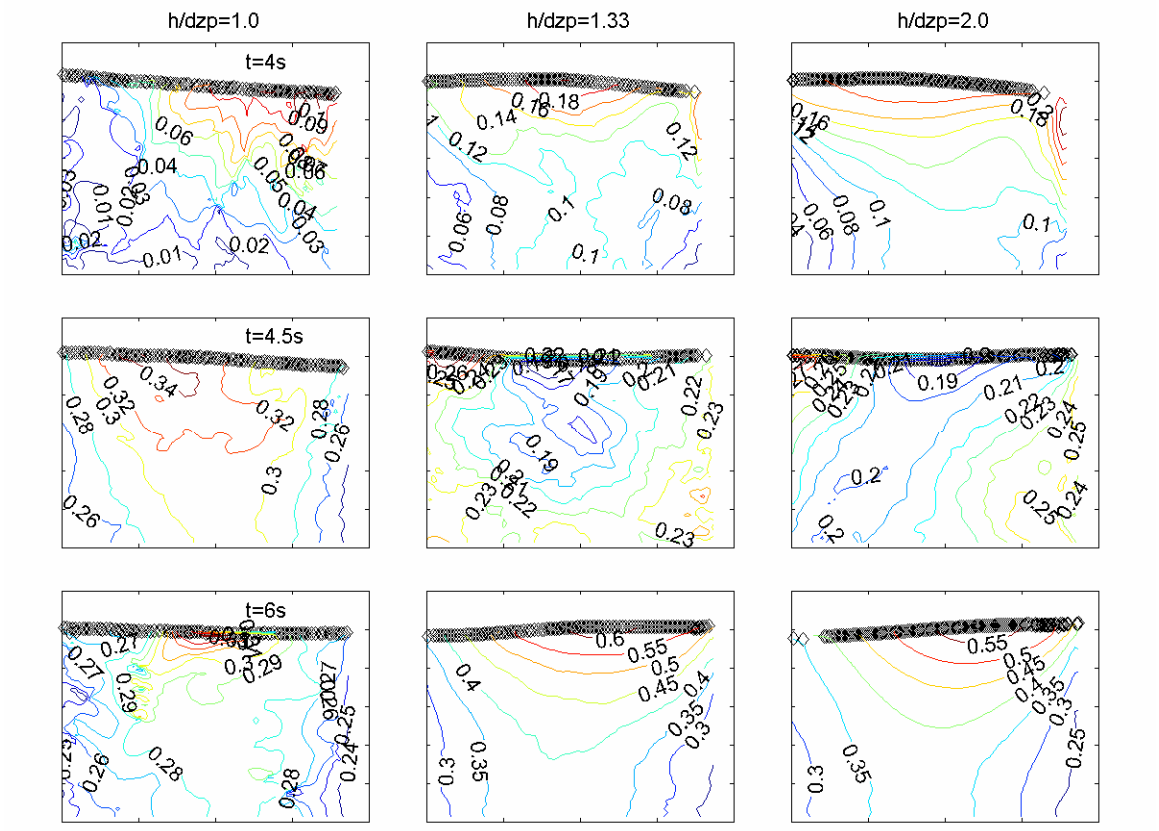

Fig. 5.10. Variation in the spatial distribution of the overall velocity and associated free surface profile with respect to the chosen *h*/*dzp* ratio.

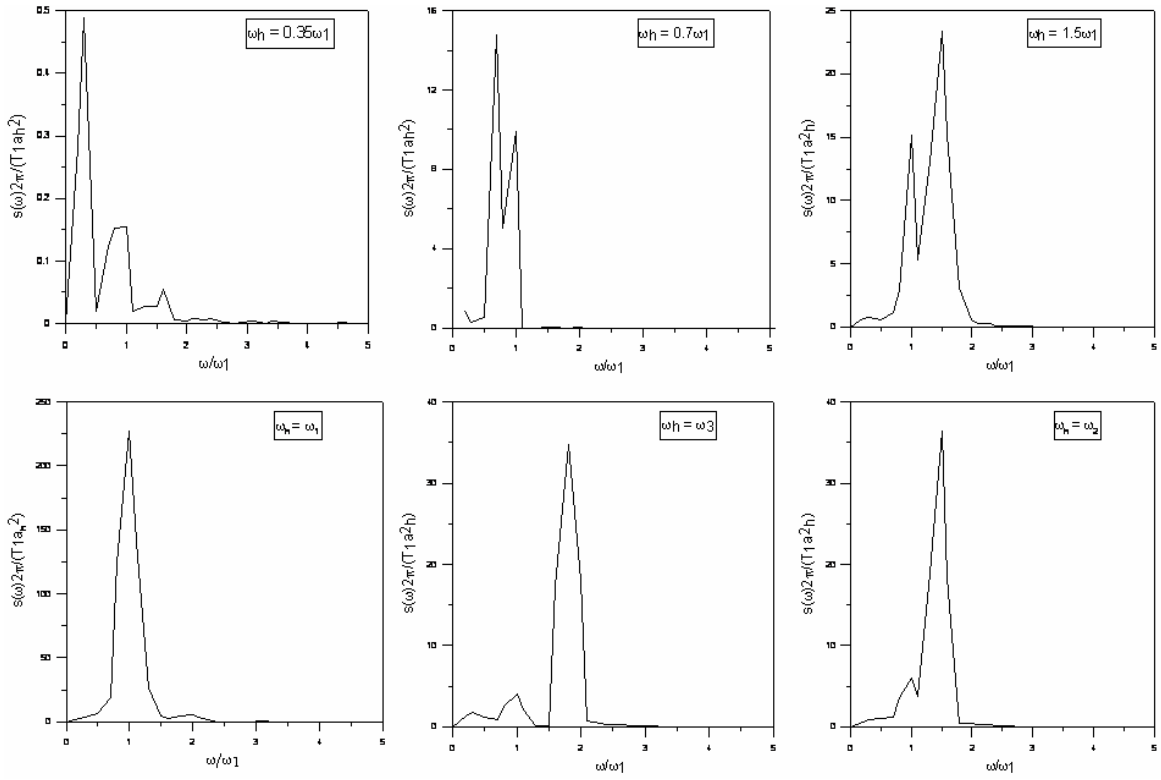

Fig. 5.11. Power spectra of the measured surface elevation at the top left corner of the tank for different excitation frequencies in regular excitation with $a_h = 0.05d$.

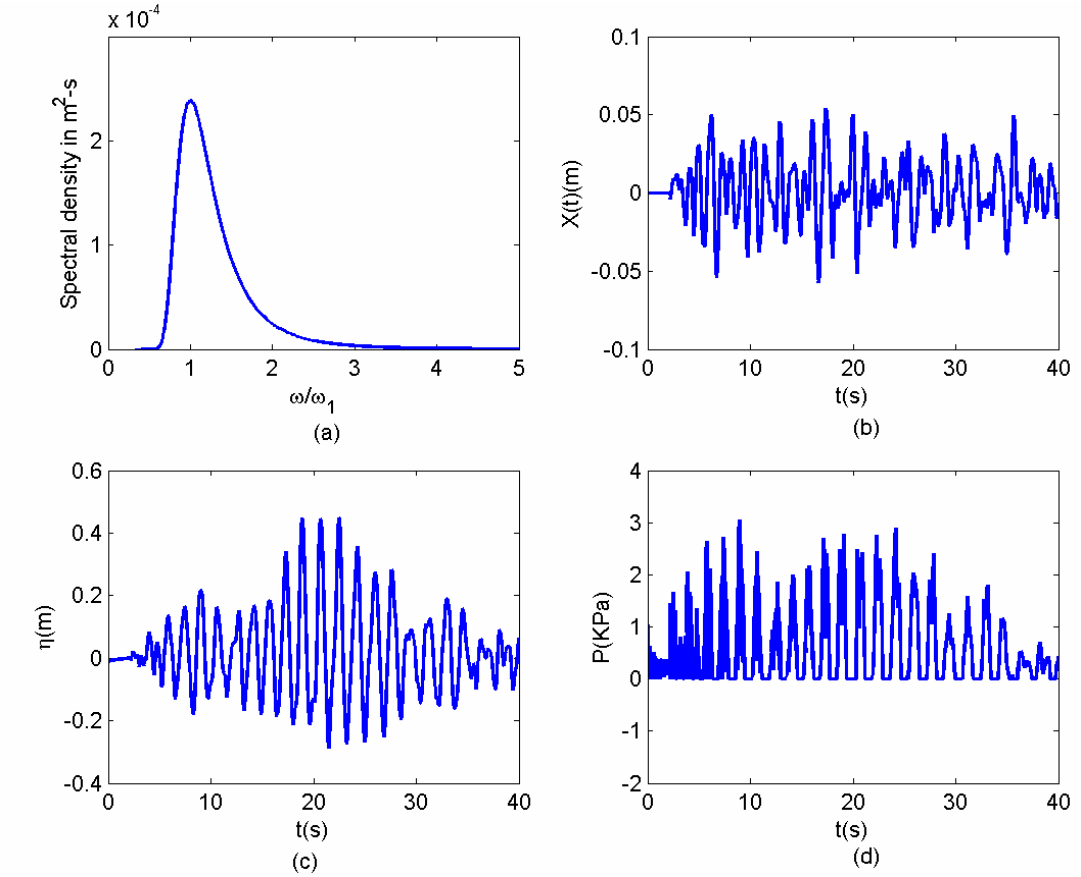

Fig. 5.12. Sloshing oscillation under random tank excitation. (a) Bretschneider spectrum prescribing random excitation; (b) Random tank excitation (horizontal) time series; (c) Measured free surface elevation at the top left corner, and (d) Time history of dynamic pressure measured at the same location.

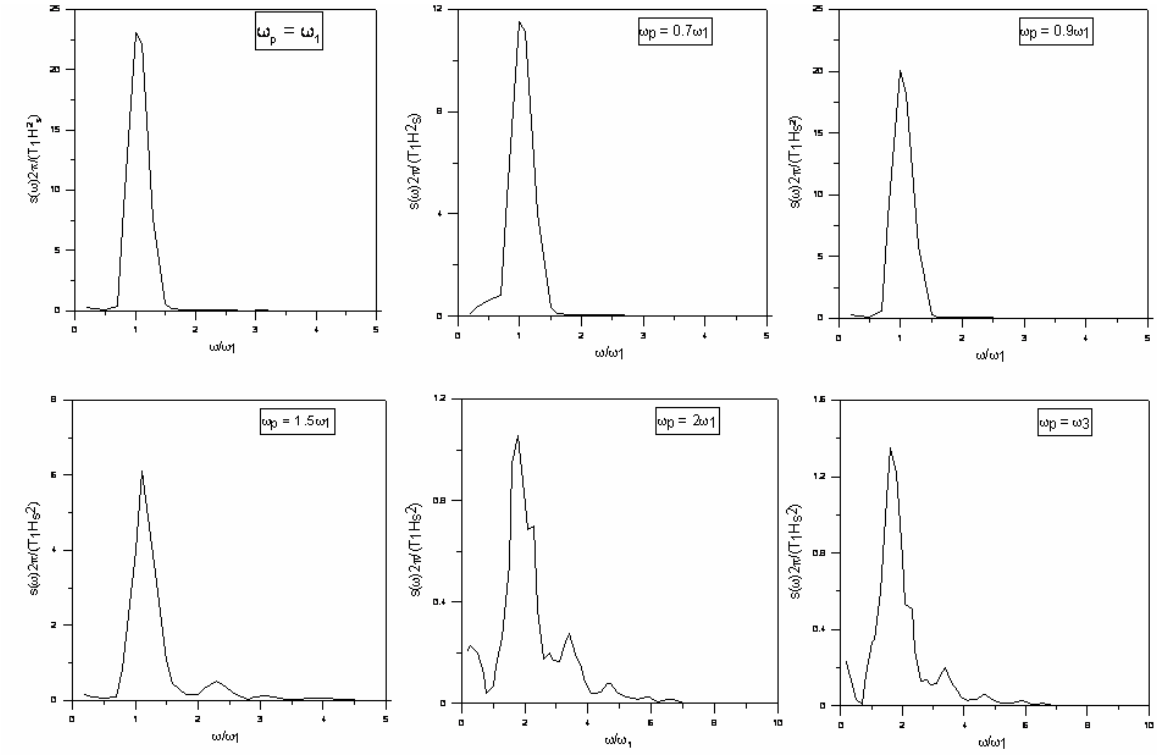

Fig. 5.13. Power spectra of the measured surface elevation at the top left corner of the tank for different random excitation peak frequencies ($H_s = 0.1d$).

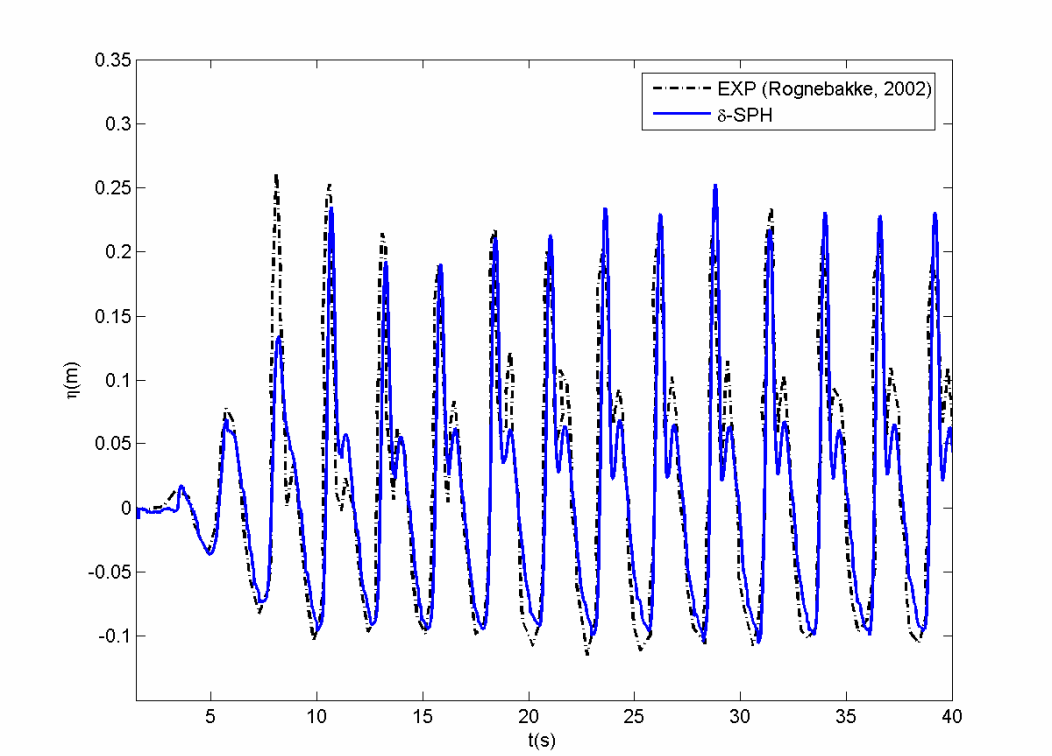

Fig. 5.14. Comparison of the free surface elevation at the given location for the DNV (Rognebakke, 2002) sloshing case.

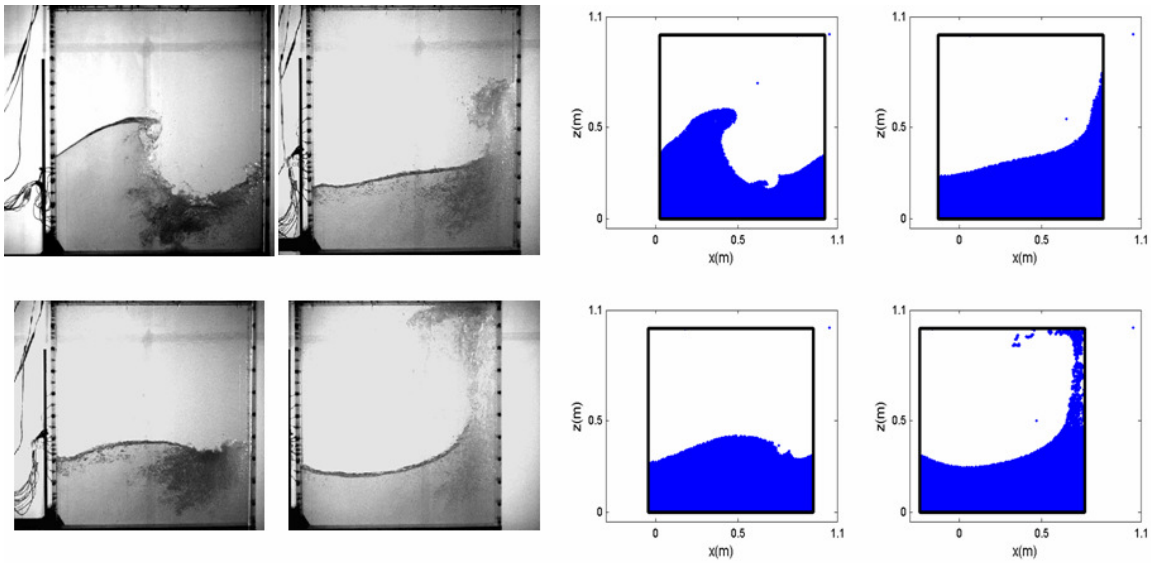

Fig. 5.15. Comparison of free surface fragmentation for the sloshing case VS- 3 between SPH model and the experimental photographs. Time increases from left to right and from top to bottom. This event repeats after every $3T_h$.

Table 5.1. Test cases considered for the SPH model in order to simulate various kinds of sloshing waves.

Sloshing case	T_h/T_1	a_h/L	**Sloshing wave features**
VS- 1	0.95	0.05	Alternate breaking of the plunging bores at the two side walls
VS- 2	0.95	0.07	Alternate breaking with prolonged plunging jet
VS- 3	0.787	0.1	Irregular behaviour of the wave with highly turbulent characteristics
VS- 4	0.87	0.07	Local splashing jets at the side walls

Note: *Th* and *T*1 are the excitation period and the period of the 1st mode of natural sloshing frequency respectively.

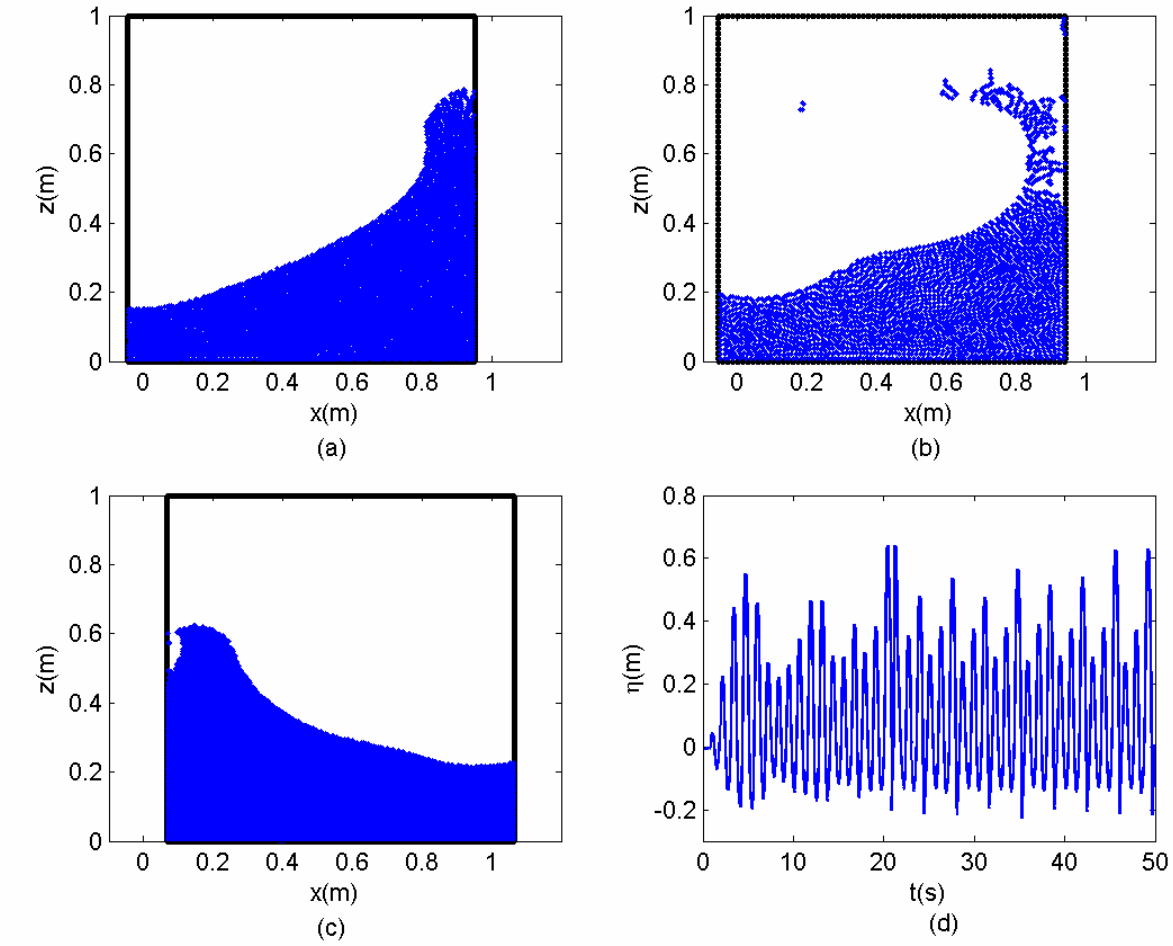

Fig. 5.16. Different kinds of violent sloshing waves as obtained for the cases as mentioned in Table 5.1: (a) case VS- 1, (b) case VS- 2 and (c) case VS- 4; (d) time history of wave elevation measured at 0.01m from the left wall for VS-1.

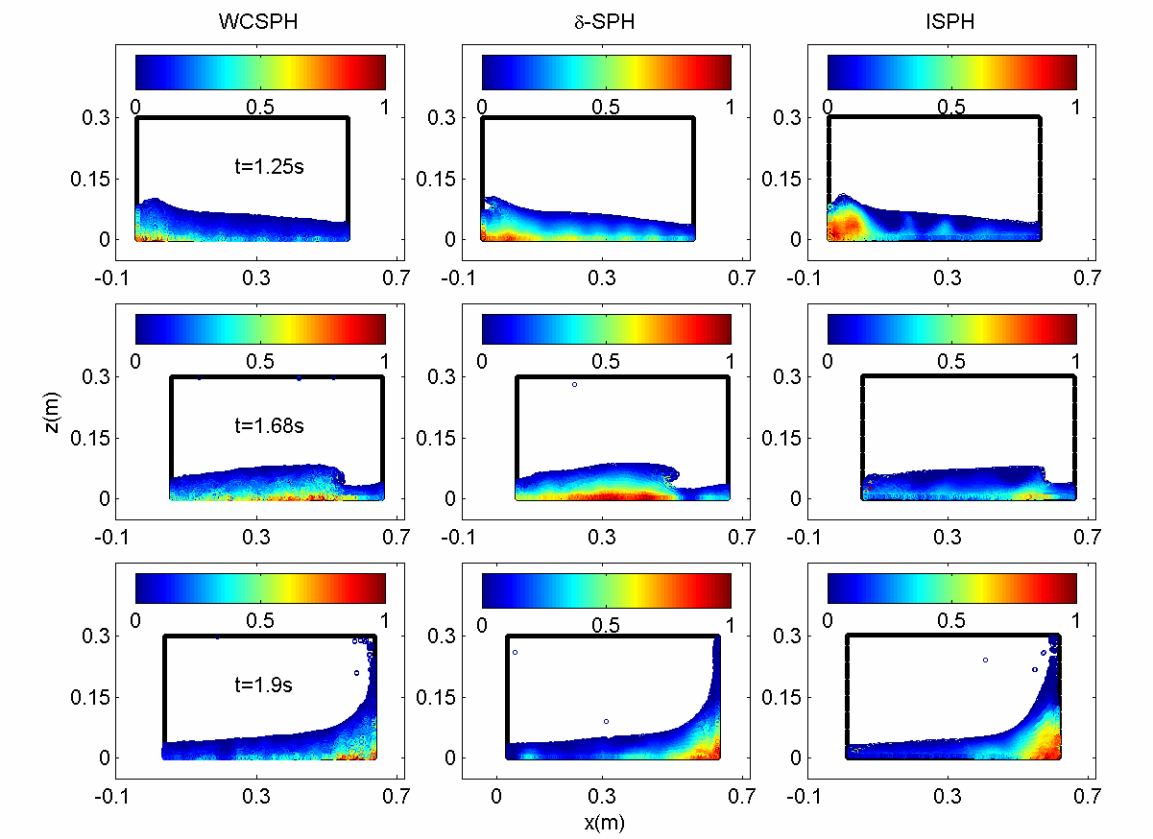

Fig. 5.17. Inter comparison of spatial distribution of total pressure field between WCSPH, *δ*- SPH and ISPH at different time instants. The colorbar is of total pressure normalized with respect to the maximum pressure.

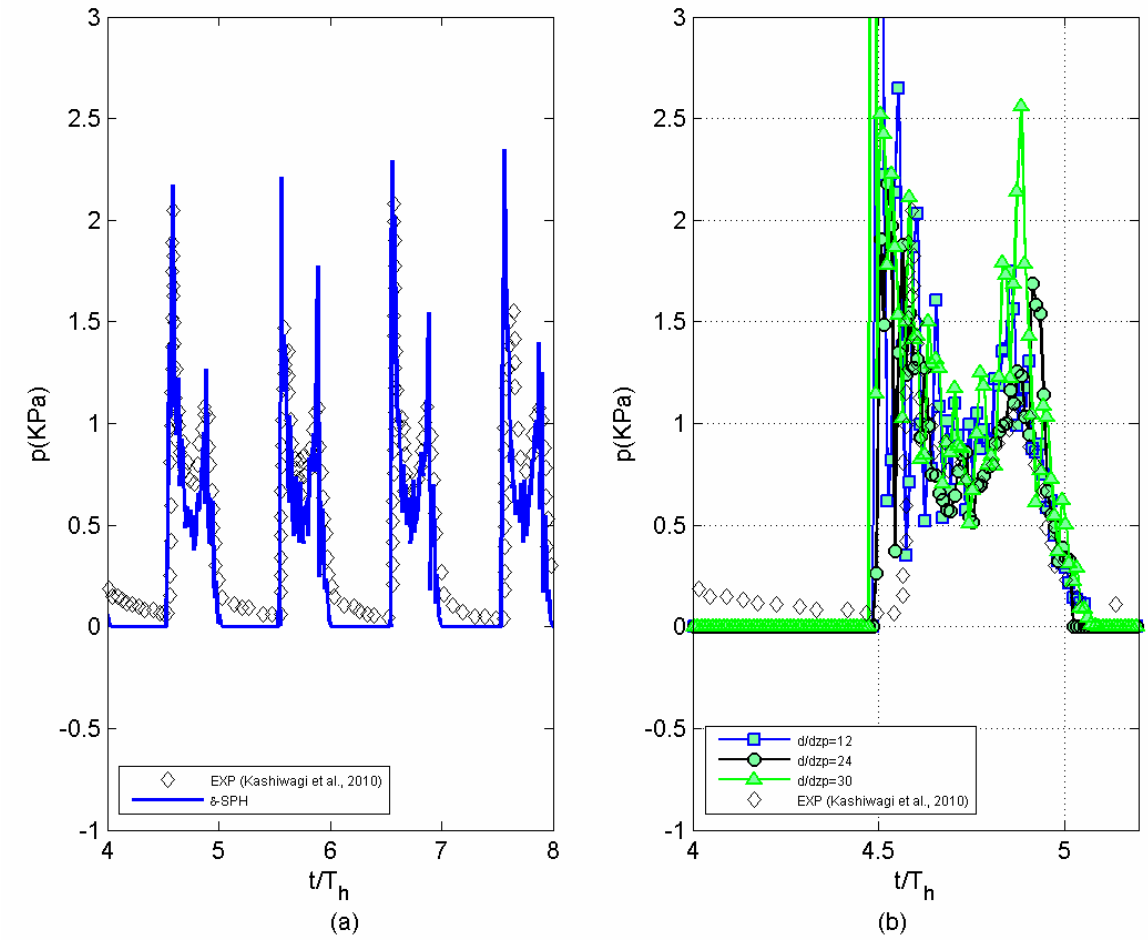

Fig. 5.18. (a) Comparison of pressure time history at the given location between δ- SPH model and experiment; (b) Variation in the pressure time history with change in resolutions.

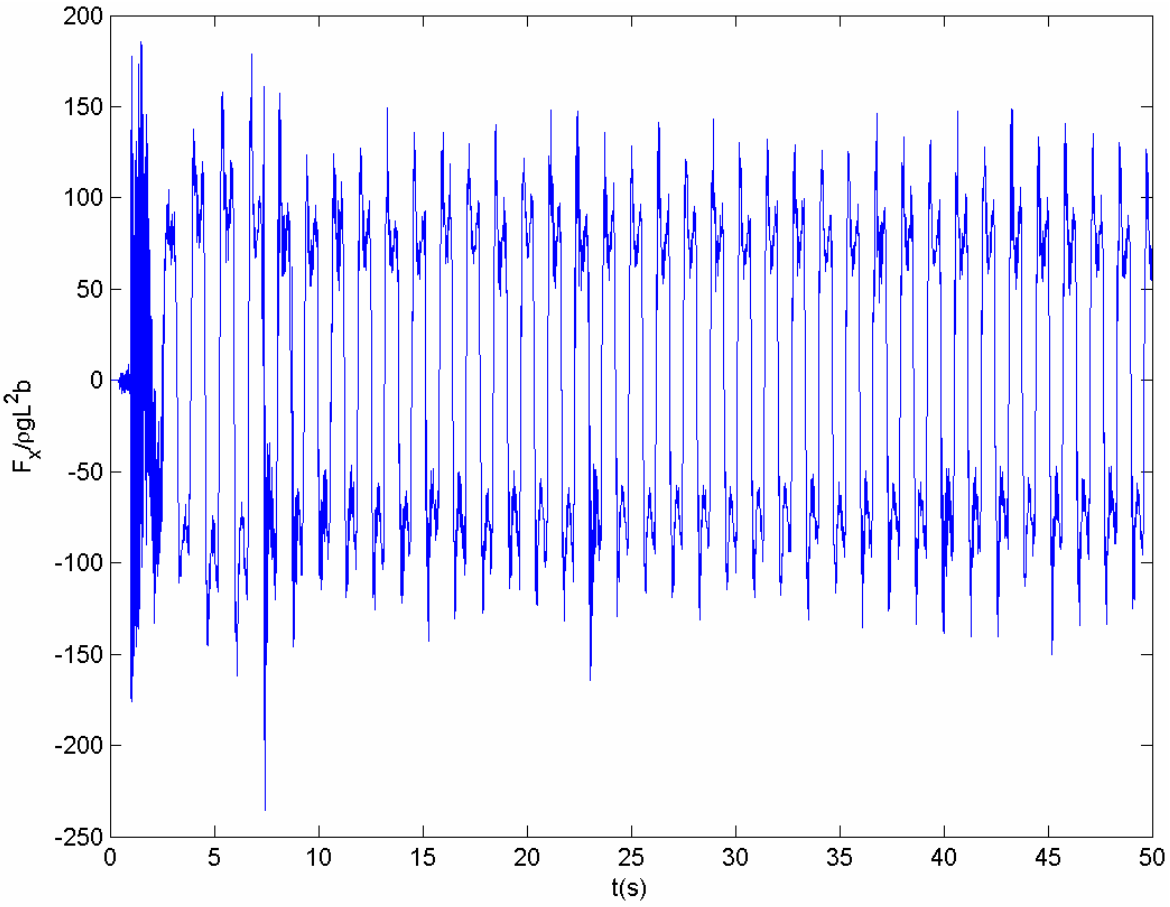

Fig. 5.19. Time history of horizontal impact force in the sloshing tank for T_h/T_1=1.02 and a_h/L_x= 0.05.

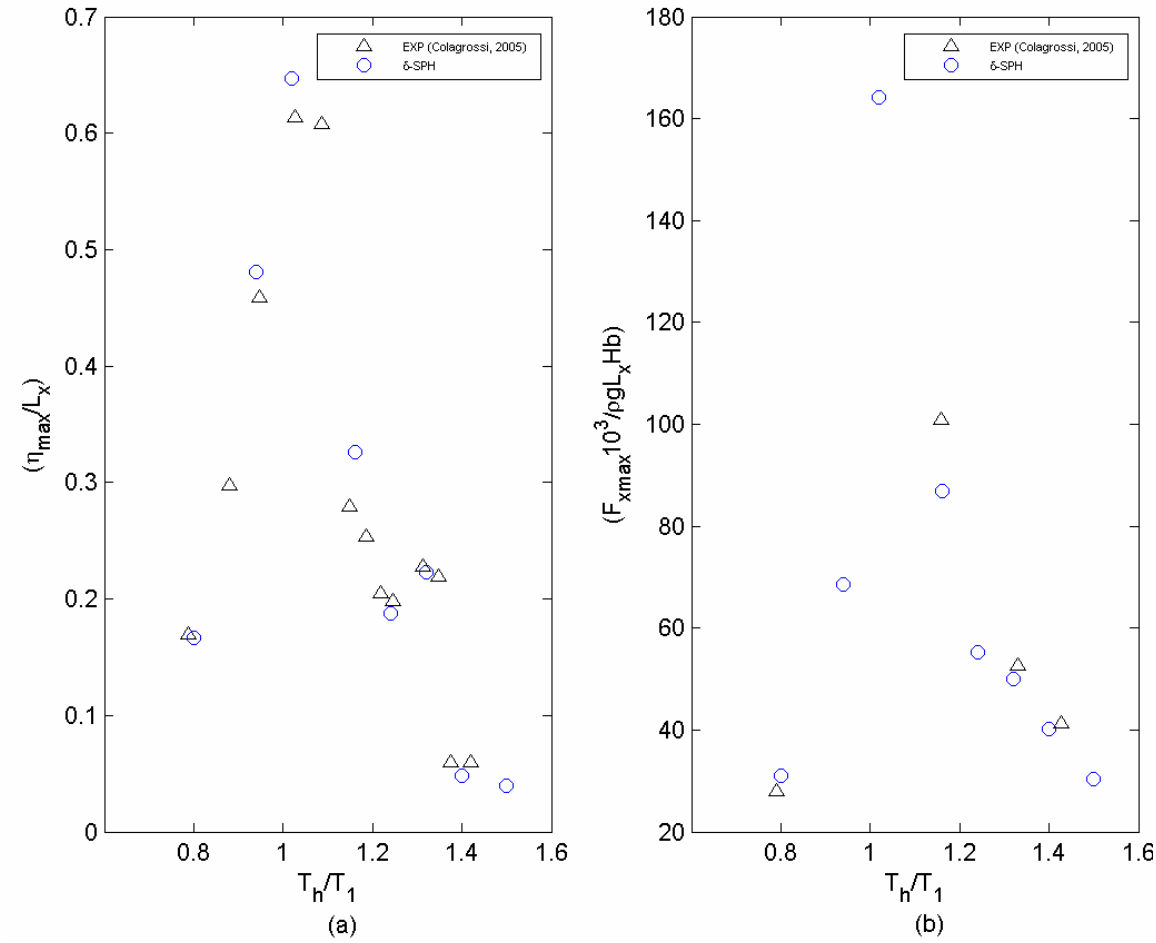

Fig. 5.20. Comparison of maximum free surface elevation and horizontal impact force between SPH and the experiments.

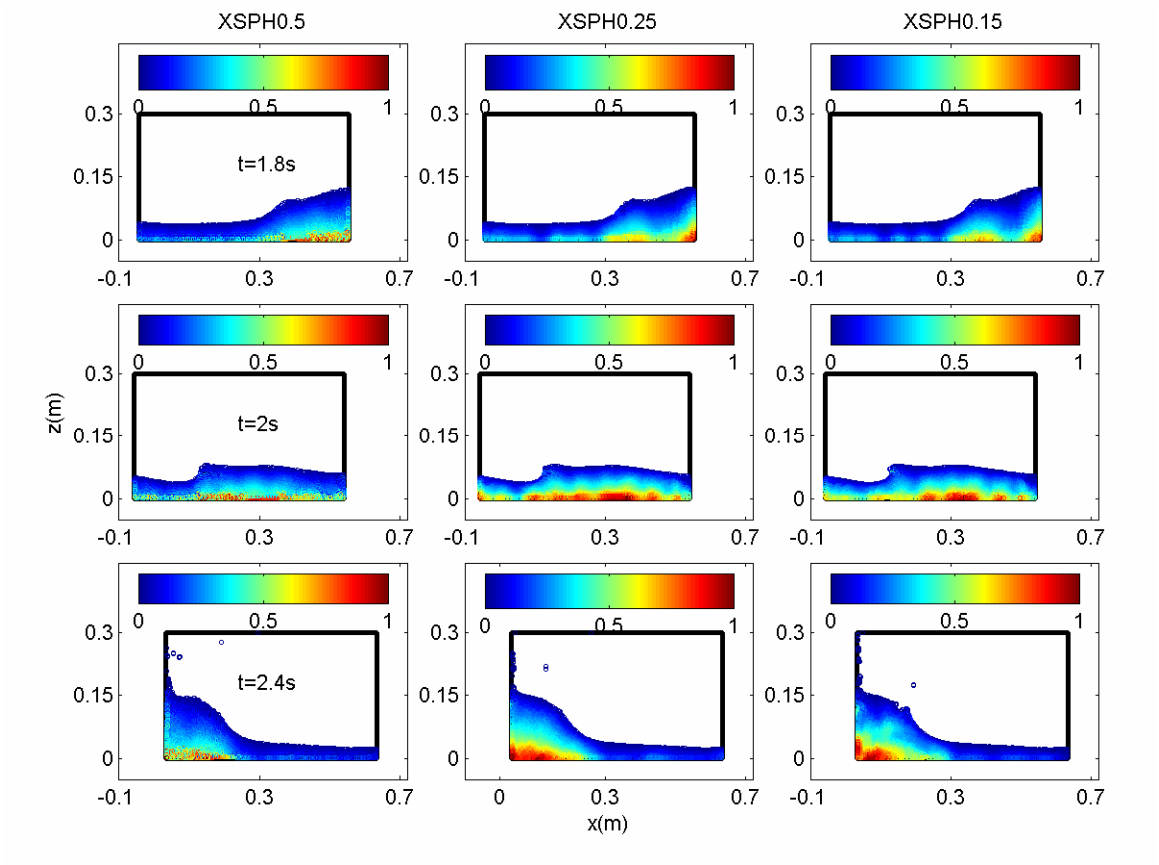

Fig. 5.21. Variation in the spatial distribution of the total pressure field in the δ- SPH model with respect to the change in XSPH velocity correction factor (ε). The colorbar is of pressure normalized with respect to the maximum pressure.

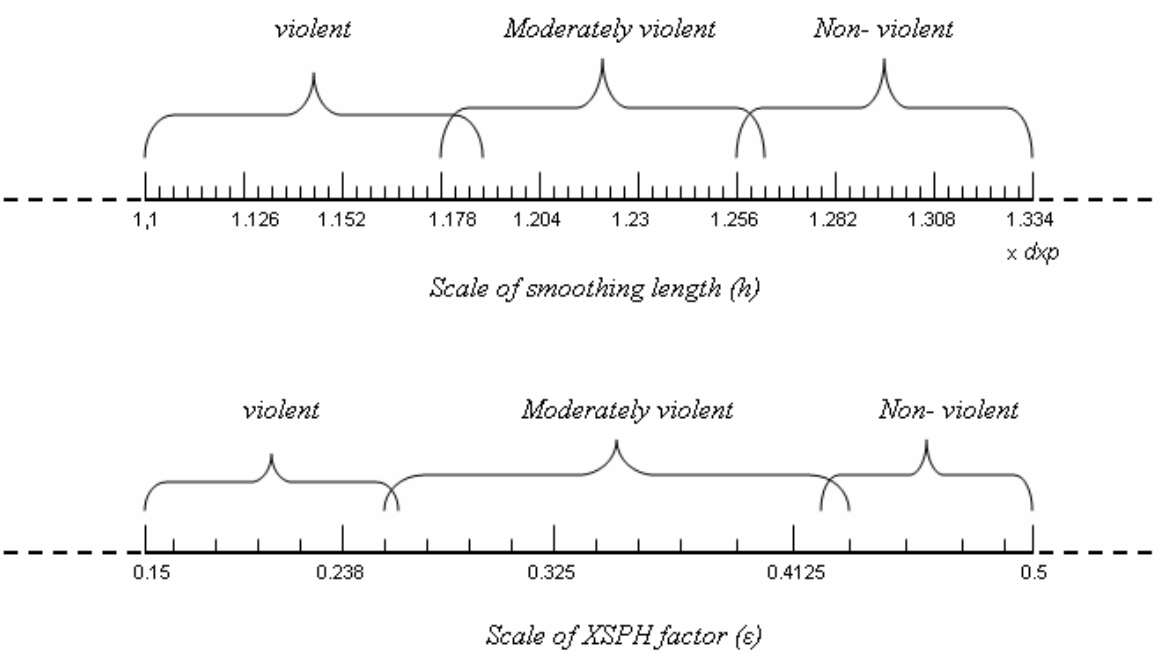

Fig. 5.22. Scale of smoothing length (h) and XSPH factor (ε) for its selections for the requirement in simulating the sloshing problem.

CHAPTER 6

WAVE INTERACTIONS WITH SEAWALLS AND OVERTOPPING

6.1. GENERAL

Wave overtopping is a phenomenon caused by spillage of water waves over coastal structures. This is one kind of a catastrophic phenomenon which mostly occurs depending on local wave climate and coastal mophology; yet, it takes a considerable focus from the bigger community dealing with environmental hydraulic engineering, for planning and designing sustainable coastal environments. Prior knowledge and estimation of overtopping water volume with respect to various incident wind/ wave conditions, help to ensure an efficient designing of coastal structures.

Measuring the volume of water discharged during the wave overtopping is indeed a critical task: both in experiment and in computation. However, numerous studies have been performed due to the prime importance of wave overtopping in the context of coastal engineering. Cox and Ortega (2002) conducted experiments to measure wave overtopping due to transient wave on a fixed horizontal deck. Troch et al. (2004) made detailed field study to investigate the wave overtopping over rubble mound breakwaters at three different shore locations. Umeyama (1993) analytically estimated wave overtopping over a vertical wall due to standing waves and made experiments to analyze the predictions. Stansby and Feng (2004) carried out PIV measurements on wave overtopping over trapezoidal obstacle and found complex vortical structures to take place in the form of interacting bores. Goda (2009) derived a set of formula for predicting overtopping based on a broad range of available data sets. McCabe et al. (2013) validated the overtopping estimated by shallow water and Boussinesq modelling with laboratory experiments. Baldock et al. (2012) made an experimental study to investigate wave overtopping due to solitary waves.

The empirical formulae so obtained from experimental data are frequently used in design practice and model set up for other physical model based studies; however, these predictions are in general limited within a certain range of data considered. Hence,

several numerical studies have also been performed for calculating wave overtopping. Stansby (2003) measured wave overtopping due to solitary wave by finite volume based shallow water Boussinesq model. Soliman (2003) also adopted the Volume of Fluid (SOLA- VOF) method to analyse two- dimensional breaking wave numerical model (2D-BWNM) solving Reynolds Averaged Navier- Stokes (RANS) including k- ε turbulence modelling. Kobayashi and Wurjanto (1989) and Hu et al. (2000) applied Nonlinear Shallow Water Equation (NLSW) for calculating wave overtopping. Li et al. (2004) provided numerous VOF solutions for wave overtopping. So, from these studies, it is learnt that solving NS is indispensable in order to compute wave overtopping. Most of them used Finite Volume based numerical schemes.

However, in the last the few decades, another numerical scheme named Smoothed Particle Hydrodynamics (SPH) has also been found to be evolving for solving NS to simulate nonlinear water waves. The major attraction in SPH, being totally free form mesh constraints, gives easy capturing of the complex shape of the free surface which is likely to emerge during all the stages of wave breaking, run up and overtopping. Currently, two versions of SPH are found to be popular for solving free surface flow related problems: the Incompressible SPH (ISPH, Cummins and Rudman, 1999; Lo and Shao, 2002) and the Weakly Compressible SPH (e.g., WCSPH, Monaghan, 1994). Gomez- Gesteira et al. (2005) simulated green water using WCSPH. Barreiro et al. (2013) has shown three dimensional simulation of wave overtopping near real like coastal environments and computed force and moment imparted in that process over the coastal structures using DualSPHysics, a WCSPH based open source solver. Crespo et al. (2008) provided the input to the SPH solver in terms of wave height as provided by a wind-wave generation/ propagation model (e.g., SWAN, WAM etc.) and computed the flow velocity pattern, overtopping rate for a given bathymetry. However, apart from the work of Issa et al. (2010), a rigorous comparison and validation of WCSPH with other numerical and experimental studies for wave overtopping were unavailable until Shao and his co authors (Shao, 2006; Shao et al., 2006) gave clear evidence of applicability of SPH in computing wave overtopping by showing comparison with other studies. But, their study was based on an ISPH solver where pressure is calculated by solving a Pressure Poisson Equation (PPE) rather than from an explicit equation of state as is

generally done in WCSPH. Even for the problem of wave propagation over both a sufficiently long time and distance, it was not clear how accurately a WCSPH based scheme simulates without much of numerical damping. This critical question has found to be first well addressed in Antuono et al. (2011) where the prediction of a WCSPH solver was compared with Mixed Eulerian Lagrangian Boundary Element (BEM) prediction and experiments. However, their WCSPH based solver utilized a separate term in continuity equation to enhance the performance of WCSPH in many aspects. Previously named as δ- SPH by Antuono et al. (2010), this model has been found to be fairly accurate in simulating various problems in nonlinear water waves like ISPH.

Therefore, δ- SPH appears to be preferable numerical scheme to study such wave overtopping. Moreover, modelling boundary in SPH with several rapid geometrical changes as encountered in a Numerical Wave Flume (NWF) is a delicate task.

In this chapter, the process of wave overtopping on different type of seawalls has been explored using the developed SPH models. Such wave interaction problems consist of wave propagation over irregular bathymetry and in which case, the model has to be capable of dealing with complex geometrical shapes/ sharp changes. The model also needs to be numerically stable enough to run for sufficiently long time duration in order to capture the relevant physical processes under consideration. These have been achieved in the present study by taking advantages of the salient aspects of the model development as discussed in Chapter 4. The δ- SPH application for the wave propagation problem in Antuono et al. (2011) applied a technique named fixed ghost particles to model boundaries. However, in this study, a separate technique proposed by Adami et al. (2012) has been implemented as discussed in Chapter 4.

This chapter is organized as follows. In the beginning, an introduction gives the brief summary of the past work carried out on the problem of wave overtopping based on laboratory measurements and various numerical techniques. Then the overtopping due to regular, random and solitary waves over a vertical sea wall has been investigated with the present SPH models. Inter comparison between WCSPH and ISPH has been performed for few selected cases. Detailed procedure has been described to calculate the overtopping water volume. A parametric study has been conducted to follow changes in overtopping rate due to changes in incident wave parameters and seawall characteristics.

This shows the potential of the present SPH model to replace the experimental based empirical formulae which have been adopted for designing sustainable coastal structures against a harsh sea environment like during wave overtopping. The second part of the chapter describes further application of the present SPH scheme in investigating hydrodynamic characteristics of curved front sea wall compared with vertical seawall under same wave conditions. The available experimental measurements form the basis for comparison and further exploration of results. All these reflect the robustness of the present SPH models in solving important coastal engineering problems.

6.2. REGULAR WAVES

The regular wave overtopping on a sloped sea wall is considered. The case study has been adopted from Shao et al. (2006) in which wave overtopping was simulated using an ISPH model. The computational domain is shown in Fig. 6.1. Shao et al. (2006) considered the same domain which ends at 0.5 m from the top of the slope as shown by point A. Particles going beyond that point were counted by a counter to measure overtopping. No further details of those particles and procedure of measuring water discharged were provided.

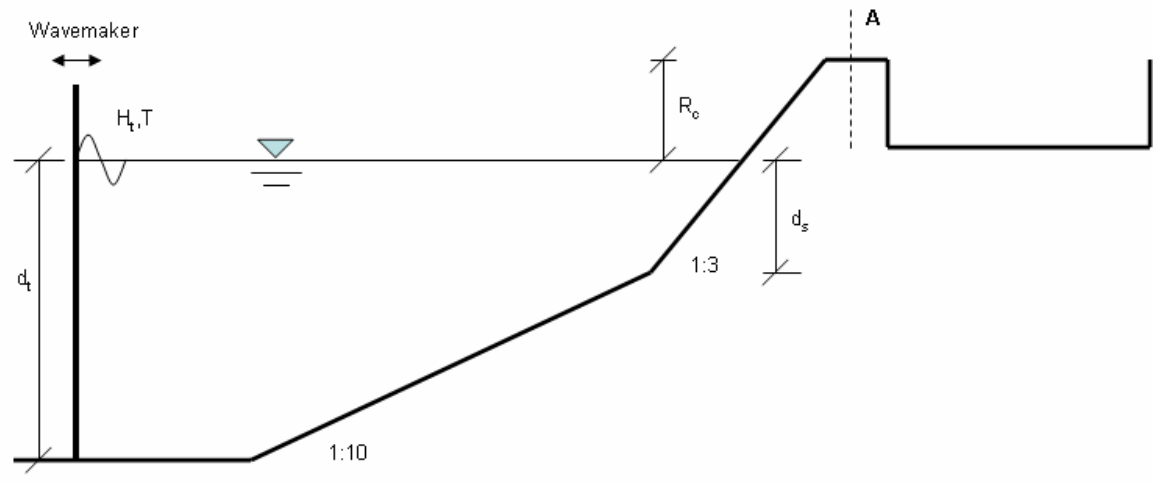

Fig. 6.1. Computational domain used for the simulation of wave overtopping

In this study, an additional storage tank has been placed after the seawall to store overtopping particles/ discharged water. Flexibility of the present boundary modelling technique has allowed it. The procedure of calculating overtopping rate is explained here.

Initially, the specific time instants of a particular wave train have been captured when the particles just start to cross the point, A. This can be detected by the local velocity field. This is shown in Fig. 6.2 (a) as initiation of the overtopping. The volume of water already contained in the tank is taken as V_b. The discharge has been found to take place during certain duration. Then, the time instant of the initiation of the run- down process (Fig. 6.2(c)) has been captured. The run down process could be identified from the local velocity field. The volume of the water in the tank is recalculated and taken as V_e. Therefore, V_e-V_b gives discharged water volume during that particular wave overtopping instant. The same procedure has been followed for the subsequent overtopping time instants.

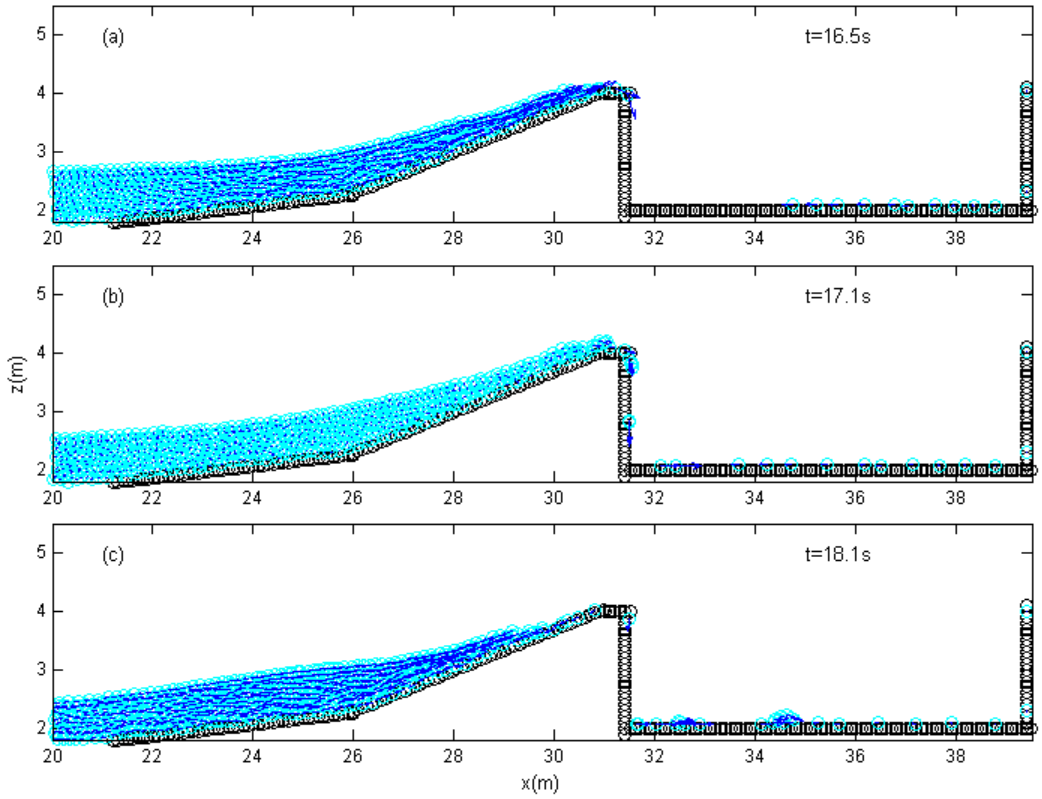

Fig. 6.2. Wave overtopping on a sloped sea wall due to 4.73s regular wave. (a) wave run up, (b) overtopping (c) and run down.

A number of several case studies have been performed to compare the overtopping predicted by the present SPH model with that of Shao et al. (2006). Few more predictions, i.e., the experimental and NLSW from Hu et al. (2000) have also been included. The details of the case study are given in Table 6.1. The comparison of the predicted rate of overtopping is shown in Fig. 6.3. The initial particle spacing is 0.1m. The average time step size is 5.5×10^{-3} s. All the computations were performed in the desktop PC. Adopting 4000- 5000 number of particles, it took around 3.5 CPU hours to complete ten wave cycles. Under same conditions, Shao et al. (2006) reported 2 CPU hrs. It is observed that the present SPH model prediction matches more closely with that of experiment and ISPH prediction of Shao et al. (2006). The maximum difference between the two SPH model predictions is about 24% (run no. 8). In overall, it confirms that present WCSPH based model is equally applicable as ISPH in estimating wave overtopping. Considering all experimental runs, the present model prediction differs on average by 25.18% which is much closer to ISPH (18%) than RANS solution (52.63%).

A parametric study has been performed to investigate changes in the predicted rate of overtopping with respect to seawall crest level and incident wave period (Fig. 6.4). The incident wave periods are 3.73s, 4.73s and 5.73s. The seawall crest level varies from 0.5m to 1.5m.

Table 6.1 Details of the case studies considered for calculating regular wave overtopping. N_p is the total number of fluid particles used.

Run no.	*Rc* (m)	*dt*(m)	*ds*(m)	*Ht*(m)	*T*(s)	N_p
1	0.5	3.0	0.75	0.95	4.73	4743
2	1.0	3.0	0.75	0.95	4.73	4743
3	0.5	3.0	1.5	0.95	4.73	4174
4	1.0	3.0	1.5	0.95	4.73	4174
5	0.67	4.0	2.0	0.99	6.55	7201
6	0.5	4.0	0.75	1.08	7.98	8368
7	1.0	4.5	0.75	1.06	7.98	10556
8	1.5	4.0	0.75	1.08	7.98	8368
9	0.5	4.0	1.5	1.08	7.98	7795
10	1.0	4.0	1.5	1.08	7.98	7795

The trend in the variation looks similar with that of Soliman (2003) for a given wave period. This shows good potential of the SPH in estimating wave overtopping to replace laboratory based empirical formulae for practical coastal engineering application.

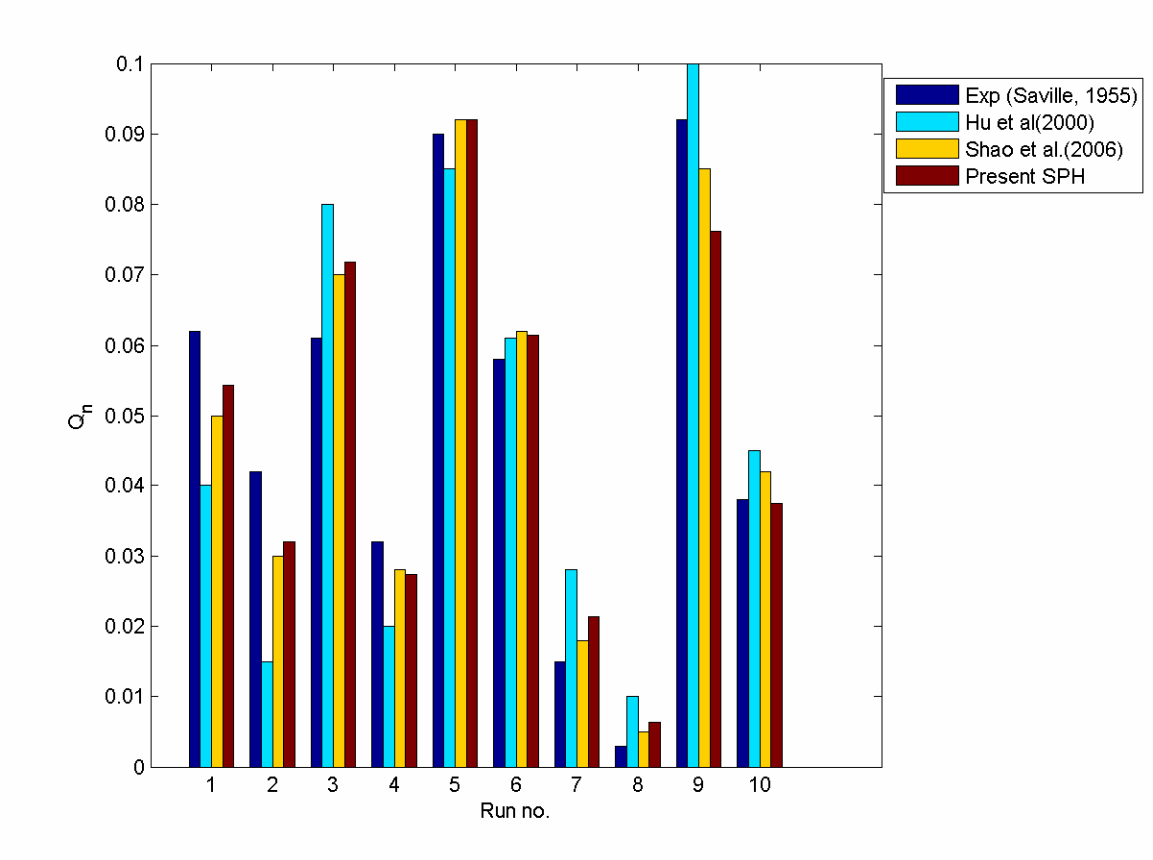

Fig. 6.3. Non- dimensional wave overtopping rate ($Q_n=Q/\sqrt{(|\boldsymbol{g}|H_0)}$), H_0 is the deep water wave height = 1m) as predicted by the present SPH model and comparison with other studies.

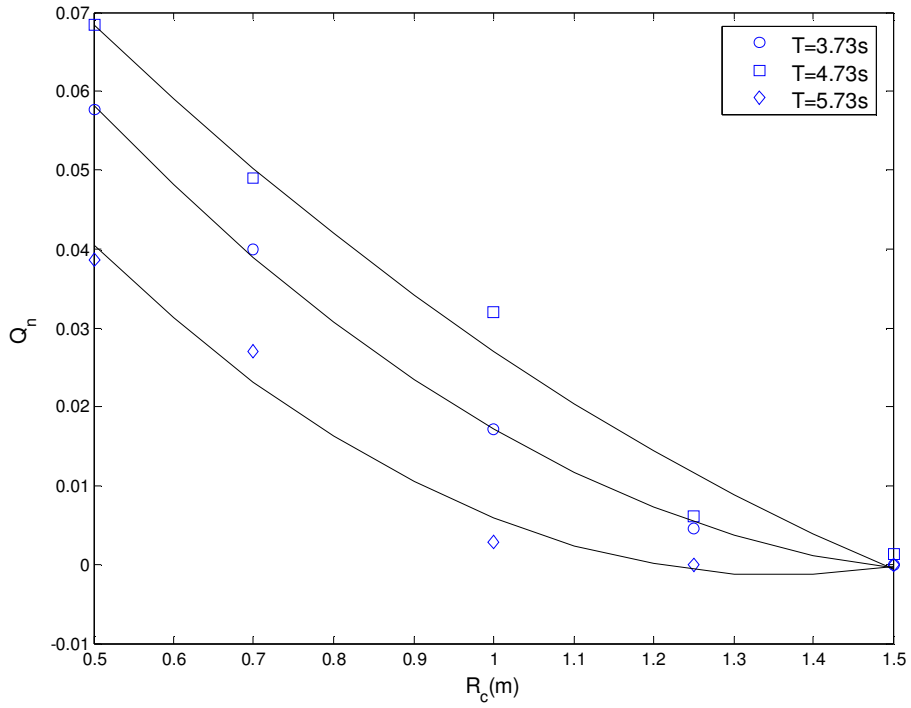

Fig. 6.4. Prediction of wave overtopping for different sea wall crest levels (R_c) and incident wave periods.

6.3. RANDOM WAVES

The numerical investigation on wave overtopping due to random wave incidence on a seawall is reported. The schematic diagram of the domain is shown in Fig. 6.5.

This domain has been adopted from Soliman (2003) and Shao et al. (2006) where the overtopping was studied through other numerical models. In the present study, additional

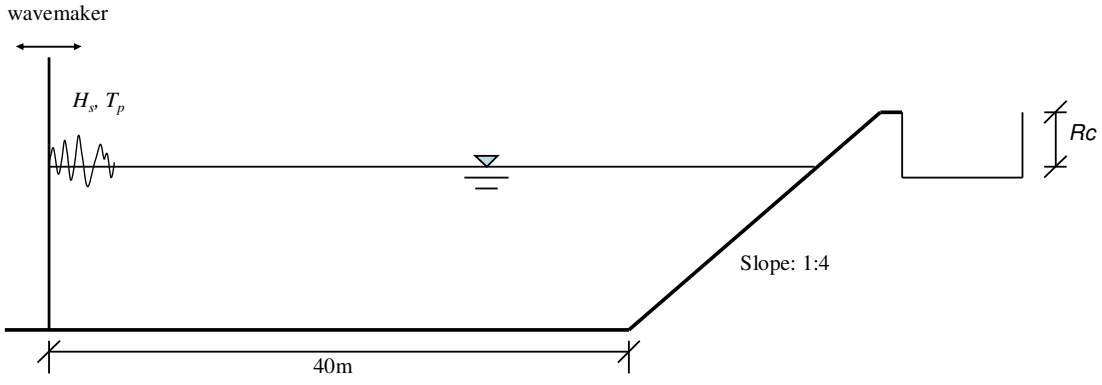

Fig. 6.5. Schematic of the domain adopted for wave overtopping.

storage tank has been included to collect the overtopping water. The standard JONSWAP spectrum was used to generate the random waves in the flume with a constant water depth of 8m from the wavemaker to the foot of the seawall. The slope of the impermeable seawall front is 1:4. Table 6.2 presents the details of various experimental runs. Here, H_s, T_p and R_c are the significant wave height, peak wave period and free board, respectively.

Fig. 6.6 presents overtopping rate averaged over few wave cycles from the prediction of the present SPH models and the ISPH model of Shao et al. (2006). The prediction from RANS solution including k- ε turbulence using SOLA- VOF model (Soliman, 2003) is also included. Fig. 6.7 shows particle snapshots from the present ISPH model during a particular wave cycle of overtopping. Even with the inclusion of storage tank, still few particles have been found to escape the given domain in unphysical way. Most of these particles escape after the jet enters into the storage tank. Since, there are less number of neighbors available for those particles, the velocity of those particles could not been calculated correctly. The particles which escaped the tank are still considered to be inside the tank while calculating rate of overtopping.

Table 6.2. Details of the runs for simulating wave overtopping due to random waves

Run No.	R_c (m)	H_s (m)	T_p (s)
1	1.0	0.78	3.53
2	1.0	1.22	4.38
3	1.0	1.7	5.19
4	1.5	1.26	4.38
5	1.5	1.75	5.16
6	1.5	2.35	6.03

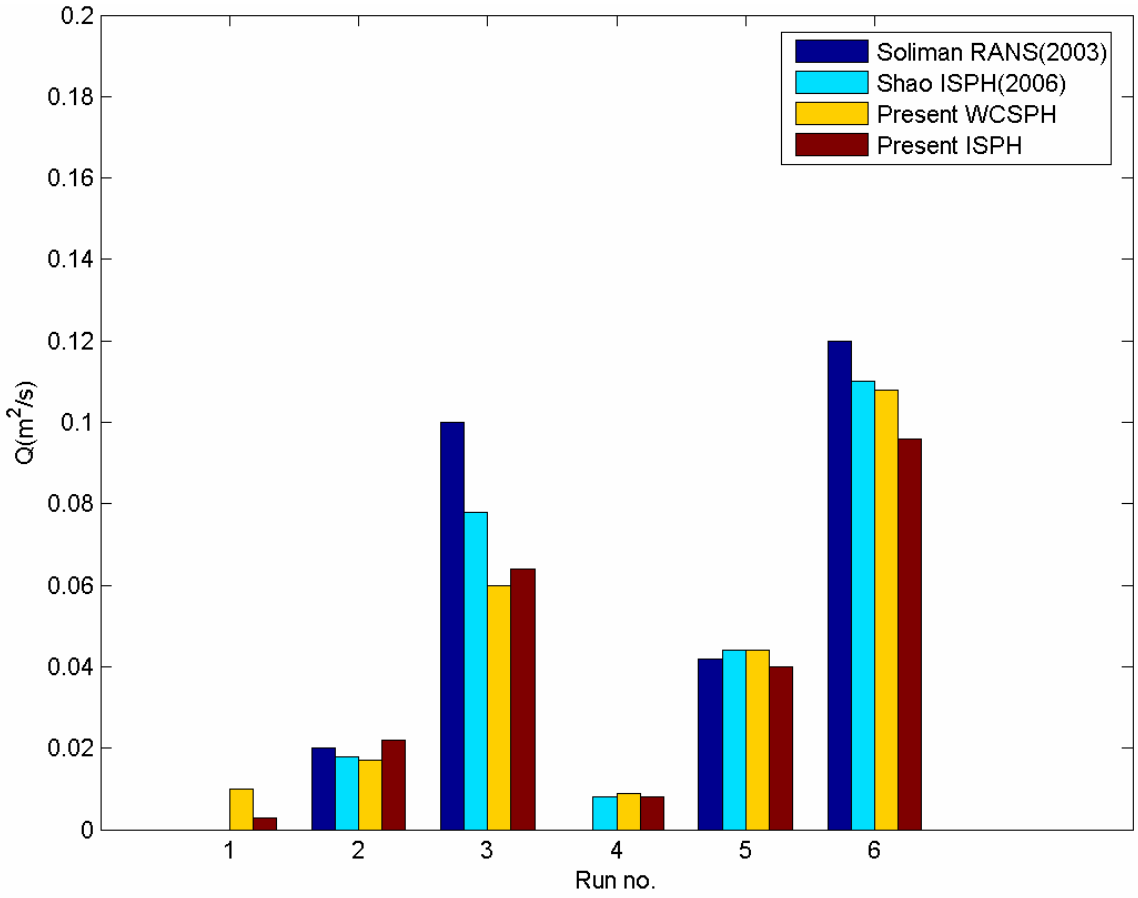

Fig. 6.6. Overtopping rate predicted by the present SPH models and comparison with other studies.

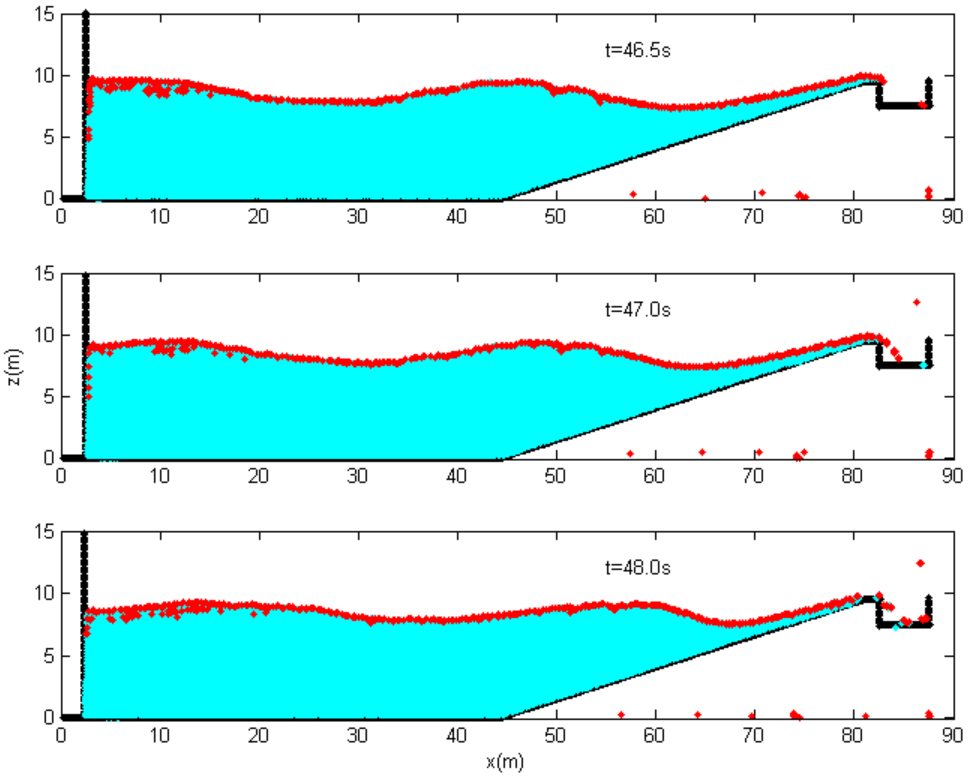

Fig. 6.7. Particle snapshots from ISPH model for random wave overtopping at different instants of time.

Considering wave overtopping as simulated by present WCSPH and ISPH models, it has been found that, in contrast to the wave impact problems as discussed in Chapter 4, predictions from these two models are almost similar subjected to same initial conditions. Therefore, both models are equally good in overtopping calculations.

6.4. SOLITARY WAVES

The present SPH models have been applied to reproduce the experimental set up of Baldock et al. (2012). The bathymetry in the physical model test consisted of a constant depth in front of the wave making boundary, followed by a sloping (slope: 0.107) artificial beach. The beach portion composed of two parts: a permanent beach below the initial Still Water Level (SWL) and a removable beach portion with the provision for placing a storage tank at a desired elevation above the SWL. For each wave climate

considered, two sets of experiments were conducted, first to estimate maximum run up and second to calculate overtopping water. The same set up was reproduced for the SPH models. The details of the model set up are provided in Fig. 6.8.

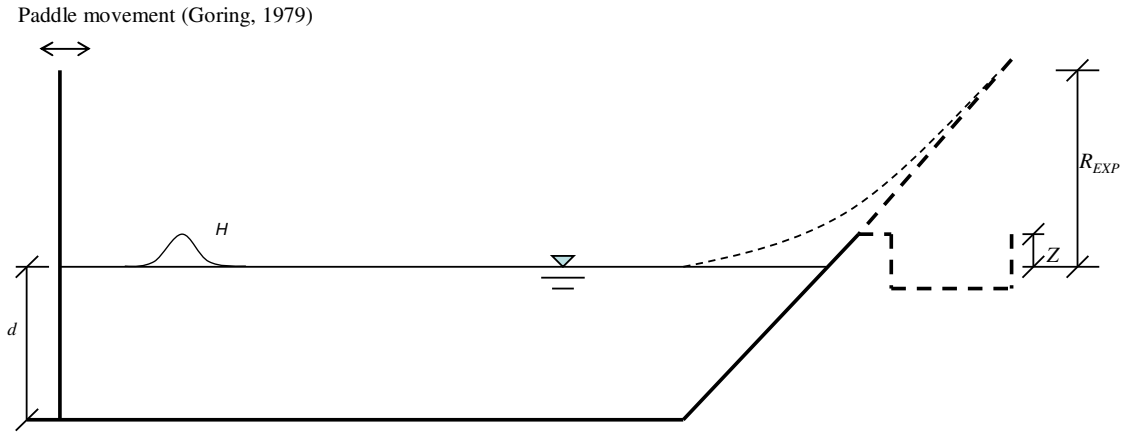

Fig. 6.8. Details of the domain considered for the investigation on wave overtopping due to solitary wave. Initial water depth is (d)= 0.26 m.

Three test cases are considered and Table 6.3 presents the parameters of experimental runs along with the measured maximum run up. R_{EXP} and R_{SPH} are the solitary wave run up measured in experiment and SPH, respectively. The agreement with experimental measurements is relatively better for a higher wave height. For solitary waves with smaller heights, very fine resolution may be required for better agreement. A high resolution is also essential for resolving the boundary layer close to the wall. Fig. 6.9 reports the comparison OF the overtopping water volume predicted by SPH with the experimental measurements. Similar performance as in the case of maximum run up is noticed.

Table 6.3. Wave overtopping parameters due to solitary wave.

Run No.	d (m)	H (m)	Z (m)	R_{EXP} (m)	R_{SPH} (m)
1	0.26	0.032	0.091	0.1012	0.1244
2	0.26	0.061	0.091	0.1714	0.15
3	0.26	0.106	0.091	0.2155	0.2153

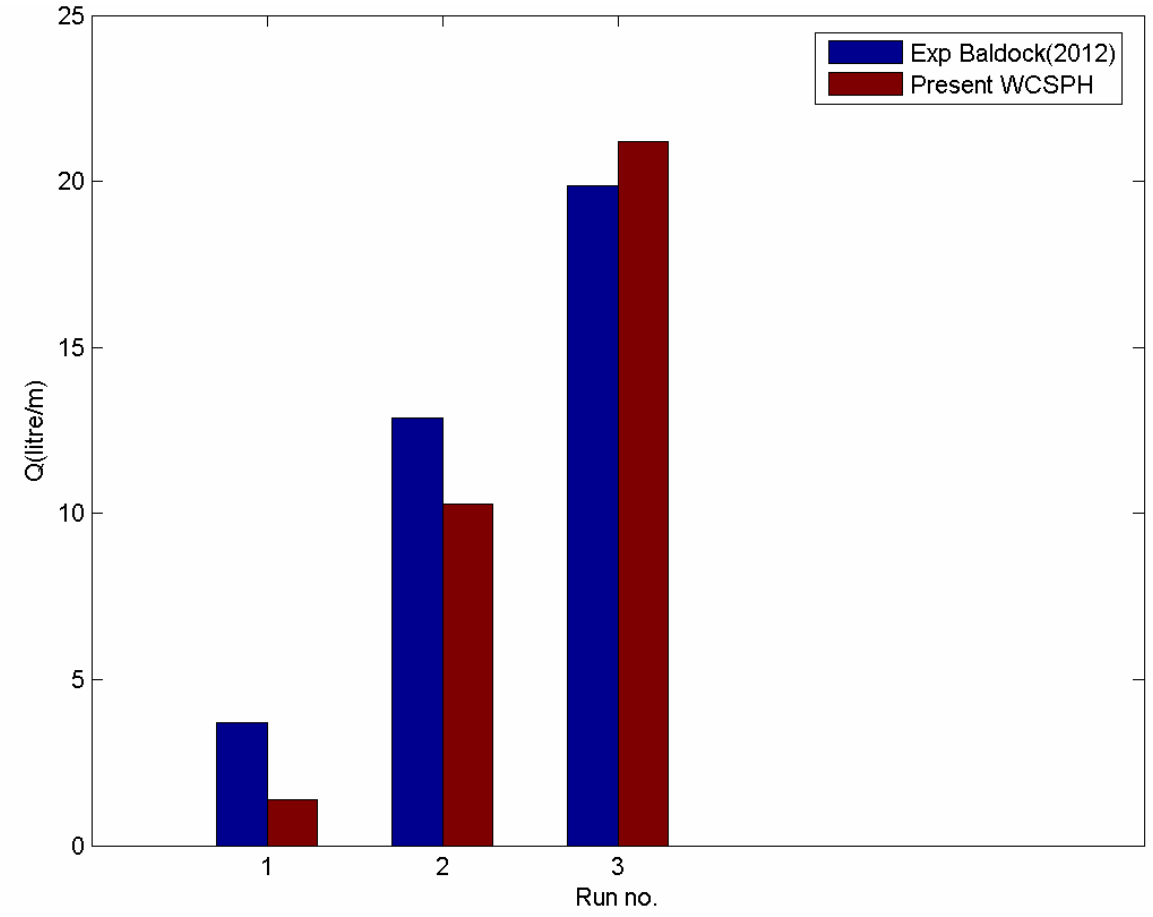

Fig. 6.9. Comparison of the volume of the overtopping water (per unit width of sea wall crest) as predicted by the present WCSPH and experiment (Baldock et al., 2012).

6.5. VERTICAL AND CURVED SEAWALLS

A Seawall is one kind of a protecting member employed in coastal zone serving multiple purposes. They are also used to prevent wave overtopping in regions where excess water may cause severe damages to civil properties (like roads passing next to the beach). Understanding the importance of wave overtopping, many studies have been conducted to understand the relation between local wave climate and coastal structures to prescribe design solutions to prevent wave overtopping (e.g., Kamikubo et al., 2003; Anand, 2010; Anand et al., 2011).

The hydrodynamic characteristics of vertical and three specific curved sea walls were investigated through physical model tests by Anand (2010). This experimental set up has been reproduced in a NWF to show the capability and robustness of the present SPH model to simulate wave interaction with structures involving a complex shape (e.g. a curved front seawall). The domain used both in experiment and numerical studies is shown in Fig. 6.10. In the laboratory, the uniform slope (1:30) was divided into two equal portions in order to conduct test with two different sea walls subjected to same wave environment at the same time.

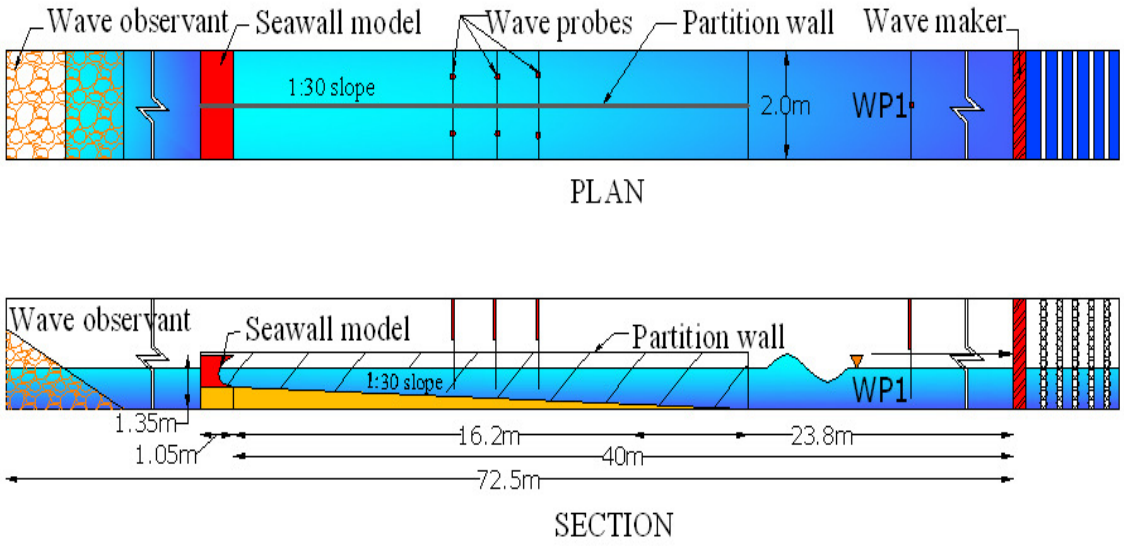

Fig. 6.10. Schematic of the domain considered for the problem of wave interaction with seawalls (from Anand, 2010).

However, in numerical studies, different sea walls are considered for each given cases under same wave conditions separately. The details of the shape and dimensions of the seawalls are provided in Fig. 6.11. These are: Vertical Wall (VW); Flaring Shaped Seawall (FSS); Galveston Seawall (GS) and Circular cum Parabolic Seawall (CPS). The seawalls discretized with particles are shown in Fig. 6.12. The locations of the pressure probes mounted on the seawall profiles are provided in Fig. 6.13. These probes are referred as: Probe 1 (+1.0m), Probe 2 (+0.88m), Probe 3(+0.76m) and Probe 4(+0.64m). The pre-processor reproduces the entire domain (Fig.6.10) considering the required seawalls (Fig. 6.12).

Among the various wave conditions considered by Anand (2010), only the condition in which the generated regular wave with a height (H) of 0.26 m and a period (T) of 3s has been adopted for the present numerical investigation. For the wave interaction with VW, the spatial distribution of total pressure at a particular time instant as predicted by WCSPH, δ- SPH and ISPH has been compared in Fig. 6.14. Due to the addition of diffusive terms in δ- SPH, the pressure field has been found to be improved compared to standard WCSPH. The pressure field in ISPH has also found to be more regular compared to WCSPH.

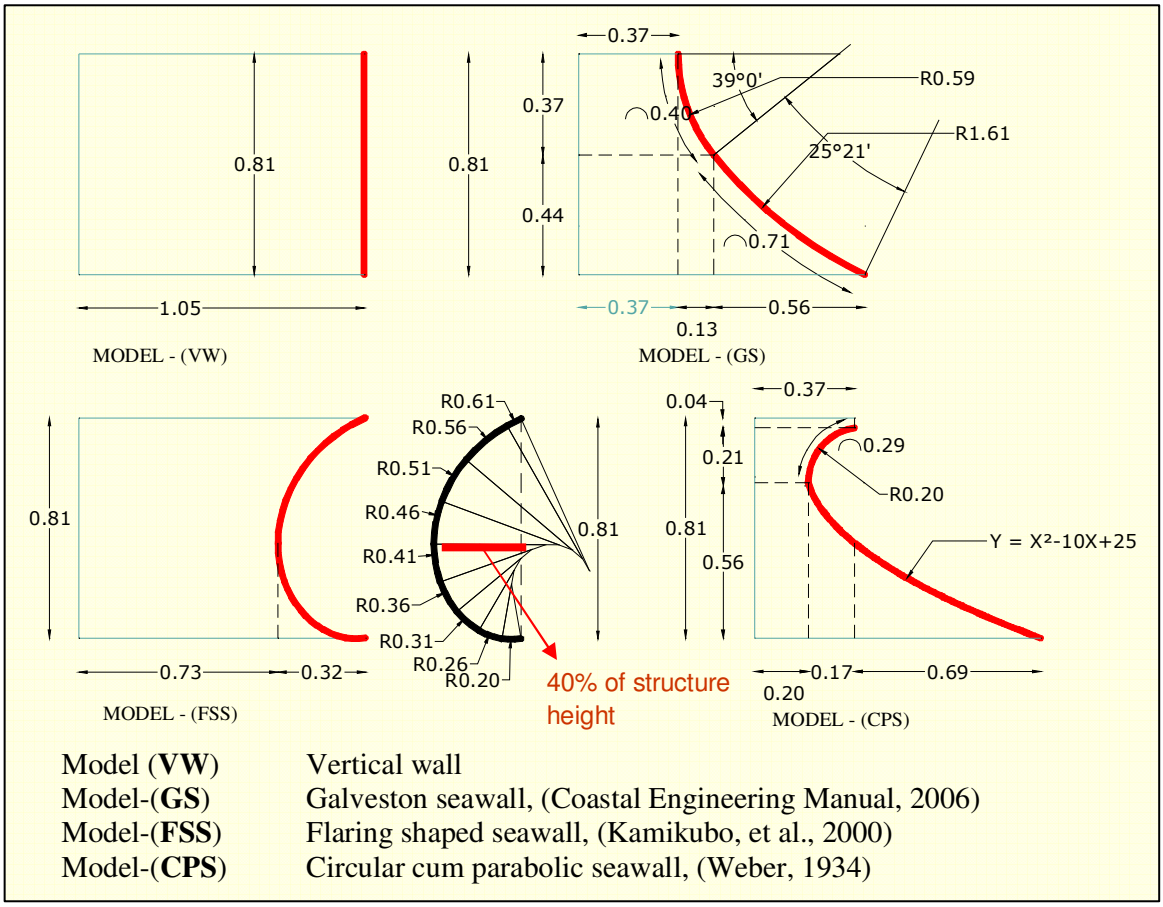

Fig. 6.11. Geometrical details of the vertical and curved sea walls (Anand, 2010).

6.5.1. Dynamic pressure

The comparison between the dynamic pressures measured in experiment (Anand, 2010) and present numerical model has been provided in Figs. 6.15 (a) to (d). Very good agreement has been achieved while comparing the δ- SPH predicted pressure time history

with experimental measurements. This is an improvement obtained in the present study compared to past attempts with SPH and similar particle methods (like MPS) while comparing pressure time history with experiment. It should also be noted that, by taking advantage of the diffusive term in δ- SPH, no spatial filtering has been applied on the predicted numerical time history. However, there is a phase lag in between experiment and numerical prediction and that has been adjusted with respect to the first pressure peak.

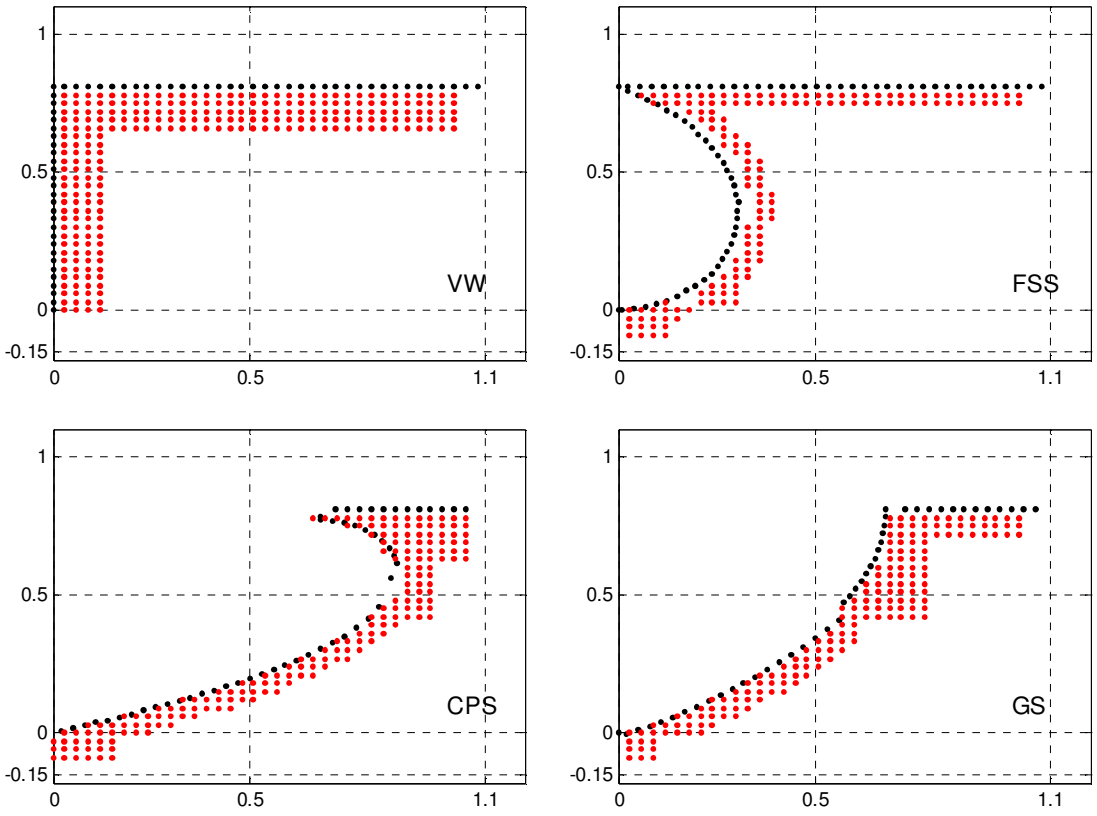

Fig. 6.12. Adopted seawalls discretized with boundary and dummy particles.

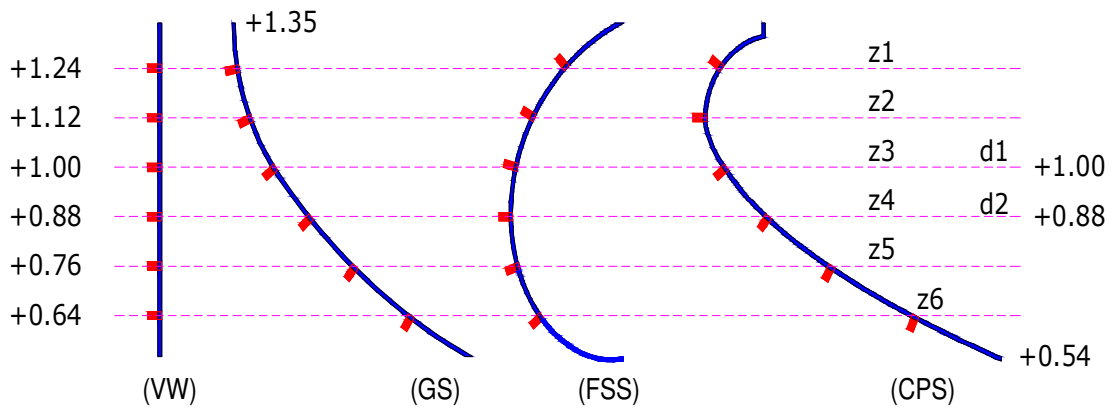

Fig. 6.13. Location of the pressure probes mounted along the seawall profile (Anand, 2010).

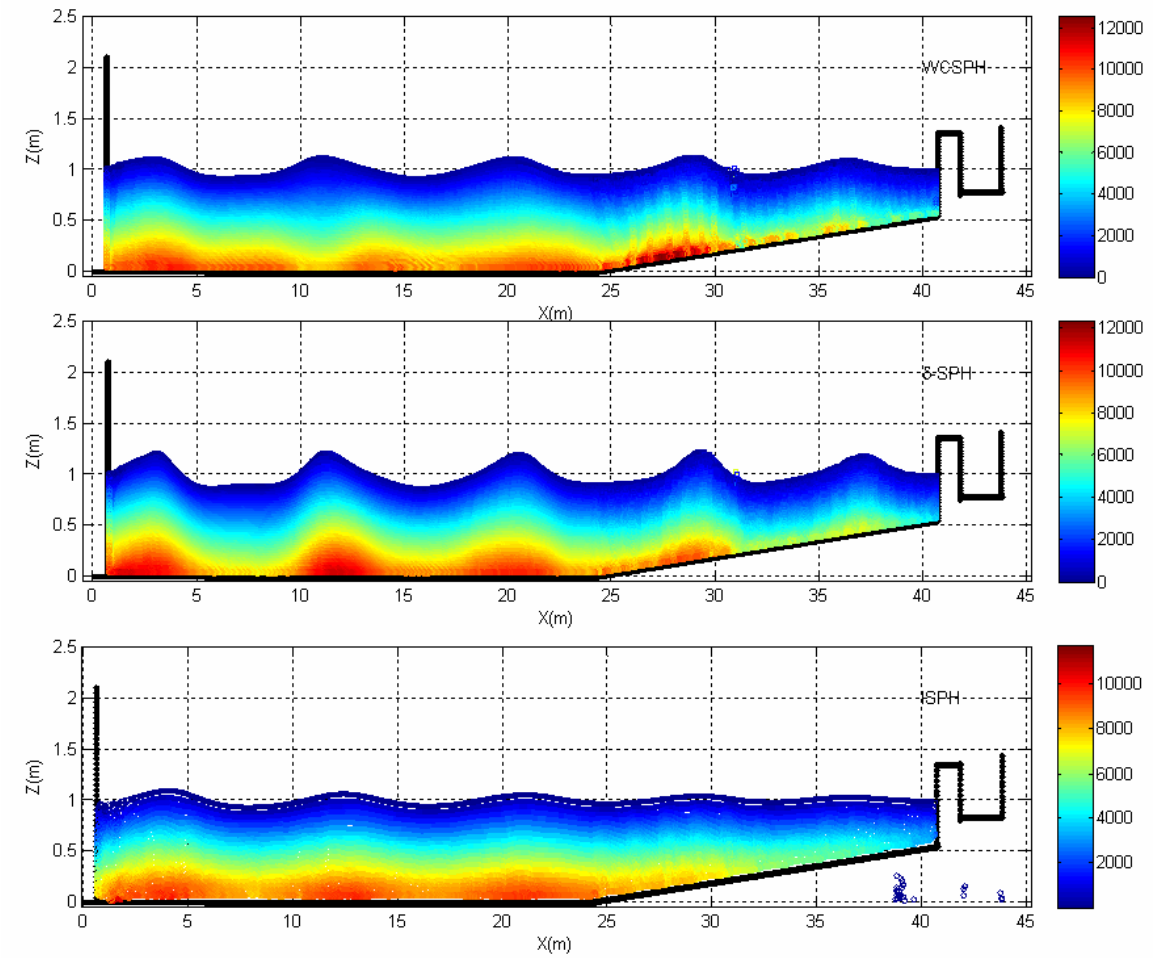

Fig. 6.14. Inter comparison for the pressure at 18 s between different SPH schemes. The colorbar is of pressure in Pa.

In case of VW and FSS, the predicted dynamic pressure time history (specifically Probe 2, Probe 3 and Probe 4) shows characteristics wave nonlinearity by the way of shallowing and broadening of trough of the signal. At the beginning (upto 5s), there are fluctuations recorded in the numerical simulation. It should be noted that, in contrast to some of the δ-SPH models (Marrone et al., 2013) or WCSPH model (Monaghan and Rafiee, 2013; Fatehi and Manzari, 2011), no relaxation has been applied to initialize the particle set up at the beginning of the simulation. However, as the numerical model proceeds further in time, predictions improve indicating the limited effect of applying initialization of the given particle states in the present case. Besides, it is found to be necessary to reduce the XSPH velocity correction factor in case of CPS (Fig. 6.15(c)) and GS (Fig. 6.15 (d)) to capture secondary peaks near the crest and trough in the pressure time history.

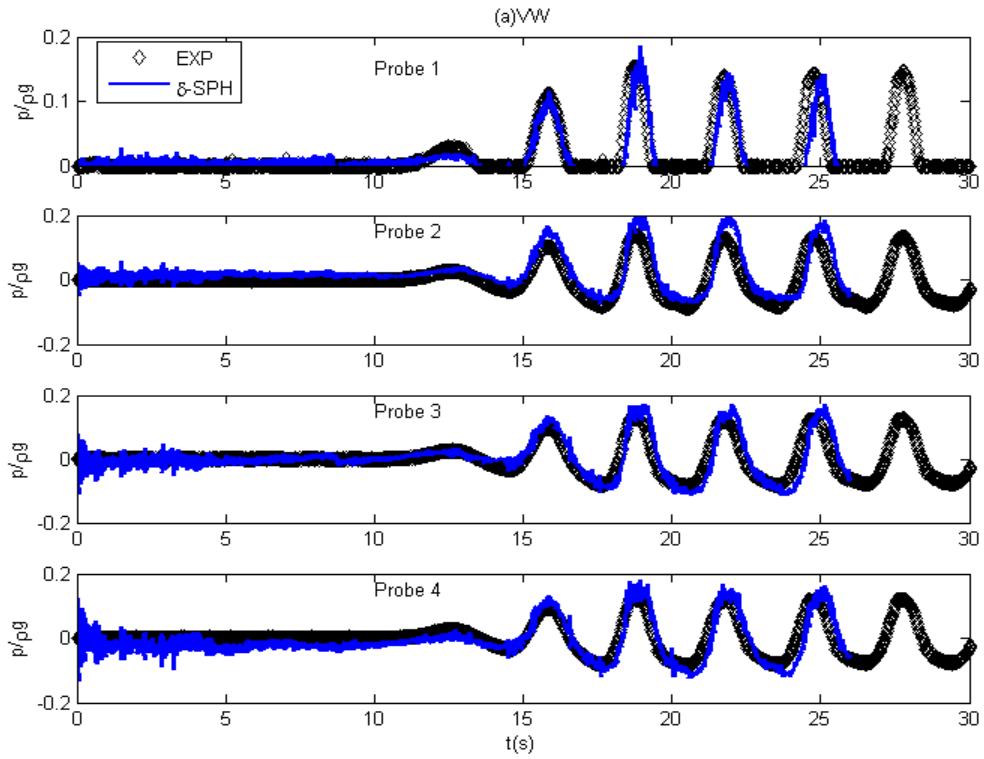

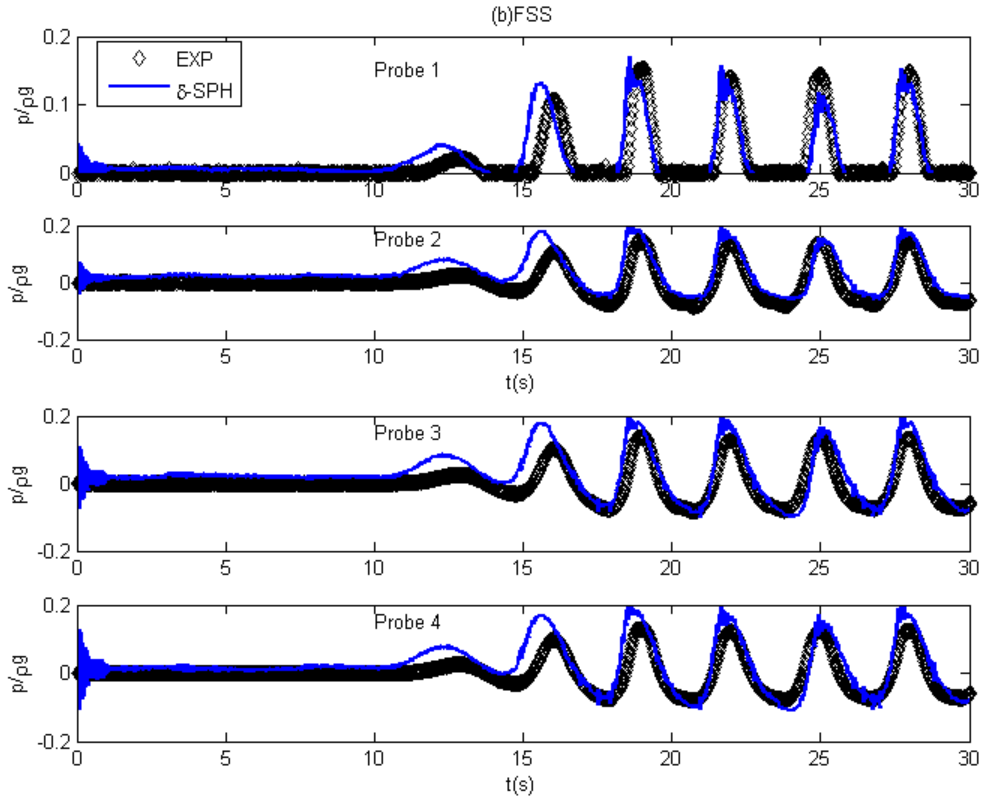
(b)FSS
EXP
δ-SPH
Probe 1
Probe 2
Probe 3
Probe 4
p/ρg
t(s)

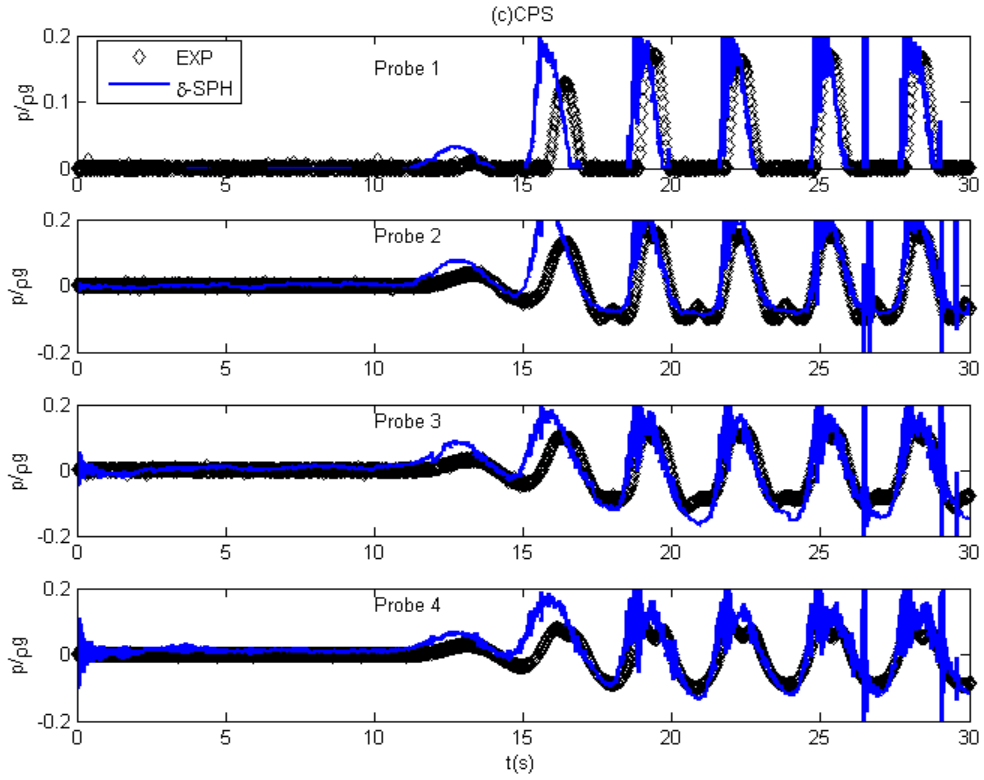
(c)CPS
EXP
δ-SPH
Probe 1
Probe 2
Probe 3
Probe 4
p/ρg
t(s)

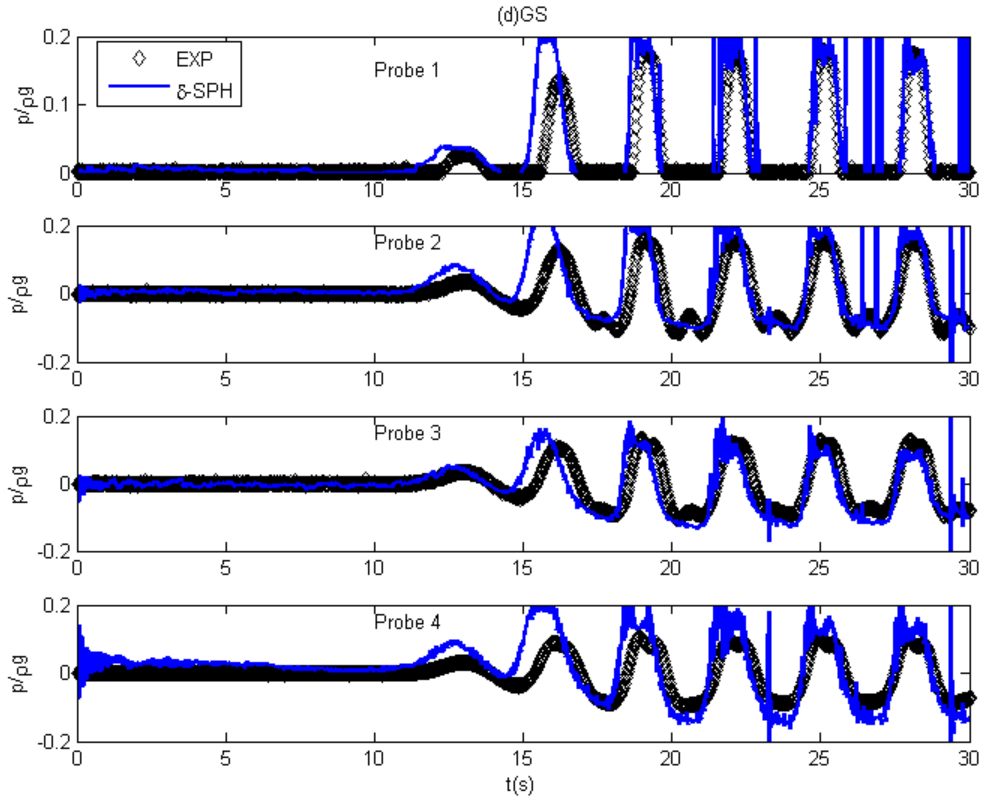

Fig. 6.15. Comparison of dynamic pressure time history between experiment and present δ- SPH due to wave interaction with (a) VW (b) FSS (c) CPS and (d) GS sea walls.

For this reason, there have been more fluctuations observed in these two cases compared to VW and FSS. Also there has been overshoot around 27s for CPS and GS. These issues should be resolved by further optimizing the XSPH velocity correction factor. In overall, these results are quite promising in adopting present SPH model in designing and modelling non linear wave structure interaction in practical coastal engineering problems.

6.5.2. Wave breaking and velocity field

From the foregoing discussion, it is seen that FSS kind of seawalls are preferred than VW as a measure of effective beach protection. Here, the total pressure field and velocity field evolution have been compared for these two kinds of seawalls subjected to same wave conditions using δ- SPH scheme. Fig. 6.16 shows the particle snapshots taken at the

instant when the wave breaks and the resulting spray formation during the violent interaction with the front sea wall. The flow dynamics have been compared with the photographs taken during experiment by Kamikubo et al. (2003). The plunging wave front has been reflected back towards the sea by the FSS both in SPH and experiment, whereas, sprays due to wave breaking overtops on the VW. However, several other physical parameters have to be considered in design for prescribing a seawall under a particular wave climate. Therefore, the velocity field and pressure field at the wave breaking stage have been studied for both of FSS and VW. Fig. 6.17 and Fig. 6.18 present the evolution of the velocity field during wave breaking in case of FSS and VW, respectively. From these two velocity fields it can be observed that at the time of maximum run up, both the sea wall induces similar maximum velocity fields, whereas, while run down, VW induces more severe velocity field compared to FSS. Actually, this is caused due to the reduction in the maximum run up occurred in case of FSS compared to VW. This was also a point of motivation while designing optimal profile for FSS in Anand (2010) in contrast to the original FSS profile proposed in Kamikubo et al. (2000).

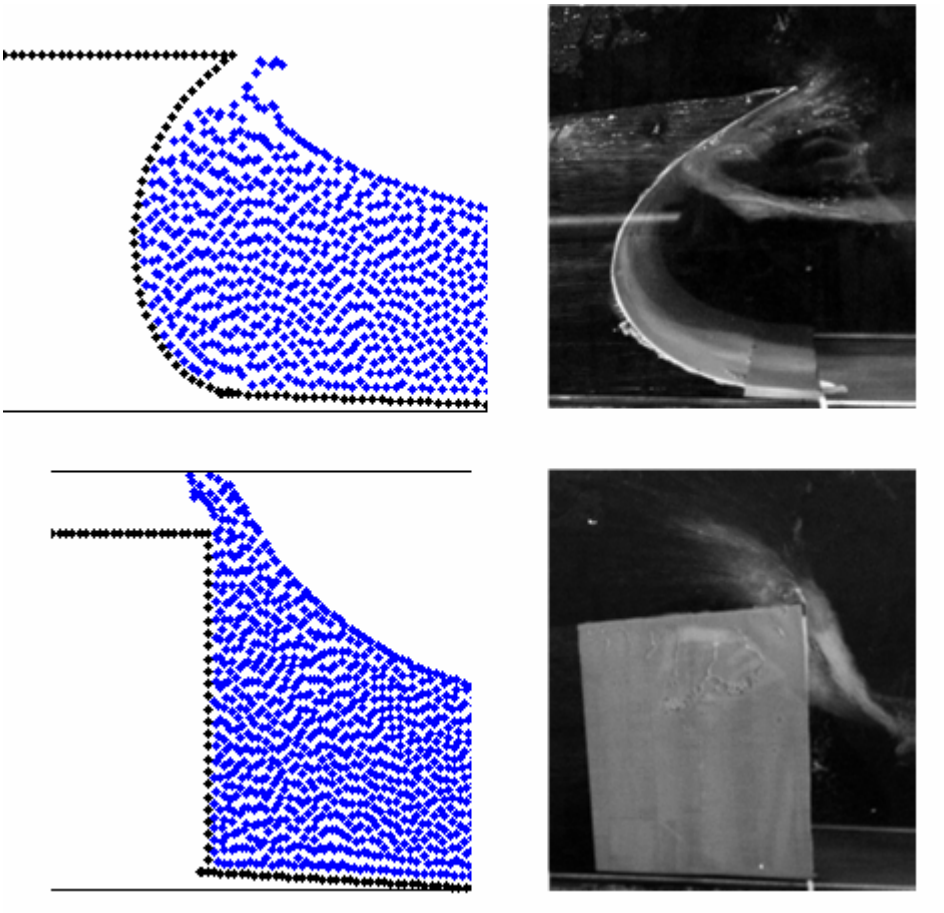

(a) Present study (b) Experiment (Kamikubo et al., 2003)

Fig. 6.16. Wave breaking in front of FSS and VW.

The increase in the velocity field magnitude in VW compared to FSS during run down thus may result in a higher shear stress field adjacent to the VW compared to FSS.

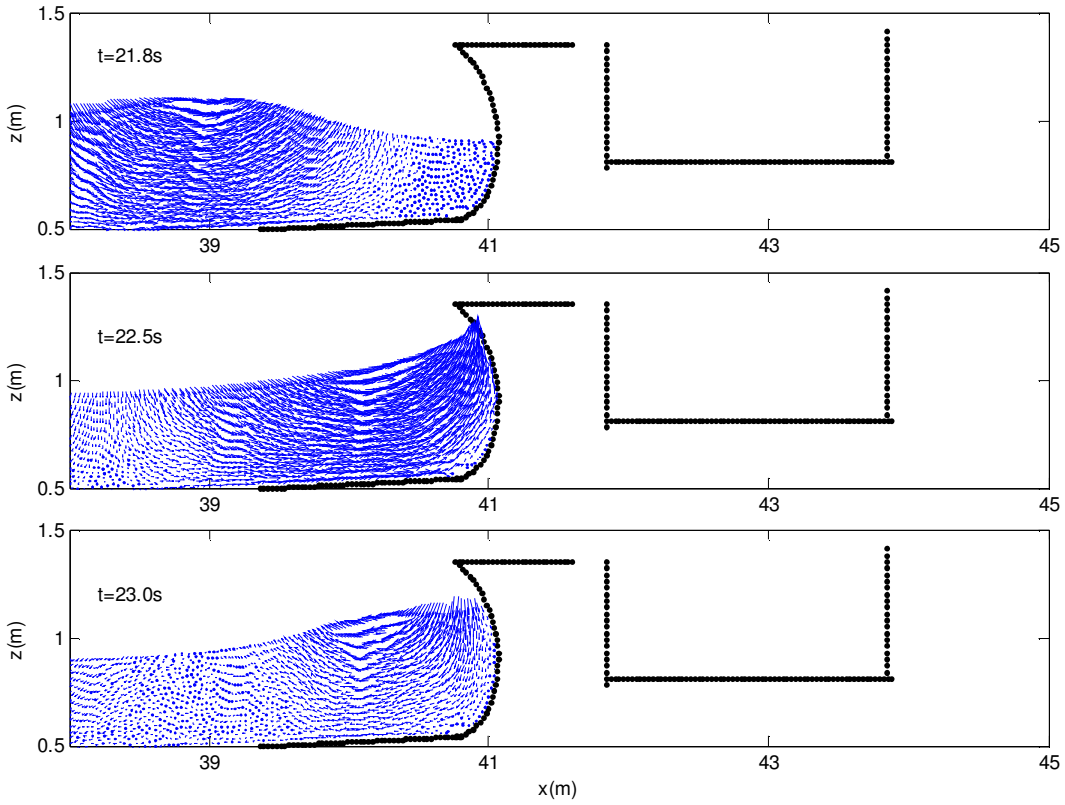

Fig. 6.17. Velocity field evolution during wave breaking on FSS.

Total pressure field corresponding to the time instants during which the vortex field evolves has been reported in Fig. 6.19 and Fig. 6.20 for FSS and VW, respectively. The spatial distribution of pressure shows a higher maximum pressure (almost of the order of 50%) in case of FSS compared to VW. The maximum increase in shoreward peak pressure is found to be 35% at the still water level, in case of FSS compared to VW from the experimental measurement by Anand et al. (2011). Therefore, proper optimization has to be carried out based on other aspects (e.g., material property) in order to adopt seawalls as beach protection measures.

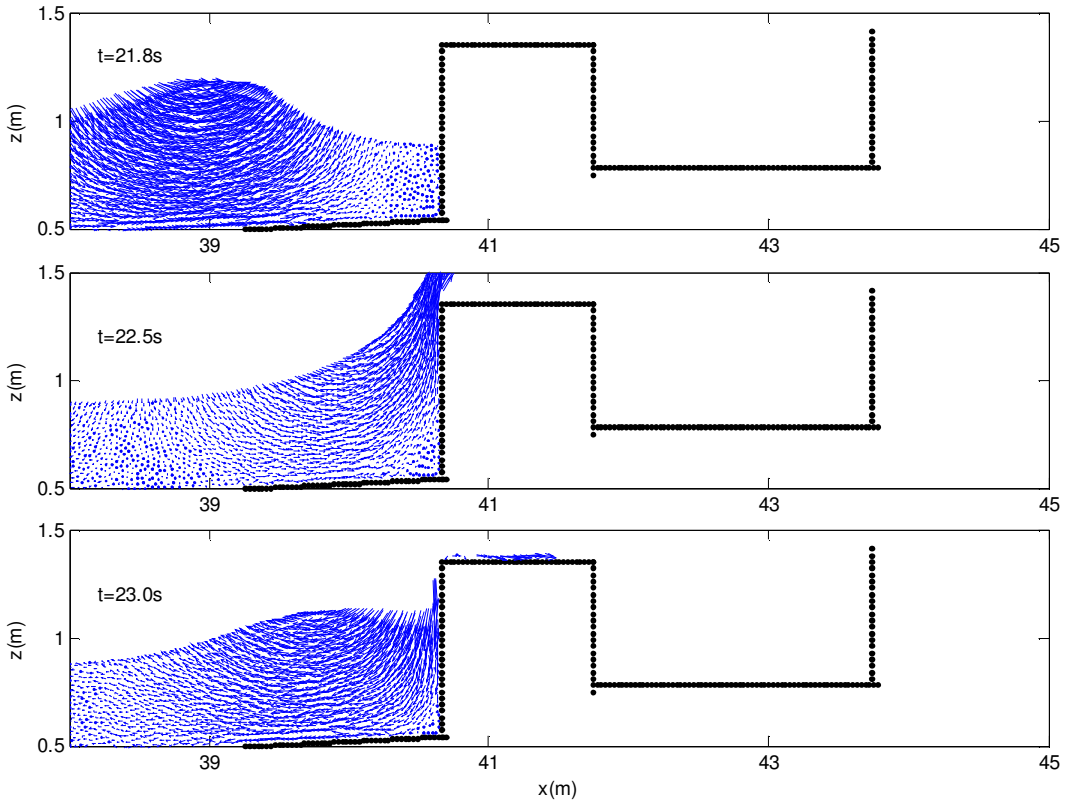

Fig. 6.18. Velocty field evolution during wave breaking on VW.

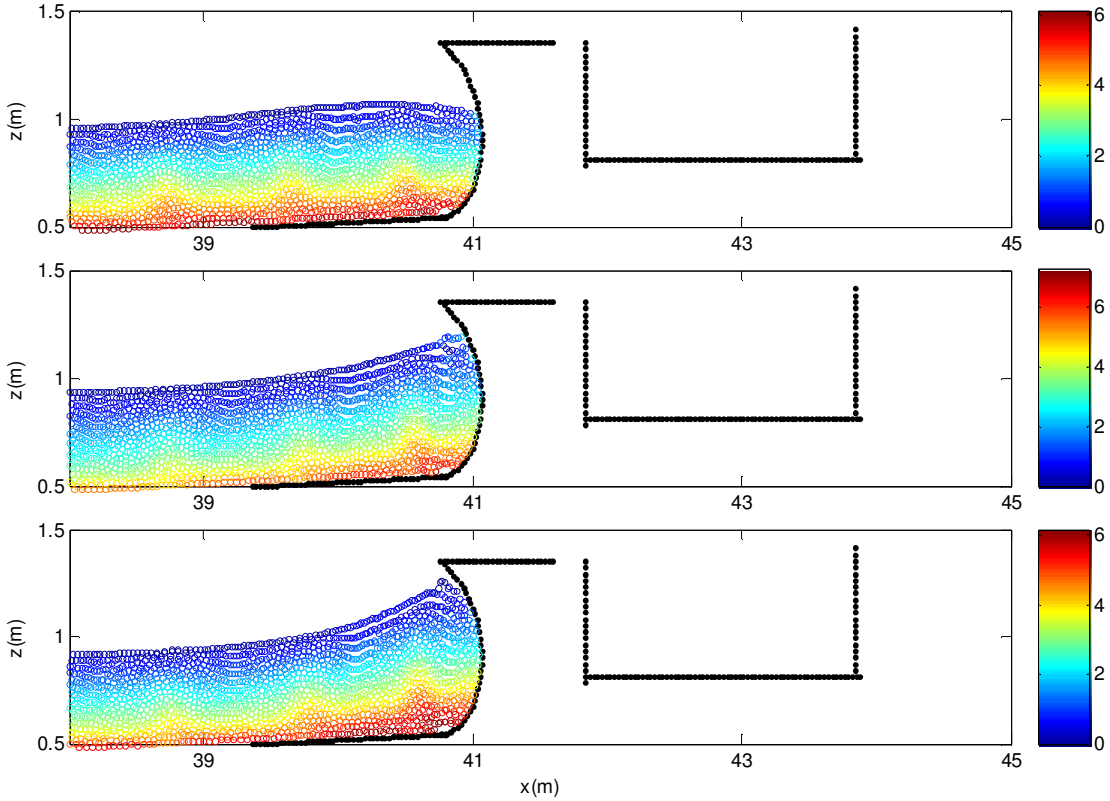

Fig. 6.19. Spatial distribution of total pressure field during wave breaking in case of FSS. The colourbar is of pressure (in Kpa).

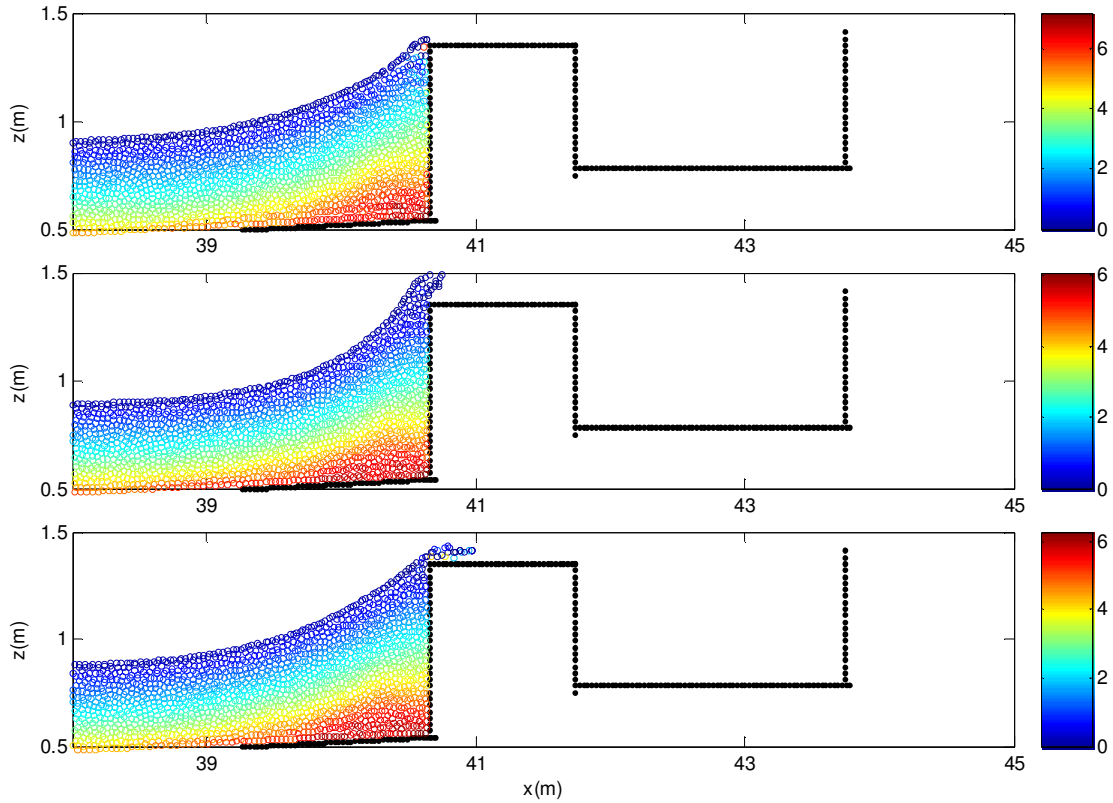

Fig. 6.20. Spatial distribution of total pressure field during wave breaking in case of VW. The colourbar is of pressure (in Kpa).

6.6. SUMMARY

In this chapter, SPH models have been applied to investigate numerically the wave overtopping over different coastal structures under different wave climate. Both WCSPH and ISPH models have been adopted. Adding diffusive term in δ- SPH has improved pressure prediction for longer time simulation and good agreement has been achieved at given locations along seawall when compared to experiment. Both ISPH and WCSPH seem to be equally applicable in predicting overtopping volume of water.

Being a mesh free particle method, SPH has emerged as a potential tool to study wave overtopping charecterised by strong flow separation. Moreover, solving full set of Navier-Stokes equations gives direct access to most of the useful flow properties. This has given the scope to investigate the details of the pressure and velocity fields with the influence of viscosity at the time of wave breaking. The vortex due to breaking has been

found to be more intense for wave interaction with VW compared to FSS. Although SPH schemes are computationally expensive, but fast and efficient computation have been shown with GPU (Barreiro et al., 2013; Hori et al., 2011 for MPS).

CHAPTER 7

SUMMARY AND CONCLUSIONS

7.1. SUMMARY

A robust numerical model based on SPH method has been developed in the present study. The model is capable of simulating a variety of problems in nonlinear water waves. The weakly compressible (WCSPH) and incompressible (ISPH) versions of SPH have been considered. The major advantage is the possibility of simulation of highly steep waves and capturing of wave breaking due to its meshfree characteristics. Flexibility of incorporating the prescribed geometry for the solid boundary by the user and options for both free slip and no slip boundary conditions for moving/ fixed boundaries are additional important features of the present numerical model. The improved WCSPH and ISPH models can perform long time simulation and capture relevant physical processes (such as prediction of identifying higher order harmonics in the sloshing oscaillation). Smooth pressure time histories have been obtained for various wave impact problems.

The following section summarizes the SPH model development and the simulation results for the considered problems. Salient conclusions from the findings observed from different case studies have been provided. This chapter also highlights the scope for prospective future extension of the present study.

7.1.1. Improved SPH models

Many of the successful simulation for the nonlinear water wave problems have been obtained from the present improved versions of the SPH models. The present versions of the WCSPH model suitable for specific problems are summarized in Table 7.1. Five versions of WCSPH have been developed to address problems of different nature. The specific problems which are addressed using different versions of WCSPH are listed. Characteristic features of few versions are combined into a new form for optimizing the advantages to successfully simulate the process under consideration. On the other hand, it is equally important to incorporate some improvements in the ISPH model to address

problems in which pressure prediction is important. This also helps for comparative study with the improved WCSPH model for specific problems. These improvements in ISPH are also provided in Table 7.2.

Table 7.1. Improved versions of the WCSPH models with their characteristic features

Version	Features	Applications
WCSPH-GP Weakly Compressible SPH with Ghost Particles.	• Basic SPH formulation with RK4 time integrator. • MLS density filtering at a given intervals of time steps. • Classical Ghost Particles to enforce free slip along the solid boundaries (both moving and fixed).	1. Benchmark Dam Break problem. 2. NWT: for validation purposes. 3. Sloshing in a prismatic tank.
WCSPH-GP-STEP WCSPH-GP with provision for a STEP.	• Corrections for formulas for assigning correct velocity and mass properties at the corners.	1. Solitary wave split up over a step replicating a continental self. 2. Breaking wave impact over a sea head located on a sloping beach.
***δ*- SPH-GP** *δ*- SPH formulation with Ghost Particles	• Solving higher order source terms in continuity equation: smooth pressure. • Higher time step. • Long time simulations.	1. Sloshing with long time simulation for capturing sub harmonics. 2. Breaking wave impact on a vertical wall.
***δ*- SPH-DP** *δ*- SPH formulation with enhanced Dummy Particle	• Accurate extrapolation of both pressure and velocity at the solid region.	1. Wave impact problem.

Technique	• Easy adoption of geometry of the domain defined by the user. • Faster computation than WCSPH-GP.	
δ- SPH-GP-DP δ- SPH with Dummy Particles for the fixed arbitrary shaped boundaries and Ghost Particles for wave maker.	• Accurate wave generation as defined by the user. • Faster computation than WCSPH-GP-STEP. • Collision model.	1. Solitary wave breaking over a sloping beach. 2. Wave overtopping. 3. Wave interactions with seawalls with prescribed shapes.

Table 7.2. Improved versions of the ISPH models with their characteristic features

Version	Features	Applications
ISPH-MHS ISPH with Multi Higher Order source terms for the PPE.	• Better stability during strong impact. • XSPH smoothing of velocity. • Faster convergence in the solution for PPE.	1. Dame Beak wave impact with and without obstacle. 2. Violent sloshing.
ISPH-DFDI ISPH with uniform particle distributions by employing both Divergence Free and Density Invariant conditions.	• Smooth pressure and velocity field. • Accurate evolution of nonlinear free surface. • Stable long time simulations.	1. Wave overtopping. 2. Wave interactions with sea walls.

7.2. CONCLUSIONS

The major findings from the present study are highlighted as follows.

7.2.1. Model development

- Ghost Particle techniques are preferred for enforcing free slip conditions along the solid boundary for both moving and fixed boundaries, if there are no geometrical complexities. In the presence of sharp changes in the boundary, implementation of ghost particle technique poses difficulties in terms of particles overlap in the ghost region. Yet, one can develop formulae to assign flow properties at singular zones; even though it is difficult to make this as general for any defined shape. Therefore, Dummy Particles are found to be a better approach for the development of robust numerical model. For the benchmark problem, the model has been found to be 30% faster using Dummy Particles than Ghost Particles irrespective of resolution used.
- In order to have a smooth pressure field, the particle coordinates have to be updated so as to retain a uniform particle distribution in overall. This has been achieved by using XSPH velocity correction with the value of the correction factor chosen optimally depending on the problem. XSPH velocity correction ensures uniform particle distribution in both WCSPH and ISPH models with sufficient resolution. However, a standard value (say, 0.5) might degrade the solution in the case of a violent flow. In such cases, a lower value (say, 0.3) might yield better pressure field. For non violent cases, the model has been found to be less sensitive with respect to the chosen value of XSPH factor.
- The role of artificial viscosity can be significantly compensated by XSPH velocity correction technique. There are empirical coefficients in the specification of artificial viscosity which need calibration and thus difficult to adopt for general purposes. It is better to avoid artificial viscosity to retain the original Re of the flow in WCSPH and ISPH models. In most of the cases, the viscous part of the Navier Stokes equation has been modelled using SPH formulation and artificial viscosity has been avoided.
- The dissipation of energy has been found to occur in both WCSPH and ISPH models even if fine resolutions are adopted. The spurious dissipation has to be controlled by properly chosen smoothing length and resolution (i.e., ratio of the characteristic length to

the initial particle spacing). In NWT problem, better comparison of the present WCSPH model with FEM has been obtained for h/dzp= 2 (h is smoothing length and dzp is the initial particle spacing used along the given water depth) than other values. The numerical solution from WCSPH has been found to converge at a faster rate with increase in h/dzp for NWT and sloshing problems. But, the computational cost has been found to increase significantly with increase of h/dzp. Therefore, an optimum value can be selected based on the requirement of the problem under consideration. For sloshing problem, the evolved free surface harmonics is found to be similar to that with h/dzp =2. Therefore, the former value has been adopted as an optimum choice.

- For violent sloshing problem, the WCSPH solution has been found to diverge with increase in resolution. This may be due to the high Re of the flow ($O(10^6)$). Therefore, the optimum resolution has been found through several numerical experiments for violent sloshing. Higher smoothing length (h) gives larger time step in WCSPH. In violent sloshing, the simulation of several flow features like wave breaking, flip through, roof impacts etc. requires smaller time step. Therefore, a relatively smaller h has been preferred in this case.
- Incorporating diffusive terms in continuity equation (δ- SPH) bring two major improvements for WCSPH: a) Pressure time history with less fluctuation and, b) Simulation with larger time step which is favourable for long time simulation of non violent water waves. In many wave impact problems, a secondary peak is observed along with primary peak in the measured pressure time history. It is difficult to extract such useful information from standard WCSPH even while applying smoothing on the predicted pressure time history. The numerical model successfully captures the secondary pressure peaks in wave impact problems as considered in the present study by taking advantages of δ- SPH.
- The preferred choice for improved WCSPH and ISPH models for wave impact problem still remains an open question among other issues. However, considering the problems considered in the present study, the order of preference can be given based on the Re of the flow as: Re($O(10^3)$)- WCSPH, ISPH; Re($O(10^4$-$10^5)$)- ISPH, WCSPH; Re($O(10^6)$)- WCSPH, ISPH. For wave overtopping problems, both models have been proven to be equally applicable.

- WCSPH model has been found to be equally preferable as ISPH model for overtopping calculation. For regular wave incidence, the overtopping prediction from WCSPH differs from experimental measurements by 25.18%, while such variation is 18% for ISPH model. However, RANS estimate deviates of about 52.63% from experimental measurements.

7.2.2. Significance of the results

- Being a Navier Stokes solver, the present numerical model gives direct prediction of the physical quantities which is important in flow analysis for the design of an object in a marine environment. For example, the difference in velocity fields as captured through the present SPH model while simulating wave interaction with seawalls can be effectively used for selecting profile of the seawall and the materials for construction.
- A number of free surface harmonics due to sloshing under regular and random external excitation has been captured by the present SPH model. This characteristic feature of sloshing oscillation can be positively utilized for an efficient operation of the sea going vessels.
- With the rapid progress in computing architecture in recent times, it is apparent that very soon it would be possible to perform fast numerical simulation with million of particles in a laptop utilizing GPU techniques. With the findings, on convergence properties of the SPH scheme for a given problem, optimum choice of input parameters and the choice of a SPH scheme can provide necessary input for the development of an optimized SPH algorithm dealing with 3D problems in addition to parallelization.

7.3. RECOMMENDATIONS FOR FUTURE WORKS

The scope of the present work was initiated with some questions as mentioned at the end of Chapter 2. Upto the current stage of this study, exploration has been made up to certain extent. This leads to the following scope for future work:

- **ISPH model**: A major advantage of ISPH model is the absence of the numerical sound speed constraints on time step. There is also no evidence reported in literature whether there is a shock problem here or not. Instead some collision model has been used. In the present study, some improvements have been incorporated in the ISPH model; yet, success could not be achieved even with these progresses in some cases. For

this reason, inter comparison could not be provided for all the cases where WCSPH based models have been applied. Possible scopes for the improvement of the ISPH model include:

- ***A higher order time integrator:*** Present ISPH model uses predictor- corrector based technique for time marching. It is known that if a higher order time integrator (e.g., RK4, Adam Bashforth) is implemented the computational cost per time step can be significantly increased; yet from numerical point of view, it would be interesting to see how far the model improves by adopting these time integrators like RK4. Because, for long time simulation, higher order time integrators are generally preferred.
- ***Alternate formulation*****:** The projection based strategies proposed by Cummins and Rudman (1999) is one way of enforcing incompressibility in SPH for water wave problems. However, there are other approaches available in literature (e.g., Lastiwaka et al., 2005; Ellero et al., 2007) to enforce incompressibility. Therefore, it would be interesting to perform a comparative study for the same benchmark problem using these different approaches for incompressibility and then investigate their performances.
- Khayyer et al. (2009) found that using an artificial sound speed in the source term of PPE in MPS method (a method similar to ISPH where pressure is obtained by solving PPE), the pressure fluctuation can be reduced. On the other hand, the quantitative equivalence between MPS and ISPH in terms of particle based differential operators has been derived by Souto- Iglesias et al. (2013). Now, combining these two works one can form a definite research path understanding whether numerical sound speed is important parameter to be considered in ISPH.

- **Provision for floating bodies:** A floating body can be incorporated in a particle based numerical model easily due to its meshfree characteristics. Koshizuka et al. (1998) proposed algorithm for simulating floating bodies in MPS. Shao (2009) extended this technique for simulating entry of an object into water using ISPH. Since the developed SPH model can provide proper pressure time history on any shape of the solid boundary, it is important to extend these techniques for modelling floating bodies.

- **Modelling turbulence**: The present SPH models have been able to simulate wave breaking. Now, the next step should be development of the turbulence scheme in order to understand energy dissipation due to turbulence while wave breaking. Issa et al. (2010) has found that choice of a particular scheme to model turbulence may effect the prediction of the free surface profile during wave breaking, particularly in post breaking stages.
- **Other problems**: With the current status of the numerical models, one can go for numerical simulation for the following two important problems in nonlinear water waves:
    - ***Wave focusing*:** In deep ocean, freak waves are generated due to directional focusing of wave groups and may lead to a breaking wave. Present SPH model can be used to study the processes of wave- wave interaction during wave focusing.
    - ***Topographic focusing*:** When a wave crest travels over a variable bathymetry, wave breaking may occur due to shoaling. Since the present SPH model can adopt user defined geometry for the solid boundary, it can be used to simulate wave breaking due to such topographic focusing.
- **Extension to 3D**: Many of the problems in wave structure interaction require the description of the nonlinear water wave in 3D. In such cases, large number of particles are required to perform accurate simulation of the complete scenario of wave generation, propagation and then interaction with structures. But the present serial version of the numerical code can model only upto a limited number of particles. In order to further extend the capabilities following approaches can be considered:
    - ***Hybrid coupling with a potential flow based solver:*** The stages from the generation and then propagation of the nonlinear water wave upto the point of breaking can be modelled using a FNPT based model. This model is computationally cheap and efficient for the same number of nodes (particles) for a NS model. Then from the time the wave starts to overturn and breaks can be modelled using present SPH model. One of the requirements for such coupling is that the pressure field in the particle based NS model has to be regular and smooth. Since the present SPH model has provided smooth pressure field in many cases, it has the potential to be used in such coupling.

- ***Parallel program:*** The computational efficiency of the present serial code can be enhanced by using OpenMP methodologies. Implementation of MPI appears to be difficult. The efficiency should be improved by adopting GPU computing techniques with CUDA programming.

APPENDIX A

ITERATIVE METHODS FOR SOLVING LARGE SPARSE SYSTEM OF MATRIX

A.1. GENERAL

Incompressible SPH (ISPH) method differs from Weakly Compressible SPH (WCSPH) method by the technique adopted to calculate pressure at each particle. These discrete pressures are required to calculate pressure gradient while solving momentum equation (Eqn. 3.29) obtained by approximating the Navier- Stokes equation (Eqn. 3.2). From continuity equation (Eqn. 3.1), it is seen that the velocity field has to be divergence free in order to satisfy the incompressibility condition for the working media (i.e., water). This leads to a Poisson equation (i.e., an equation of the form $\nabla^2\varphi = F$, where both of φ and F are variables) for pressure (which is generally known as Pressure Poisson Equation (PPE)), as explained in section 3.6. To solve PPE, it is required to write it in a matrix form $AX=B$ which actually represents a simultaneous linear system of algebraic equation. Suppose, there are N_p number of fluid particles and N_b number of wetted boundary particles. Then the sizes of A, X and B will be $n \times n$, $n \times 1$ and $n \times 1$, respectively. Here, $n= N_p + N_b$[1]. A is the coefficient matrix (obtained after expanding Eqn. (3.45) for each particle and writing p_{ij} as $p_i - p_j$), X is the unknown vector ($X=\{p_1,p_2,p_3,\ldots.p_n\}^T$) to be solved for pressure and B is the source term (obtained from right hand side of Eqn. (3.44) for each particle) of the PPE. In most cases, n is quite large since a sufficient number of particles are required to perform proper simulation. For a standard 2D problem, the number of neighbouring particles should be in the range of 20 ~50 for a given particle. Hence, for any given row in A, there are numerous empty spaces. Therefore, A is diagonally dominant and sparse. Solving such a matrix by using direct techniques like

[1] N_b may vary in nonlinear water wave problems. Suppose, we need to simulate wave interaction with a structure. In such case, N_b increases when there is a wave run up and N_b decreases when there is a wave run down. Hence in the ISPH model, provision has to be kept in order to consider the varying size of the PPE in time steps.

Gauss Elimination, LU decomposition or Back substitution may be very CPU time consuming. Hence, an iterative method is preferred for such purpose.

In literature pertaining to scientific computing, many iterative methods are available to solve a large sparse matrix. However, the choice closely depends on the properties of the matrix A. This appendix provides an introduction to the principles of constructing iterative schemes and the key factors required to make a choice among the various ones for the ISPH method. A brief numerical test has been reported for the comparative study on a few iterative techniques/ solvers for a given matrix.

The idea presented here is largely based on a comprehensive article by Shewchuk (1994) and some open source Conjugate Gradient (CG) solvers.

A.2. ITERATIVE TECHNIQUE

A.2.1. Principle

An iterative technique provides solution for system of equations written in the matrix form as,

$$AX = B \tag{A.1}$$

An iterative technique is most useful when it is difficult to get exact solutions for X and, an approximate solution is sought. This technique consists of starting with an initial guess for X, choosing a proper direction towards the solution based on current X in hand and then checking the status of error. The basic flow chart for this loop is shown in Fig. A.1. Here, ε is the tolerance criteria imposed on limiting the error. The loop continues until convergence is achieved in terms of the tolerance (i.e., the error does not vary significantly with increase in later iteration steps) or, the error comes below a threshold or, the loop reaches the maximum number of iteration steps permitted. The various iterative techniques differ from each other by the technique adopted to choose the direction towards the correct X and calculate X_{i+1}. The method of steepest descent is the most fundamental among those techniques.

Before discussing the algorithm of steepest descent, it is required to mention the interpretation of Eqn. (A.1) in finding minima of a quadratic form.

A quadratic form for a vector X can be written as,

$$f(X) = \frac{1}{2} X^T AX - BX + c \tag{A.2}$$

Taking derivative with respect to X on both sides of Eqn. (A.2), $f'(X)$ is obtained as,

$$f'(X) = AX - B \tag{A.3}$$

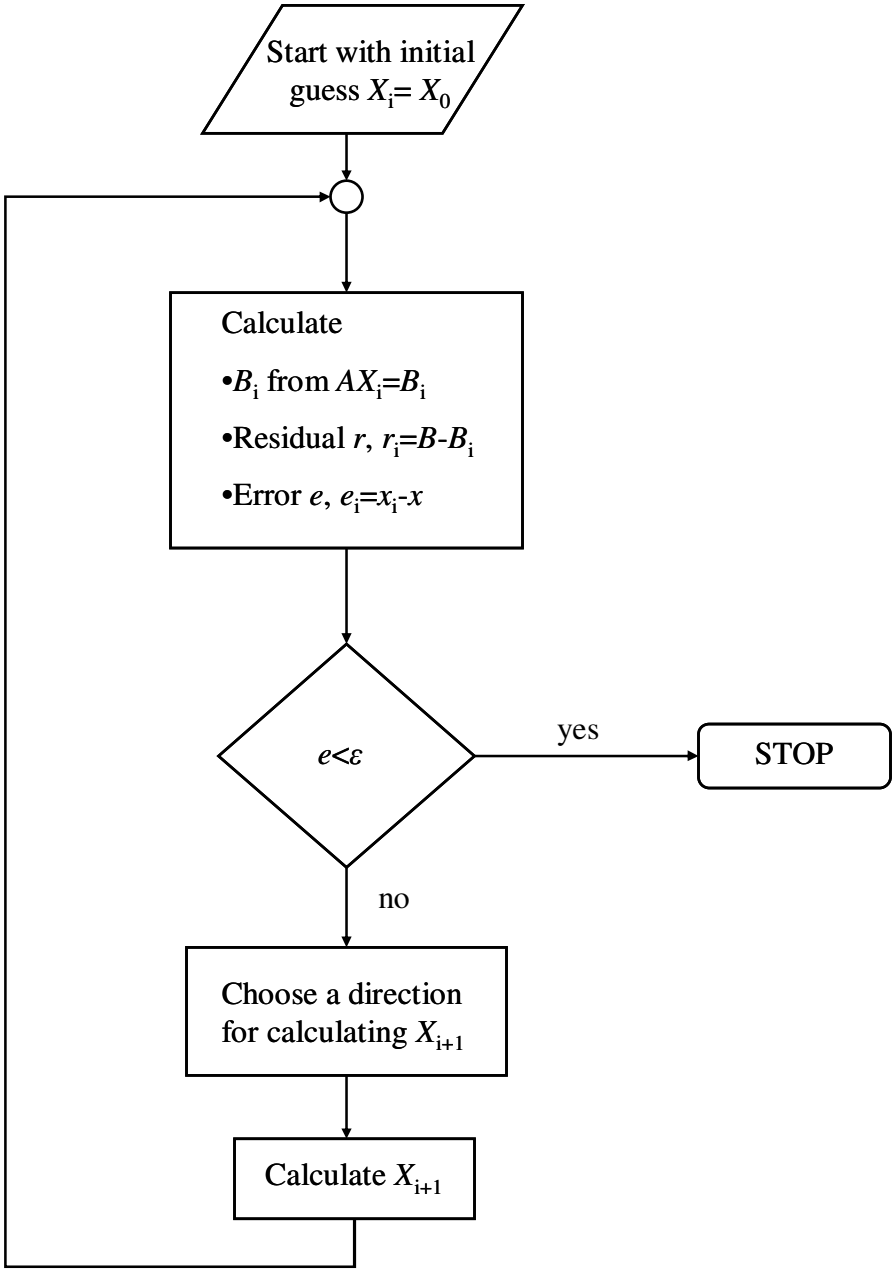

Fig. A.1. Flow chart for a solver using iterative technique.

where, it is assumed that A is symmetric (i.e., $A^T=A$). Therefore, the solution of Eqn. (A.1) can be interpreted as finding minima of Eqn. (A.2) by setting $f'(X)$ in Eqn. (A.3) as zero.

A.2.2. Method of steepest descent

It starts with an initial guess located over the space defined by Eqn. (A.2). With the definition of residual (r) and error (e) shown in Fig. A.1, it can be found that $r_i=-f'(X_i)$. Therefore, at any iteration step, the residual directs opposite to the gradient calculated at X_i over the space of $f(X)$. To calculate X for the next iteration step (i.e., X_{i+1}), one needs a direction (which may be defined by a parameter α) to which one needs to advance towards the correct X as,

$$X_{i+1} = X_i + \alpha r_i \tag{A.4}$$

It is required to consider the following relationship that holds between the residual at the current iteration step (r_i) and at the next step (r_{i+1}).

$$\frac{dX_{i+1}}{d\alpha} = f'\left(X_{i+1}\right)^T \frac{dX_{i+1}}{d\alpha} = -r_{i+1}{}^T r_i \tag{A.5}$$

In each iteration step $f(X)$ is tried to be minimized. For a given point on $f(X)$ this can be achieved by considering the intersection of the planes of $f(X)$ and same given by Eqn. (A.4). Now, for a given X, $f(X)$ is minimized when minima is sought by setting $dX_{i+1}/d\alpha=0$ in Eqn. (A.5). Eventually this leads r_i and r_{i+1} to be orthogonal (since, $r^T_{i+1}r_i=0$). Then substituting r_{i+1} as $B- AX_{i+1}$ and substituting X_{i+1} in terms of X_i from Eqn. (A.4) to Eqn. (A.5), we have α as:

$$\alpha = \frac{r_i^T r_i}{r_i^T A r_i} \tag{A.6}$$

This procedure of finding α is known as line search. In summary, the method of steepest descent is given by,

$$\begin{aligned} r_i &= B - AX_i, \\ \alpha_i &= \frac{r_i^T r_i}{r_i^T A r_i}, \\ X_{i+1} &= X_i + \alpha_i r_i. \end{aligned} \tag{A.7}$$

A.2.3. Conjugate Gradient (CG) method

In the method of steepest descent, there are chances that a particular search direction is taken multiple times. Hence, this process can be made more efficient if a number of search directions, mutually orthogonal are chosen simultaneously and then for each direction, an iterative step is taken. To improve the efficiency further, these directions are made *A* orthogonal. In Conjugate- Gradient (CG) method, this is achieved as

$$\left.\begin{aligned} d_0 &= r_0 = B - AX_0, \\ \alpha_i &= \frac{r_i^T r_i}{d_i^T A d_i}, \\ X_{i+1} &= X_i + \alpha_i d_i, \\ r_{i+1} &= r_i - \alpha_i A d_i, \\ \beta_{i+1} &= \frac{r_{i+1}^T r_{i+1}}{r_i^T r_i}, \\ d_{i+1} &= r_{i+1} + \beta_{i+1} d_i. \end{aligned}\right\} \quad \text{(A.8)}$$

In most of the cases, the condition number (i.e., the ratio of maximum to minimum eigen values) of matrix *A* is improved by multiplying it with another matrix (P^{-1}) so that the product has a better condition number and therefore ensure faster convergence. *P* is chosen in such a way that it is easy to invert (like an identity matrix or a matrix containing only the diagonal parts of *A*). *P* is called a Preconditioner.

A.2.4. Bi- Conjugate Gradient Method

The CG method requires matrix *A* to be positive definite. However, due to meshfree nature of SPH, in some time steps, it may not be assured that *A* will remain positive definite. Therefore, it is required that the adopted CG method is capable to work with square, symmetric but not necessarily positive definite matrix. This can be done by using Bi- Conjugate Gradient method. Along with a Preconditioner (*P*), the resulting algorithm is known as Preconditioned Bi- Conjugate Gradient (PBCG) method. Here, we have two additional set of vectors *z* and $\bar{z}$, defined by

$$\left.\begin{aligned} Pz_i &= r_i \\ P^T \bar{z}_i &= \bar{r}_i \end{aligned}\right\} \tag{A.9}$$

vectors r and $\bar{r}$ are related through the biorthogonality condition,

$$\bar{r}_i.r_j = r_i.\bar{r}_j = 0, \quad for\ j<i \tag{A.10}$$

With these, the PBCG method is obtained by the following recurrence.

$$\left.\begin{aligned} \alpha_i &= \frac{\bar{r}_i z_i}{\bar{d}_i A d_i}, \\ r_{i+1} &= r_i - \alpha_i A d_i, \\ \bar{r}_{i+1} &= \bar{r}_i - \alpha_i A^T \bar{d}_i, \\ X_{i+1} &= X_i + \alpha_i d_i, \\ \beta_i &= \frac{\bar{r}_{i+1} z_{i+1}}{\bar{r}_i z_i}, \\ d_{i+1} &= z_i + \beta_i d_i, \\ \bar{d}_{i+1} &= \bar{z}_i + \beta_i \bar{d}_i. \end{aligned}\right\} \tag{A.11}$$

where, vectors d and $\bar{d}$ are related by biconjugacy condition.

$$\bar{d}_i A d_j = d_i A^T \bar{d}_j = 0, \quad for\ j < i \tag{A.12}$$

The Bi- Conjugate gradient method reduces to CG method when A is symmetric and, $\bar{r}_i = r_i$ and $\bar{d}_i = d_i$, for all i.

A.2.5. Generalized Minimum Residual Method (GMRES)

There is another variant of CG is available which can work with symmetric, square and non positive definite matrix. In such case, $\bar{r}_i = Ar_i$ and $\bar{d}_i = Ad_i$ for all i. Also, all inner products between a general matrix a and vector B, aB is replaced by aAB. The algorithm is known as Generalized Minimum Residual Method (GMRES) which acts by minimizing function, $\Phi(X)$ given by

$$\Phi(X) = \frac{1}{2} r.r = \frac{1}{2} \left| AX - B \right|^2 \tag{A.13}$$

through iterations.

A.3. NUMERICAL TEST

A suitable solver is adopted for the ISPH method based on a series of numerical tests on a given square, symmetric and positive definite matrices (A). In these tests, following solvers have been used:

- BICGSTAB: In built Bi- Conjugate solver in MATLAB®.
- Gauss: Direct inversion of a given matrix based on Gaussian Elimination by using '/' operator in MATLAB®. (source: http://www.mathworks.in/help/matlab/ref/inv.html).
- DGMRES : GMRES solver available in FORTRAN library DLAP for solving sparse linear systems. DLAP has been developed and released in public domain by SLATEC (acronym for Sandia, Los Alamos, Air Force Weapons Laboratory Technical Exchange Committee). Details about SLATEC are available in SLATEC user guide (Fong et al., 1993).
- DBCG: Bi- Conjugate Gradient solver available in DLAP.
- linbcg: A PBCG solver detailed by Press et al. (1986).

These tests consist of two parts: Firstly, a square, symmetric and positive definite matrix of a given size is generated in MATLAB® and stored as A. B is taken as a unit vector. Secondly, for the same A and B, X is solved by BICGSTAB and Gauss (in MATLAB®) and linbcg. The purpose of the test is to understand the pattern of the solution X varies, as its' size increases (i.e., when the size of A increases). When the size is $O(1000)$, DGMRES and DBCG are also applied. Same tests are repeated for multiple times for A for a given size in order to ensure that the results are independent of the ways in which A is generated in MATLAB®.

Fig. A.2 reports the comparative studies for the performances of the above mentioned solvers. Following observations are noted:

- When the number of unknowns is $O(50\text{-}100)$, the solutions from all the solvers matches exactly (Figs. A.2, (a) and (b)). For both of the iterative solvers, BICGSTAB and linbcg, convergence is achieved within about twenty iteration steps. There are also no significant differences in terms of elapsed CPU time for the iterative methods when compared to a direct one like Gauss.

- For the number of unknowns in the range [150- 200], the solution from linbcg matches more closely to Gauss than BICGSTAB (Figs. A.2, (c) and (d)).
- When the number of unknowns in the range [250- 800], the solution from the iterative methods diverges from the direct one (Figs. A.2. (e) and (f)). Even with the increase in the maximum number of iteration steps allowed, no significant changes observed in the results. With the further increase in the number of unknowns (Fig. A.2 (g)), i.e., $O(1000)$, the elapsed CPU time in direct method like Gauss is very large compared to others. Solutions from DGMRES and linbcg match more closely than others. Hence, in ISPH model, one of these two solvers is used.

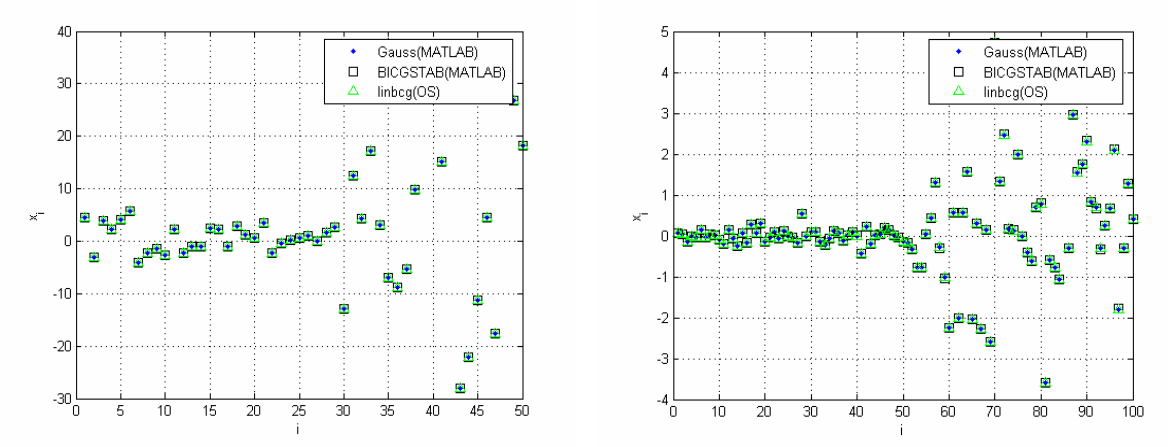

(a) (b)

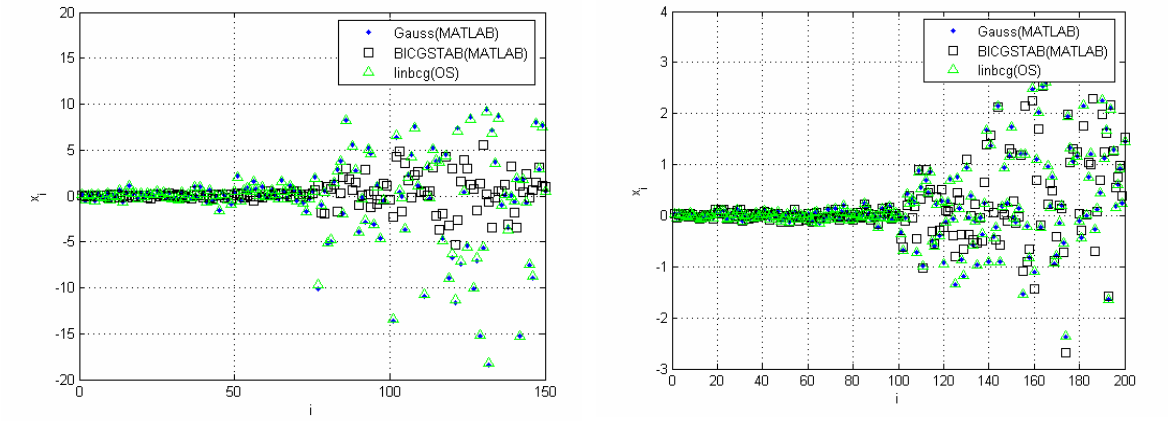

(c) (d)

Fig. A2. Performances of the iterative solvers with reference to the direct solver (Contd..)

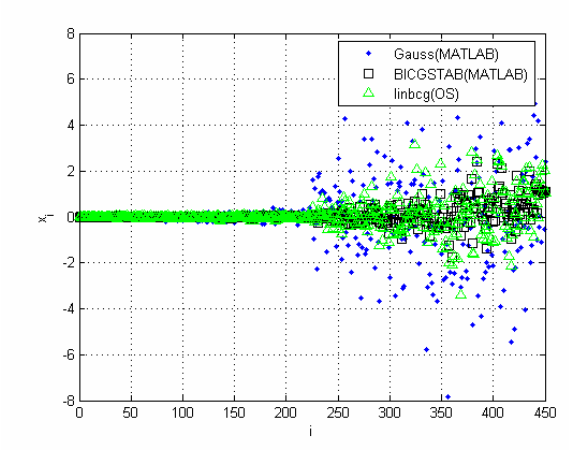

(e)

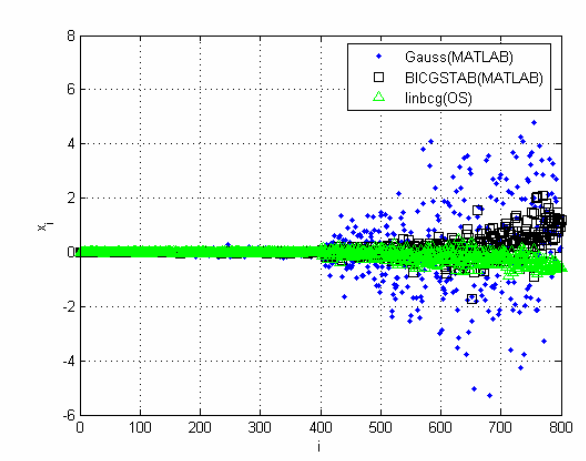

(f)

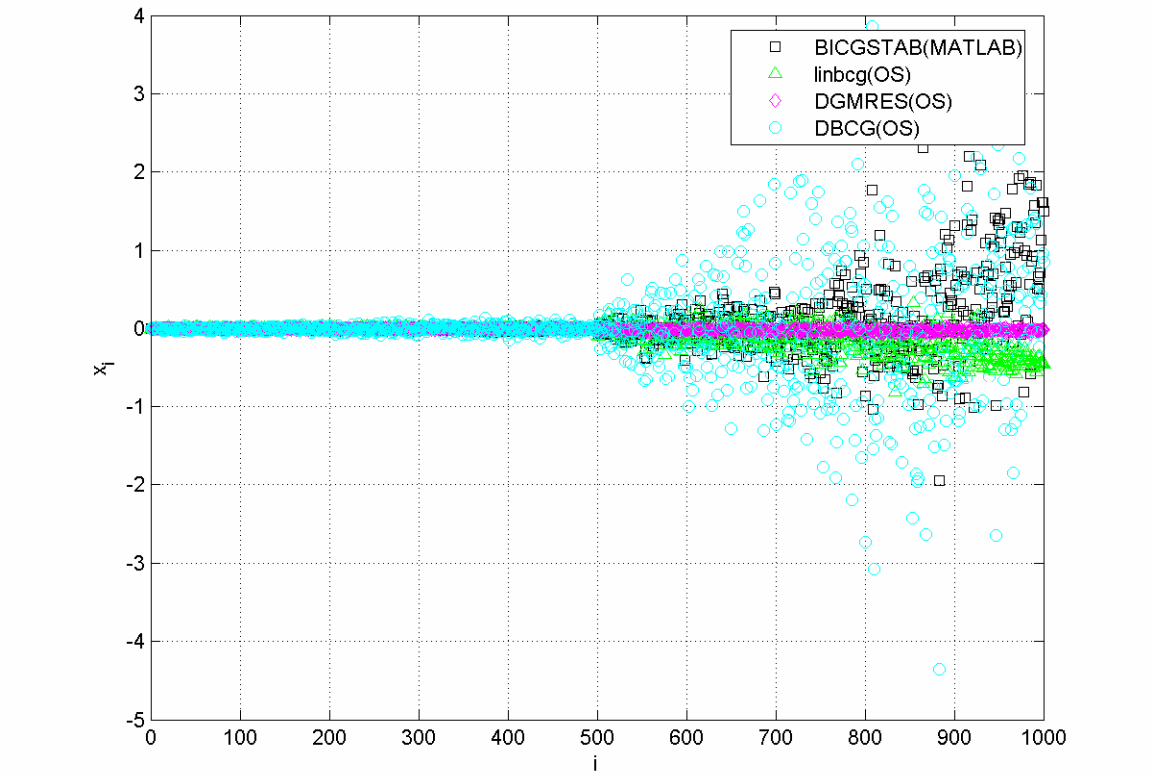

(g)

(Contd..) Fig. A.2. Performances of the iterative solvers with reference to the direct solver.

APPENDIX B
GENERATION OF SOLITARY WAVE

In the present study, solitary wave has been generated in the NWF by prescribing a displacement to the wavemaker (section 4.2.2). The equations (Eqns. (4.5) and (4.6)) that are required to be solved to obtain a piston displacement time series are implicit in form (Goring, 1979). These equations can be solved by an iterative technique. This appendix lists the MATLAB® code (Table B.1) which solves these equations using a simple iterative solver.

The output of the code contains piston displacement time history. This becomes input to the paddle in the NWF to generate a solitary wave of required height for a given initial water depth.

Fig. B.1. shows a typical piston displacement (X_p) time history for a target solitary wave height of 0.1m in a water depth of 1m.

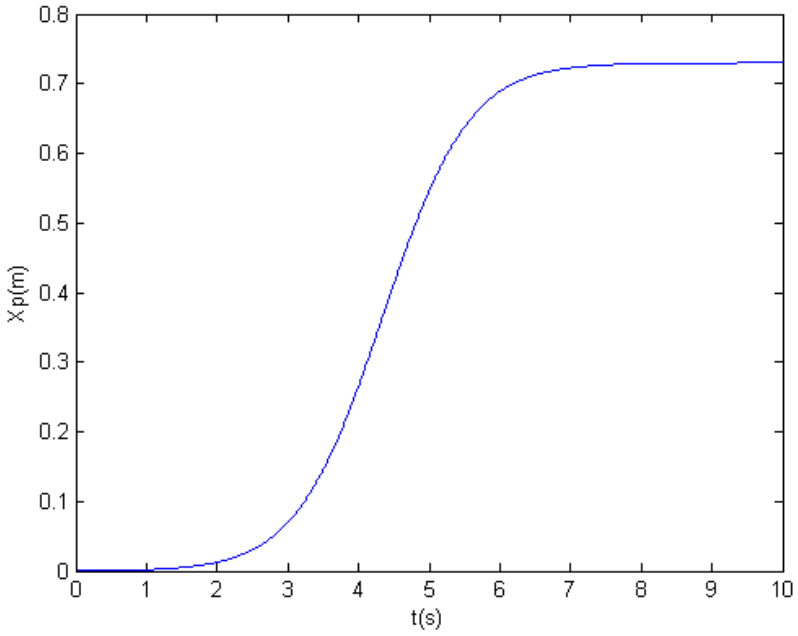

Fig. B.1. Piston displacement time history to generate a solitary wave of height 0.1m in a water depth of 1m.

Table B.1. MATLAB® code for generating piston displacement time history corresponding to a solitary wave

```
clc;
%input target wave height and initial water depth
H=0.1;h=1.0;
g=9.8;
k=((3.0*H)/(4.0*h))^0.5;
cel=(g*(h+H))^0.5;
lambda=3.8/k;

%enter end time
tend=10.0;

tini=0.0;
dt=0.01;
nt=int16((tend-tini)/dt) + 1;
ta(1:nt)=0.0;
for i=2:nt
    ta(i)=ta(i-1)+dt;
end

%initialize working arrays
Xp(1:nt)=0.0;
Vp(1:nt)=0.0;
Xp(1)=0.0;
Vp(1)=0.0;

%define tolerance and maximum number of iteration steps
tol=1.00e-10;
itmax=2000;

x=0.0;

for i=2:nt              % the time integration loop
    x=0.00;
    it=0;
    chi=(k/h)*(cel*ta(i)-x-lambda);
    x2=(H/k)*(tanh(chi)+tanh(k*lambda/h));
    ct=x2-x;
    while(ct>=tol | it<=itmax)          %iteration loop
    x1=x;
    chi=(k/h)*(cel*ta(i)-x1-lambda);
    x2=(H/k)*(tanh(chi)+tanh(k*lambda/h));
    ct=x2-x1;
    x=x2;
    it=it+1;
    end
    Xp(i)=x2;
    chi=(k/h)*(cel*ta(i)-Xp(i)-lambda);
    Vp(i)=(cel*H)/(h*((cosh(chi))^2 + (H/h)));

end

plot(ta,Xp);            %plot displacement time history
xlabel('t(s)');
ylabel('Xp(m)');

M(1:nt,1:2)=0.0;
for i=1:nt
    M(i,1)=ta(i);
    M(i,2)=Xp(i);
end
dlmwrite('wavmker.txt',M,'delimiter','\t')  %store piston displacement time history
```

REFERENCES

Adami S., Hu X.Y. and Adams N.A. 2012. A generalized wall boundary condition for smoothed particle hydrodynamics. *Journal of Computational Physics* (231), 7057- 7075.

Anand K.V. 2010. Hydrodynamic characteristics of curved front face and vertical seawalls. MS Thesis, Department of Ocean Engineering, IIT Madras, India.

Anand K.V., Sundar V. and Sannasiraj S.A. 2011. Hydrodynamic Characteristics of Curved Front Sea Walls Models Compared With Vertical Seawall under Regular Waves. *Journal of Coastal Research* (27(6)), 1103- 1112.

Anderson J.D. 1995. Computational Fluid Dynamics The Basics with Applications. McGrawhill Incorporation, Singapore.

Antuono M., Colagrossi A., Marrone S. and Molteni D. 2010. Free- surface flows solved by means of SPH schemes with numerical diffusive terms. *Computer Physics Communications* (181), 532- 549.

Antuono M., Colagrossi A., Marrone S., Lugni C. 2011. Propagation of gravity waves through an SPH schemes with numerical diffusive terms. *Computer Physics Communications* (182), 866- 877.

Antuono M., Bouscasse B, Colagrossi A. and Lugni C. 2012. Two- dimensonal modal method for shallow- water sloshing in rectangular basins. *Journal of Fluid Mechanics* (700), 419- 440.

Asai M., Aly A.M., Sonoda Y. and Sakai Y. 2012. A Stabilized Incompressible SPH Method by Relaxing the Density Invariance Condition. *Journal of Applied Mathematics* (2012), 1- 24.

Atluri S.N. and Zhu T. 1998. A New meshless local Petrov- Galerkin (MLPG) approach in computational mechanics. *Computational Mechanics* (22), 117- 127.

Babanin A. and Chalikov D. 2012. Nuemrical investigation of turbulence generation in non- breaking potential waves. *Journal of Geophysical Research* (117), 1-14.

Baldock T. E., Peiris D., Hogg J. 2012. Overtopping of solitary waves and solitary bores on a plane beach. *Proceedings of the Royal Society London* (468 A), 3496- 3516.

Balsara D.S. 1995. Von Neumann Stability Analysis of Smoothed Particle Hydrodynamics- Suggestions for Optimal Algorithms. *Journal of Computational Physics* (121), 357- 372.

Barcaloro D.A., Le Touze D. and de Vuyst F. 2012. Incompressible Smoothed Particle Hydrodynamics : proposition and validation of a fully- explicit algorithm. in Proceeding: 7th SPHERIC conference.

Batchelor G.K. 1974. An introduction to fluid dynamics, second edition, Cambridge University Press, New York.

Barreiro A., Crespo A.J.C, Dominguez J.M. and Gomez- Gesteira M. 2013. Smoothed Particle Hydrodynamics for coastal engineering problems. *Computers and Structures* (120), 96- 106.

Benz W. 1984. 3D models of rotating magnetic gas clouds I. Time evolution, mass spectrum and angular momentum. *Astronomy and Astrophysics* (139), 378- 388.

Benz W. 1988. Application of smooth particle hydrodynamics (SPH) to astrophysical problems. *Computer Physics Communications* (48), 97- 105.

Benz W. 1989. Smoothed particle hydrodynamics: a review, NATO Wokshop, Les; Arcs, France.

Belytchsko T., Lu Y.Y. and Gu L. 1994. Element- Free Galerkin methods. *International Journal for Numerical Methods in Engineering* (37), 229- 256.

Bockmann A., Shipilova O., Skeie G. 2012. Incompressible SPH for free surface flows. *Computers and Fluids* (67), 138- 151.

Bonet J. and Lok T.-S.L. 1999. Variational and momentum preservation aspects of Smooth Particle Hydrodynamic formulations. *Computer methods in Applied Mechanics and Engineering* (180), 97- 115.

Bonet J. and Kulasegaram K. 2001. Remarks on tension instability of Eulerian and Lagrangian corrected smooth particle hydrodynamics (CSPH) methods. *International Journal for Numerical Methods in Engineering* (52), 1203- 1220.

Bouscasse B., Colagrossi A., Marrone S. and Antuono M. 2013a. Nonlinear water wave interaction with floating bodies in SPH. *Journal of Fluids and Structures* (42), 112-129.

Bouscasse B., Antuono M., Colagrossi A. and Lugni C. 2013b. Numerical and Experimental Investigation of Nonlinear Shallow Water Sloshing. *International Journal of Nonlinear Sciences and Numerical Simulation*. (14(2)) 123- 138.

Brookshaw L. 1985. A Method of Calculating Radiative Heat Diffusion in Particle Simulations. *Proceedings of the Astronomical Society of Australia* (6(2)), 207- 210.

Camield F.E. and Street R.L. 1968. Shoaling of solitary waves and small slopes. *Journal Waterways and Harbour Division*. (95).

Chalikov D and Sheinin D. 2005. Modeling extreme waves based on equations of potential flow with a free surface. *Journal of Computational Physics* (210), 247- 273.

Chandrasekhar S. 1939. An introduction to the study of stellar structure. Dover Publications Incorporation, New York.

Chandrasekhar S. 1969. Ellipsoidal figures of equilibrium. New Heaven: Yale University Press. London.

Chorin A.J.1968. Numerical solution of Navier- Stokes equations. *Math Comput* (22), 745- 62.

Chen Z., Zong Z., Li H. T., Li J. 2013. An investigation into the pressure on solid walls in 2D sloshing using SPH method. *Ocean Engineering* (59), 129- 141.

Colagrossi A. and Landrini M. 2003. Numerical simulation of interfacial flows by smoothed particle hydrodynamics. *Journal of Computational Physics* (191) 448-475.

Colagrossi A. 2005. A Meshless Lagrangian Method for Free- Surface and Interface Flows with Fragmentation. PhD Thesis, Department of Mechanical Engineering, University of Rome, La Sapienza, Italy.

Colagrossi A., Palladino F., Greco M., Lugni C., Faltinsen O. M. 2006. Experimental and numerical investigation of 2D sloshing: scenarios near the critical filling depth. in Proceeding: 21st IWWWFB.

Colagrossi A., Antuono M., Le Touze D. 2009. Theoretical considerations on the free-surface role in the smoothed- particle- hydrodynamics model. *Physical Review E.* (79(5)) 056701: 1- 13.

Colagrossi A., Souto- Iglesias A., Antuono M. and Marrone S. 2013. Smoothed- particle-hydrodynamics modeling of dissipation mechanisms in gravity waves. *Physical Review E.* (87 (2)) 023302: 1-15.

Cox D.T. and Ortega J.A. 2002. Laboratory observations of green water overtopping a fixed deck. *Ocean Engineering* (29), 1827- 1840.

Crespo A.J.C., Gomez- Gesteira M., Carracedo P. and Dalrymple R.A. 2008. Hybridation of generation propagation models and SPH model to study severe sea states in Galician Coast. *Journal of Marine Systems* (72), 135- 144.

Cummins S.J. and Rudman M. 1999. An SPH Projection Method. *Journal of Computational Physics* (152) 584-607.

Cleary P.W. 1998. Modeling confined multi-material heat and mass flows using SPH. *Applied Mathematical Modelling* (22), 981- 993.

Dalrymple R.A. and Rogers B.D. 2006. Numerical modelling of water waves with the SPH method. *Coastal Engineering* (53), 141- 147.

Das A.K. and Das P.K. 2009. Bubble evolution through submerged orifice using smoothed particle hydrodynamics: Basic formulation and model validation. *Chemical Engineering Science* (64), 2281- 2290.

Dirac P.A.M. 1930. The principles of quantum mechanics. Oxford University Press, UK.

Dean R.G. and Dalrymple R.A. 1984. WATER WAVE MECHANICS for Engineers and Scientists. Prentice- Hall Incorporation, New Jersey.

Delorme L., Colagrossi A., Souto-Iglesias A., Zamora-Rodríguez R., Botía-Vera E. 2009. A set of canonical problems in sloshing, Part I: Pressure field in forced roll-comparison between experimental results and SPH. *Ocean Engineering* (36), 168-178.

Di Monaco A., Maneti S., Gallati M., Sibilla S., Agate G. and Guandalini R. 2011. SPH modeling of solid boundaries through a semi- analytic appraoch. *Engineering Application of Computational Fluid Mechanics* (5(1)), 1-15.

Durisen R.H., Gingold R.A., Tohline J.E. and Boss A. 1986. Dynamic fission instabilities in rapidly rotating n=3/2 polytropes: A comparison of results from finite- difference and smoothed particle hydrodynamics codes. *The Astrophysical Journal* (305), 281-308.

Dilts G.A. 1999. Moving- Least- Square- Particle Hydrodynamics- I. Consistency and Stability. *International Journal for Numerical Methods in Engineering* (44), 1115-1155.

Dilts G.A. 2000. Moving- Least- Square- Particle Hydrodynamics- II. conservation and boundaries. *International Journal for Numerical Methods in Engineering* (48), 1503-1524.

Dyka C.T. and Ingel R.P. 1995. An approach for tension instability in smoothed particle hydrodynamics (SPH). *Computers and Structures* (57(4)), 573- 580.

Dyka C.T., Randles P.W. and Ingel R.P. 1997. Stress points for tension instability in SPH. *International Journal for Numerical Methods in Engineering* (40), 2325- 2341.

Eatock Taylor R., Wang B.T. and Wu G.X. 1994. On the transient analysis of the wavemaker. in Proceeding: 9th IWWWFB.

Ellero M. and Tanner R.I., 2005. SPH simulations of transient viscoelastic flows at low Reynolds number. *Journal of Non- Newtonian Fluid Mechanics* (132(1-3)), 61- 72.

Ellero M., Serrano M. and Espanol P. 2007. Incompressible smoothed particle hydrodynamics. *Journal of Computational Physics* (226), 1731- 1752.

Faltinsen O.M. and Timokha A.N. 2002. Asymptotic modal approximation of nonlinear resonant sloshing in a rectangular tank with small fluid depth. *Journal of Fluid Mechanics* (470), 319- 357.

Fatehi R. and Manzari M.T. 2011. A remedy for numerical oscillations in weakly compressible smoothed particle hydrodynamics. *International Journal For Numerical Methods in Fluids* (67), 1100- 1114.

Fatehi R. and Manzari M.T. 2012. A consistent and fast weakly compressible smoothed particle hydrodynamics with a new wall boundary condition. *International Journal for Numerical Methods in Fluids* (68), 905- 921.

Ferrand M., Laurence D.R., Rogers, B.D., Violeau, D. and Kassiotis C. 2013. Unified semi-analytical wall boundary conditions for inviscid, laminar or turbulent flows in the meshless SPH method. *International Journal For Numerical Methods in Fluids* (71), 446- 472.

Fochesato C. Dias F. 2006. A fast method for nonlinear three- dimensional free-surface waves, Proceedings of the Royal Society of London A (462), 2715- 2735.

Fong K.W. Jefferson T.H., Suyehiro T., Walton L. 1993. Guide to SLATEC Common Mathematical Library.

Frandsen J.B. 2004. Sloshing motion in excited tanks. *Journal of Computational Physics* (196) 53-87.

Gingold R.A. and Monaghan J.J. 1977. Smoothed particle hydrodynamics: theory and application to non- spherical stars. *Monthly Notices of Royal Astronomical Societies* (181), 375- 389.

Gingold R. and Monaghan J.J. 1978. Binary fission in damped rotating polytropes. *Monthly Notices of Royal Astronomical Societies* (184), 481- 499.

Gingold R.A. and Monaghan J.J. 1981. The collapse of a rotating non- axisymmetric isothermal gas cloud. Monthly Notices of Royal Astronomical Societies (197), 461-475.

Goda Y., Fukumori T. 1972. Laboratory investigation of wave pressures exerted upon vertical and composite walls. Report of the Port and Harbour Research Institute, Ministry of Transport, Japan (11(2)), 3- 45.

Goda Y. 2009. Derivation of Unified wave overtopping formulas for seawalls with smooth, impermeable surfaces based on selected CLASH datasets. *Coastal Engineering* (56), 385- 399.

Gomez- Gesteira M., Cerqueiro D., Crespo C. and Dalrymple R.A. 2005. Green water overtopping analyzed with a SPH model. *Ocean Engineering* (32), 223- 238.

Goring D.G. 1979. Tsunamis-The propagation of long waves onto a shelf. PhD dissertation, California Institute of Technology, USA.

Gotoh H., Shibahara T., Sakai T. 2001. Sub-particle-scale turbulence model for the MPS method-Lagrangian flow model for hydraulic engineering, *CFD Journal* (9(4)), 339-347.

Grenier N., Antuono M., Colagrossi A., Le Touze D. 2009. An Hamiltonian interface SPH formulation for muti- fluid and free surface flows. *Journal of Computational Physics* (228), 8380- 8393.

Grenier N., Le Touze D., Colagrossi A., Antuono M. and Collichio G. 2013. Viscous bubbly flows simulation with interface SPH model. *Ocean Engineering* (69), 88-102.

Grilli S.T., Svendsen I.A., Subramanya R. 1997. Breaking criterion and characteristics for solitary waves on slopes. *Journal of Waterway Port Coastal and Ocean Engineering* (123(3)), 102- 112.

Grilli S.T. and Subramanya R. 1996. Numerical modelling of wave breaking induced by fixed or moving boundaries. *Computational Mechanics* (17), 374- 391.

Guo L.C., Zhang S., Morita K and Fukuda K. 2012. Fundamental validation of the finite volume particle method for 3D sloshing dynamics. *International Journal for Numerical Methods in Fluids* (68), 1- 17.

Hammersley J.M. and Handscomb D.C. 1964. Monte Carlo Methods. Methuen, London.

Hockney R.W. and Eastwood J.W. 1988. Computer simulations using particles, Adamhilger, New York.

Hietel D., Steiner K. and Struckmeier J. 2000. A finite volume particle method for compressible flows. *Mathematical Models and methods in Applied Science* (10), 1363- 1382.

Hernquist L. and Katz N. 1989. TreeSPH- A unification of SPH with the hierarchical tree method. *The Astrophysical Journal Supplement Series* (70), 419- 446.

Hori C., Gotoh H., Ikari H., Khayyer A. 2011. GPU- acceleration for Moving Particle Semi- Implicit method. *Computers and Fluids* (51), 174- 183.

Hosseini S.M., Manzari M.T. and Hannani S.K. 2007. A fully explicit three- step SPH algorithm for simulation of non- Newtonian fluid flow. *International Journal of Numerical Methods for Heat and Fluid Flow* (17(7)), 715- 735.

Hirt C.W. and Nichols B.D. 1981. Volume of fluid (VOF) method for dynamics of free boundaries. *Journal of Computational Physics* (39), 201-225.

Hu K., Mingham C.G. and Causon D.M., 2000. Numerical simulation of wave overtopping of coastal structures using non- linear shallow water equations. *Coastal Engineering* (41), 433- 465.

Hu X.Y. and Adams N.A. 2007. An incompressible multi- phase SPH method. *Journal of Computational Physics* (227), 264- 278.

Hu Z., Zheng X., Duan W. and Ma Q. 2011. K2_SPH method and its application for 2-D water wave simulation, *Journal of Marine Science and Applications* (10), 399- 412.

Hughes J.P., Graham D.I. 2010. Comparison of incompressible and weakly- compressible SPH models for free- surface water flows. *Journal of Hydraulic Research* (48), 105-117.

Ibrahim Rouf A. 2005. Liquid sloshing dynamics theory and application, first edition. Cambridge University Press, UK.

Issa R., Violeau D., Lee E.-S. and Flament H., 2010. Modelling nonlinear water waves with RANS and LES SPH models, in Advances in Numerical Simulation of Non-linear Water Waves, edited by Q.W. Ma, 497-537. World scientific, Singapore.

Idelsohn S.R., Oñate E. and Del Pin F. 2004. The particle finite element method: a powerful tool to solve incompressible flows with free-surfaces and breaking waves. *International Journal for Numerical Methods in Engineering* (61), 964- 989.

Idelsohn S.R., Marti J., Limache A. and Oñate E. 2008. Unified Lagrangian formulation for elastic solids and incompressible fluids: Application to fluid- structure interaction problems via the PFEM. Computer methods in Applied Mechanics and Engineering (197), 1762- 1776.

Inutsuka S. 2002. Reformulation of Smoothed Particle Hydrodynamics with Riemann Solver. Journal of Computational Physics (179), 238- 267.

Kamikubo Y., Murakami K., Irie I., and Hamasaki Y. 2000. Study on Practical Application of a Non-Wave Overtopping Type Seawall. in Proceeding: 27th ICCE conference (126) 2215-2228.

Kamikubo Y., Murakami K., Irie I., Kataoka Y. and Takehama N. 2003. Reduction of Wave Overtopping and Water Spray with Using Flaring Shaped Seawall. in Proceeding: 13th ISOPE (3), 671- 676.

Kashiwagi M., Hu C., Sueyoshi M. 2010. Numerical computation methods for strongly nonlinear wave-body interactions, in Advances in Numerical Simulation of Non-linear Water Waves, edited by Ma Q.W., 429- 464. World Scientific, Singapore.

Kim Y. 2001. Numerical simulation of sloshing flows with impact load. *Applied Ocean Research* (23), 53- 62.

Kim K.S., Lee B.H., Kim M.H. and Park J.C. 2011. Simulation of Sloshing Effect on Vessel Motions by Using MPS (Moving Particle Simulation). *Computer Modeling in Engineering and Sciences* (79(3)), 201-221.

Kishev Z.R. Hu C and Kashiwagi M. 2006. Numerical simulation of violent sloshing by a CIP-based method. *Journal of Marine Science and Technology* (11), 111- 122.

Kobayashi N. and Wurjanto A. 1989. Wave Overtopping on Coastal Structures. *Journal of Waterway Port Coastal and Ocean Engineering* (115(2)), 235- 251.

Koh C.G., Gao M. and Luo C. 2012. A new particle method for simulation of incompressible free surface flow problems. *Computer methods in Applied Mechanics and Engineering* (89), 1582- 1604.

Koh C.G., Luo M., Gao M. and Bai W. 2013. Modelling of liquid sloshing with constrained floating baffle. *Computer and Structures* (122), 270- 279.

Koshizuka S. and Oka Y. 1996. Moving- particle semi- implicit method for fragmentation of incompressible fluid. *Nuclear Science and Engineering* (123(3)), 421- 434.

Koshizuka S, Nobe A and Oka Y. 1998. numerical analysis of breaking waves using the moving particle semi implicit method. *International Journal for Numerical Methods in Fluids* (26), 751- 769.

Koukouvinis P.K., Anagnostopoulos J.S. and Papantonis D. 2013. An improved MUSCL treatment for the SPH- ALE method : comparsion with the standard SPH method for the jet impingement case. *International Journal For Numerical Methods in Fluids* (71), 1152- 1177.

Khayyer A. 2008. Improved Particle Methods by Refined Differential Operator Models for Free-Surface Fluid Flows. PhD Thesis, Department of Civil and Earth Resources Engineering, Kyoto University, Japan.

Khayyer A., Gotoh H. and Shao S.D. 2008. Corrected Incompressible SPH method for accurate water- surface tracking in breaking waves. *Coastal Engineering* (55), 236- 250.

Khayyer A, Gotoh H and Shao S. 2009. Enhanced predictions of wave impact pressures by incompressible SPH methods. *Applied Ocean Research* (31), 111-131.

Khayyer A. and Gotoh H. 2009a. Modified Moving Particle Semi- implicit methods for the prediction of 2D wave impact pressure. *Coastal Engineering* (56), 419- 440.

Khayyer A. and Gotoh H. 2009b.Wave Impact Pressure Calculations by Improved SPH Methods. *International Journal of Offshore and Polar Engineering* (19(4)), 300-307.

Khayyer A. and Gotoh H. 2011. Enhancement of stability and accuracy of the moving particle semi- implicit method. *Journal of Computational Physics* (230), 3093- 3118.

Khayyer A. and Gotoh H. 2013. Enhancement of performance and stability of MPS mesh- free particle method for multiphase flows characterized by high density ratios. *Journal of Computational Physics* (242), 211- 233.

Kulasegaram S., Bonet J., Lewis R.W. and Profit M. 2004. A variational based contact algorithm for rigid boundaries in two dimensional SPH applications. *Computational Mehcanics* (33), 316- 325.

Lastiwka M., Basa M. and Quinlan N. 2005. Incompressible Smoothed Particle Hydrodynamics using a Clebsh- Weber Decomposition. in Proceeding: ECCOMAS Thematic Conference on Meshless Methods (Meshless 2005), B13.1- B13.8.

Lastiwka M., Basa M. and Quinlan N.J. 2009. Permeable and non- reflecting boundary conditions in SPH. *International Journal for Numerical Methods in Fluids* (61), 709-724.

Lattanzio J.C., Monaghan J.J., Pongracic H. and Schwarz M.P. 1985. Interstellar cloud collisions. *Monthly Notices of Royal Astronomical Societies* (215), 125- 147.

Le Touze D., Colagrossi A. and Collichio G. 2006. Ghost technique for right angles applied to solution of benchmarks of 1 and 2. in Proceeding: 1st SPHERIC workshop.

Lee E.S., Moulinec C., Xu R., Violeau D., Laurence D. and Stansby P.K. 2008. Comparisons of weakly compressible and truly incompressible algorithms for the SPH mesh free particle method. *Journal of Computational Physics* (227), 8417-8436.

Lee B-H., Park J-C., Kim M-H., Jung S-J., Ryu M-C. and Kim Y-S. 2010. Numerical simulation of impact loads using a particle method. *Ocean Engineering* (37), 164-173.

Lee B-H., Park J-C., Kim M-H. and Hwang S-C. 2011. Step-by-step improvement of MPS method in simulating violent free-surface motions and impact-loads. *Computer methods in Applied Mechanics and Engineering* (200), 1113- 1125.

Li Y., Raichlen F. 2003. Energy balance model for breaking solitary wave runup. *Journal of Waterway Port Coastal and Ocean Engineering* (129(2)), 47–59.

Li T., Troch P. and De Rouck J. 2004. Wave overtopping over a sea dike. *Journal of Computational Physics* (198), 686- 726.

Li J., Liu H., Gong K., Keat Tan S. and Shao S. 2012. SPH modelling of solitary wave fissions over uneven bottoms. *Coastal Engineering* (60), 261- 275.

Libersky L.D., Petscheck A.G., Carney T.C. and Hipp J.R. 1993. High Strain Lagrangian Hydrodynamics. *Journal of Computational Physics* (109), 67- 75.

Lighthill J. 2001. Waves in Fluids. second edition. Cambridge University Press, New York.

Lind S.J., Xu R., Stansby P.K. and Rogers B.D. 2012. Incompressible smoothed particle hydrodynamics for free- surface flows: A generalized diffusion- based algorithm for stability and validations for impulsive flows and propagating waves. *Journal of Computational Physics* (231), 1499- 1523.

Liu W.K., Jun S. and Zhang Y.F. 1995. Reproducing Kernel Particle Methods, *International Journal for Numerical Methods in Fluids* (20) 1081- 1106.

Liu G.R. 2002. Meshfree Methods: moving beyond the finite element method, CRC Press.

Liu G.R. and Liu M.B. 2003. Smoothed Particle Hydrodynamics a meshfree particle method. World Scientific, Singapore.

Liu X., Xu H., Shao S. Lin P. 2013. An improved incompressible SPH model for simulation of wave-structure interaction. *Computers and Fluids* (71), 113- 123.

Lo E.Y.M. and Shao S. 2002. Simulation of near-shore solitary wave mechanics by an incompressible SPH method. *Applied Ocean Research* (24), 275-286.

Löhner R., Ynag C., Oñate E. 2006. On the simulation of flows with violent free surface motion. *Computer methods in Applied Mechanics and Engineering* (195), 5597-5620.

Lucy L.B. 1977. A numerical approach to the testing of fission hypothesis. *The Astronomical Journal* (82(12)), 1013- 1024.

Ma Q.W. and Zhou J.T. 2009. MLPG_R Method for Numerical Simulation of 2D Breaking waves. *Computer Modeling in Engineering and Sciences* (43(3)), 277-303.

Ma Q.W. 2005a. Meshless local Petrov-Galerkin method for two-dimensional nonlinear water wave problems. *Journal of Computational Physics* (205), 611- 625.

Ma Q.W. 2005b. MLPG Method Based on Rankine Source Solution for Simulating Nonlinear Water Waves. *Computer Modeling in Engineering and Sciences* (9(2)), 193- 209.

Maciá F., Antuono M., González L.M. and Colagrossi A. 2011. Theoretical Analysis of the No- Slip Boundary Condition Enforcement in SPH Methods. *Progress of Theoretical Physics* (125(6)), 1091- 1121.

Macià F., Sánchez J.M., Souto-Iglesias A. and González L.M. 2012. WCSPH viscosity diffusion processes in vortex flows. *International Journal for Numerical Methods in Fluids* (69), 509- 533.

Maciá F., Gonzalez L. M., Cercos- Pita J. L. and Souto- Iglesias A. 2013. A Boundary Integral SPH Formulation, Consistency and Applications to ISPH and WCSPH. *Progress of Theoretical Physics* (128(3)), 439- 462.

Marrone S., Antuono M., Colagrossi A., Colicchio G. and Le Touze D. Graziani G. 2011a. δ-SPH model for simulating violent impact flows. *Computer methods in Applied Mechanics and Engineering* (200), 1526-1542.

Marrone S., Colagrossi A., Antuono M., Lugni C., Tulin M.P. 2011b. A 2D+*t* SPH model to study breaking wave pattern generated by fast ships. *Journal of Fluids and Structures* (27), 1199- 1215.

Marrone S., Bouscasse B., Colagrossi A., Antuono M. 2012. Study of ship breaking patterns using 3D parallel SPH simulations. *Computers and Fluids* (69), 54- 66.

Marrone S., Colagrossi A., Antuono M., Collichio G. and Graziani G. 2013. An accurate SPH modeling of flows around bodies at low and moderate Reynolds numbres. *Journal of Computational Physics* (245), 456- 475.

Martin J.C. and Mouce W.J. 1952. An experimental study of the collapse of the liquid columns on a rigid horizontal plane. *Philosophical Transaction of Royal Society A*, 244-312.

Mayrhofer A., Rogers B.D., Violeau D. and Ferrand M. 2013. Investigation of wall bounded flows using SPH and the unified semi- analytical wall boundary conditions. *Computer Physics Communications* (184), 2515- 2577.

Mayrhofer A., Ferrand M., Kassiotis C., Violeau D. and Morel F-X. 2014. Unified semi-analytical wall boundary conditions in SPH: analytical extension to 3-D. *Numerical Algorithms*.

Miyama S.M., Hayashi C. and Narita S. 1984. Criteria for collapse and fragmentation of rotating, isothermal clouds. *The Astrophysical Journal* (279), 621- 632.

Monaghan J.J. and Gingold R.A. 1983. Shock simulation by the particle method SPH. *Journal of Computational Physics* (52), 374- 389.

Monaghan J.J. and Lattanzio J.C. 1985. A refined particle method for astrophysical problems. *Astronomy and Astrophysics* (149), 135- 143.

Monaghan J.J. 1989. On the Problem of Penetration in Particle Methods. *Journal of Computational Physics* (82), 1-15.

Monaghan J.J. 1992. Smoothed Particle Hydrodynamics. *Annual Review of Astronomy and Astrophysics* (30), 543- 574.

Monaghan J.J. 1994. Simulating Free Surface Flows with SPH. *Journal of Computational Physics* (110), 399- 406.

Monaghan J.J., Kocharyan A. 1995. SPH simulation of multi-phase flow. *Journal of Computational Physics* (87), 225- 235.

Monaghan J.J. and Kos A. 1999. Solitary Waves On A cretan Beach. *Journal of Waterway, Port and Ocean Engineering* (125), 145-153.

Monaghan J.J. 2000. SPH without a Tension Instability. *Journal of Computational Physics* (159), 290- 311.

Monaghan J.J. and Rafiee A. 2013. A simple SPH algorithm for muti- fluid flow with high density ratios. *International Journal for Numerical Methods in Fluids* (71), 537-561.

Molteni D. and Colagrossi A. 2009. A simple procedure to improve the pressure evaluation in hydrodynamic context using the SPH. *Computer Physics Communications* (180), 861- 872.

Molteni D., Grammauta R. and Vitanza E. 2013. Simple absorbing layer conditions for shallow wave simulations with Smoothed Particle Hydrodynamics. *Ocean Engineering* (62), 78- 90.

Morris J.P., Fox P.J. and Zhu Yi. 1997. Modeling Low Reynolds Number Incompressible Flows Using SPH. *Journal of Computational Physics* (136), 214- 226.

McCabe M.V. Stansby P.K. and Apsley D.D. 2013. Random wave runup and overtopping a steep sea wall: Shallow- water and Boussinesq modelling with generalised breaking and wall impact algorithms validated against laboratory and field measurements. *Coastal Engineering* (74), 33-49.

Nelson R.P. and Papaloizhou J.C.B. 1994. Variable smoothing lengths and energy conservation in smoothed particle hydrodynamics. *Monthly Notices of Royal Astronomical Societies* (270), 1- 20.

Nestor R.M., Basa M., Lastiwka M and Quinlan N.J. 2009. Extension of the finite volume particle method to viscous flow. *Journal of Computational Physics* (228), 1733- 1749.

Oger G., Doring M., Alessandrini B. and Ferrant P. 2006. Two-dimensional SPH simulations of wedge water entries. *Journal of Computational Physics* (213), 803-822.

Oñate E., Idelsohn S.R., Zienkievicz O.C. and Taylor R.L. 1996. A finite point method in computational mechanics, applications to convective transport and fluid flow. *International Journal for Numerical Methods in Engineering* (39(22)), 3839- 3886.

Oñate E., Idelsohn S.R., Celigueta M.A. and Rossi R. 2006. Advances in the particle finite element method for fluid-structure interaction problems. in Proceedings: 1st South- East European Conference on Computational Mechanics (SEECCM-06).

Parshikov A., Medin S.A., Loukashenko I.I. and Milekhin V.A. 2000. Improvements in SPH method by means of interparticle contact algorithm and analysis of perforation tests at moderate projectile velocities. *International Journal of Impact Engineering* (24), 779- 796.

Price D.J. 2004. Magnetic fields in Astrophysics. PhD Thesis, Institute of Astronomy and Churchill College, University of Cambridge, UK.

Press W.H., Teukolsky S.A., Vetterling W.T., Flannery B.P. 1986. NUMERICAL RECIPES IN FORTRAN The Art of Scientific Computing. Cambridge University Press. UK.

Puri K. and Ramachandran P. 2014. A comparison of SPH schemes for the compressible Euler equations. *Journal of Computational Physics* (256(1)), 308- 333.

Quinlan N. J., Basa M. and Lastiwka M. 2006. Truncation error in mesh- free particle methods. *International Journal for Numerical Methods in Engineering* (66), 2064- 2085.

Rabzcuk T., Belytschko T. and Xiao S.P. 2004. Stable particle methods based on Lagrangian kernels. *Computer methods in Applied Mechanics and Engineering* (193), 1035- 1063.

Rafiee A. and Thiagarajan K.P. 2009. An SPH projection method for simulating fluid-hypoelastic structure interaction. *Computer methods in Applied Mechanics and Engineering* (198), 2785- 1795.

Rafiee A., 2011. SPH modeling of multi-phase and energetic flows. PhD Thesis, School of Mechanical Engineering. Faculty of Engineering, Computing and Mathematics, The University of Western Australia, Australia.

Rafiee A., Pistani F. and Thiagarajan K. 2011. Study of liquid sloshing: numerical and experimental approach. *Computational Mechanics* (47), 65- 75.

Rafiee A., Cummins S., Rudman M. and Thiagarajan K. 2012. Comparative study on the accuracy and stability of SPH schemes in simulating energetic free- surface flows. *European Journal of Mechanics B/ Fluids* (36), 1- 16.

Repalle N., Rafiee A, Thiagarajan K.P. and Kantharaj M. 2011. Simulation of free surface benchmark problems using level set and SPH methods. in Proceeding: 30th OMAE conference.

Rogers B.D., Dalrymple R.A. and Stansby P.K. 2010. Simulation of caisson breakwater movement using 2-D SPH. *Journal of Hydraulic Research* (48), 135- 141.

Rognebakke O. 2002. Sloshing in rectangular tanks and inetractions with ship motions. PhD Thesis, Department of Marine Hydrodynamics, Norwegian University of Science and Technology, Norway.

Ryzhakov P., Rossi R., Viña A. and Oñate E. 2013. Modelling and simulation of the sea-landing of aerial vehicles using the Particle Finite Element Method. *Ocean Engineering* (66), 92- 100.

Saville T.(Jr.). 1955. Laboratory data on wave runup and overtopping on shore structures. Technical Memo No. 64. U.S. Army, Beach Erosion Board, Document Service Center, Dayton, Ohio.

Seabra-Santos F.J., Renourd D.P. and Temperville A.M. 1987. Numerical and experimental study of the transformation of a solitary wave over a shelf or isolated obstacle. *Journal of Fluid Mechanics* (176), 117-134.

Shadloo M.S., Zainali A., Sadek S.H. and Yildiz M. 2011. Improved Incompressible Smoothed Particle Hydrodynamics method for simulating flow around bluff bodies. *Computer methods in Applied Mechanics and Engineering* (200), 1008- 1020.

Shakibaeinia A. and Jin Y-C. 2010. A weakly compressible MPS method for modeling of open-boundary free-surface flow. *International Journal for Numerical Methods in Fluids (*63), 1208- 1232.

Shao S. 2006. Incompressible SPH simulation of wave breaking and overtopping with turbulence modelling. *International Journal for Numerical Methods in Fluids* (50), 597- 621.

Shao S., Ji C., Graham D.I., Reeve D.E., James P.W. and Chadwick A.J. 2006. Simulation of wave overtopping by an incompressible SPH model. *Coastal Engineering (*53), 723- 735.

Shao S. 2009. Incompressible SPH simulation of water entry of a free- falling object. *International Journal for Numerical Methods in Fluids* (59), 91- 115.

Shao J.R., Li H.Q., Liu G.R., Liu M.B. 2012. An improved SPH method for modeling liquid sloshing dynamics. *Computers and Structures*. 100- 101 (2012) 18- 26.

Shewchuk J.R. 1994. An introduction to the Conjugate Gradient Method Without the Agonizing Pain.

Sod G.A. 1978. A survey of several finite difference methods for systems of hyperbolic conservation laws. *Journal of Computational Physics* (27), 1- 31.

Soliman A. 2003. Numerical study of irregular wave overtopping and overflow. PhD thesis, The University of Nottingham, UK.

Souto-Iglesias A., Macià F., González L.M. and Cercos-Pita J.L. 2013. On the consistency of MPS. *Computer Physics Communications* (184), 732- 745.

Springel V., Yoshida N. and White S.D.M. 2001. GADGET: a code for collisions and gasdynamical cosmological simulations. *New Astronomy* (6), 79- 117.

Sriram V., Sannasiraj S.A. and Sundar V. 2006a. Simulation of 2-D nonlinear waves using finite element method with cubic spline approximation. *Journal of Fluids and Structures* (22), 663- 681.

Sriram V., Sannasiraj S.A. and Sundar V. 2006b. Numerical simulation of 2D sloshing waves due to horizontal and vertical random excitation. *Applied Ocean Research* (28), 19-32.

Sriram V. 2008. Finite Element Simulation of Nonlinear Free Surface Waves. PhD Thesis, Department of Ocean Engineering, Indian Institute of Technology Madras, India.

Sriram V., Ma Q.W. and Schlurmann T. 2012. Numerical Simulation of Breaking Waves using Hybrid Coupling of FNPT and NS Solvers. in Proceeding: 22nd ISOPE conference (3), 1118- 1124.

Sriram V. and Ma Q.W. 2012. Improved MLPG_R method for simulating 2D interaction between violent waves and elastic structures. *Journal of Computational Physics* (231), 7650- 7670.

Stansby P.K. 2003. Solitary wave run up and overtopping by a semi-implicit finite-volume shallow-water Boussinesq model. *Journal of Hydraulic Research* (41(6)), 639- 647.

Stansby P.K. and Feng T. 2004. Surf zone wave overtopping a trapezoidal structure: 1-D modelling and PIV comparison. *Coastal Engineering* (51), 483- 500.

Swegle J.W., Hicks D.L. and Attaway S.W. 1995. Smoothed Particle Hydrodynamics Stability Analysis. *Journal of Computational Physics* (116), 123- 134.

Takeda H., Miyama S. M. and Sekiya M. 1994. Numerical Simulation of Viscous Flow by Smoothed Particle Hydrodynamics. *Progress of Theoretical Physics* (92(5)), 939-960.

Tartakovsky A., Meakin P., Schiebe T.D. and Eichler West R.M. 2007. Simulations of reactive transport and precipitation with smoothed particle hydrodynamics. *Journal of Computational Physics* (222(2)), 654- 672.

Troch P., Geeraerts J., Van de Walle B., De Rouck J., Damme L. V., Allsop W. and Franco L. 2004. Full- scale wave overtopping measurements on the Zeebrugge rubble mound breakwater. *Coastal Engineering* (51), 609- 628.

Umeyama M. 1993.Wave overtopping on vertical boundary and water–surface displacement. *Journal of Waterway Port Coastal and Ocean Engineering* (119 (3)), 243–260.

USACE (U.S. Army Corps of Engineers). 2006. Coastal Engineering Manual. Vicksburg, Mississippi: Coastal and Hydraulics Laboratory, Engineer Research and Development Center Report EM 1110-2-1100.

Vacondio R., Mignosa P. and Pagani S. 2013. 3D SPH numerical simulation of the wave generated by the Vajont rockslide. *Advances in Water Resources* (59), 146- 156.

Vanaverbeke S., Keppens R., Poedts S. and Boffin H. 2009. GRADSPH: A parallel smoothed particle hydrodynamics code for self- gravitating astrophysical fluid dynamics. *Computer Physics Communications* (2009), 1164- 1182.

Violeau D. 2009. Dissipative forces for Lagrangian models in computational fluid dynamics and application to smoothed particle hydrodynamics. *Physical Review E.* (80) 036705: 1-15.

Von Neumann J. and Richtmyer R.D. 1950. A method for the numerical calculation of hydrodynamic shocks. *Journal of Applied Physics* (21), 232- 247.

Wood D. 1981. Collapse and fragmentation of isothermal gas clouds. *Monthly Notices of Royal Astronomical Societies* (194), 201- 218.

Wood D. 1982. Fragmentation in rotating interstellar gas clouds. *Monthly Notices of Royal Astronomical Societies* (199), 331- 343.

Wedland H. 1995. Piecewise polynomial, positive definite and compactly supported radial functions of minimal degree. *Advances in Computational Mathematics (*4), 389- 396.

Weib D., Grenier A., Lienemann J and Korvink J.G. 2013. SPH based optimization of electrowetting- driven digital microfluidics with advanced actuation patterns. *International Journal of Modern Physics C*. (24(12)).

Weber C. 1934. Seawall. U.S. Patent 1,971,324, filed Jul. 18, 1934, issued Aug. 21, 1934.

Wu G.X., Ma Q.W. and Eatock Taylor R. 1998. Numerical simulation of sloshing waves in a 3D tank based on a finite element method. *Applied Ocean Research* (20) 337-355.

Wu G.X. 2007. Second- order resonance of sloshing in a tank. *Ocean Engineering* (34), 2345- 2349.

Xie Z. 2012. Numerical study of breaking waves by a two-phase flow model. *International Journal for Numerical Methods in Fluids* (70), 246- 268.

Xie Z. 2014. Numerical modelling of wind effects on breaking solitary waves. *European Journal of Mechanics B/ Fluids* (43), 135- 147.

Xu R., Stansby P., Laurence D. 2009. Accuracy and stability in incompressible SPH (ISPH) based on the projection method and a new approach. *Journal of Computational Physics* (228), 6703- 6725.

Yan S. and Ma Q.W. 2010. QALE-FEM for modelling 3D overturning waves. *International Journal for Numerical Methods in Fluids* (63), 743- 768.

Yildiz M., Rook R.A. and Suleman A. 2009. SPH with multiple boundary tangent method. *International Journal for Numerical Methods in Engineering* (77), 1416-1438.

Zainali A., Tofighi N., Shadloo M.S. and Yildiz M. 2013. Numerical investigation of Newtonian and non- Newtonian mutiphase flows using ISPH method. *Computer methods in Applied Mechanics and Engineering* (254), 99- 213.

Zhang Y. and Wan D. 2012. Apply MPS Method to Simulate Liquid Sloshing in LNG Tank. in Proceeding: 22nd ISOPE conference (3), 381- 391.

Zhou Z.Q., Kat J.O.D. and Buchner A. 1999. A nonlinear 3D approach to simulate green water dynamics on deck. in Proceeding: 7th International Numerical Ship Hydrodynamics Conference.

Zhou J.T. and Ma Q.W. 2010. MLPG method Based on Rankine Source Solution for Modelling 3D Breaking Waves. *Computer Modeling in Engineering and Sciences* (56(2)), 179- 210.

Zhou J. T. 2010. Numerical investigation of breaking waves and their interactions with structures using MLPG_R method. PhD Thesis, School of Engineering and Mathematical Sciences, City University London, UK.

PUBLICATIONS

A. National Seminars/Workshops attended

1. De Chowdhury S. and Sannasiraj S. A. 2012. A Comparative study on different SPH methods for simulating 2D wave impact pressures. National Conference on Hydraulics, Water Resources, Coastal and Environmental Engineering (HYDRO-2012), IIT Bombay, India.
2. De Chowdhury S. and Sannasiraj S. A. 2013. Application of sloSPHing2D for Numerical Simulation of Sloshing. NRB Workshop on Numerical Simulation of Nonlinear Free Surface Waves, 16th- 18th March, 2013. Dept. of Ocean Engineering, IIT Madras, Chennai, India.

B. International Conferences

1. De Chowdhury S. and Sannasiraj S. A. 2011. SPH simulation of sloshing due to horizontal tank excitation. 2nd international conference on particle-based methods, fundamentals and application, PARTICLES'011, Barcelona, Spain, 26-28th October, 2011.
2. De Chowdhury S. and Sannasiraj S. A. 2012. Numerical simulation of water waves using SPH method. 8th international conference on coastal and port engineering in developing countries, COPEDEC 2012, Chennai, India, 20-24th February, 2012.
3. De Chowdhury S. and Sannasiraj S. A. 2013. Numerical Simulations of 2D Wave Impact Pressures Using SPH Schemes. 23rd Offshore (Ocean) Polar Engineering Conference (ISOPE 2013), Anchorage, Alaska, USA, 30th June- 05th July.
4. De Chowdhury S. and Sannasiraj S. A. 2013. Numerical Simulation of Wave Overtopping Using Meshfree SPH Method. 35th IAHR World Congress. Chengdu, PRC, 8th- 13th September.
5. De Chowdhury S. and Sannasiraj S. A. 2013. Comparison between incompressible and weakly compressible SPH schemes in simulating breaking wave impact.

HYDRO 2013 INTERNATIONAL, conference on Hydraulics, Water resources, coastal and Environmental Engineering, Chennai, India, 4th- 6th December.

6. De Chowdhury S. and Sannasiraj S. A. 2014. A Study on Wave Overtopping and Sea Wall Stability Using SPH Schemes. Paper accepted for 24th Offshore (Ocean) Polar Engineering Conference (ISOPE 2014), Busan, Korea, June 15- 20.

C. Referred Journals

1. De Chowdhury S. and Sannasiraj S. A. 2012. Numerical Simulation of Solitary waves using Smoothed particle Hydrodynamics method, International Journal of Ocean and Climate systems; 3(3), 187- 202.
2. De Chowdhury S. and Sannasiraj S. A. 2013. SPH simulation of shallow water wave propagation, Ocean Engineering; 60, 41- 52.
3. De Chowdhury S. and Sannasiraj S. A. 2014. Numerical Simulation of 2D Sloshing Waves Using SPH With Diffusive Terms, Applied Ocean Research; 47, 219- 240.